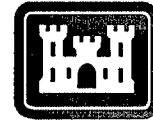


ERDC/ITL TR-02-6

Information Technology Laboratory



US Army Corps
of Engineers®
Engineer Research and
Development Center

Fragility Analysis of Concrete Gravity Dams

Paulos B. Tekie and Bruce R. Ellingwood

September 2002

20021129 068

The contents of this report are not to be used for advertising, publication, or promotional purposes. Citation of trade names does not constitute an official endorsement or approval of the use of such commercial products.

The findings of this report are not to be construed as an official Department of the Army position, unless so designated by other authorized documents.



PRINTED ON RECYCLED PAPER

ERDC/ITL TR-02-6
September 2002

Fragility Analysis of Concrete Gravity Dams

by Paulos B. Tekie, Bruce R. Ellingwood
Georgia Institute of Technology
School of Civil & Environmental Engineering
790 Atlantic Dr.
Atlanta, GA 30332

Final report

Approved for public release; distribution is unlimited

TABLE OF CONTENTS

PREFACE	I
CHAPTER 1. INTRODUCTION	1
1.1. Statement of the Problem.....	1
1.2. Review and Critical Appraisal of Current Policies and Design Procedures.....	2
1.3. Goals and Objectives of Research	5
1.4. Outline of Report	6
CHAPTER 2. PERFORMANCE OF CONCRETE GRAVITY DAMS	9
2.1. Current Design Basis	10
2.2. Structural Behavior and Performance States	13
2.3. Past Performance	14
2.4. Failure Criteria.....	16
2.4.1. Concrete.....	16
2.4.2. Foundation Rock.....	17
Hoek-Brown Failure Criterion.....	19
2.4.3. Dam-Foundation Interface	21
CHAPTER 3. NATURAL HAZARDS	24
3.1. Hydrologic Hazard.....	25
3.2. Seismic Hazard	28
3.3. Sampling Errors and Uncertainty Analysis.....	30

CHAPTER 4. STRUCTURAL MODELING OF DAM BEHAVIOR.....	36
4.1. Rigid Body Model.....	36
4.2. Linear Finite Element Model (FElt)	39
4.2.1. Description of Model	39
4.2.2. Uplift Force.....	40
4.2.3. Structural Response	41
4.3. Nonlinear Finite Element Model (Abaqus).....	43
4.3.1. Modeling for Hydrologic (Static) Analysis	43
4.3.1.1. Description of Model	44
4.3.1.2. Structural Response	45
4.3.2. Modeling for Seismic (Dynamic) Analysis	48
4.3.2.1. Contact Surface Model	49
4.3.2.2. Infinite Elements.....	50
4.3.2.3. Input Mechanism of Ground Motion.....	50
4.3.2.4. Boundary Conditions	52
4.3.2.5. Dam-Water-Foundation Interaction.....	53
4.4. Discrete Element Method	63
CHAPTER 5. FRAGILITY MODELING.....	102
5.1. Probabilistic Safety Assessment	102
5.2. Fragility Modeling	105
5.3. Limit States	110
5.4. Hydrologic Fragility.....	113
5.4.1. Uncertainty Modeling	113
5.4.2. Fragility Analysis.....	115
5.4.2.1. Fragilities: Rigid body model	115
5.4.2.2. Fragilities: Linear FE model	116
5.4.2.3. Fragilities: Nonlinear FE model.....	117
5.4.2.4. Comparison of fragilities	118
5.5. Seismic Fragility	120
5.5.1. Uncertainty Modeling	120

5.5.2. Fragility Analysis.....	122
5.5.2.1. Sampling Procedure.....	122
5.5.2.2. Fragility analysis.....	123
5.6. Sensitivity Studies.....	125
5.6.1. Hydrologic Fragility.....	125
5.6.2. Seismic Fragility.....	127
5.7. Additional Data Needs.....	127
CHAPTER 6. INSIGHTS AND PERSPECTIVES ON RISK.....	160
6.1. Interpretation Guidelines	160
6.2. Fully Coupled Risk Analysis	163
6.2.1. Basic Concepts.....	163
6.2.2. Risk De-aggregation	164
6.2.3. Limit State Probabilities	165
6.2.3.1. Computation.....	165
6.2.3.2. Risk Balancing.....	166
6.3. Acceptable Risk	167
6.3.1. Decision-Making Agencies.....	167
6.3.2. Social Risk Perception	168
6.3.3. Acceptable levels of risk.....	170
6.4. Simplified Risk Analysis Models	172
6.4.1. Statistical Simplification.....	172
6.4.2. Structural Simplification.....	174
CHAPTER 7. CONCLUSIONS AND RECOMMENDATIONS	197
Recommendations for Further Research.....	200
APPENDIX – BLUESTONE DAM.....	203
Estimated hydrologic hazard for Bluestone Dam	
BIBLIOGRAPHY.....	207

LIST OF FIGURES

Fig. 2.1.	Array of loads used in current design practices (Novak et al., 1996).....	23
Fig. 3.1.	Hydrologic hazard for Bluestone Dam	33
Fig. 3.2.	Seismic hazard for Bluestone Dam.....	34
Fig. 3.3.	Illustration of epistemic uncertainty in seismic hazard at Zion Nuclear Power Plant.....	35
Fig. 4.1.	Non-overflow monolith no. 12 at Bluestone Dam.....	69
Fig. 4.2.	Linear finite element model of Bluestone monolith no. 12	70
Fig. 4.3.	Uplift pressure at base of dam	71
Fig. 4.4.	Normal stress distributions at the base of dam	72
	a) For different pool elevations.....	72
	b) For pool elevation of 1360 ft (415 m)	72
	c) For pool elevation of 1556 ft (474 m).....	73
Fig. 4.5.	Shear stress distribution at base of dam.....	74
Fig. 4.6.	Relative deformation of the top of the dam with respect to heel	75
Fig. 4.7.	Deformed shape of dam-foundation system	76
	a) Pool elevation = 1360 ft.....	76
	b) Pool elevation = 1556 ft	76
Fig. 4.8.	Stress distribution at the neck of the dam	77
	a) Normal stress distribution.....	77
	b) Shear stress distribution.....	77
Fig. 4.9.	Comparison of stresses observed vs. Hoek-Brown criterion at elevation of 1556 ft (474 m)	78
	a) Compression failure.....	78
	b) Shear failure.....	78

Fig. 4.10. Relative deformation at top of the dam.....	79
Fig. 4.11. Normal stress distribution at the base of dam, with modified modulus of elasticity.....	80
Fig. 4.12. Shear stress distribution at base of dam, with modified modulus of elasticity.....	81
Fig. 4.13. Nonlinear FE model of Bluestone monolith no. 12.....	82
Fig. 4.14. Normal stress distribution at the base of dam.....	83
Fig. 4.15. Comparison of normal stresses at base of dam.....	84
a) Pool elevation of 1360 ft (415 m).....	84
b) Pool elevation of 1556 ft (474 m).....	84
Fig. 4.16. Shear stress distribution at base of dam.....	85
Fig. 4.17. Comparison of shear stresses at base of dam.....	86
a) Pool elevation of 1360 ft (415 m).....	86
b) Pool elevation of 1556 ft (474 m).....	86
Fig. 4.18. Normal stress distribution at the neck of dam.....	87
Fig. 4.19. Comparison of normal stresses at neck of dam.....	88
a) Pool elevation of 1360 ft (415 m).....	88
b) Pool elevation of 1556 ft (474 m).....	88
Fig. 4.20. Relative deformation of top of dam.....	89
Fig. 4.21. Sliding response at the interface around the heel.....	90
Fig. 4.22. Cracking at the interface around the heel.....	91
Fig. 4.23. Plastic strain (in vertical direction) in foundation, near the toe of dam.....	92
Fig. 4.24. One-dimensional idealization of a horizontally layered soil deposit over a uniform half-space (Idriss and Sun, 1992).....	93
Fig. 4.25. Nonlinear FE model of monolith no. 12 – seismic.....	94
Fig. 4.26. Construction of the two-parameter model (Darbre, 1998).....	95

Fig. 4.27. Normal Stress (S22) [ksf] at the heel; El-Centro scaled to S_a 0.9 g (With and without vertical component)	96
Fig. 4.28. Normal Stress [ksf] at neck of dam; El-Centro scaled to S_a 0.9 g (With and without vertical component)	97
a) Upstream side of the neck.....	97
b) Downstream side of the neck.....	97
Fig. 4.29. Relative deformation [ft] of top of dam; El-Centro scaled to S_a 0.9 g (With and without vertical component)	98
Fig. 4.30. Cracking [ft] at the heel of dam; El-Centro scaled to S_a 0.9 g (With and without vertical component)	99
Fig. 4.31. Sliding [ft] at the interface of dam; El-Centro scaled to S_a 0.9 g (With and without vertical component)	100
Fig. 4.32. Plastic strain in foundation – toe of dam; El-Centro scaled to S_a 0.9 g (With and without vertical component)	101
a) Plastic strains at points in foundation (Area 1).....	101
b) Area-averaged plastic strains.....	101
Fig. 5.1.a. Simplified event tree model of dam-reservoir system	130
Fig. 5.1.b. Inclusive event tree model of a dam-reservoir system (Stedinger, 1996).....	131
Fig. 5.2. Fragilities for progressively severe limit states	132
Fig. 5.3. Conceptual illustration of fragility showing both epistemic and aleatory uncertainty	133
Fig. 5.4. Hydrologic Fragility of Monolith 12 – rigid body analysis.....	134
Fig. 5.5. Hydrologic Fragility of Monolith No. 12 – linear FE analysis.....	135
Fig. 5.6. Hydrologic Fragilities for LS1 with different modeling assumptions	136
Fig. 5.7. Hydrologic Fragilities for LS2 with modified modulus of elasticity.....	137
Fig. 5.8. Hydrologic Fragility of Monolith No. 12 – nonlinear FE analysis.....	138
a) for LS1, LS2, and LS4.....	138
b) for LS5, LS6, and LS7.....	138

Fig. 5.9. Comparison of Hydrologic Fragilities – LS1 and LS2	139
Fig. 5.10. Comparison of Hydrologic Fragilities – LS5 and LS7	140
Fig. 5.11. Response spectra of selected earthquake records – scaled to 1.0 g at $w_n = 6.12$ Hz.....	141
Fig. 5.12. Seismic Fragility of Monolith No. 12 LS4 – Tensile Stress & Cracking	142
Fig. 5.13. Seismic Fragility of Monolith No. 12 LS5 – Nonlinear behavior in foundation	143
Fig. 5.14. Seismic Fragility of Monolith No. 12 LS6 – Sliding.....	144
Fig. 5.15. Seismic Fragility of Monolith No. 12 LS7 – Relative Deformation.....	145
Fig. 5.16. Comparison of Seismic Fragilities.....	146
Fig. 5.17. Hydrologic Fragility – Effect of uplift area	147
Fig. 5.18. Hydrologic Fragility – Effect of tail water elevation.....	148
Fig. 5.19. Hydrologic Fragility – Effect of drain efficiency	149
Fig. 5.20. Hydrologic Fragility – Effect of grout efficiency	150
Fig. 5.21. Hydrologic Fragility – Effect of drain and grout efficiencies (perfectly correlated).....	151
Fig. 5.22. Hydrologic Fragility – effect of effective uplift area; LS1 and LS2.....	152
Fig. 5.23. Hydrologic Fragility – effect of effective uplift area; LS5 and LS6.....	153
Fig. 5.24. Hydrologic Fragility – effect of coefficient of friction; LS1 and LS2.....	154
Fig. 5.25. Hydrologic Fragility – effect of coefficient of friction; LS5 and LS6.....	155
Fig. 5.26. Seismic Fragility – effect of uplift area; LS4 and LS5	156
Fig. 5.27. Seismic Fragility – effect of uplift area; LS6 and LS7	157
Fig. 5.28. Seismic Fragility – effect of coefficient of friction; LS4 and LS5	158
Fig. 5.29. Seismic Fragility – effect of coefficient of friction; LS6 and LS7	159
Fig. 6.1. Frequency distribution of estimated limit state probability	181

Fig. 6.2.	Determination of limit state probability.....	182
Fig. 6.3.	Hydrologic hazard and Limit States for Cracking	183
Fig. 6.4.	Hydrologic hazard and LS5, LS6, and LS7	184
Fig. 6.5.	Seismic hazard and LS4 (Tensile Stress & Cracking).....	185
Fig. 6.6.	Seismic hazard and LS5 – Plastic Strains.....	186
Fig. 6.7.	Seismic hazard and LS6 – Sliding	187
Fig. 6.8.	Seismic hazard and LS7 – Relative Deformation.....	188
Fig. 6.9.	Proposals for F-N curves (adapted from Hoeg, 1996).....	189
Fig. 6.10.	Approximate fragility analysis by scaling upward from design conditions.....	190
Fig. 6.11.	Approximate Hydrologic Fragility for LS1 and LS2.....	191
Fig. 6.12.	Approximate Hydrologic Fragility for LS5 and LS7.....	192
Fig. 6.13.	Approximate Seismic Fragilities for LS6 – Sliding.....	193
Fig. 6.14.	Approximate Seismic Fragilities for LS5 – Plastic Strains	194
Fig. 6.15.	Approximate Seismic Fragilities for LS4 – Tensile Cracking.....	195
Fig. 6.16.	Approximate Seismic Fragilities for LS7 – Relative Deformation	196

PREFACE

The research work reported herein was supported in part by awards from the U.S. Army Corps of Engineers (USACE), under Contract No. DACW31-99-P-0479, "Fragility Analysis of Concrete Gravity Dams," through Black & Veatch (B&V) Research Corporation and the U.S. Army Engineer District, Baltimore. Funding was provided by the Reliability Models from Major Rehabilitation Program, for which Mr. H. Wayne Jones of the Information Technology Laboratory (ITL), U.S. Army Engineer Research and Development Center (ERDC), is the ERDC program manager. Messrs. James Waller (B&V) and Jerry Foster and Peter Rossbach (USACE) served as program directors. This support is gratefully acknowledged by the authors.

At the time of publication of this report, the Director of ITL was Dr. Jeffery P. Holland. Director of ERDC was Dr. James R. Houston, and the Commander and Executive Director was COL John W. Morris III, EN.

Chapter 1

INTRODUCTION

1.1. STATEMENT OF THE PROBLEM

Concrete gravity dams are an important part of the nation's infrastructure, serving as part of the inland waterway transportation system as well as providing for conservation and for recreational facilities. Approximately 10% of the major dams in the United States are of this type. Many have been in service for over 50 years. During this period of service, some degradation in a dam may have occurred as a result of operating conditions, environmental forces, deterioration in materials from natural causes, and wearout of mechanical equipment such as gates, pipes and valves. Many of the nation's dams now are in need of rehabilitation (National, 1985; DeSena, 1998). Potential economic or property losses from dam failures, both direct (flood damage, loss of reservoir) and indirect (environmental damage, loss of economic opportunity), may be significant (Ellingwood et al, 1993). Moreover, the database on natural phenomena hazards such as floods and earthquakes has expanded significantly in recent years. With this expansion, design-basis events, such as the Probable Maximum Flood (PMF) or Maximum Credible Earthquake (MCE), often have been revised upward (National, 1985; Lave et al, 1990). Many existing dams fail to

meet these revised (and usually more conservative) safety criteria incorporating this new information on natural hazards. Questions have arisen as to whether certain existing dams have the capacity in their current condition to withstand extreme environmental events beyond the original design basis during a future service period with an acceptable margin of safety.

Under criteria currently in use, dams are designed to withstand or resist hazards that conceivably could occur in their lifetimes. However, it is not possible to provide "absolute" safety against all hazards. Extreme events that exceed the dam's capacity to resist them can occur, although they may have very low probabilities of occurrence. Decisions regarding condition assessment, whether corrective action should be initiated and, if so, to what level, are difficult (Lave et al, 1990). Structural rehabilitation to allow high-hazard dams to meet newly revised criteria is extremely costly, and indeed may not be feasible in some cases (Dawdy and Lettenmaier, 1987). It is reasonable to ask whether retrofitting a dam to meet a newly defined and larger natural hazard is an appropriate strategy for managing its risk. Such questions can best be answered within the framework of a formal probabilistic safety analysis (PSA) of the dam.

1.2. REVIEW AND CRITICAL APPRAISAL OF CURRENT POLICIES AND DESIGN PROCEDURES

Current dam safety policies strive to balance the benefits of making dams safer against the cost of increasing safety and to reduce any risks to acceptable proportions

(National, 1985). A summary of such a policy of the U.S. Army Corps of Engineers (USACE), a major dam owner, builder and operator of dams in the US, is summarized in the Corps' document, "Dam Safety Assurance Program" (Dam, 1995). The policy is to determine the population at risk with and without dam failure, and to consider loss of life in assigning project hazard categories. The hazard classification, summarized in Table 1.1, is not used to evaluate hydrologic or seismic adequacy of the dam structure. It only defines general performance expectations. The qualitative classification in Table 1.1 is not tied to any engineering analyses and does not provide any quantitative basis for safety/ risk evaluation of the dam. Rather, the dam is considered "hazardous" if its failure would cause one more fatality than would have occurred had the dam not failed.

This USACE policy is limited in its ability to distinguish the risk implications of alternate strategies for safety assurance. The policy detailed in "Dam Safety Assurance Program" (Dam, 1995), for example, considers important parameters in the safety evaluation as deterministic. These parameters include the bearing capacity of the foundation soil /rock, strength of concrete and the hydrologic or seismic hazards. The hazards are defined simply by estimates of the largest event that could possibly occur at the site; namely, the PMF (Probable Maximum Flood) and MCE (Maximum Credible Earthquake). Because of the limitation in the supporting databases, the procedures for the estimation of these values are not robust, and thus different analysts often come up with different estimates of "largest events". This becomes a significant problem in condition assessment of existing facilities.

Traditional methods for analyzing the structural behavior of the dam-foundation system have relied on simple rigid body analysis. Only recently have more exact methods

of analyses (e.g. finite element analyses) been employed (e.g. Dewey et al, 1994). The rigid body analysis implements rudimentary measures of performance, such as the location of the resultant force with respect to the base of the dam, for design criteria. It is not capable of distinguishing the different performance states of the dam-foundation system, ranging from cracking /minor damage to incipient instability /catastrophic failure. The recent finite element procedures have been more successful at capturing the essential features of dam performance at high hazard levels; however, they have been largely deterministic in nature.

Accordingly, these procedures and USACE policies do not provide a rational basis for handling the uncertainties involved in dam performance and safety assessment. The traditional approach of dealing with uncertainties is through use of factors of safety (ignorance). These safety factors are applied separately at different stages, and inconsistently in the processes of analysis, design, and condition assessment, leading to an unknown but unpredictable margin of safety.

Procedures that provide a more rational way of assessing safety of concrete gravity dams are required to establish priorities on allocation of limited resources to mitigate risk by rehabilitation, dam inspection and/ or by changes in policy. Such procedures should be based on modern principles of structural/geotechnical engineering. Moreover, a probabilistic framework is required to manage the various sources of uncertainty that may impact dam performance and decisions related thereto (National, 1985). Fragility analysis, which depicts the uncertainty in the safety margin above specified hazard levels, including the design-basis and review-level events, is a central tool in this probabilistic framework.

1.3. GOALS AND OBJECTIVES OF RESEARCH

This study presents a methodology for development of fragilities of concrete gravity dams to assess their performance against hydrologic and seismic hazards. Structural models of varying degrees of complexity and with different assumptions, including those capable of handling the essential features of the non-linear response of the dam-foundation system are utilized. Computational support for the fragility assessment is provided by statistical/ probabilistic tools for analysis of uncertainties. Guidelines for the use, interpretation and implementation of fragilities within the context of probabilistic dam safety assessment are provided. The methodology is illustrated using the Bluestone Dam on the New River in West Virginia, which was designed in the late 1930's and has recently been the subject of a re-assessment of performance under a revised PMF. A description of this dam is provided in the appendix to this report. The governing design condition involved a combination of hydrostatic pressure and earthquake effects.

The essential ingredients of this study include:

- Identification of performance limit states
- Development of structural/ numerical models
- Procedures for analyzing sources of uncertainty
- Sensitivity studies to identify areas of additional data requirements
- Quantitative risk metrics to be used for decision analysis

This study is confined to the fragility modeling of concrete gravity dams, and does not address economic or social consequences of dam failure to the population at risk. Methods are available for developing cost accounting stances and for evaluating failure costs (Baecher, et al, 1980; Ouelette, et al, 1985; Ellingwood, et al, 1993).

1.4. OUTLINE OF REPORT

This report is organized around three themes: review of basic design concepts and performance measures, structural modeling and probabilistic analysis of dam performance at different levels of natural hazard, and interpretation and implementation of fragilities in facility risk management. Chapters 2 and 3 provide an overview of the basic concepts and background necessary in the discussion of the probabilistic safety assessment of concrete gravity dams. Chapter 2 reviews and critiques the current standards and requirements used in the design of dams. It discusses the structural behavior of dams subjected to hydrologic and earthquake hazards, and presents a brief review of the causes and statistics of dam failures. In addition, it depicts failure criteria for construction materials of concrete gravity dams, which are subsequently used in fragility analyses. Chapter 3 characterizes the major natural hazards that challenge concrete gravity dams: extreme hydrologic events and earthquakes. It introduces the notions of probabilistic hazard analysis, and the modeling of uncertainties in natural hazard intensity.

Structural models of concrete gravity dams are presented in Chapter 4. Models of increasing complexity, from rigid body to linear and nonlinear finite element (FE) methods, are considered. The structural responses obtained from these models are compared and critiqued. The basic concepts of fragility analysis in the context of a probabilistic safety assessment (PSA) are presented in Chapter 5. Performance limit states that are pertinent to structural behavior of concrete gravity dams are identified. Hydrologic and seismic fragilities, obtained from different structural models, are presented and their

differences/similarities discussed. Sensitivity analyses, carried out to assess the sensitivity of the fragility to various modeling assumptions, are also described.

Chapter 6 presents guidelines for the interpretation and implementation of fragilities in the decision-making process. It also illustrates how fragilities are used in a fully coupled PSA, with a description of various performance limit states and a comparison with socially “acceptable risks”. The use of approximate procedures of fragility analysis for preliminary risk assessment purposes is investigated. The key findings of this are presented in Chapter 7, where areas for further research are recommended.

Table 1.1. Hazard potential classification for civil works projects[‡]

<u>Category</u>	<u>Low</u>	<u>Significant</u>	<u>High</u>
Loss of life	None expected	Uncertain	Certain
Lifeline losses	No disruption	Disruption of essential facilities.	Disruption of critical facilities.
Property losses	Private only	Major public/ private	Extensive public /private
Environmental losses	Minimal	Major - mitigation required	Extensive - mitigation difficult

[‡] The essential features of Table E-1 of ER 1110-2-1155 (1995) are summarized. More details are provided in the original table.

Chapter 2

PERFORMANCE OF CONCRETE GRAVITY

DAMS

A concrete gravity dam is a massive structure with an essentially triangular profile that consists of rigid monoliths (40-50 ft/ 12-15 m wide) situated side by side. Its axis runs straight from one end to the other (as opposed to an arch dam, which has a curved axis). The structural stability of a concrete gravity dam is derived entirely from its weight. Unlike other types of concrete dams (e.g. buttress, arch, cupola dams) it has a relatively large base area, reducing the stresses on the foundation. Construction is carried out by pouring concrete in a series of lifts of 1-10 ft (0.3-3 m) high, depending on dam size and construction method, creating construction joints within each monolith. An indispensable feature of concrete gravity dams is the spillway, which is used to discharge water safely during floods and/ or when the reservoir is full. Auxiliary features of concrete gravity dams that are necessary for the safe and serviceable operation and effective maintenance include: penstocks and associated valves and gates, internal galleries and shafts, cofferdams (for diversion during construction), cut-offs, drain pipes and grout curtains (to reduce seepage

under and around the dam). Concrete gravity dams make up about 10% of those dams with heights greater than 50 ft (15 m) in the United States (USCOLD, 1988).

2.1. CURRENT DESIGN BASIS

A dam is designed to impound and store water behind it safely throughout its lifetime. It thus has to maintain its structural integrity in the face of a range of hazards or loading conditions that arise during construction, normal operation, and extreme environmental events. Specifically, concrete gravity dams are designed to remain operational under normal conditions, to sustain minimal damage under infrequent operative conditions and to prevent total loss of reservoir under extreme events. The primary load affecting concrete gravity dams arises from the differential hydrostatic head that occurs during hydrologic events up to and including the Probable Maximum Flood (PMF)[†]. Associated with the hydrostatic head are substantial uplift forces arising from interstitial/pore water pressures that develop within the dam and the foundation. These uplift forces must be included in the overall equilibrium analysis of the monolith. The neglect of these forces results in the compressive stresses in the foundation being underestimated (De Boer and Ehlers, 1990; Yeh and Baier, 1992).

Other loads of lesser magnitude or importance are considered secondary loads, which may or may not be considered in design: the sediment load (earth pressure due to silt deposits in the reservoir), dynamic wave pressure at the surface of the reservoir, ice load (due to formation of thick ice sheets on the reservoir), and thermal loads (due to temperature gradients caused by cement hydration and ambient and water temperature

[†] The PMF is discussed in more detail in Chapter 3, which deals with natural hazards.

variations). In areas of seismic risk, dynamic loads due to earthquake ground motions up to an intensity associated with the maximum credible earthquake (MCE)[†] must be considered.

Current procedures for design of concrete gravity dams are based on static, deterministic analyses. These involve rigid body analysis of static equilibrium for monolith stability and foundation stresses ("Gravity," 1958). Where required, seismic loads are approximated by psuedo-static forces obtained using a seismic coefficient analysis, i.e. the inertia and hydrodynamic forces are calculated in terms of the acceleration maxima selected for design and considered as equivalent to additional static loads (Novak et al, 1996). A typical array and distribution of loads used in current design practices is shown in Fig. 2.1.

The governing criteria in design of concrete gravity dams are that the dam must be safe from overturning, sliding and bearing failure in the dam or foundation. Factors of safety are utilized in design to provide a margin of safety. These factors vary depending on the importance of the structure and on the hazard, lower factors of safety being assigned to structures considered less important and to check against events with lower perceived probability of occurrence. The safety check against bearing failure requires that the computed stresses be limited to less than the allowable stress in compression for concrete or allowable bearing pressure for foundation materials. It is also general practice that the location of the resultant at any horizontal section in the dam must be kept within the kern (middle third of dam) to ensure no tensile stresses are produced under any pool elevation. The sliding stability of the dam is checked by using a factor of safety that compares the shear resistance with the total horizontal load. For overturning stability, the restoring and

[†] The MCE is discussed in more detail in Chapter 3, which deals with natural hazards.

overturning moments about the toe of the monolith are compared. These factors of safety may vary for each criterion and are sometimes very conservative.

The simplifications inherent in these design procedures are considerable. For one thing, the distribution of stresses on any horizontal plane is not necessarily linear. For another, the analysis does not take into account the constitutive properties of the concrete and the foundation and the resulting dam-foundation interaction. The potential of a crack or a major opening developing at the dam-foundation interface under extreme later force is not considered. In the seismic case, the treatment of the dynamic loads is very simplistic. The dynamic behavior of the dam and the content of the earthquake ground motion are not fully incorporated into the analysis. The complex dam-foundation-reservoir interaction is neglected, in both the hydrologic and seismic cases.

In recent years, there has been a move towards the use of advanced analytical/numerical methods (such as the finite element (FE) analysis) to gain a more comprehensive picture of dam behavior. Typical of this move are studies on the crack propagation at the heel of the dam (e.g. Dewey et al, 1994), on dynamic response and behavior of dam-foundation system (e.g. Chavez and Fenves, 1995), and on treatment of uplift forces on FE analysis (e.g. Yeh and Baier, 1992). Increased computational capabilities and advances in numerical analysis theories have encouraged this trend.

2.2. STRUCTURAL BEHAVIOR AND PERFORMANCE STATES

The structural behavior of concrete gravity dams is a complex phenomenon. Structural and geotechnical issues are interlocked in understanding the mechanics of dam behavior. Concrete gravity dams progress through several stages of behavior (limit/performance states) under increasing levels of hazard. At low levels, the dam-foundation system remains essentially elastic, displacements are small, drains are fully effective, and full control of the reservoir is maintained. In the elastic range, there are no permanent deformations and the dam behaves mostly as a rigid body. Following the onset of nonlinear behavior, material cracking occurs, deformations may become permanent, drainage characteristics of the dam and operation of gates begin to be affected, and 3-D structural actions within the dam are initiated. At this stage, 2-D rigid body analysis of a dam monolith may no longer provide a good model of structural action. Rather, a nonlinear finite element model of the dam-foundation system may be required. Excessive deformations may cause visually objectionable cracking and functional disruption. Finally, at ultimate conditions prior to impending failure, the drains become ineffective due to large deformations and structural behavior becomes unstable and unpredictable due to sliding, flotation, or loss of bearing capacity of the foundation material. In extreme cases, loss of reservoir control may occur. Although design typically focuses on one limit state (e.g., that related to overall failure), multi-stage performance limits provide a more complete depiction of dam performance under increasing levels of hazard.

With the advance of computational capabilities, advanced numerical models of structural behavior of dams have become more feasible and manageable. The development of more comprehensive and accurate models should be accompanied by the identification

of significant performance limit states that would be meaningful in the structural evaluation of a structure. These models should be coupled with the study and analysis of databases on dam failures. Studies have already indicated that modeling errors and insufficient databases are significant sources of uncertainty in prediction of dam performance (e.g. Bury and Kreuzer, 1985). The development of more comprehensive models and databases would reduce significantly the uncertainties involved in prediction of dam performance.

2.3. PAST PERFORMANCE

The main source of information on dam failures incidents (failures and accidents) is the International Commission on Large Dams (ICOLD), which maintains the World Register of Dams (ICOLD, 1998) where more than 34,000 dams from over 80 countries are registered. ICOLD has published reports on dam failure and incidents around the world (ICOLD, 1971, 1983). Similar reports have been published for incidents in the US (USCOLD, 1976, 1988). Studies based on these data (e.g. Wahlstrom, 1975, Johnson and Illes, 1976, Blind, 1983, Duffaut, 1986, Douglas et al, 1999) indicate that the main sources of dam failure have been: overtopping, foundation failure, slides of banks or dam slopes, design and construction errors, cracks in dam, thermal effects, earthquakes, and acts of war. A statistical survey of all kinds of dams throughout the world showed that 35% of failures were a direct results of floods exceeding the spillway capacity, 25% resulted from foundation problems (such as seepage, piping, excess pore pressures, inadequate cutoff, fault movement, settlement and rock slides), and the remaining 40% resulted from other causes (improper design and/ or construction, material failure, misuse and acts of war) (Johnson and Illes, 1976). Concrete gravity dams, however, are less vulnerable to

overtopping (compared to embankment dams). The majority of failures or damages in concrete gravity dams have been associated with flaws in the foundation. Unlike the dam, which is above ground and easy to inspect, flaws in the foundation may not be detected until major damage has been incurred. A statistical study of concrete dam failures (Kalustyan, 1983) and incidents indicated that 34% were related to seepage in the foundation, 29% were caused by shearing, formation of cracks, and displacement of the dam along the foundation, another 29% were related to drainage failure and increased uplift and the remaining 8% were due to erosion of the foundation by the surface flow and slides due to the interaction of the dam-foundation system. Kalustyan's study (1983) also established that 64% of the incidents occurred during filling of the reservoir, 28% occurred as a result of floods, 6% were related to earthquakes and 2% were due to the effect of temperature. The majority of dams that failed either did not have a monitoring or warning system or the system was malfunctioning (Blind, 1983).

Studies of past records of dam failures and incidents generally suggest that annual probability of failure is on the order of 10^{-4} to 10^{-3} . In this case, failure is defined as (a) major structural failure involving the complete abandonment of the dam or (b) severe damage to the dam, which can be successfully repaired and used. For example, it was reported (Cheng, 1993) that the annual probability of failure of gravity dams is 1.1×10^{-3} , while for concrete gravity dams that were commissioned from 1930-1992 and have been in service for at least 5 years, it is 1.4×10^{-5} (Douglas, 1999). It was also shown that this probability varies with age, time of service and height of the dam. For example, for gravity dams completed in 1941-1950, the annual probability of failure after 5 years of service was 6.1×10^{-4} , while for dams of height greater than 165 ft (50 m) the probability of failure was

given as 4.0×10^{-4} (Cheng, 1993). It is worth noting that human error in design, construction or operation of dams, quality assurance, inspection and maintenance scheduling, and early warning systems has often played a role in dam incidents and failures.

2.4. FAILURE CRITERIA

Identification of structural failure criteria for dams requires an extensive knowledge of the mechanical properties of the engineered materials in the dam and foundation. This section describes the mechanical properties of the materials concrete gravity dams and their associated failure criteria. These failure criteria must be defined so as to be compatible with the responses computed from a finite element analysis.

2.4.1. Concrete

The mechanical properties of concrete as a construction material have been extensively studied over the years. The density of normal-weight concrete is about 140-160 lb/ft³ (2200-2600 kg/m³) with a thermal coefficient of about $9.9 \times 10^{-6}/^{\circ}\text{C}$. Its elastic modulus is related to its specified compressive strength and its Poisson's ratio ranges from 0.15-0.25. Concrete with mean compressive strength of about 4000 psi (28 MPa) is common in massive structures. The cumulative distribution function (CDF) of concrete compressive strength can be modeled with a normal distribution, having a coefficient of variation (for in-situ concrete) of about 12%-15% (e.g. Shalon and Reintz, 1955, Rusch

et al, 1969, Mirza et al, 1979), depending on quality control. The tensile strength of concrete (measured from a split cylinder test) has been described as (Mirza et al, 1979):

$$f_{sp} = 6.4 \sqrt{f_c} \quad (2.1)$$

where: f_{sp} = splitting strength of concrete (psi)

f_c = compressive strength of concrete (psi)

Its CDF also is depicted to be normal with a coefficient of variation of about 20%.

Test results (e.g. Tasuji et al, 1979) have shown that the strength of concrete in biaxial loading is greater than in uniaxial loading. Depending on the principal stress ratio, an increase in compressive strength up to 20% has been achieved in biaxial compression, and an increase in tensile strength of up to 10%-20% has been observed in biaxial tension.

Modest increases in strength of concrete have been observed for rapid loading rates, such as would occur when subjected to earthquakes (Mirza et al, 1979; Raphael, 1984; Earthquake, 1990). However, the limiting tensile strength of a concrete gravity dam is across construction lift surfaces, where there may be some reduction in tensile strength. Thus, this phenomenon is not considered in this study.

2.4.2. Foundation Rock

Rock, in its natural state, is a complex material that usually contains interconnected pores/ cavities, isolated crystals of other origins, and microfissures. These fissures and pores reduce the tensile strength of the rock, create nonlinear load/ deformation response (especially at low stress levels), contribute to the variability and scatter in test results and

introduce scale effects into prediction of behavior (Goodman, 1989). Rock foundations also exhibit weakness planes, which include joints, bedding planes, faults and stratifications. A single joint in a rock mass decreases the shear strength in the tangential direction and reduces the tensile strength to practically zero in the perpendicular direction. The orientation and distribution of joints, thus, produces significant non-homogeneity and anisotropy in the strength of a rock mass.

In rock mechanics, the use of empirical failure criteria is widely accepted. Theoretical failure criteria have so far been limited in their scope and application, partly to the complex behavior of rock masses described above. Some rock failure criteria allow for adjustments for rock strength based on rock type classifications. Because of physical limitations on experimental set-up, most failure criteria are two-dimensional, i.e. they are described in terms of major (σ_1) and minor (σ_3) principal stresses. The effect of the intermediate (σ_2) principal stress is generally ignored, though there exists some experimental evidence that it may influence failure to some extent, at least for some rocks (Sheorey, 1997). Empirical failure criteria that have been proposed so far use stress, and not strain, as their defining parameter (e.g. Balmer, 1952, Bienawski, 1974, Hoek and Brown, 1980, and Sheorey, 1989). This is because defining a strain value at failure proves to be difficult and also because it is easier to measure stress in experiments. Brief descriptions of empirical and theoretical failure criteria can be found in Sheorey (1997).

In this study, the Hoek-Brown criterion (Hoek and Brown, 1997) has been chosen for the evaluation of the performance of foundation rock. The Hoek-Brown criterion is used extensively in practice and is applicable to jointed rock masses without significant anisotropy. It has been developed from regression analysis of triaxial test data of different

rock types and has evolved, since it was first published in 1980, to include a wide variety of rock characteristics. The Hoek-Brown criterion is relatively easy to implement in a finite element analysis and relates the rock mass strength to a widely recognized rock mass classification.

Hoek-Brown Failure Criterion

The Generalized Hoek-Brown (Hoek and Brown, 1997) failure criterion for jointed rock masses is defined by:

$$\sigma_1' = \sigma_3' + \sigma_{ci} \left(m_b \frac{\sigma_3'}{\sigma_{ci}} + s \right)^a \quad (2.2)$$

where σ_1' and σ_3' are, respectively, the maximum and minimum effective stresses at failure, σ_{ci} is the uniaxial compressive strength of the intact rock, and m_b , s and a are given by:

$$m_b = m_i e^{\left(\frac{GSI-100}{28} \right)} \quad (2.3)$$

$$s = e^{\left(\frac{GSI-100}{9} \right)} \quad \text{and} \quad a = 0.5 \quad (2.4)$$

for $GSI > 25$, i.e. rock masses of good to reasonable quality. For $GSI < 25$, i.e. rock masses of very poor quality,

$$s = 0 \quad \text{and} \quad a = 0.65 - \frac{GSI}{200} \quad (2.5)$$

In Eqns 2.3 – 2.5, GSI is the Geological Strength Index (Hoek, 1994 and Hoek, et al, 1995), and m_i is a constant which depends on the characteristics of the rock mass. Eqn. 2.2 is based on the observed behavior of rock masses, model studies to simulate the failure mechanism of jointed rock, and triaxial compression tests of fractured rock. The tensile strength of the rock mass is;

$$\sigma_{tm} = \frac{\sigma_{ci}}{2} \left(m_b - \sqrt{m_b^2 + 4s} \right) \quad (2.6)$$

The Mohr failure envelope corresponding to the empirical failure criterion defined by Eqn. 2.2 is given by (Hoek, 1983);

$$\tau = \left(\cot \phi'_i - \cos \phi'_i \right) \frac{m_b \sigma_{ci}}{8} \quad (2.7)$$

where τ is the shear stress at failure, ϕ'_i is the instantaneous friction angle at the given values of τ and σ'_n is the effective normal stress. The instantaneous friction angle ϕ'_i is given by (Hoek, 1983):

$$\phi'_i = \tan^{-1} \left(4h \cos^2 \theta - 1 \right)^{-1/2} \quad (2.8)$$

where:

$$h = 1 + \frac{16(m_b \sigma'_n + s \sigma_{ci})}{3m_b^2 \sigma_{ci}} \quad (2.9)$$

$$\theta = \frac{1}{3} \left[90 + \tan^{-1} \left(h^3 - 1 \right)^{-1/2} \right] \quad (2.10)$$

Most finite element software provide the Mohr-Coulomb failure criterion with constant parameters c (cohesion) and ϕ (angle of friction) as a feature. A simple linear regression of the Hoek-Brown failure criterion can be performed (Hoek and Brown, 1997) to determine the associated Mohr-Coulomb constants and to implement them in available software.

In order to incorporate the effects of joints and fractures in a rock mass, Hoek and Brown (Hoek and Brown, 1997) suggested the use of a modified modulus of elasticity in the analysis. This modified modulus is:

$$E_m [GPa] = \sqrt{\frac{\sigma_{ci}}{100}} 10^{\frac{(GSI - 10)}{40}} \quad (2.11)$$

Eqn. 2.11 is a modification of the relationship proposed by Serafim and Pereira (Serafim and Pereira, 1983), which relates the in-situ modulus of deformation and Bienawski's RMR classification (Bienawski, 1976; Bienawski, 1989). The original relationship proposed by Serafim and Pereira, based upon analysis of dam foundation deformations, in which the modulus was calculated from the deformation and stresses that were measured, has been found to be suitable for better quality rocks, but overpredicts the deformation modulus for poor-quality rock masses ($\sigma_{ci} < 100$ MPa) (Hoek and Brown, 1997). The modified relationship suggested in Eqn. 2.11 is based on observations and analysis of excavation behavior in poor quality rock masses.

2.4.3. Dam-Foundation Interface

The behavior at the dam-foundation interface is assumed to obey the Mohr-Coulomb relationship, i.e. the shear strength depends on the frictional resistance and the

intact shear strength or cohesion. These are related as follows:

$$\tau = c + \sigma \mu \quad (2.12)$$

in which c = the cohesion, σ = is the normal stress and

$$\mu = \tan \phi \quad (2.13)$$

where ϕ = is the angle of internal friction. In the direction perpendicular to the interface, it is assumed that the interface cannot transmit any tensile stresses. These assumptions have also been utilized in other studies of gravity dams (e.g. Chopra and Chakrabarti, 1981; Fenves and Chopra, 1984a).

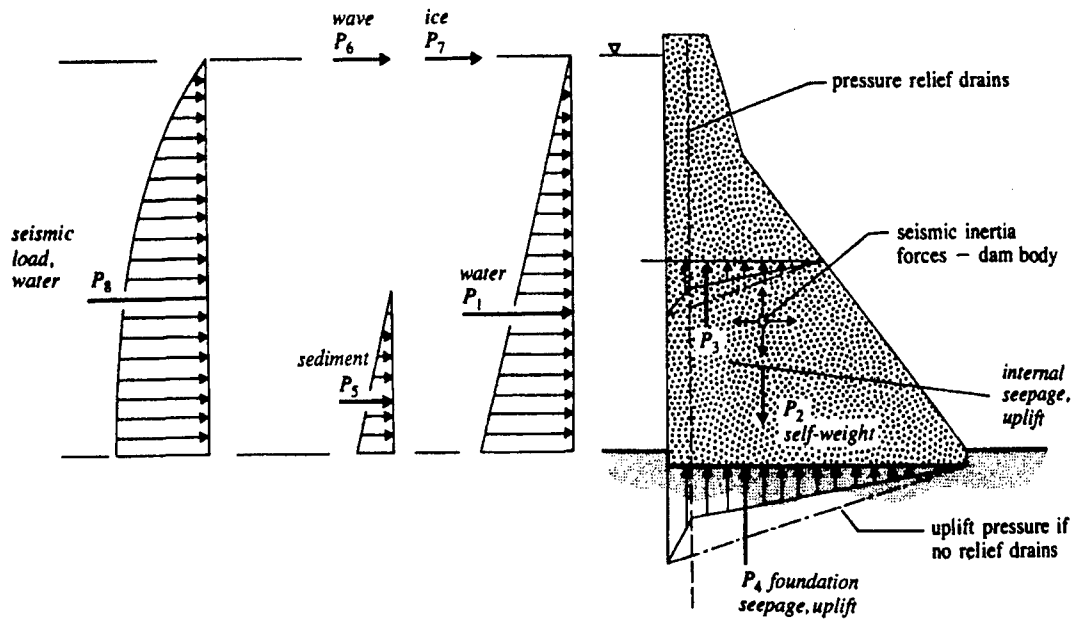


Fig. 2.1. Array of loads used in current design practices (Novak et al, 1996)

Chapter 3

NATURAL HAZARDS

Hazards that challenge the integrity of civil structures can be classified as natural or man-made. Natural hazards include earthquakes, floods, tornadoes, and hurricanes. Man-made hazards could be human error, accidents, sabotage, or acts of war. In a probabilistic safety assessment (PSA) of a civil infrastructure system, a few hazards are selected for detailed analysis, depending on their frequencies, magnitudes and consequences. In this selection process, the geologic, seismologic, hydrologic and meteorological characteristics of the site, in addition to the present and projected industrial activities, must be reviewed (Casciati and Faravelli, 1991). General methods for determining these hazards to develop siting and design criteria for other critical facilities, such as Department of Energy facilities and nuclear power plants (Natural, 1994), are available and should be used for safety assessment of critical civil infrastructure facilities, wherever possible.

The main objective of a hazard analysis is the description, in probabilistic terms, of the inherent randomness in occurrence and magnitude. This is displayed through a "hazard curve," a complementary cumulative distribution function (CCDF),

$$G_Y(y) = P[Y > y] = \sum_{\xi \geq y} P[Y = \xi] \quad (3.1)$$

which expresses the probability that event intensity Y exceeds specific intensities, y , in a given period of time. Knowledge of the CCDF of the hazard is important for determining those events that are likely to have a significant impact on risk. A single parameter is usually used to characterize the hazard. [This parameter must also be used in the fragility analysis (discussed in Chapter 5) in order to interface with the hazard. For complex hazard phenomena, a multi-variate description of the hazard is avoided by using the interface parameter in the hazard curve and including the other parameters in the fragility analysis.] In a fully coupled risk assessment, the hazard also is required to obtain a point or interval estimate of risk.

This chapter summarizes procedures for modeling the two major natural phenomena hazards affecting concrete gravity dams in the United States, namely: extreme hydrologic events and earthquakes. It also discusses the uncertainties involved in hazard analysis.

3.1. HYDROLOGIC HAZARD

All dams are exposed to flood hazard to varying degrees. Extreme hydrologic events, caused by river flooding, precipitations, snow melt, seiches, failure of upstream dams or dikes, etc, may produce flows of water with which the spillway cannot cope and thus may overtop the dam. The estimation of the frequency and magnitude of such extreme events with reasonable accuracy is essential for dam safety analysis.

The Probable Maximum Flood (or PMF), a hypothetical flood height that is considered to define the upper range of flood potential, is used by the US Army Corps of Engineers (USACE) as a design criterion for flood protection. It represents professional

judgment on the largest flood that should be considered for design and is derived from the probable maximum precipitation (PMP) (Chow, 1964; Linsley et al, 1975; Newton, 1983). Based on the coincidence of a set of conservative meteorological and hydrological assumptions concerning precipitation from the principal storm and its areal distribution, storm positioning, antecedent conditions (preceding storms, if any, snowpack, moisture, etc.) that may affect ground saturation and degree of runoff, size and topography of drainage basin, reservoir level, and dam operating conditions, a flood inflow hydrograph is synthesized. This inflow hydrograph is routed through the reservoir-dam system, i.e. the available reservoir storage and the spillway and other outlet works. The resulting PMF level and spillway capacity are then used in design.

Contrary to common belief, the PMF does not provide for "zero-risk" against hydrologic hazard. In fact, there have been instances where the PMF has been exceeded (Dawdy and Lettenmaier, 1987). Moreover, the basic methodology for determining the PMF, which dates back to the 1930's, is not robust as it involves a great deal of subjective judgment in the estimation of parameters. Given the same basic meteorological information and data, different analysts may arrive at different estimates of the PMF for a particular site.

The PMF has no statistical basis and its determination depends on the reliability of information, the advance of modeling techniques and the accuracy of the analysis. Moreover, the conservatisms in parameter assignment propagate through the analysis and are compounded in an unpredictable way. Estimation of the PMF at a given site may have changed over time, as additional meteorological and hydrological information have been collected (Lave et al, 1990; Reed and Field, 1992), usually being revised upward. While the

probability of exceeding the PMF cannot be determined with any confidence, independent estimates of this probability range from $10^{-4}/\text{yr}$ to $10^{-6}/\text{yr}$ (National, 1985). There is no reason to believe that the probability of exceeding the PMF is uniform from site to site. In magnitude, the PMF tends to be on the order of 3 - 6 times the 100-year return period flood (National, 1985), which is a more familiar measure of flood hazard. Thus, it is very conservative by any objective measure.

In contrast to the PMF, a probabilistic model for hydrologic hazard displays a relation between the annual probabilities of being exceeded and the flood height. Consequently, the hydrologic fragility of a concrete gravity dam (Chapter 5) must use the flood height (pool elevation) as the demand variable in order to interface with the hydrologic hazard. The U.S. Water Resources Council (1977) has postulated that the annual extreme flood discharge can be modeled by a log-Pearson Type III CDF. The implication is that the natural logarithms of the annual extremes can be described by a gamma distribution (Ang and Tang, 1974). Other probability distributions, e.g., the lognormal distribution (Karlsson and Haimes, 1989) and the Gumbel distribution (Bury and Kreuzer, 1985) also have been proposed for modeling hydrologic hazard. One recent model for precipitation is the Generalized Extreme Value (GEV) distribution (Hosking et al, 1985):

$$G_Y(y) = \left[1 - \frac{ky}{a} \right]^{1/k} \quad ; \text{ for } k \neq 0 \quad (3.2a)$$

$$G_Y(y) = e^{-y/a} \quad ; \text{ for } k = 0 \quad (3.2b)$$

The probabilistic approach of determining the hydrologic hazard provides a rational mechanism for incorporating additional data that the PMF approach does not provide. However, this procedure also may not be robust due to insufficiencies in the available database (Stedinger et al, 1996). While the CDF's of precipitation or flood hazard are positively skewed, seldom is there sufficient data to show that one skew-positive distribution is preferable to another. The variability in flood elevation depends on the site of the dam.

The revised hydrologic hazard for Bluestone Dam (Appendix) is illustrated in Fig. 3.1, which has been adapted from a report by the US Army Corps of Engineers on frequency of reservoir filling of the Bluestone Lake. The design flood level, the old PMF of 1520 ft, now is believed to have a return period of around 150 years. The new, revised PMF of 1556 is shown to have a return period of about 30,000 years. None of the probabilistic models above provides a particularly good description of the hazard depicted in Fig. 3.1 over its entire range.

3.2. SEISMIC HAZARD

Earthquakes are caused by sudden release of energy deep in the earth's crust. Most earthquakes occur near tectonic plate margins or faults and are associated with the tectonic forces that produce mountains, rift valleys, mid-oceanic ridges, and ocean trenches. There have also been reports of reservoir-induced earthquakes (e.g. Koyna dam, India; Hsingfengkiang dam, China), in which increased seismic activity has been observed in areas of low-historical seismicity, after initial filling of reservoir. The focus of this study is on earthquake hazard generated by tectonic forces.

Seismic activity in the Western US is dominated by the interaction of the various Pacific and North American tectonic plates. Such faults are not apparent in the Eastern US, where the intervals between large earthquakes are large and as a result there is little or no experience with their impact in that part of the country. Nonetheless, their damage potential should be considered in risk assessment of large concrete gravity dams because of their potential impact on the economy and on public safety.

In current design practice by the US Army Corps of Engineers, the seismic hazard is estimated by an "upper bound" intensity of ground motion, the maximum credible earthquake (MCE). It is considered as the largest possible earthquake that can be expected to occur at a site. Estimation of the MCE requires information on location and geometry of faults, duration and magnitude of earthquake at source, and requisite physical properties of soil/ rock. Return periods associated with MCE's are believed to be on the order of 500 to 1,000 years (National, 1985). Thus, the MCE may be on the order of 10 to 1000 times more likely to occur than a PMF. Since the consequences of a MCE or PMF to the structural integrity of the dam are potentially the same (if pool control is lost), it follows that the risks between these two competing hazards may not be properly balanced (Ellingwood, 1994).

A probabilistic model of seismic hazard, $G_Y(y)$, shows the annual probability of exceeding ground motion parameter y , generally defined as instrumental peak ground acceleration or, more recently, spectral acceleration at the fundamental period of the structure. The seismic fragility analysis (subsequently conducted in Chapter 5), uses the spectral acceleration as its demand/ interface variable. The other parameters that characterize ground motion, such as frequency content, magnitude/ intensity of earthquake, duration of excitation, epicentral distance, site rock/ soil condition, geographical location

and earthquake mechanism are subsumed in the fragility analysis. The seismic hazard curve can be described by a Type II distribution of largest values (Cornell, 1968),

$$G_Y(y) = 1 - e^{-\left(\frac{y}{u}\right)^{-k}} \quad (3.3)$$

in which u and k are parameters of the distribution. Parameter k determines the slope of the hazard curve, and is related to the coefficient of variation (COV) in Y . The value of k tends to be larger in seismically active areas, decreasing from about 5 (COV = 0.32) in San Francisco, CA to approximately 2 (COV = 1.38) at Boston, MA and Memphis, TN. For the Bluestone Dam (Appendix), values of $k = 1.46$ and $u = 0.17$ were computed based on spectral accelerations (at period of 0.2 sec (cf. Chapter 5)) provided by the US Geological Survey (USGS) for the area (<http://www.usgs.gov/>). Fig. 3.2 illustrates the seismic hazard curve for Bluestone Dam constructed using these values.

Seismic hazard analysis carries with it the largest component of uncertainty in the process leading to earthquake forces on engineered facilities (Reiter, 1990). In the Eastern US, for example, the variability in earthquake demand is an order of magnitude greater than that of flood level.

3.3. SAMPLING ERRORS AND UNCERTAINTY ANALYSIS

Natural hazards are inherently random and thus uncertainties are associated with every step of their analysis. These uncertainties can be aleatory (inherent) or epistemic (knowledge-based). The problem of handling inherent uncertainty in natural hazards is compounded by the limited database available. Quantitative flood and earthquake data are

limited to approximately the past 100 years (or less) at most sites in the United States. To get the design values, the data are extrapolated to return periods much greater than the period represented by the database. It is possible that different fundamental physical mechanisms might control the hazard at such levels. In the south-central part of the US, for example, the CCDF of annual extreme wind speeds is determined by extratropical storms at return periods less than about 150 years, but by tornadoes at greater return periods. Similarly, extrapolating the CCDF of flood hazard out to the return period range speculated for the PMF (10,000 - 1,000,000 years of Fig. 3.1.) is problematic. Furthermore, for seismic hazard, the potential earthquakes from different seismic zones (often determined with a heavy dose of professional judgment) are attenuated from the source to the site and then summed (integrated) over all possible earthquake sources and magnitudes (Algermissen et al, 1982), adding considerable uncertainties in the estimation of the earthquake intensity.

Epistemic uncertainties in hazard analysis are manifested, in part, by the “tail-sensitivity” of the chosen CCDF. The upper fractile of any distribution is highly distribution-dependent at return periods in excess of the length of the record, and one must be very careful in estimating these distributions for risk analysis purposes simply from historical data. For example, suppose the coefficient of variation in the annual extreme intensity is 0.30 (not atypical for meteorological phenomena). Two candidate CCDFs with the same mean are considered: the normal and the lognormal. The ratio of lognormal/normal 100-year return period intensities is about 1.11, which is manageable. However, the ratio of 100,000-year intensities is 1.47. Even when an appropriate distribution has been identified, sampling errors in estimating the distribution parameters

may lead to large uncertainties in the estimates of return period values much in excess of 100 years.

Another manifestation of epistemic uncertainty is in the analysis of propagation of events. Hazard scenarios are postulated in which extreme events are propagated, giving rise to consequences that are significant for decisions regarding public safety. Each scenario is assigned a probability and a hazard curve constructed for it. The family of curves thus developed displays the knowledge-based (or epistemic) uncertainty associated with the hazard analysis. An illustration of a seismic hazard curve family for the Zion Nuclear Power Plant, sited approximately 45 miles north of Chicago, IL, is presented in Fig. 3.3. The “relative likelihoods” are weights assigned to the various seismogenic hypotheses on which the individual hazard curves are based. At very large return periods, the estimated hazard varies over two orders of magnitude.

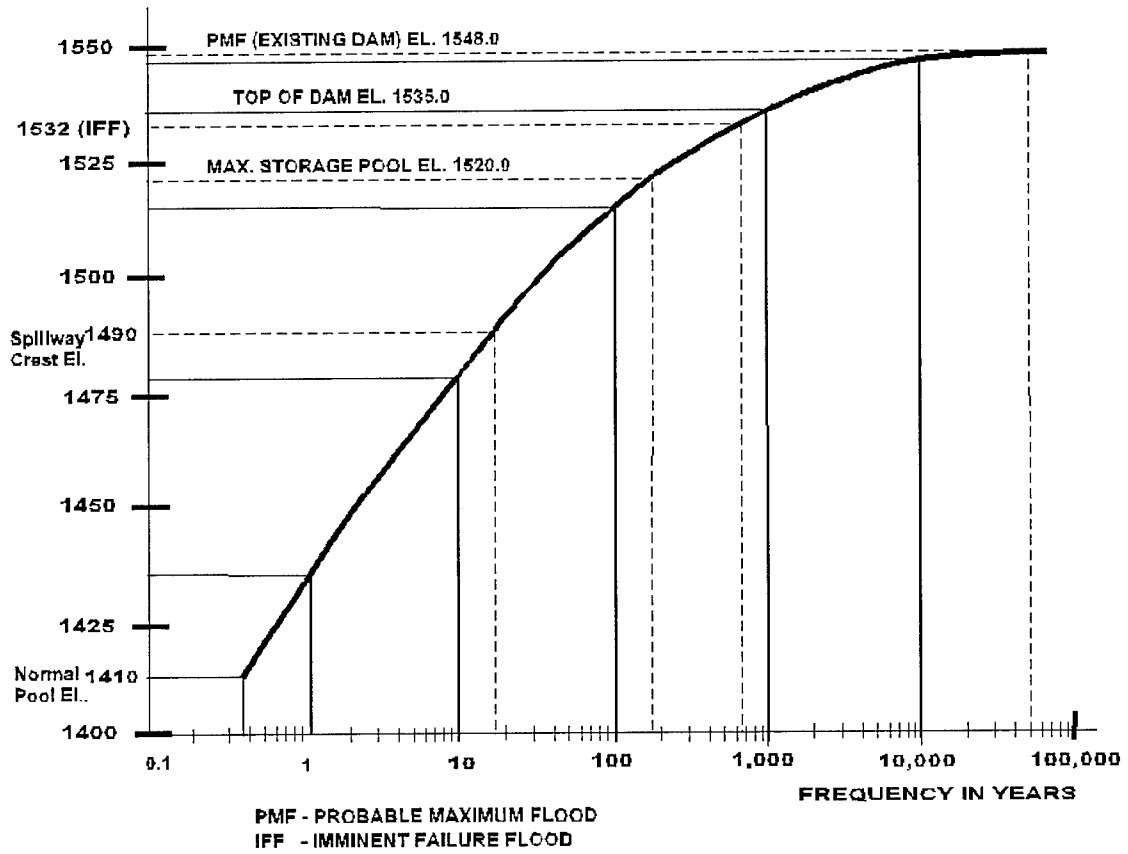


Fig. 3.1. Hydrologic hazard for Bluestone dam

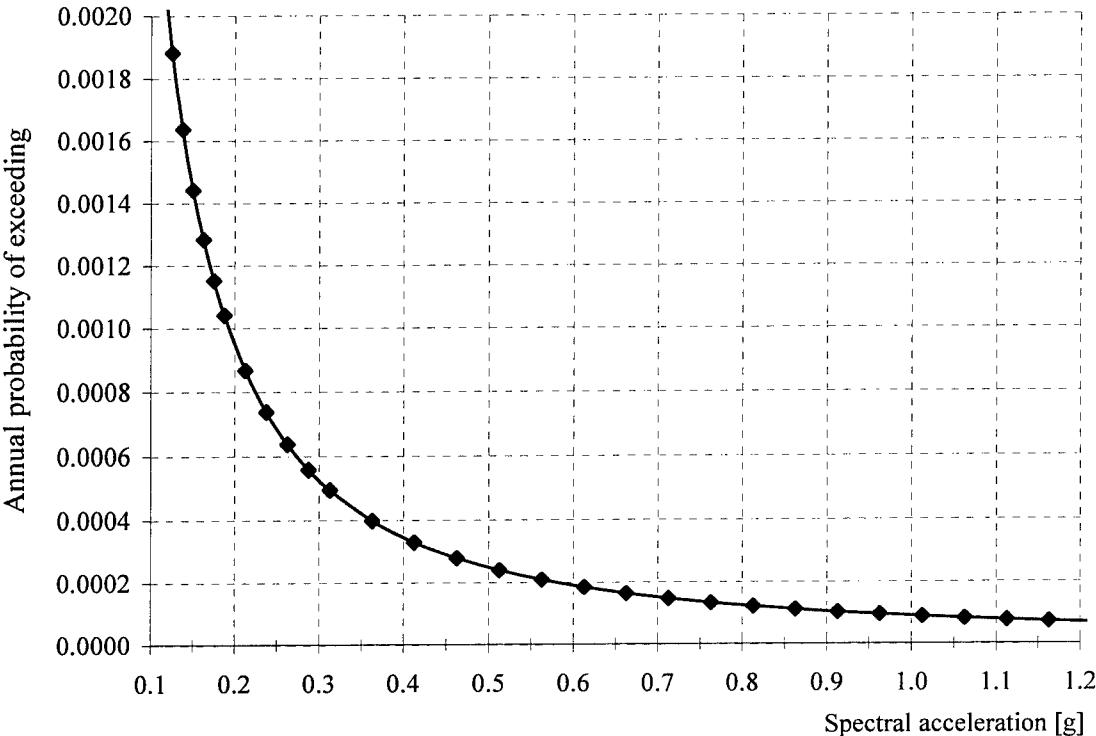


Fig. 3.2. Seismic hazard for Bluestone Dam

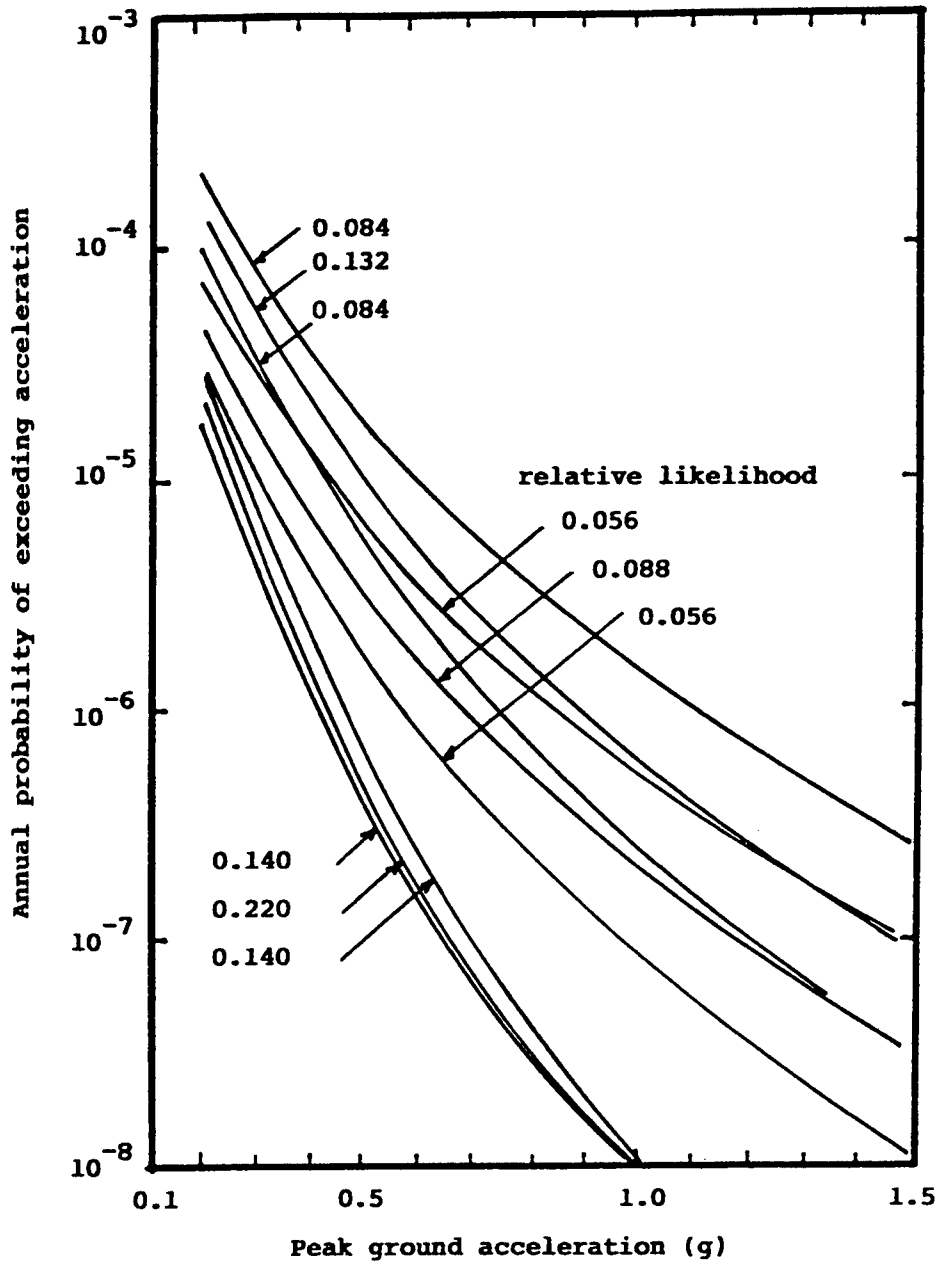


Fig. 3.3. Illustration of epistemic uncertainty in seismic hazard at Zion Nuclear Power Plant

Chapter 4

STRUCTURAL MODELING OF DAM BEHAVIOR

This chapter develops and unifies the concrete gravity dam modeling/ structural mechanics to support the risk analysis to follow in later chapters. Models of varying degree of complexity and with different assumptions, from rigid body to the linear and nonlinear finite element models, are presented. Structural responses obtained using those models are presented. Based on the study of these results, the models are critiqued and their limitations and/ or merits are investigated. Finally, a brief description of the discrete element method is provided, and its use in modeling the structural behavior of concrete gravity dams is discussed.

4.1. RIGID BODY MODEL

The rigid body model, traditionally used in design of concrete gravity dams, is based solely on principles of equilibrium and assumes the dam and foundation to be rigid. It also is assumed that there is no interaction between adjacent monoliths and that no differential movements affecting the dam or foundation occur (Novak et al, 1996). Using this model it is possible to compute the stresses at the dam-foundation interface and/or on

sections within the dam. The rigid body analysis of the dam was performed to provide a benchmark against which subsequent, more complex models and analyses could be compared.

The typical non-overflow Monolith No. 12 of the Bluestone Dam (Appendix), illustrated in Fig. 4.1, was selected for analysis. The loads applied on the dam include its self-weight, the horizontal hydrostatic pressures on the upstream (from the impounded water) and downstream (from the tail water) faces of the dam, uplift force at the base of the dam, vertical weights of water upstream and downstream of the dam, and ice pressure of 20,000 lb/ft (292 kN/m) applied to the dam at the pool elevation of the reservoir. Consistent with current practice, the uplift pressure distribution at the interface is modeled as piecewise linear, decreasing from 100% hydrostatic head at the heel of the dam to head defined by the higher of the drain gallery or tail water elevations, and then to tail water elevation at the toe of the dam. This distribution was confirmed in a separate finite element analysis described in the next section.

The vertical stresses at the heel and toe of the dam are computed as:

$$\sigma_z = \frac{\sum V}{B} \left(1 \pm \frac{6e}{B} \right) \quad (4.1)$$

where V = the vertical forces, B = the width of the base, and

$$e = \frac{\sum M}{\sum V} \quad (4.2)$$

is the location of resultant measured from the toe of the dam, in which M are the moments about the toe, and .

Horizontal shear stresses are obtained as (Novak et al, 1996):

$$\tau_u = (\sigma_{zu} - p_w) \tan \phi_u \quad (4.3)$$

$$\tau_d = \sigma_{zu} \tan \phi_d \quad (4.4)$$

where τ_u and τ_d are shear stresses at the upstream and downstream faces, respectively, p_w is the hydrostatic pressure head at the upstream face, and ϕ_u and ϕ_d are the angles between the upstream and downstream face slopes and the vertical. Principal stresses can be obtained using Mohr's stress state relations:

$$\sigma_{1,3} = \frac{\sigma_z + \sigma_y}{2} \pm \tau_{\max} \quad (4.5)$$

$$\text{where } \tau_{\max} = \sqrt{\left(\frac{\sigma_z + \sigma_y}{2}\right)^2 - \tau^2} \quad (4.6)$$

Note that the upstream and downstream faces are planes of zero shear, and thus, they are planes of principal stresses.

The rigid body model allows no deformation in either the foundation or the concrete dam. In addition, the normal stresses at the interface obtained from this analysis have a linear distribution. The effect of the discontinuity at the dam-foundation interface on the structural behavior of the dam, or the nonlinear behavior of the material is also not accounted for in this model.

4.2. LINEAR FINITE ELEMENT MODEL (FEIt)

A simple linear, elastic, 2-D finite element (FE) analysis of Monolith No. 12 of the dam, including the foundation, was implemented. A finite element program, *FEIt*, with an advanced graphical user interface, generation and post-processing capabilities was downloaded from the web (Atkinson, D. and Gobat, J., 2000). This program was thoroughly tested and validated on problems with known solutions prior to being used in this study.

4.2.1. Description of Model

The dam-foundation system was modeled by constant-strain triangular elements. The FE program allows the use of different materials in the monolith and foundation; however, each material is homogeneous and isotropic within each zone. The FE model of the dam-foundation system is shown in Fig. 4.2. The rock/foundation zone was modeled as being 590x250 ft (180x76 m). This size was found to be sufficient to minimize errors due to modeling the foundation zone as having a finite size, when in fact it is a semi-infinite half-space.

The mechanical properties for the materials are taken from Table 4.1. Information in this table was provided by the US Army Corps of Engineers, which stated that the foundation rock consists of interlaminated orthoquartzite and shale. The elements around the concrete-rock interface and around the grout curtain and the drain areas have been made finer to better capture the behavior of the dam in these key areas. Hydrostatic, uplift, ice and body forces are applied as nodal forces or as tractions on the edges of elements.

4.2.2. Uplift Force

A separate FEA was carried out to determine the uplift pressure distribution at the concrete-rock interface. In this FE model, the problem was idealized as having a dimensionless 100% hydrostatic pressure head, h_w , at the heel of the dam in foundation and a pressure head of 15% of h_w , at the toe of the dam from tail water. It was also assumed that the rock-concrete interface is impermeable. Three different cases were considered:

- i. grout curtain or drains absent
- ii. grout curtain and drains present, and with an assumed zero pressure at the drains,
- iii. grout curtain and drains present, with pressure head of 25% of h_w assumed at the drains.

This FE model took into consideration the presence of the grout curtain in (ii) and (iii) by assuming that the curtain has a very low permeability relative to the surrounding rock. Uplift pressures determined from the above analyses are presented in Fig. 4.3. They compare very well with results in other studies (Casagrande, 1961; Amadei, et al, 1991; Dewey, et al, 1994) and with pressure distributions commonly assumed used in dam evaluations. It is observed that the pressure distribution is nearly piece-wise linear (for cases (i) and (iii)). However, the water from the drain holes is drained out of the gallery by gravity. Thus, the pressure at the drains is the hydrostatic pressure of the column of water up to the floor of the drain gallery. Hence, in the structural FEA of the dam, the uplift pressure is modeled by a piece-wise linear distribution, with 100% hydrostatic pressure head at the heel, hydrostatic pressure head measured from the floor of the drain gallery at the drains and pressure head equal to tail water elevation at the toe of the dam. If the tail

water elevation is above the floor of the floor gallery, however, the hydrostatic pressure is measured using the tail water elevation as reference, as the gallery itself is flooded and under pressure greater than one atmosphere.

4.2.3. Structural Response

The linear FE analysis of the dam-foundation system was conducted at increasing pool elevations corresponding to filling the reservoir. As in the rigid body analysis, the forces applied are: hydrostatic force against the upstream face of the dam, weight of concrete and rock masses, uplift forces at the interface and assumed ice pressure of 20,000 lb/ft (292 kN/m) applied at the pool elevation of the reservoir. The uplift force is conservatively assumed to act over 100% of the area to which it is applied. The stresses (in the vertical direction) at the concrete-rock interface for various pool elevations are presented in Fig. 4.4.a. They compare very well with stresses computed from rigid body analyses (Figs. 4.4.b and 4.4.c). Fig. 4.5 presents the shear stress distribution at the concrete-rock interface and Fig. 4.6 shows the relationship between the horizontal deformation of the top of the dam (relative to the heel) and the pool elevation. The total deformations of the dam-foundation system at pool elevations of 1360 ($h = 0$ ft.) and 1556 ft. ($h = 196$ ft.), respectively, are depicted in Figs. 4.7.a and 4.7.b. Normal and shear stresses at the neck (line AA' on Fig. 4.2) are presented in Figs. 4.8.a and 4.8.b. These stresses are of the same order of magnitude as the stresses at the concrete-rock interface. In particular, stresses at the downstream side of the neck of the dam are comparable to stresses at the toe of the dam. These stresses, however, are well below the compressive strength of

the concrete in the dam. Tensile stresses in the concrete at the upstream side of the neck of the dam are approximately 45 psi (0.3 MPa), an order of magnitude less than the estimated splitting strength of 452 psi (3.1 MPa) (according to Eqn. 2.1). Comparisons of the Hoek-Brown failure criteria with principal stresses (in foundation elements) and shear stress (in elements along the dam-foundation interface) for a pool elevation of 1556 ft. are presented in Figs. 4.9.a and 4.9.b, respectively. Those elements exhibiting stress states beyond the failure surfaces for both principal stresses and shear are situated around the heel of the dam near the concrete-dam interface. Note that almost all of these elements show tensile principal stresses beyond the tensile strength of the rock mass.

Using the modified modulus of elasticity of Eqn. 2.11 yields higher values of deformation, as shown in Fig. 4.10. The normal and shear stress distributions also differ considerably, as shown in Figs. 4.11 and 4.12, respectively, with higher stress values indicated at the toe of the dam.

The elastic FE model improves on the rigid body model by incorporating the constitutive models of the foundation and concrete in the structural analysis of the dam. However, it is not capable of modeling cracks or joints at the concrete-rock interface or elsewhere in the system. It also is not capable of modeling nonlinear constitutive relationships and post-yield behaviors. Moreover, the uplift pressure within such cracks is not accounted for in the analysis. Consequently, results from the elastic FE analysis exhibit some peculiarities, particularly when the reservoir pool is raised above the design level (1520 ft). The element at the heel shows relatively high tensile stresses compared to adjacent elements. Similarly, relatively high compressive stresses are observed for elements near the toe of the dam. Refining the mesh size does not smooth out these singularities. The

elastic FE analysis also does not model the development of pore water pressures within the foundation, which may lead to a significant decrease in strength of many rocks. These deficiencies can be remedied by using a more sophisticated FE analysis, as described in the following section.

4.3. NONLINEAR FINITE ELEMENT MODEL (ABAQUS)

The commercially available software, *Abaqus* (Abaqus, 2001) was used to carry out the nonlinear analysis of the Bluestone dam. *Abaqus* is capable of modeling the complex behavior of the dam in a way that improves on the modeling assumptions made in the rigid body and linear FE models, as described subsequently. It is widely used in research and industry and its various features have been tested and validated thoroughly.

4.3.1. Modeling for Hydrologic (Static) Analysis

The nonlinear FE model of monolith no. 12, illustrated in Fig. 4.13, used 8-node, biquadratic, porewater-stress coupled elements for concrete and foundation material. The model incorporated the behavior of dam-foundation interface (with the possibility of cracking and sliding) as well as the nonlinear constitutive behavior of dam and foundation materials. The concrete-rock interface is assumed to be horizontal at elevation 1360 ft and to obey the Coulomb friction law. It is assumed that the friction angle of the interface is equal to that of the foundation and that there is no bonding (or cohesion) between the foundation and the monolith. The foundation material was assumed to be a Mohr-Coulomb material, with its nonlinear behavior defined as perfectly plastic.

4.3.1.1. Description of Model

The concrete in the monolith was modeled as an impervious material. Pore pressures in the concrete do not play a significant role in the analysis due to the drain holes that run from the top of the dam to the gallery. Accordingly, pore water pressure in the concrete is assumed to have a negligible impact on the performance of this particular dam. Moreover, the stresses observed are much lower than the concrete strength in tension or compression.

The model for the contact interface between the concrete and rock did not allow any relative motion of the surfaces until the shear forces are greater than the frictional resistance. This condition is enforced by imposing additional constraints (done internally by *Abaqus*) on the nodes of the contact surfaces. These constraints increase the computational cost due to the addition of more degrees of freedom to the model, and thus often increase the number of iterations required for convergence. But it captures accurately the magnitude of slippage that would occur and the additional computational cost was not unmanageable. The contact behavior in the normal direction was modeled as a “softened” contact relationship (in contrast to “hard” contact), in which the surfaces begin to transmit normal pressures before the clearance/ opening between the contacting surfaces is zero. This model was considered to be realistic, as the space between the two surfaces is full of rubble and thus normal pressures get transmitted gradually. This model also has an advantage computationally, as it softens the contact behavior, and the FE solutions usually converge easily.

As *Abaqus* is not capable of modeling the Hoek-Brown criteria, the foundation material was assumed to be described by a Mohr-Coulomb relationship. However, the Mohr-Coulomb relationship used herein is a linear equivalent, for the range of stresses of interest, of the Hoek-Brown failure criteria used in the linear FE analyses. It was obtained by a simple least-squares fit to the Hoek-Brown criterion. To simulate far-field response of the foundation, so called “*infinite*” elements were used at the boundaries. It was found that the “infinite” elements perform reasonably well in simulating the far-field response in these static analyses; their performance in dynamic analysis was poor, as illustrated in later sections.

4.3.1.2. Structural Response

As with rigid and linear FE analyses, the nonlinear FE analysis was conducted at increasing pool elevations. The forces applied are as described in the previous sections. Since the loads and assumptions for these three different analyses are consistent, comparison of results is possible.

Fig. 4.14 shows the normal stresses obtained by the *Abaqus* FE analysis at the interface of the dam for different pool elevations. The results compare very well with the rigid body and linear FE analyses for lower pool elevations, as shown in Fig. 4.15.a. But for higher pool elevations, (e.g. 1556 ft), as depicted in Fig. 4.15.b, the stresses around the heel for the nonlinear FE analyses show values close to zero and no tensile stresses. This is because the nonlinear model for the interface does not allow tensile stresses to be carried by the elements, but forces the contact surfaces to open up instead. On the other hand, the

compressive stresses observed around the toe of the dam are much lower than the compressive strength of concrete (240 psi vs. 5000 psi). Thus, the toe of the dam is considered safe from crushing of concrete even at high pool elevations. The shear stress distribution across the dam-foundation interface from the nonlinear FE model is shown in Fig. 4.16. In contrast with the reasonable agreement of normal stresses, the shear stress from linear and nonlinear FE analyses differ in their distribution across the interface (Fig. 4.17), though the stresses are of the same order of magnitude. This shows that the way the modeling of the mechanical behavior affects the shear stress distribution more than the normal stress distribution at the dam-foundation interface.

The normal stresses at the neck of the dam are presented in Fig. 4.18. The results show a rapid increase in tensile stress at the upstream face of the dam above the design PMF (1520 ft). This behavior corresponds well with the design criteria that provides for no tension at any horizontal section of the dam at pool elevation at or below the design basis. Comparison of the results with those obtained from the linear FE analyses is shown in Fig. 4.19. It is observed that the compressive stresses are of the same order of magnitude as those observed at the toe of the dam (well below the strength of concrete in tension or compression), and would not impact the safety of dam subjected to hydrologic hazard. The relative deformation of the top of the dam with respect to the heel for increasing pool elevations is depicted in Fig. 4.20. The magnitude of this deformation is quite small (less than 0.02% of the height of the dam), an indication that the dam behaves (nearly) as a rigid body.

The nonlinear responses at the dam-foundation interface are presented in Figs. 4.21 through 4.23. The results for the relative sliding of the dam with respect to the foundation

are presented in Fig. 4.21 (where node 1 and 9 are at 0 ft and 50 ft, respectively, from the heel of the dam). The magnitude of slippage obtained is very small (maximum of 0.08 in) even for very high pool elevations. Fig. 4.22 shows the cracking response around the heel of the dam. The cracking has propagated for about 50 ft (node 9) at pool elevation of 1556 ft (revised PMF). This crack length is of comparable magnitude to that obtained in studies of similar monoliths (e.g. Dewey et al, 1994; Saouma, 1995). Nonlinear response of the foundation material is presented in Fig. 4.23, showing the plastic strains (in the vertical direction) at representative points in the foundation near the toe of the dam. These strain magnitudes are very small (on the order of 10^{-4}), an indication that the nonlinear behavior in the foundation due to hydrologic loads upto the PMF should be minimal.

The nonlinear model of the dam-foundation system used to assess hydrologic events incorporates the nonlinearities due to the discontinuity at the dam-foundation interface and the nonlinear constitutive behavior of the foundation. The slippage and cracking at this interface can thus be computed. It also models the presence of pore-water pressure in the foundation. The far-field response of the foundation rock is simulated by “infinite” elements, which provide stiffness at the FE boundaries and thereby maintain the necessary equilibrium conditions. Results obtained from nonlinear FE analyses compare very well with other studies and with the rigid body and linear FE analyses performed herein.

The model, however, does not correct for the uplift pressure in cracks at the dam-foundation interface that form at higher pool elevations. Once the crack forms, the uplift pressure within the crack should be adjusted to the full hydrostatic pressure head at the upstream tip of the crack. But there is no feature in *Abaqus* that iteratively adjusts the uplift

pressure while the analysis progresses. Although the model did not consider the possibility of concrete fracturing at the neck of the dam, this was deemed unnecessary, as the response at the neck was essentially linear and the stresses observed were an order of magnitude less than the splitting strength of concrete.

4.3.2. Modeling for Seismic (Dynamic) Analysis

The modeling of the dam-foundation system for seismic/ dynamic analysis must incorporate the dam-reservoir interaction (the hydrodynamic forces on the upstream face of the dam), the dam-foundation interaction, and the water-foundation interaction. An appropriate mechanism for input of selected earthquake ground motions to the FE model has to be chosen. Moreover, the effects of the boundary conditions to be imposed on the FE mesh have to be considered. The seismic analysis of the dam-foundation system is carried out in the time domain because of the nonlinear nature of the problem. Dynamic (and nonlinear) time domain analysis of concrete gravity dams is computationally very expensive, and a model that reasonably reduces the computational cost without compromising accuracy is highly desirable. The basic structural model for this analysis was as described above in hydrologic/ static modeling. However, the following modifications and/or additions are included.

4.3.2.1. Contact Surface Model

The contact surface between the concrete and the rock/foundation (modeled as a Coulomb friction surface) is allowed an “elastic slip” in the seismic analysis (as opposed to the hydrologic analysis). In other words, this model for friction uses a penalty method that permits some relative motion of the surfaces when they should be sticking (ABAQUS, 2001). This relative motion, limited to the “elastic slip” specified, can take place while the shear forces are less than the frictional resistance. This model was chosen as the use of “Lagrange constraints” (effectively setting the “elastic slip” to zero) in the model sometimes led to numerical instability in the solution and increased the computational cost excessively. Allowing an “elastic slip” of 0.005 in (0.127 mm) was found to be small enough that it did not adversely affect the accuracy of the analysis and made the computation more efficient.

The contact behavior in the normal direction was described by the “soft” contact model, as in the hydrologic analysis. The use of the alternate “hard” contact model in *Abaqus* requires the solution of impulse equations between nodes that are coming into contact with each other. These equations are solved at time increments of the order of 10^{-6} step units, giving rise to incessant impact or “chattering” between the nodes in the contact surfaces. On the other hand, a single increment involves the solution of a large number of impulse equations, leading to unacceptably high computational costs in simulation-based fragility modeling. On the contrary, the “soft” contact model improves the computational efficiency significantly. More importantly, the “soft” contact model, as described in the hydrologic model, is a more realistic representation of the normal stress transmission between the contact surfaces at the dam-foundation interface.

4.3.2.2. Infinite Elements

The infinite elements provide stiffness in static analysis. In dynamic analysis they maintain the static forces that were present at the start of the dynamic analysis on the boundary between the FE model and the infinite elements. They also introduce additional normal and shear tractions on the FE boundary that are proportional to the normal and shear components of the velocity of the boundary and are meant to minimize the reflection of dilatational and shear wave energy back into the FE mesh (ABAQUS, 2001). However, these boundary damping forces introduced by the infinite elements were observed to deform excessively the elements in their vicinity. An alternate solution was devised in which the infinite elements were replaced by constraints on the nodes at the edges of the FE mesh (as described in detail below). The forces at the edges of the FE mesh required for static equilibrium were retained.

4.3.2.3. Input Mechanism of Ground Motion

The standard input for earthquake ground motion where the foundation is assumed to be rigid is at the base of a dam. This analysis neglects the dam-foundation interaction, which has been found to be important in the study of the seismic behavior of concrete gravity dams (e.g. Chakrabarti and Chopra, 1973; Chopra and Gupta, 1980; Fenves and Chopra, 1984a, 1984b). To include this interaction, the foundation has to be modeled and incorporated into the system, and the ground motion then has to be input at the bottom of

the FE mesh of the foundation. But databases on earthquake ground motion contain records of free-field ground level accelerations or accelerations at some point on or within a structure. These free-field records are not entirely appropriate for the purpose at hand, as they do not represent the ground motion at the base of the FE model of the foundation. Rather, the free-field records must be deconvolved in such a way that when they are input at a certain depth in the foundation, they reproduce the recorded free field ground motion at the surface.

A program for such purposes, *SHAKE*, has been developed at the University of California at Berkeley (Schnabel et al, 1972). In this study, a modified version of the program, *SHAKE91*, (Idriss and Sun, 1992) was used for the deconvolution process. The program computes the response of a semi-infinite horizontally layered soil deposit overlying a uniform half-space subjected to vertically propagating shear waves. The analysis is done in the frequency domain and therefore, for any set of properties, it is a linear analysis (Idriss and Sun, 1992).

SHAKE91 idealizes the soil profile as a system of homogeneous, visco-elastic sublayers of infinite horizontal extent (See Fig.4.24). The responses in the soil profile are caused by the upward propagation of shear waves from the underlying rock half-space, essentially reducing it to a 1-D problem. Each sublayer is assumed to be completely defined by its shear modulus, damping ratio, unit weight and thickness. An equivalent linear procedure is used to account for the nonlinearity of the soil using an iterative procedure to obtain values for modulus and damping that are compatible with the equivalent uniform strain induced in each layer.

Leger and Boughoufalah (1989), in their report of the study of different input mechanisms, confirmed the validity of this method and showed that the standard rigid-base input model produces excessive amplifications. Others (e.g. Anandarajah, 1995) have used this deconvolution process in their studies successfully and have shown that analysis and experimental results match closely.

In conjunction with the above approach to modeling ground motion, two factors need to be noted. The deconvolution of the earthquake ground motion is an essentially linear, 1-D process. The deconvolved ground motion is applied at the base of the FE model of the foundation. Conducting a seismic analysis of the foundation (without the dam) in *Abaqus* would not reproduce the free field ground motion acceleration exactly, as the problem is no longer 1-D and the analysis is nonlinear. Thus, as the base of the foundation model is deepened, the difference between recorded free field ground motion and the one obtained from *Abaqus* using the deconvolved ground motion increases. On the other hand, the dam-foundation interaction is modeled better by the use of a larger (spatially) FE mesh. Hence, a balance between these competing factors has to be sought. The FE mesh shown in Fig. 4.25 was found, from comparison of different model sizes, to be adequate for both the above issues.

4.3.2.4. Boundary Conditions

The bottom boundary of the FE mesh is the application point of the deconvolved seismic ground motion, as described above. Thus, the earthquake input motion serves as the boundary condition at the base of the FE mesh. Different boundary conditions,

however, must be imposed on the nodes on the vertical boundaries of the FE mesh of the foundation. These nodes, representing the outlying nodes where the effect of dam-foundation interaction has been attenuated (and thus assumed to move in unison in the horizontal direction), are constrained to move together in the horizontal direction. In other words, the spatial variation of the earthquake ground motion across the base of the model is neglected and, these outlying nodes are constrained to move together in the horizontal direction. Those nodes in the vicinity of the base of the dam will be affected by the dam-foundation interaction. The above provisions (i.e. the FE mesh, the boundary conditions imposed and the ground motion input mechanism) provide an adequate model for the dam-foundation interaction. This modeling approach has also been successfully utilized in other studies (e.g. Anandarajah et al, 1995).

4.3.2.5. Dam-Water-Foundation Interaction

The seismic modeling of a concrete gravity dam must account for the dynamic interactions among the reservoir, the dam and the foundation. The dynamic equilibrium of the dam-foundation system is expressed as (Chopra and Chakrabarti, 1981):

$$M \ddot{\mathbf{r}} + C \dot{\mathbf{r}} + K \mathbf{r} = -M \mathbf{1} \mathbf{a}(\mathbf{t}) + R(t) \quad (4.7)$$

in which M , C , K are the mass, damping and stiffness matrices, \mathbf{r} is the vector of nodal point displacements relative to the free-field ground displacement at the base of the dam, $\mathbf{a}(\mathbf{t})$ is the free-field ground acceleration, and $\mathbf{1}$ is a unit column vector. The force vector $R(t)$ includes the hydrodynamic forces due to the dam-reservoir interaction. These forces

are expressed in terms of accelerations of the upstream face of the dam and the reservoir bottom, thus introducing acceleration-dependent terms to the right side of Eqn. 4.7. These hydrodynamic pressures are governed by the two-dimensional wave equation (assuming water to be linearly compressible and neglecting its internal viscosity) (Chopra and Chakrabarti, 1981; Chopra and Gupta, 1981; Darbre, 1998):

$$\frac{\partial^2 p(x, y, t)}{\partial x^2} + \frac{\partial^2 p(x, y, t)}{\partial y^2} = \frac{1}{c_w^2} \frac{\partial^2 p(x, y, t)}{\partial t^2} \quad (4.8)$$

in which $p(x, y, t)$ is the hydrodynamic pressure (in excess of the hydrostatic pressure) and c_w is the velocity of sound in water,

$$c_w = \sqrt{K/\rho_w} \quad (4.9)$$

where K and ρ_w are the bulk modulus and density of water, respectively. Assuming that the upstream face of the dam is vertical, solutions to Eqn. 4.8 are obtained by imposing the following boundary conditions (Chopra and Chakrabarti, 1981; Wepf, Wolf and Bachman, 1988, Darbre, 1998):

- i. At the surface of the reservoir (neglecting surface waves);

$$p(x, 0, t) = 0 \quad (4.10)$$

- ii. At the upstream face of the dam;

$$\frac{\partial p(0, y, t)}{\partial x} = -\rho_w \frac{\partial^2 r_u(t)}{\partial t^2} \quad (4.11)$$

- iii. At the reservoir bottom;

$$\frac{\partial p(0,y,t)}{\partial y} = -\rho_w \frac{\partial^2 r_v(t)}{\partial t^2} \quad (4.12)$$

iv. And reservoir absorption at the reservoir bottom;

$$\frac{\partial p(x,0,t)}{\partial y} - q \frac{\partial p(x,0,t)}{\partial t} = 0 \quad (4.13)$$

where $r_u(t)$ are horizontal displacements of nodes on the upstream face of the dam, and $r_v(t)$ vertical displacements of the nodes on the reservoir bottom, and q is the damping coefficient of the reservoir bottom, defined as (Darbre, 1998),

$$q = \frac{1}{c_w} \frac{1-\alpha}{1+\alpha} \quad (4.14)$$

where α = the wave reflection coefficient ($\alpha = 0$ means full absorption and $\alpha = 1$ is full reflection of hydrodynamic waves impinging on the reservoir bottom). Boundary conditions (ii) and (iii) are the coupling terms in the problem, representing the hydrodynamic and water-foundation interactions, respectively.

These interactions have been intensively studied and reported. A seminal paper on the dam-water (hydrodynamic) interaction was presented by Westergaard (1933), in which solutions were derived for the system of equations that govern the motion of the water and thus the associated hydrodynamic pressures. Westergaard's analysis was based on a concrete gravity dam with a triangular cross-section on a rigid base and a simple harmonic excitation. The response of the dam was assumed to be rigid and all points in the dam had the same acceleration as the base. Westergaard concluded that the problem could be visualized as if a certain body of water were forced to move back and forth with the dam

while the remainder of the reservoir is left inactive; hence the name “added mass” by which the method is usually identified. This method has been used in design of concrete gravity dams, including the Bluestone Dam, for decades. Over the years, a number of studies that investigated the effects of the various assumptions in Westergaard’s work appeared. A brief summary of these studies through up to the late 1960’s is included in Chopra (1967). More recently, interest in this subject has been revived; several articles representative of these more recent various approaches to modeling dam-reservoir interaction are briefly reviewed and critiqued below.

One approach to modeling these interactions, epitomized by the work of Chopra and his colleagues, is the solution of the governing equations in the frequency domain. This approach has evolved from the earlier studies (Chopra, 1970; Chakrabarti and Chopra, 1973) that assumed the foundation as rigid to improvements (Chopra and Gupta, 1980; Chopra and Chakrabarti 1981) that included the dynamic effects of the impounded water, flexible foundation and the simultaneous application of the horizontal and vertical components of earthquake ground motions. The dam-water-foundation system, idealized as consisting of three substructures – the dam, the fluid domain and the foundation rock - is assumed to exhibit linear behavior. These studies were further extended to include the effects of the alluvium and sediments invariably present at the bottom of actual reservoirs (Fenves and Chopra, 1984a, 1984b). A further modification was made by Chopra and Zhang (1992) to compute the earthquake-induced sliding of concrete gravity dams. However, this study was did not consider the dam-foundation interaction and/or the flexibility of the foundation. Fenves and Chavez (1996) utilized a hybrid frequency-time domain (HFTD) procedure (Darbre and Wolf, 1998), which iterates over each segment of

time in three major steps: linearization of the equations of motion, solution of the equations of motion in the frequency domain, and determination of sliding/ sticking state in the time domain. Thus the bulk of the computations are done in the frequency domain, in which the frequency- dependent hydrodynamic pressures are easily accounted for.

Wolf and his colleagues pursued a different approach, one that directly calculates the hydrodynamic-stiffness matrix (Wolf and Paronesso, 1992) by using a lumped-parameter model with frequency-independent springs, dashpots and masses and with only a few additional internal degrees of freedom. Similar approaches that used the boundary element method to construct the dynamic stiffness matrix have also been presented (e.g. Wepf et al, 1988; Tsai and Lee, 1990). Leger and Bhattacharjee (1992) proposed a slightly different approach in which added matrix coefficients that represent the reservoir interaction coefficients were used in conjunction with so-called “mock” fluid elements.

Darbre (1998) presented a relatively simple two-parameter model that illustrates the way water contained in a reservoir influences the dynamic response of a dam. The model consists of an incompressible water mass attached in series to dampers. The dampers are fixed to the upstream face of the dam. As the model is discrete, it can be implemented directly in a nonlinear, time-domain analysis. The model is motivated from observations that:

1. At low structural frequencies, the hydrodynamic pressure exerted on the upstream face of the dam is equivalent to the inertia pressure exerted by an entrained mass of incompressible water (Fig. 4.26);
2. At high structural frequencies, waves propagate upstream and the pressure exerted on the face of the dam is equivalent to that exerted by dampers attached

to the dam. The dampers are uniformly distributed along the upstream face of the dam and have a value of $\rho_w c_w$ (Fig. 4.26), where ρ_w is the mass density of water and c_w is the pressure waves' velocity.

These two fundamental features are combined in the two-parameter phenomenological model (Fig. 4.26), where an incompressible body of water is attached to the dam through distributed dampers. The model duplicates the asymptotic behavior exactly: at low frequencies of motion, the dampers do not deform and the pressure originates from the water's inertia forces only (proportional to acceleration); at high frequencies, the water mass remains still and the pressure initiates from the deformation of the dampers (proportional to velocity).

The interaction coefficients derived from this model were shown (Darbre, 1998) to duplicate the overall trends of the exact analytical solution well. The differences between the exact curves and the two-parameter model tend to diminish for increasing levels of reservoir bottom absorption of incident waves (e.g. when $\alpha = 0.5$ in Eqn. 4.14). It was shown (Darbre, 1998) that the two-parameter model is a valid approximation when both the frequency content of the excitation and the significant natural frequencies of the dam extend over several resonant frequencies of the reservoir. An application of such a model in a direct analysis of a dam also reinforces the above observations (Darbre, 1996). Darbre's discrete model, as shown in Fig. 4.26, was thus chosen for the nonlinear seismic analyses of the Bluestone concrete gravity dam. The physical parameters of the model, in addition to those described in the nonlinear hydrologic modeling, are:

$$\begin{aligned} \text{damping} &= \rho_w c_w = (1.94 \text{ slugs/ft}^3 * 1485 \text{ ft/sec}) \\ &= 2.882 \text{ kips/ft/sec per linear foot} \end{aligned}$$

added mass according to Chopra and Zhang (1992), which, assuming a rigid structure, is defined as:

$$m_a(y) = p_0(y) = \frac{8\rho_w h}{\pi^2} \sum_{n=1}^{\infty} \frac{(-1)^{n+1}}{(2n-1)^2} \cos(\lambda_n y) \quad (4.15)$$

$$\text{where: } \lambda_n = \frac{(2n-1)\pi}{2h} \quad (4.16)$$

and h = height of dam

For the seismic analysis of the Bluestone concrete gravity dam the pool elevation was fixed at 1480 ft, i.e. the elevation necessary to drive all the five turbines for power production. (The probability that an earthquake coincides with an extreme flood is negligible.) A static analysis of the dam-foundation system is first carried out with the loads applied as described in previous sections. This represents the state of the dam before an earthquake occurs. Then, a time-domain dynamic analysis is performed with the deconvolved seismic ground motion applied at the base of the FE model of the foundation. To determine the dynamic properties of the system, the natural frequencies were extracted before this dynamic analysis. Table 4.2 shows the results of this analysis for the first ten modes. The fundamental frequency is 6.12 Hz (period = 0.163 sec) with relatively high components of effective mass/ participation factor in the horizontal direction. The second mode is 7.80 Hz (period = 0.128 sec) and has a relatively high associated effective mass/ participation factor in the vertical direction. This indicates that the Bluestone dam-foundation system response in the vertical direction might be considerable. Note, however, that the eigenproblem for natural frequency extraction involves a linear system, and does

not take into consideration the nonlinearities that might dominate the overall response of the dam. The higher modes also exhibit similar tendencies, e.g. modes 2 and 3 are horizontal and mode 5 is vertical. A 5% damping ratio is assumed for modes 1 and 3 (Chopra and Zhang, 1992; Fenves, 1996), which is then used to determine the constants for Rayleigh damping.

The behavior of the dam subjected to earthquake ground motion is illustrated by its response to the ElCentro, Imperial Valley, CA (1940) earthquake. The horizontal component of this ground motion is first deconvolved using *SHAKE91* and then scaled to yield a spectral acceleration of 0.9g at the fundamental frequency of the dam-water-foundation model (i.e. 6.12 Hz). Proportional scaling is also applied to the vertical ground motion. The dam-foundation-reservoir system, with a pool elevation of 1480 ft, is thus subjected to this scaled, deconvolved ground motion at the base of the FE model of the foundation. The analyses were carried out with and without the vertical ground motion, to investigate its influence on the seismic behavior of the concrete gravity dam.

Results are presented in Figs. 4.27 – 4.32, in which the first 6 time units represent the hydrostatic loading up to pool elevation of 1480 ft, and time=6 to time=26 units represent the seismic analysis of a duration of 20 seconds. Fig. 4.27 depicts the time history of normal stress at a point near the heel of the dam. No tensile stress is observed and the maximum compressive stress is about 90 ksf (625 psi), which is much lower than the bearing capacity of the concrete (5000 psi). The two time histories shown represent results from analysis with and without the vertical component of the ground motion. It is noted that the vertical ground motion does not have much effect on the observed maximum stress. A similar conclusion can be drawn from the time histories of normal stress at points on the

neck of the dam (Fig. 4.28.a and b). Both the upstream and downstream faces of neck of the dam exhibit maximum tensile stresses around 60 ksf (420 psi), with and without vertical ground motion. According to the Eqn. 2.1, the splitting strength of a 5000 psi (Table 4.1) concrete is around 450 psi (65 ksf), which is very close to the estimated tensile stresses at the neck of the dam. Hence, some cracking might be expected at the neck of the dam when subjected to an earthquake of this magnitude. However, the maximum compressive stress is much lower than the compressive strength of concrete; in particular, the compressive stresses on the upstream face of the neck of the dam are less by about 50% than that of the downstream face. The relative deformation of the top of the dam with respect to the heel is shown in Fig. 4.29. A maximum value of about 0.05 ft (0.6 in) is observed, which, like the stresses, was not affected much by the presence/ absence of the vertical component of ground motion. This deformation is approximately 0.03% of the height of the dam, suggesting that the dam responds nearly as a rigid body.

The development of cracking, sliding and plastic strains are illustrated in Figs. 4.30 – 4.32. The cracking response around the heel of the dam is depicted in Fig. 4.30. The time history shows that the initial and final/ residual crack openings are zero, with intermittent closures and openings during seismic excitation. This intermittent closure/ opening does not allow enough time for full uplift pressure to build up in the crack, though the maximum value observed, around 0.015 ft (0.18 in) is big enough for the development of pore pressures. Hence, the cracking response of the dam-foundation interface is not deemed an essential aspect of the safety of concrete gravity dams subjected to seismic hazard. In contrast, the sliding response at the dam-foundation interface, shown in Fig. 4.31, proves to be a very important feature of seismic safety analysis. Responses of the heel and toe of the

dam (nodes 1 and 23, respectively) indicate that the monolith sliding is an essentially rigid body phenomenon. A substantial increase in the sliding response is observed with the simultaneous application of the horizontal and vertical components of the ground motion. The residual sliding response is about 0.13 ft (1.56 in), while it is about 40% less if the vertical component of ground motion is not included. These results are consistent with findings in other studies (Chopra and Gupta, 1980; Chopra and Chakrabarti 1981; Fenves and Chopra, 1984a, 1984b; Fenves and Chavez 1996). The magnitude of sliding estimated would impair the functionality of the drainage system, which would increase the uplift pressure at the interface. This in turn would increase the sliding response of the dam. Though not regarded as a probable direct cause, the sliding response thus observed could pave the way for the loss of control of the reservoir.

The nonlinear behavior of the foundation around the toe of the dam is shown in Figs. 4.32.a and b. The time history of plastic strains for elements comprising of an area of $25.3 \times 24 \text{ ft}^2$, with the vertical component of ground motion included in the analysis, is depicted in Fig. 4.32.a. It also shows an area-averaged value, which is indicative of the severity of local yielding in the foundation. Fig. 4.32.b shows area-averaged plastic strains for two different areas for analyses performed with and without the vertical component of ground motion. It is noted that the vertical ground motion intensifies the plastic strain/ local yielding in the foundation.

In seismic analysis of concrete gravity dams, the contribution of the vertical component of the ground motion to the total response of a dam, including hydrodynamic effects, depends on the relative phasing of the responses to horizontal and vertical ground motion, which in turn depends on the phasing of the ground motion component and the

vibration properties of the dam (Chopra and Gupta, 1980; Chopra and Chakrabarti 1981). As noted above, these differences in phasing seem to decrease the influence of the vertical ground motion on the observed values of stresses in the dam. However, both sliding and plastic yielding were greatly affected by the simultaneous application of the horizontal and vertical ground motion. This was also corroborated by Chopra and Zhang (1992), who showed that vertical ground motion increases the cumulative sliding displacement of the dam.

4.4. DISCRETE ELEMENT METHOD

The discrete element method (DEM) has been suggested and illustrated for the analysis of the stability of dams in several recent studies (e.g. Shi, 1992; Wei and Hudson, 1998; Lemos and Cundall, 1999). The DEM is a numerical analysis technique that focuses on discontinuities between multiple bodies and whose emphasis is on the solution of contact and impact between those bodies (Pande et al, 1990). It can simulate large scale slipping or openings of discontinuities and rotations or complete separation between a large number of blocks. In contrast, continuum modeling techniques, such as the finite difference method (FDM), the finite element method (FEM) and the boundary element method (BEM), are limited in the number of discontinuities they can model without developing numerical instability. Since its early inception by Cundall (1971), the DEM has developed into a complex engineering analysis tool, with extensive applications in problems involving discontinua: e.g. in stability of underground openings (e.g. Goodman et al, 1984), in ice mechanics (e.g. Williams et al, 1986, Mustoe et al, 1986) and in soil mechanics at the

microscopic level (e.g. Cundall and Strack, 1979; Anandarajah, 1995). Many variations of the DEM exist, including the rigid block method, the distinct element method, discontinuous deformation analysis, discrete finite element method, coupled DEM-FEM and coupled DEM-BEM methods.

The DEM, like the FEM, is completely general in its ability to handle a wide range of material constitutive behavior, interaction laws and arbitrary geometries. It models each element (or block) as a discrete body, and displacement continuity need only be satisfied within each element (Choi, 1992). The method solves the dynamic equilibrium equations for each discrete element subject to body and boundary interaction forces. The governing equation of dynamic equilibrium is thus:

$$\mathbf{m}\ddot{\mathbf{u}}_i + \mathbf{c}\dot{\mathbf{u}}_i + \mathbf{k}\mathbf{u}_i = \mathbf{f}_i \quad (4.17)$$

where \mathbf{m} , \mathbf{c} , \mathbf{k} represent the mass, damping coefficient and stiffness, \mathbf{f}_i is the i^{th} component of an external applied force and \mathbf{u}_i is the i^{th} component of displacement. The interaction between discrete elements is handled by a suitable constitutive law, such as the simple penalty function approach (Cundall and Strack, 1979):

$$\Delta\mathbf{f}_i = \mathbf{k}_i \Delta\mathbf{u}_i \quad (4.18)$$

where \mathbf{k}_i , $\Delta\mathbf{u}_i$ and $\Delta\mathbf{f}_i$ are the i^{th} components of the inter-element stiffness, incremental displacement and incremental contact force. Methods for solving Eqns. 4.18 and 4.19 are given elsewhere (e.g. Cundall and Strack, 1979; Pande et al, 1990). Because of the explicit nature of the solution methods and the decoupling of the dynamic equilibrium equations, a highly nonlinear constitutive model can easily be incorporated, if necessary (Choi, 1992).

The elements in the DEM can be idealized as either rigid or deformable blocks. Only contact, separation and slip are considered for rigid blocks. For deformable blocks, the motion is decomposed into mean rigid body motion and relative motion. It is also possible to idealize each block by a FE model (Barbosa and Ghaboussi, 1989). In this coupled DEM-FEM model, continuum deformations within each element are handled by FEM while the DEM takes care of the interactions and contacts between elements. The constitutive laws for the interactions between blocks thus become very important in a DEM formulation. This is generally an explicit relationship (like Eqn. 4.18) between the relative displacements and contact stresses. Another important aspect of the DEM formulation is the contact detection and determination of the contact geometry. This requires the use of programs/ algorithms that are capable of recognizing geometrical relationships, similar to those implemented in computer graphics or computer/ robotic vision. Thus, the DEM trades geometrical complexity for simplicity in material constitutive laws and parameters, with the advantage of a more realistic representation of the problem (Jing, 1998).

Discrete element methods have been extended to incorporate fluid flow through the fracture network in the foundation. The dynamic algorithm of the method also makes it suitable for seismic analysis, provided that appropriate boundary conditions are introduced (Lemos, 1999). Fully-coupled mechanical-hydraulic analyses can be performed in order to obtain the initial conditions for the dynamic analysis. Increased water flow through the foundation has been sometimes observed immediately after seismic events. One of the possible causes of these occurrences is the change in permeability due to shearing of dilatant joints. Furthermore, with the DEM it is easier to handle material discontinuities, nonlinearities and large deformations.

These advantages, however, are not significant in most concrete dam studies. Most dams cannot withstand large motions and failure can usually be identified by means of small-displacement analyses. The use of DEM also requires exact knowledge of the orientation and geometry of the joints and/ or faults in the foundation, which in practice is rarely available. Moreover, there are some difficulties with DEM implementation (Choi, 1992), which include: the appropriate application/ choice of correct type of damping, limitations in modeling of brittle fracture of rock, imposition of kinematic constraints, contact detection and contact force calculation, and energy radiation in dynamic problems. It is therefore concluded that at its present state-of-the-art, the DEM does not possess a particular advantage in fragility modeling over the nonlinear FEM used in this study.

Table 4.1. Summary of selected strength parameters.
(source: US Army Corps of Engineers)

Parameters	Phi	Cohesion	Strength
<u>Foundation</u>			
Peak shear strength	46°	28 psi	
Sliding shear strength	32°	6 psi	
Sliding resistance, sawn surface	27.5°	1.5 psi	
Compressive strength			10,500 psi
Allowable bearing pressure			5,250 psi
Tensile strength			1,000 psi
Unit weight			165 pcf
Elastic (Young's) modulus			3.952 x 10 ⁶ psi
Poisson's ratio			0.165
<u>Concrete</u>			
Compressive strength			5,000 psi
Elastic (Young's) modulus			4.867 x 10 ⁶ psi
Poisson's ratio			0.255

$$1 \text{ psi} = 6.895 \text{ kPa}$$

$$1 \text{ pcf} = 16.0185 \text{ kg/m}^3$$

Table 4.2. Dynamic modeling parameters for Bluestone Monolith no. 12

Natural frequencies

MODE NO	EIGENVALUE	FREQUENCY		GENERALIZED MASS
		(RAD/TIME)	(CYCLES/TIME)	
1	1477.1	38.433	6.1168	8.9325
2	2403.9	49.03	7.8034	103.31
3	3999.7	63.243	10.066	4.7926
4	10397	101.97	16.229	3.0508
5	22972	151.57	24.122	24.321
6	24216	155.62	24.767	8.9319
7	33795	183.83	29.258	20.064
8	38844	197.09	31.368	12.948
9	49071	221.52	35.256	13.274
10	62309	249.62	39.728	11.291

Participation factors

MODE NO	X-COMPONENT	Y-COMPONENT	X-ROTATION	Y-ROTATION
1	3.1186	0.48498	0.00E+00	0.00E+00
2	-0.17746	1.1742	0.00E+00	0.00E+00
3	-3.2559	-0.47506	0.00E+00	0.00E+00
4	1.4088	0.23917	0.00E+00	0.00E+00
5	-4.37E-03	-0.18797	0.00E+00	0.00E+00
6	-0.28208	0.19736	0.00E+00	0.00E+00
7	-6.66E-02	0.16278	0.00E+00	0.00E+00
8	-8.88E-02	-0.21816	0.00E+00	0.00E+00
9	3.72E-02	5.41E-02	0.00E+00	0.00E+00
10	-0.15421	6.06E-03	0.00E+00	0.00E+00

Effective mass

MODE NO	X-COMPONENT	Y-COMPONENT	X-ROTATION	Y-ROTATION
1	86.874	2.101	0.00E+00	0.00E+00
2	3.2532	142.43	0.00E+00	0.00E+00
3	50.805	1.0816	0.00E+00	0.00E+00
4	6.0546	0.17451	0.00E+00	0.00E+00
5	4.64E-04	0.85931	0.00E+00	0.00E+00
6	0.71069	0.3479	0.00E+00	0.00E+00
7	8.89E-02	0.53165	0.00E+00	0.00E+00
8	1.02E-01	0.61625	0.00E+00	0.00E+00
9	1.83E-02	3.88E-02	0.00E+00	0.00E+00
10	0.26851	4.15E-04	0.00E+00	0.00E+00

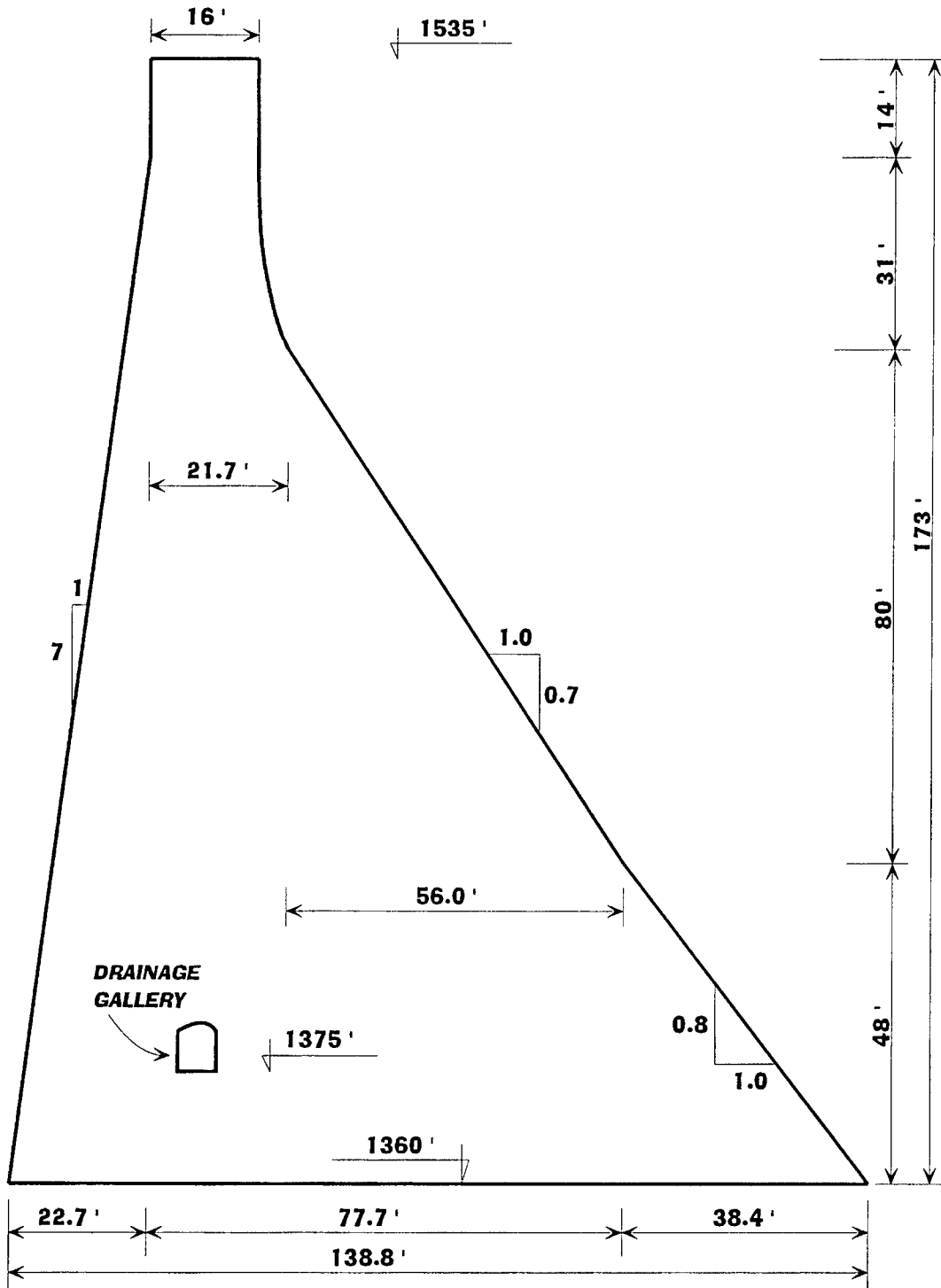


Fig. 4.1. Non-overflow monolith no. 12 at Bluestone dam

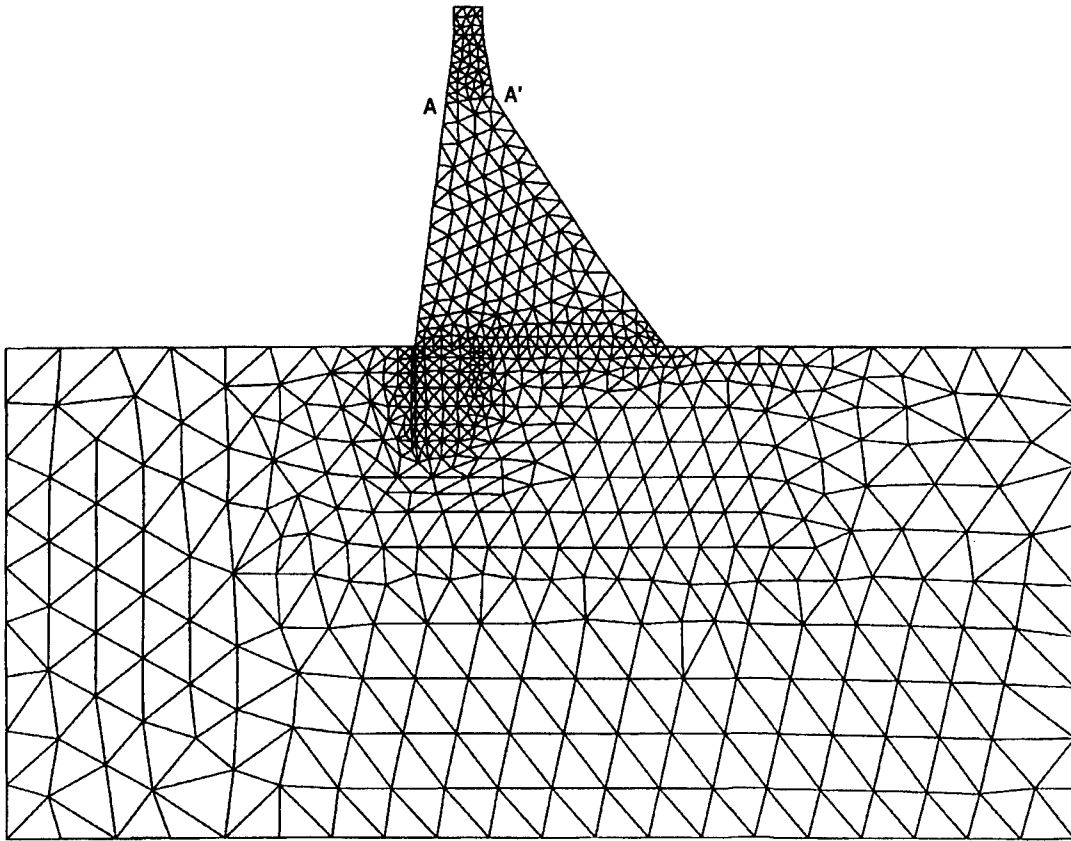


Fig. 4.2. Linear finite element model of Bluestone monolith no. 12

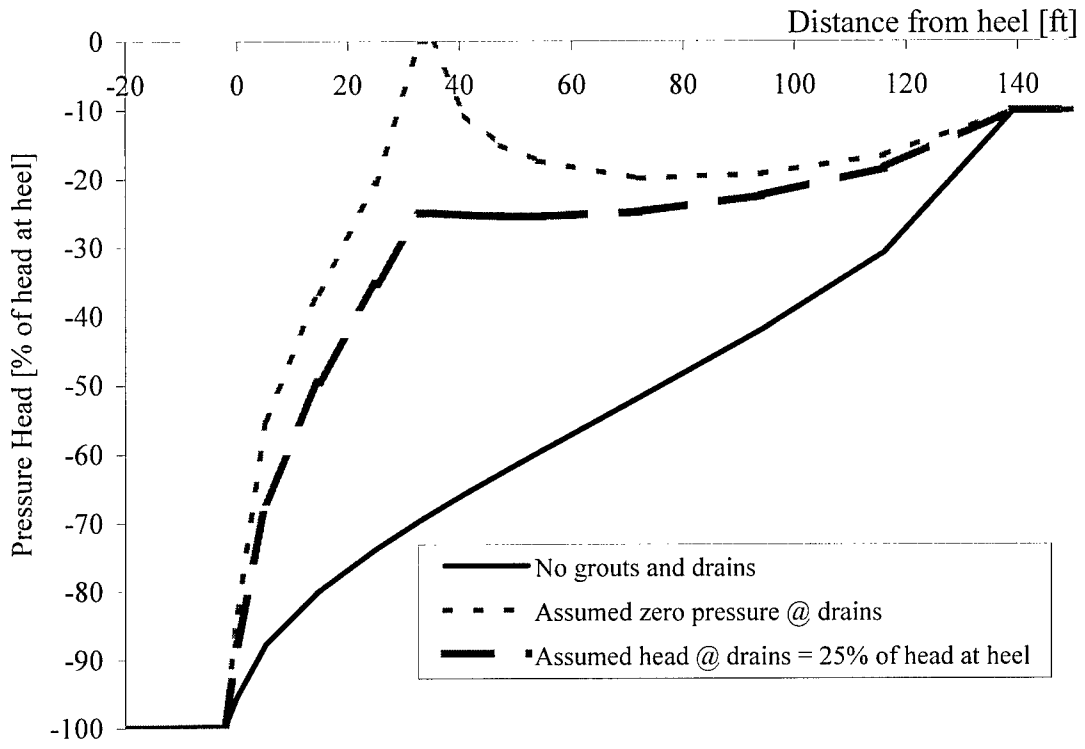
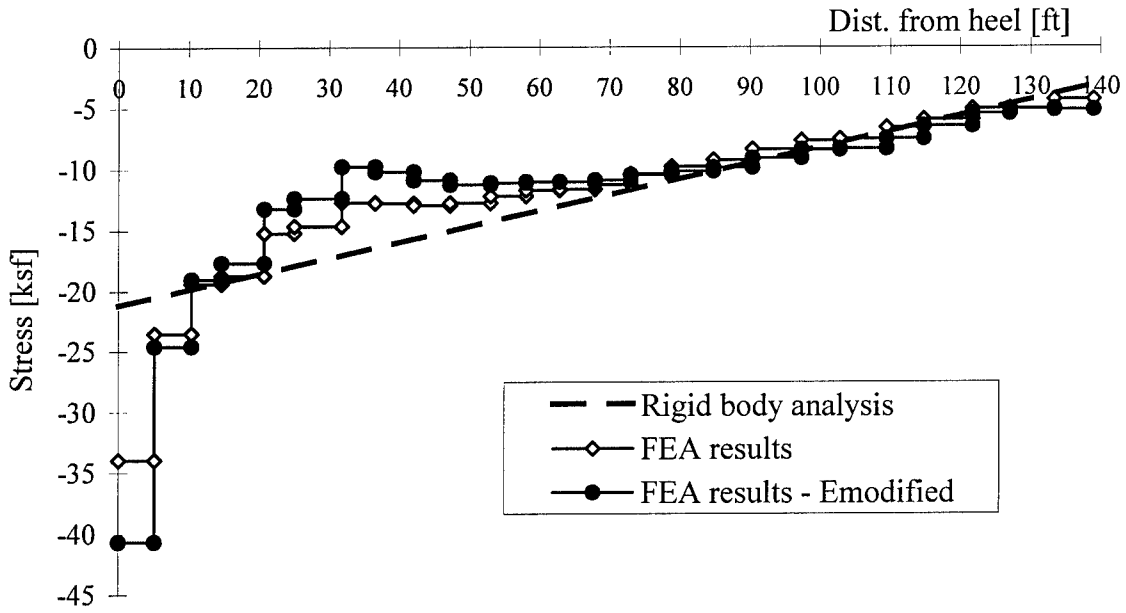
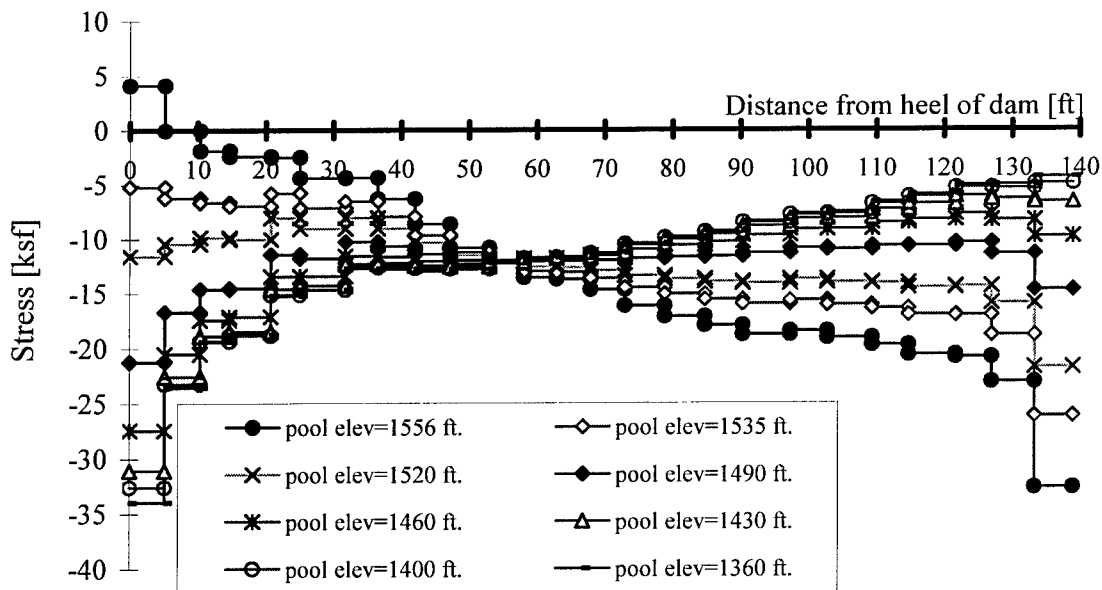


Fig. 4.3. Uplift pressure at base of dam

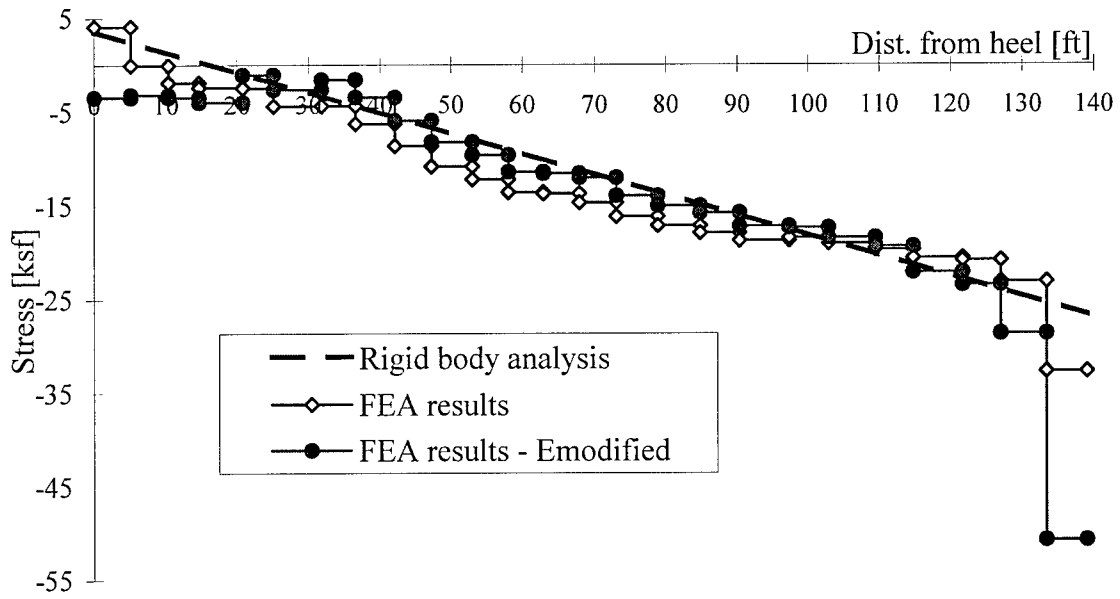


a) For different pool elevations



b) For pool elevation of 1360 ft (415 m)

Fig. 4.4. Normal stress distributions at the base of dam



c) For pool elevation of 1556 ft (474 m)

Fig. 4.4. (Cont'd). Normal stress distributions at the base of dam

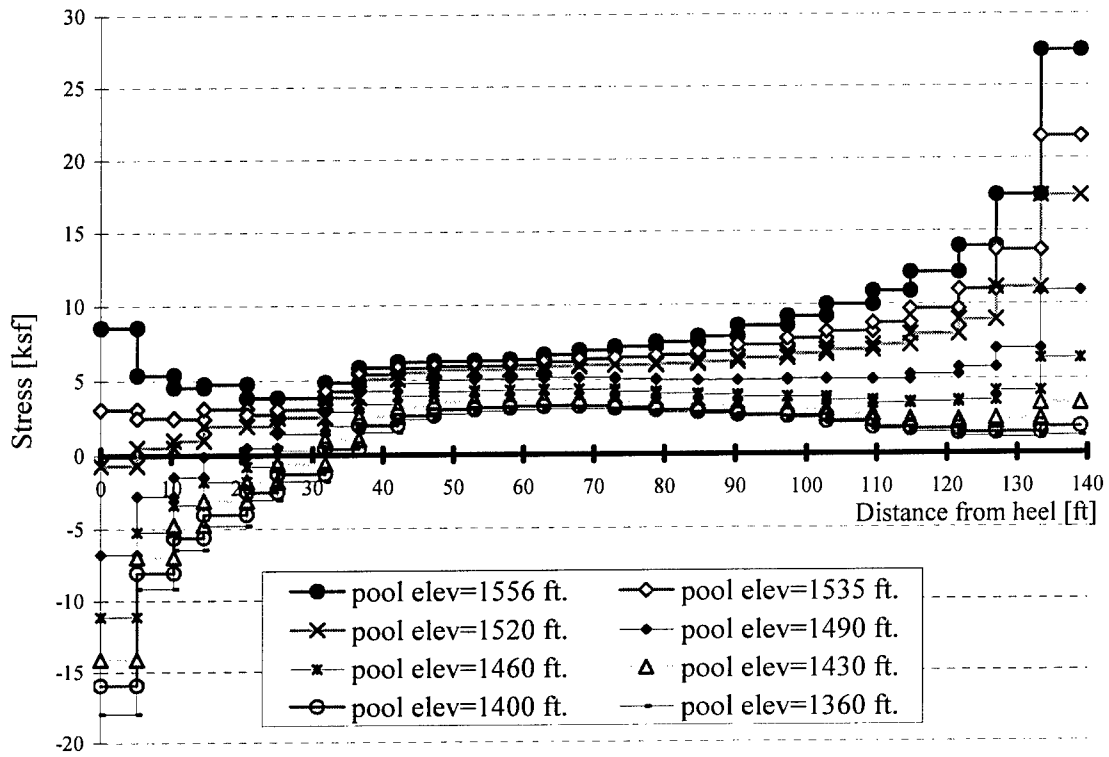


Fig. 4.5. Shear stress distribution at base of dam

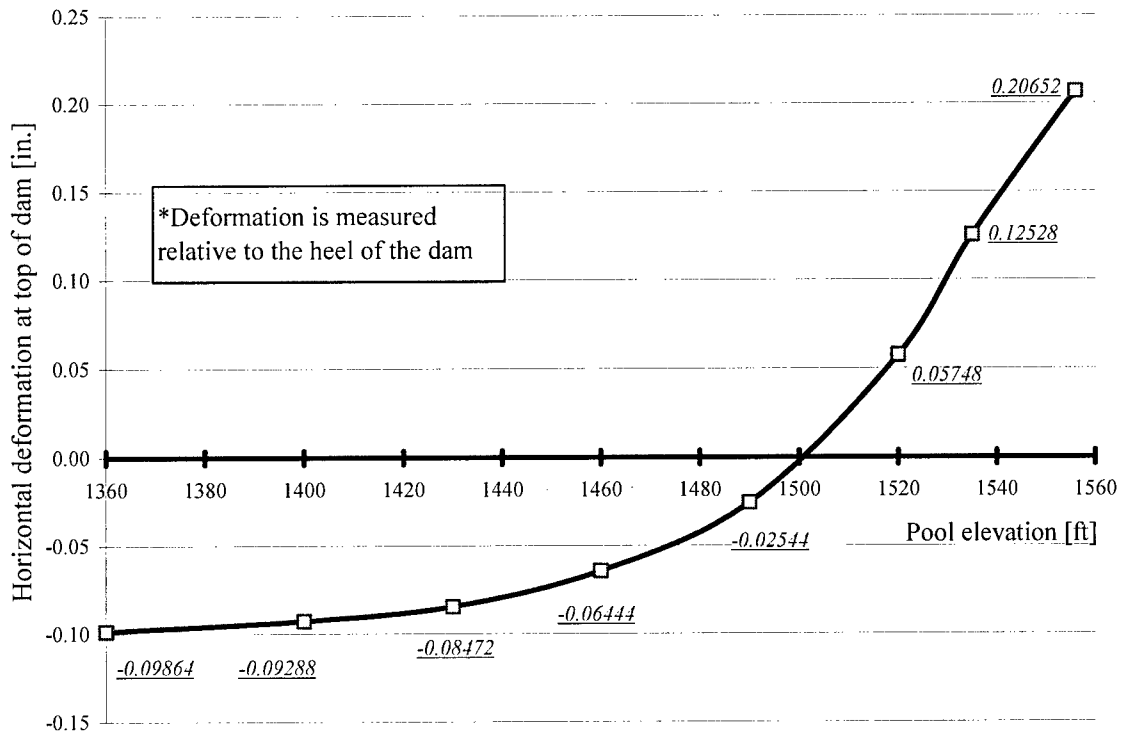
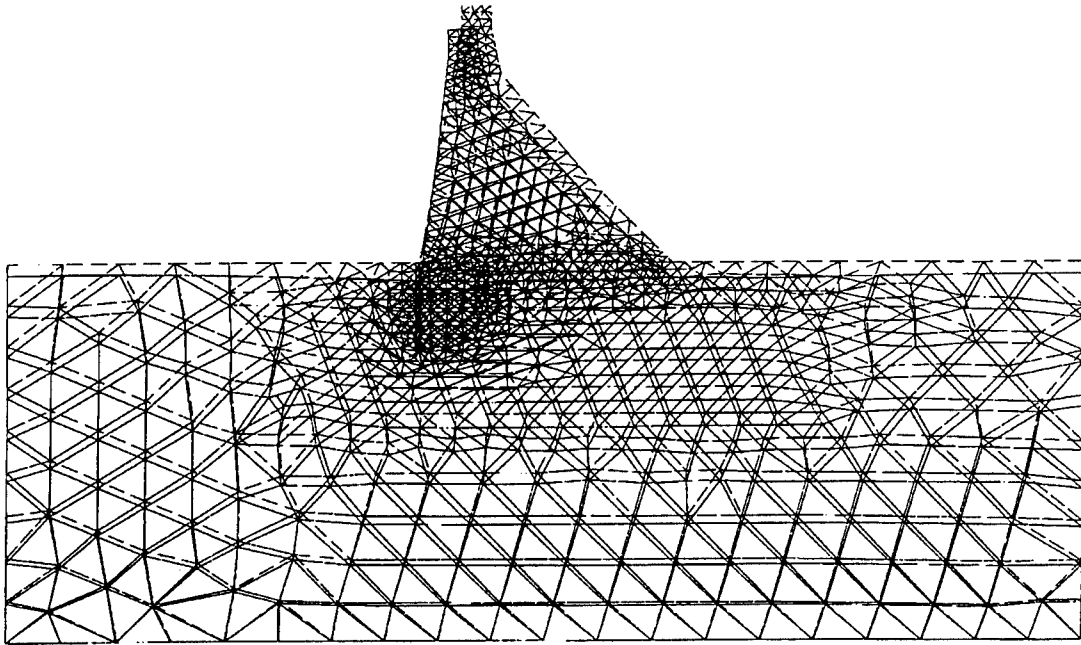
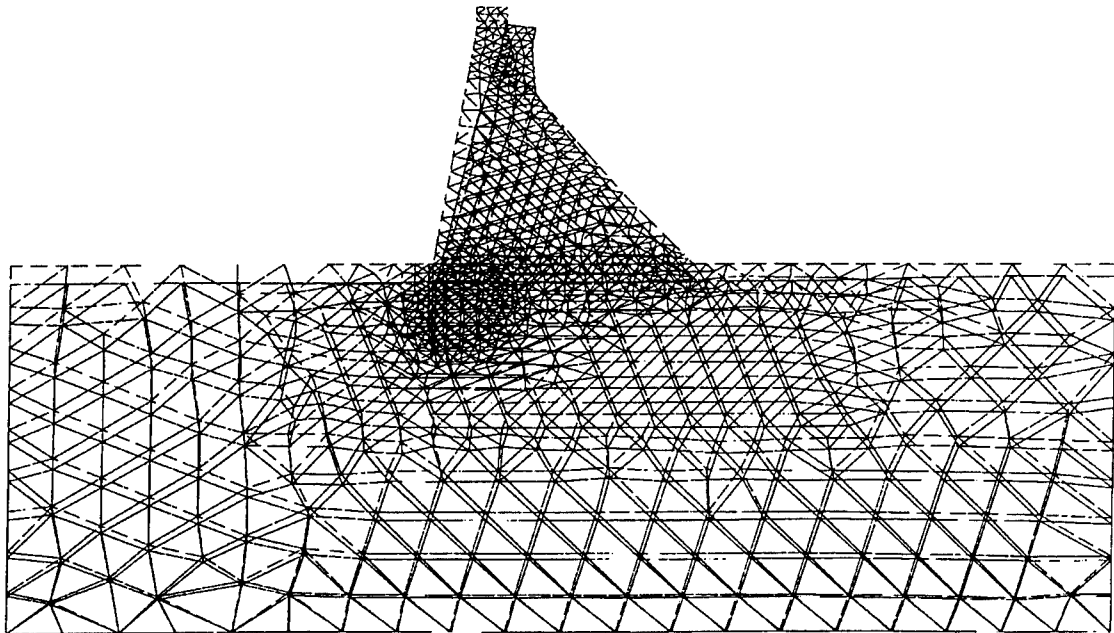


Fig. 4.6. Relative deformation of the top of the dam with respect to heel

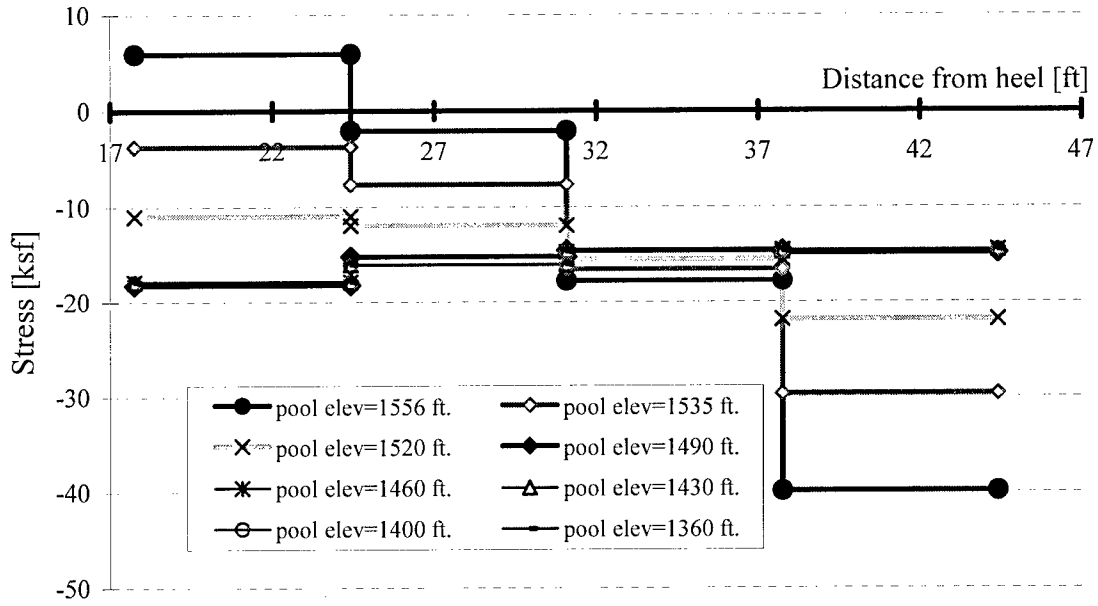


a) Pool elevation = 1360 ft.

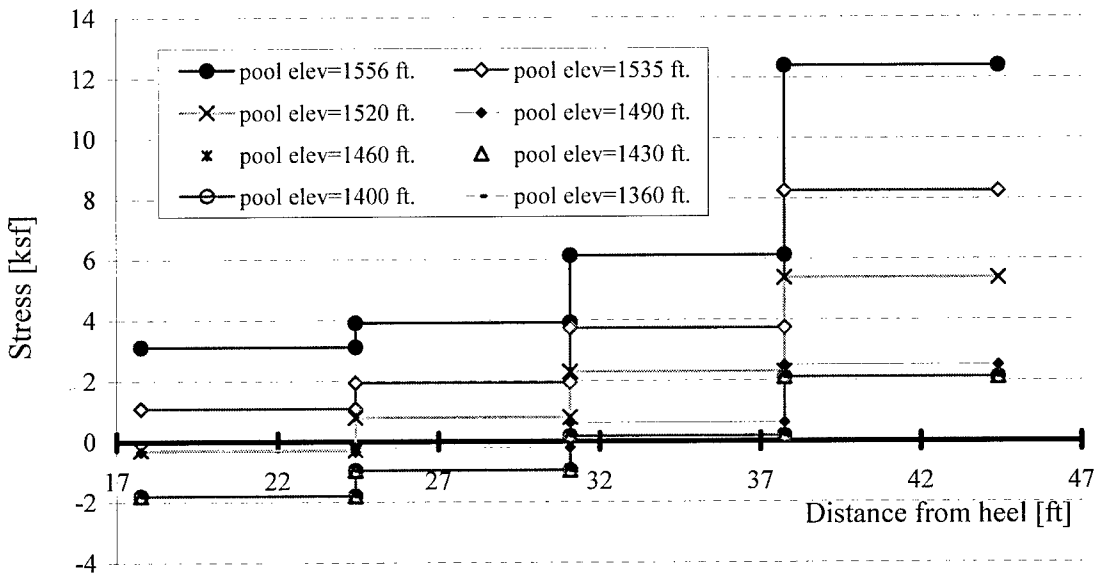


b) Pool elevation = 1556 ft.

Fig. 4.7. Deformed shape of dam-foundation system

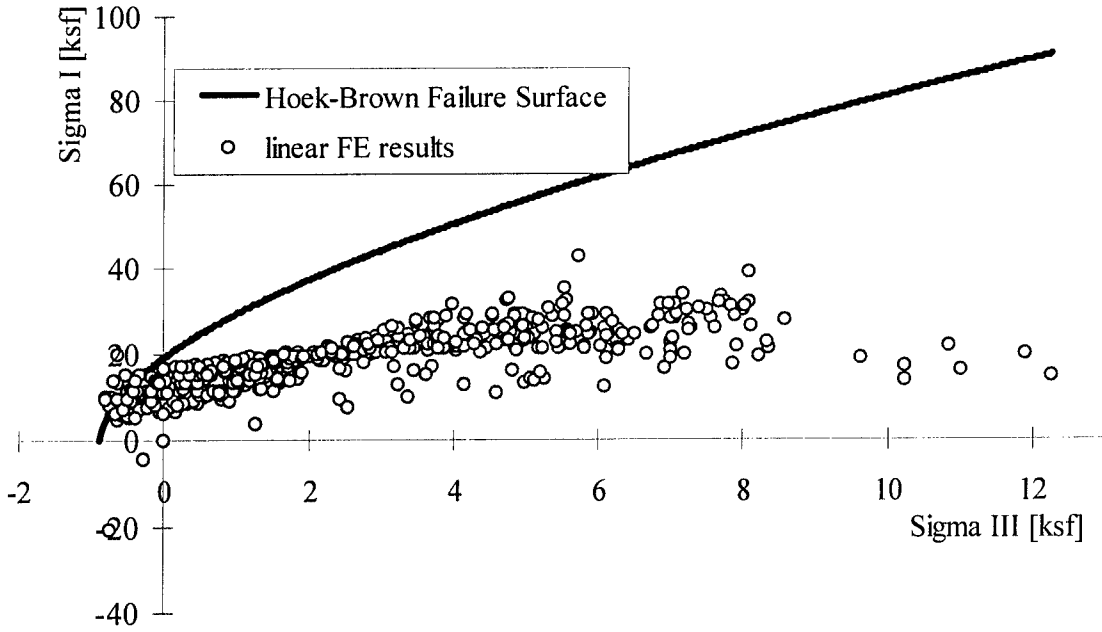


a) Normal stress distribution

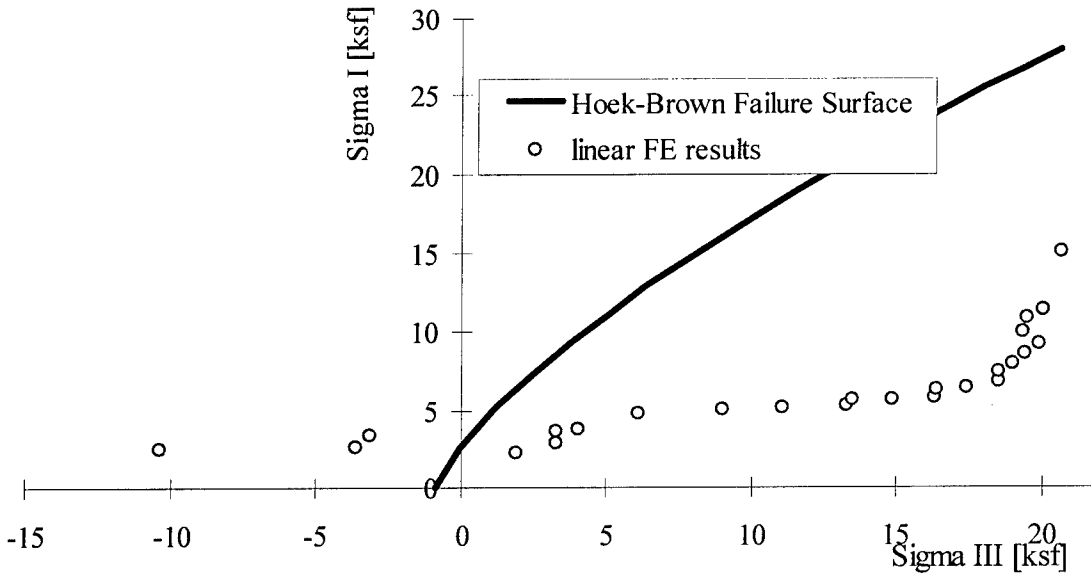


b) Shear stress distribution

Fig. 4.8. Stress distribution at the neck of the dam



a) Compression failure



b) Shear failure

Fig. 4.9. Comparison of stresses observed vs. Hoek-Brown criterion at elevation of 1556 ft (474 m)

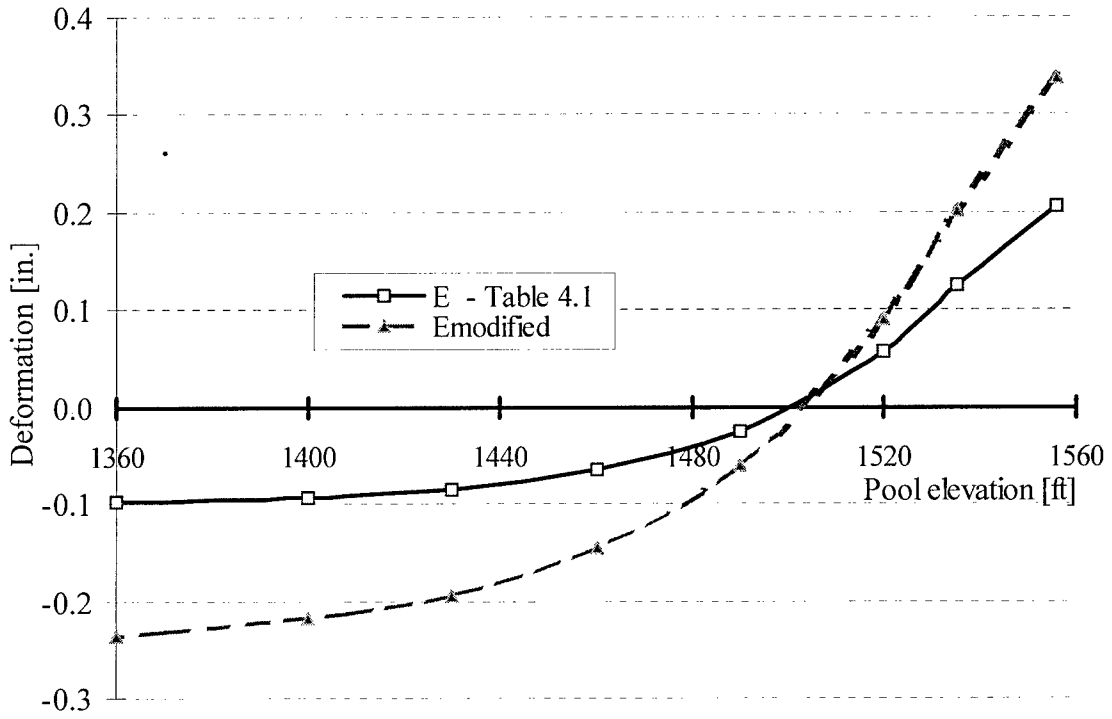


Fig. 4.10. Relative deformation at top of the dam

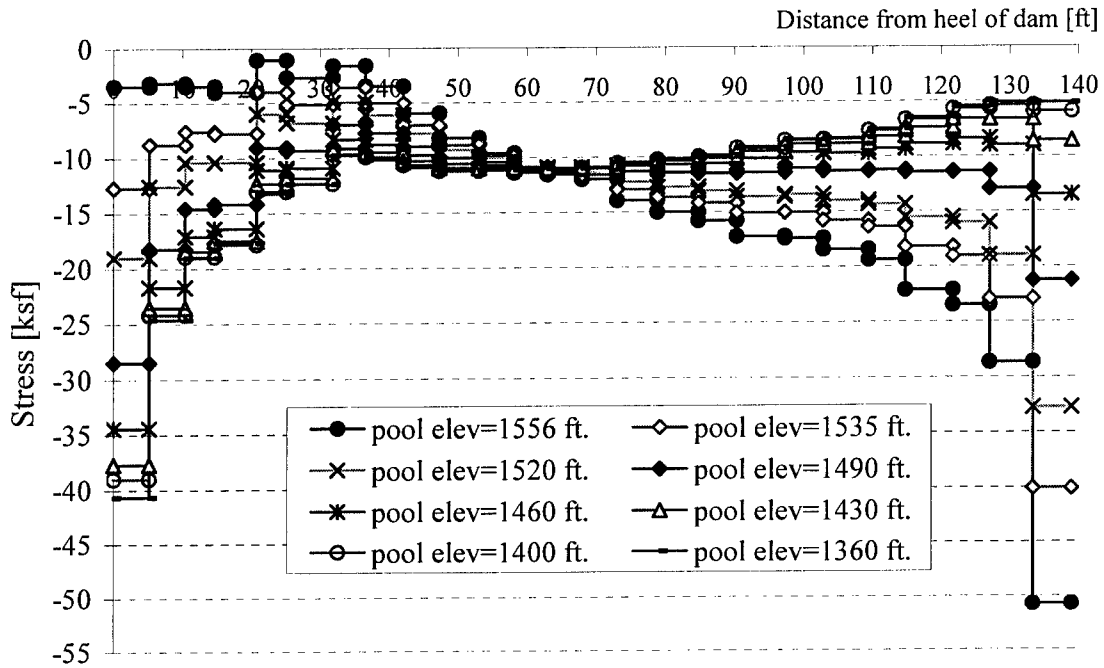


Fig. 4.11. Normal stress distribution at the base of dam, with modified modulus of elasticity

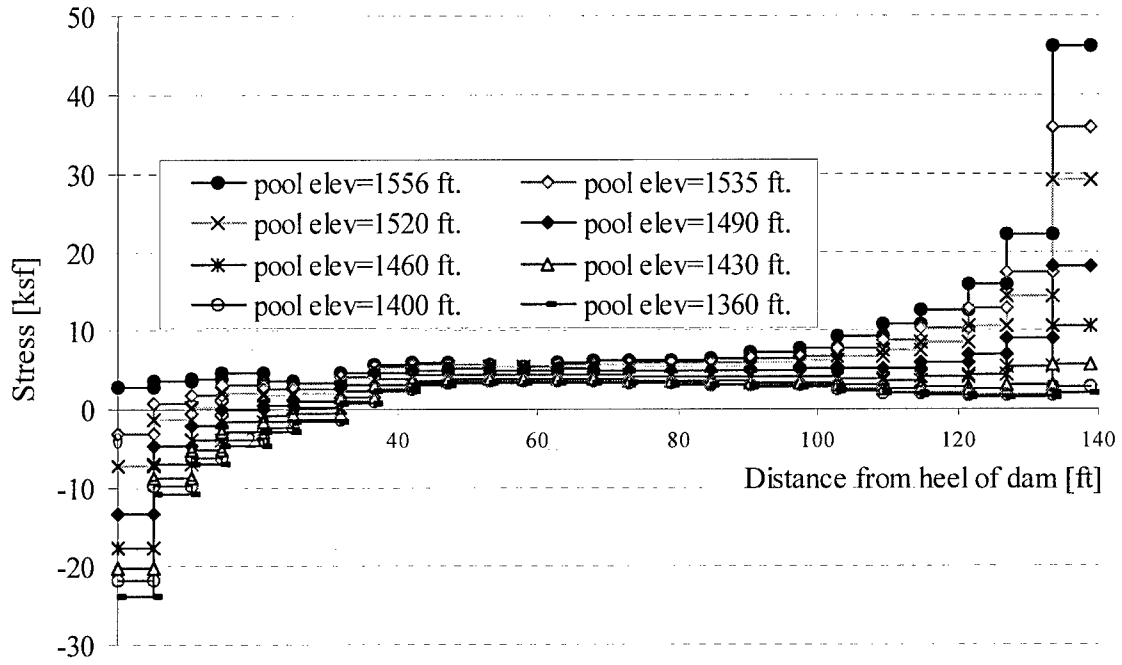


Fig. 4.12. Shear stress distribution at base of dam, with modified modulus of elasticity

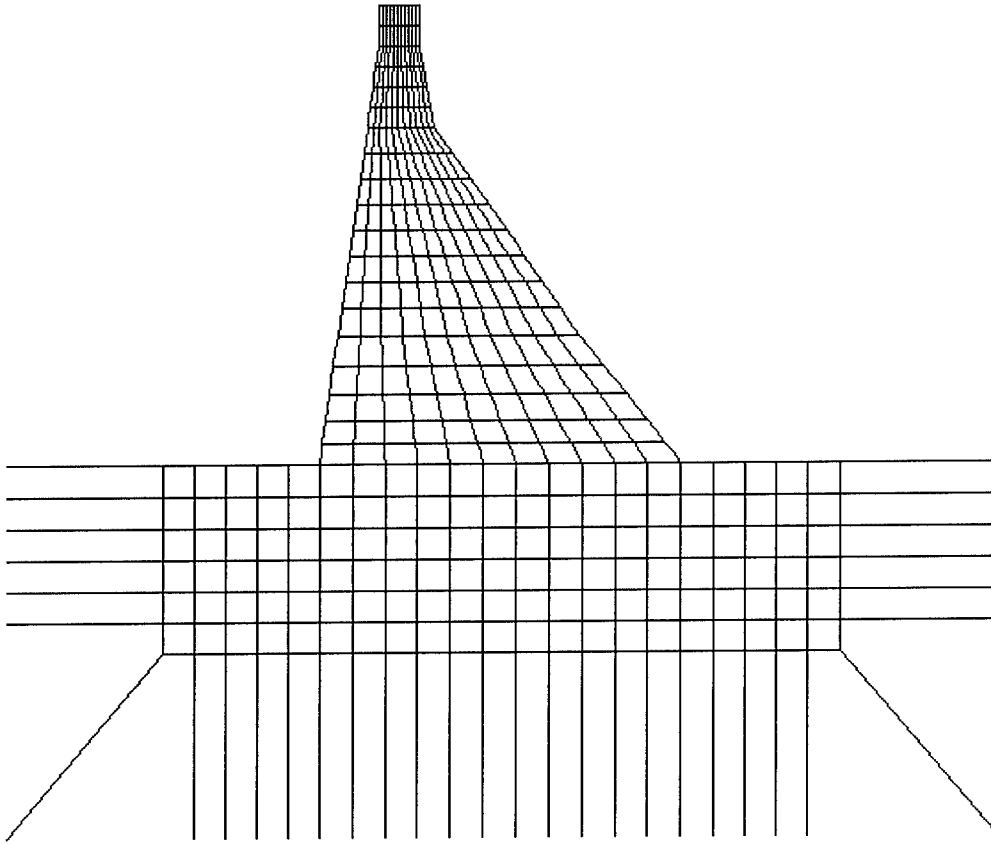


Fig. 4.13. Nonlinear FE model of Bluestone monolith no. 12

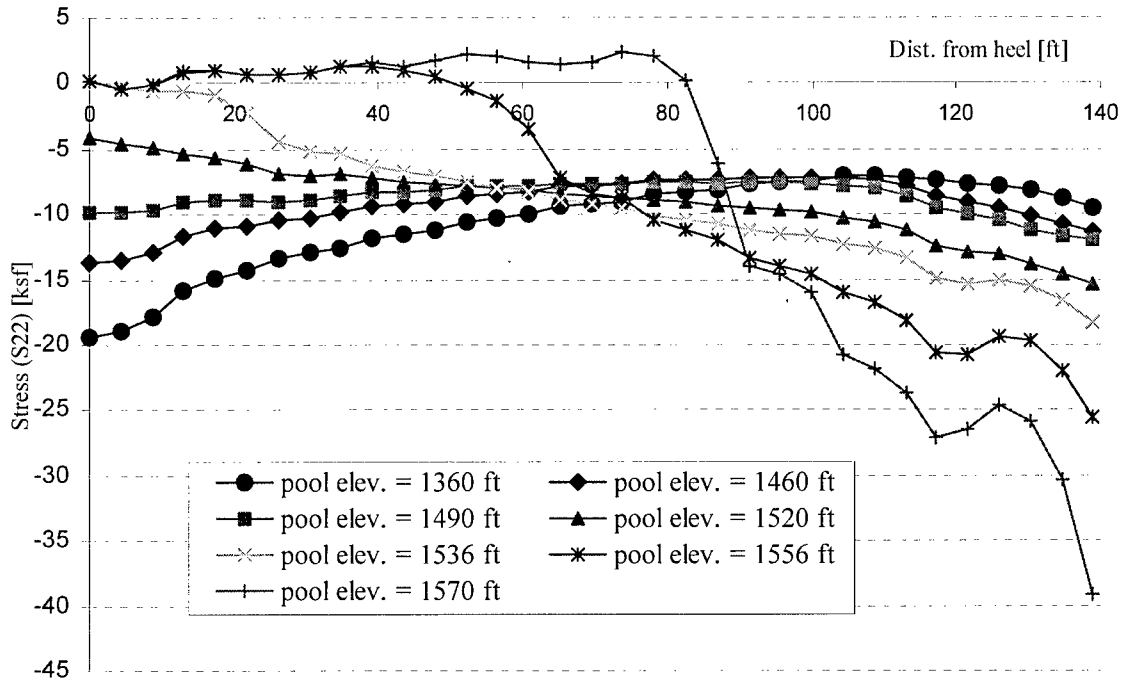
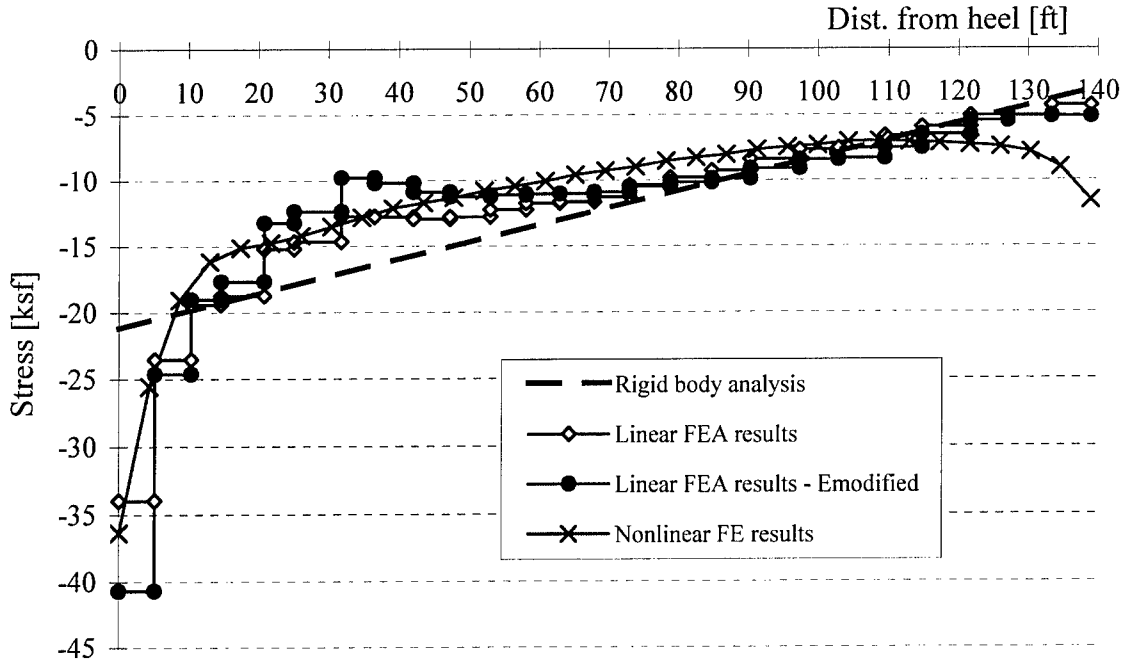
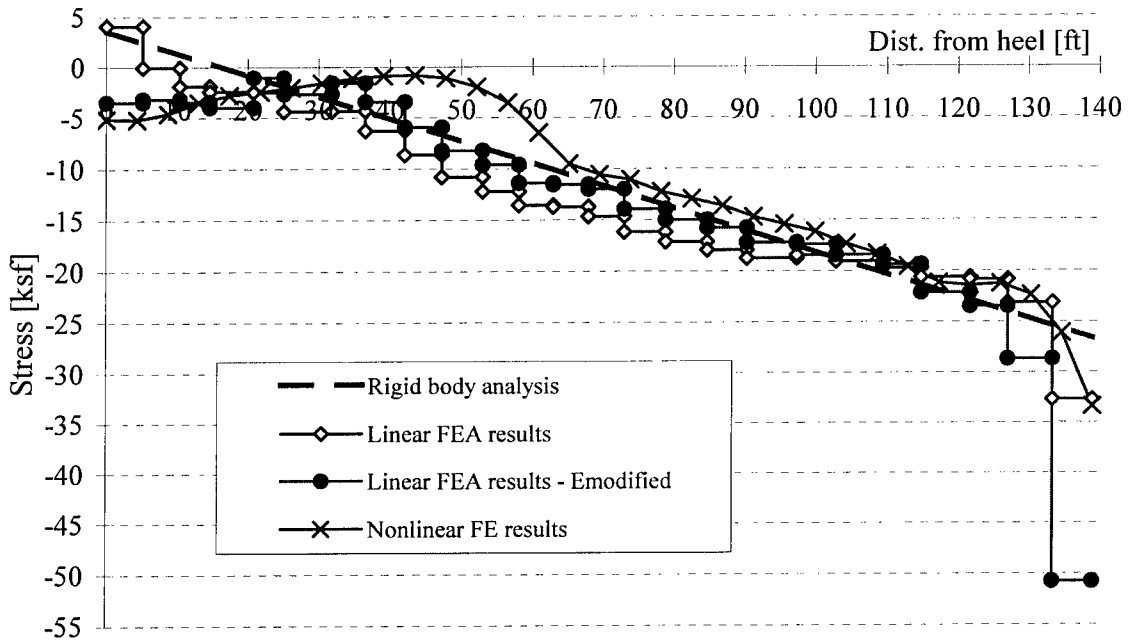


Fig. 4.14. Normal stress distribution at the base of dam



a) Pool elevation of 1360 ft (415 m)



b) Pool elevation of 1556 ft (474 m)

Fig. 4.15. Comparison of normal stresses at base of dam

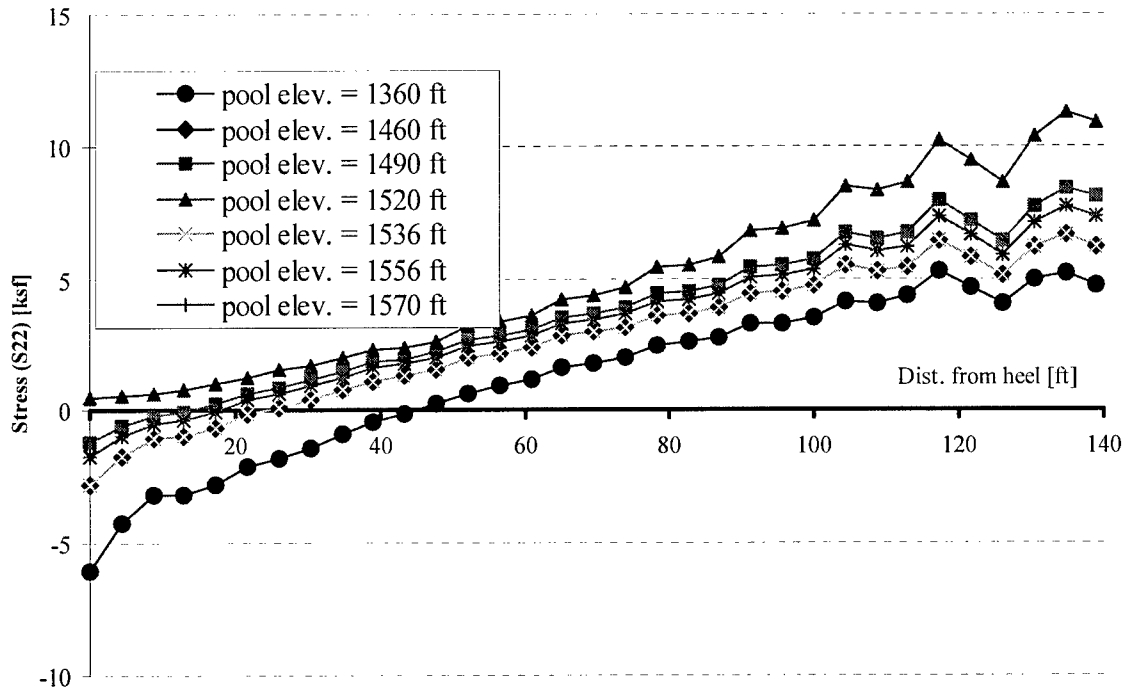
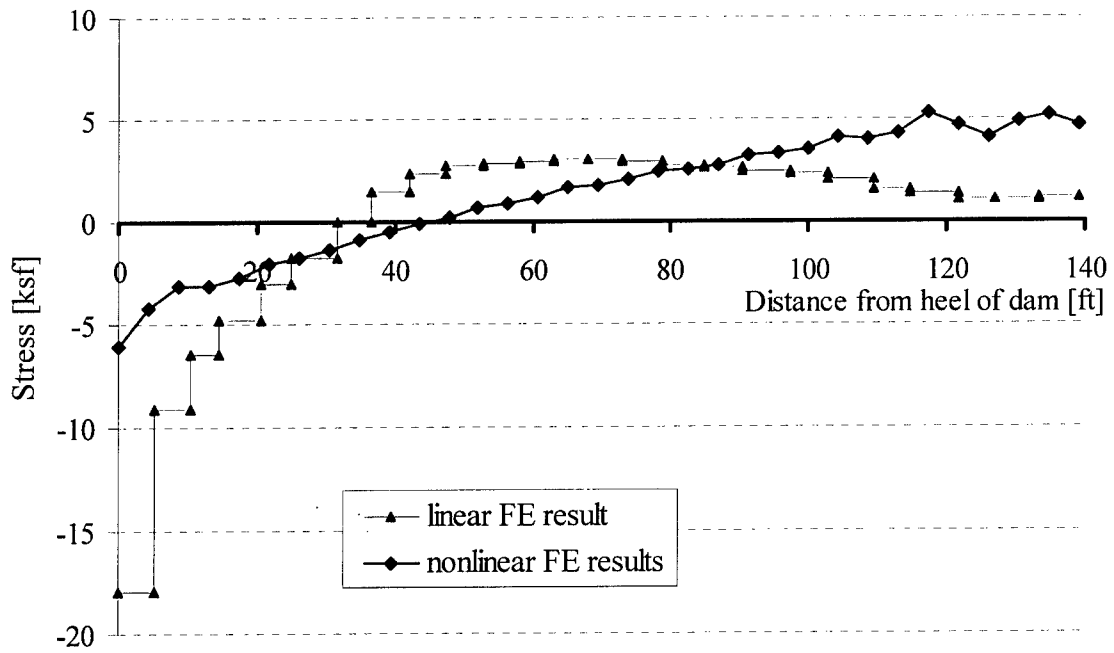
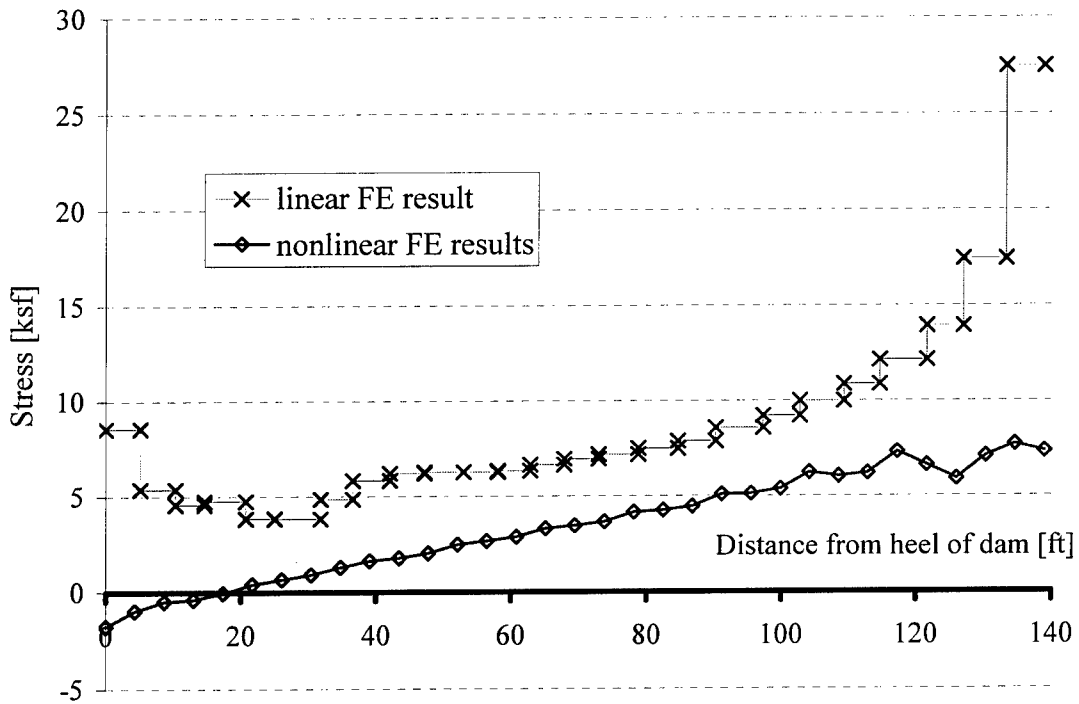


Fig. 4.16. Shear stress distribution at base of dam



a) Pool elevation of 1360 ft (415 m)



b) Pool elevation of 1556 ft (474 m)

Fig. 4.17. Comparison of shear stresses at base of dam

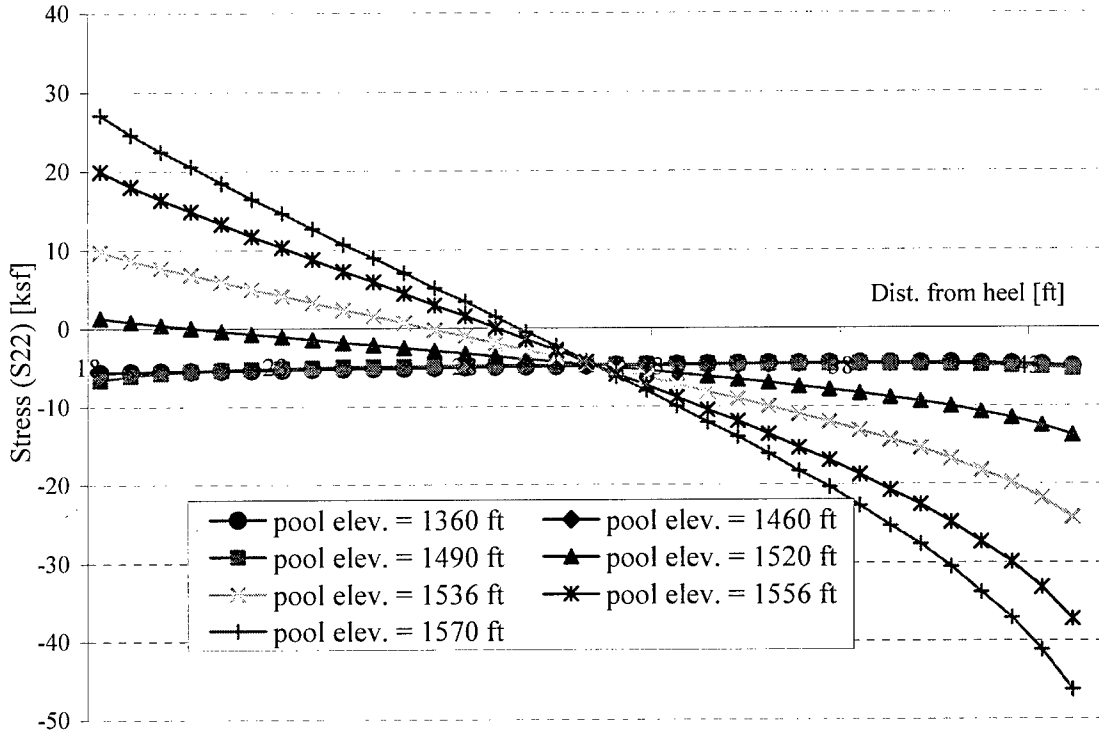
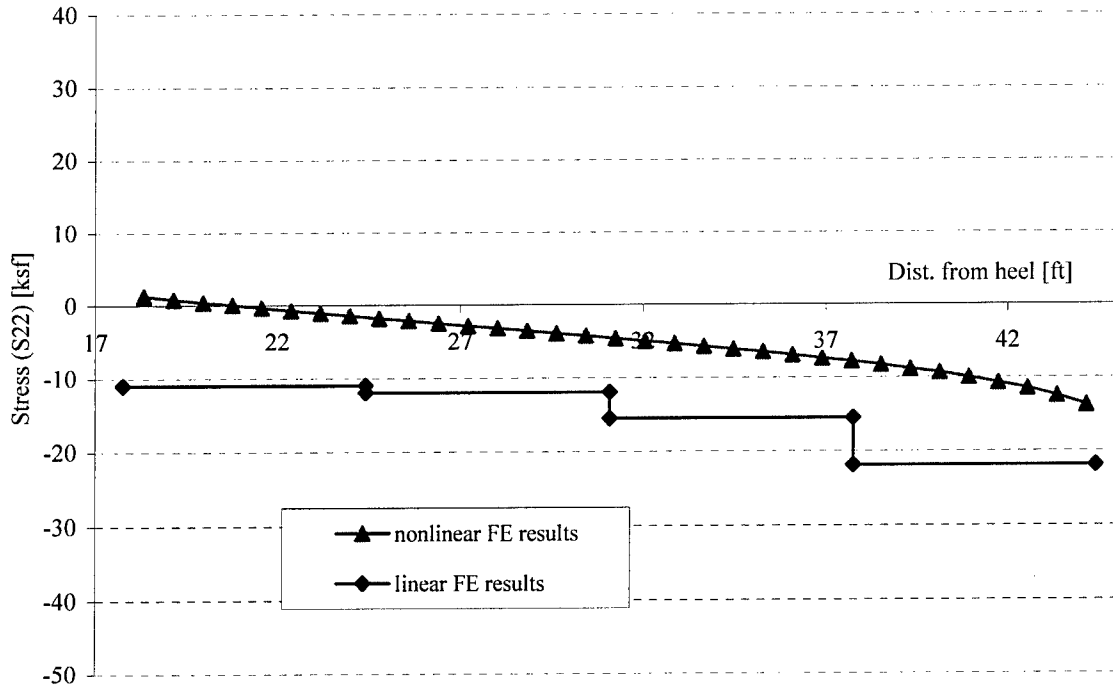
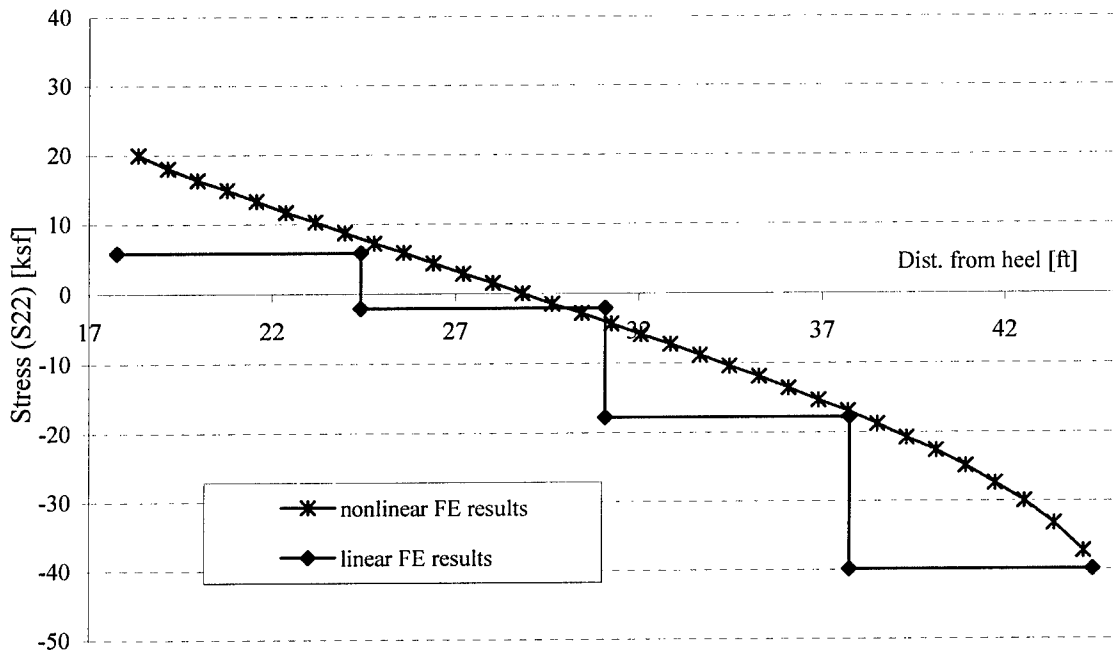


Fig. 4.18. Normal stress distribution at the neck of dam



a) Pool elevation of 1360 ft (415 m)



b) Pool elevation of 1556 ft (474 m)

Fig. 4.19. Comparison of normal stresses at neck of dam

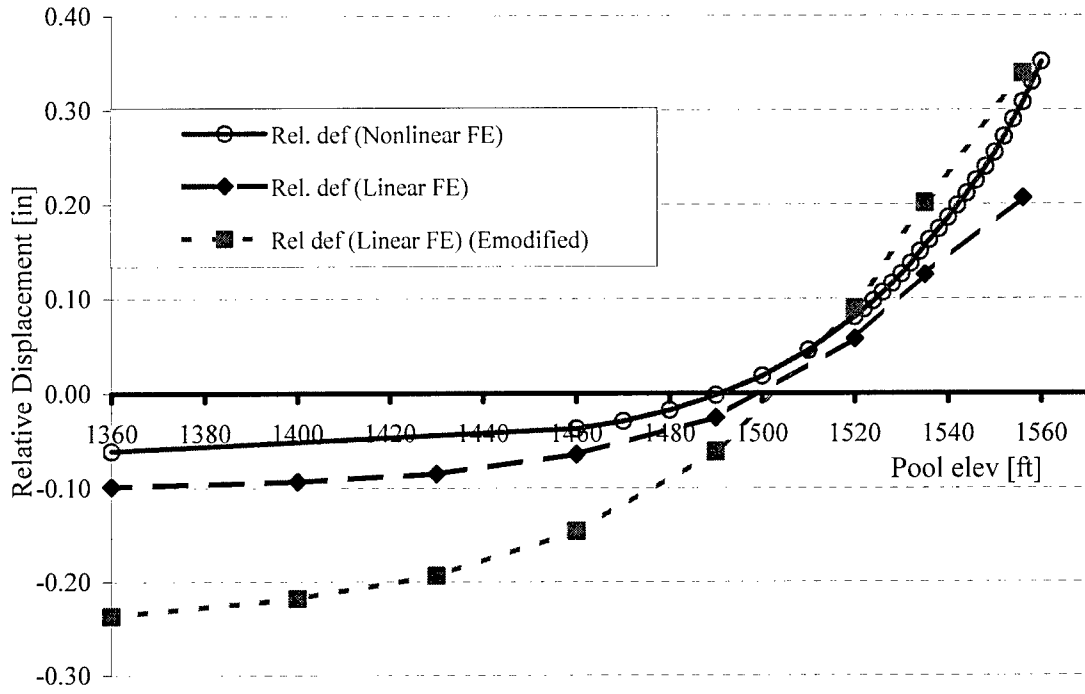


Fig. 4.20. Relative deformation of top of dam

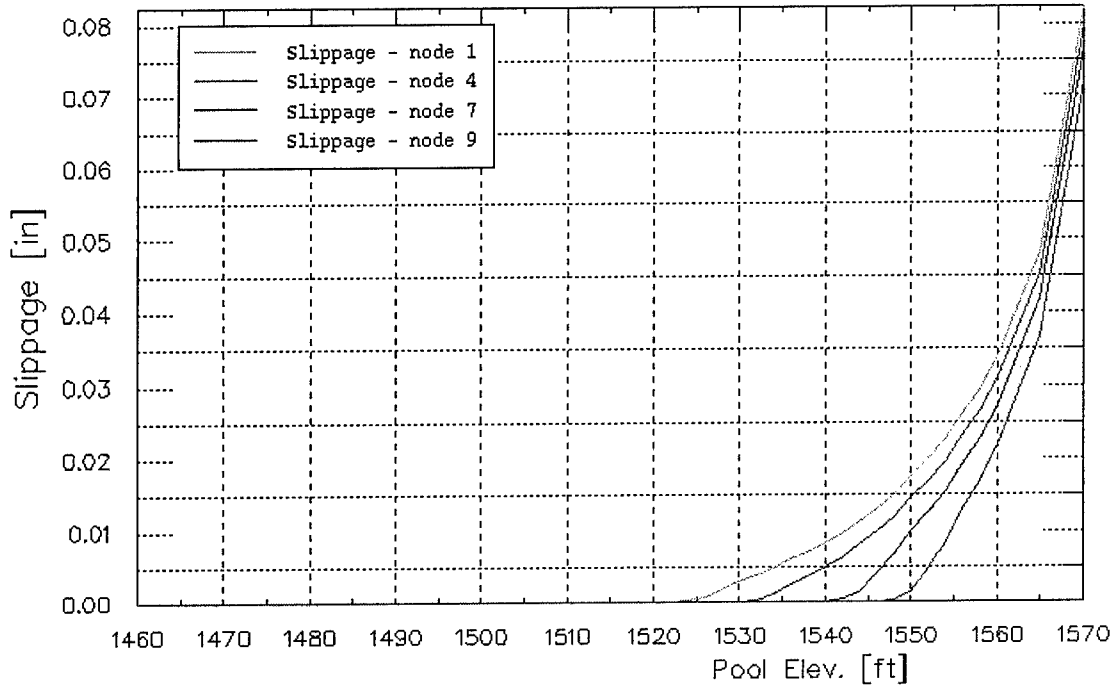


Fig. 4.21. Sliding response at the interface around the heel

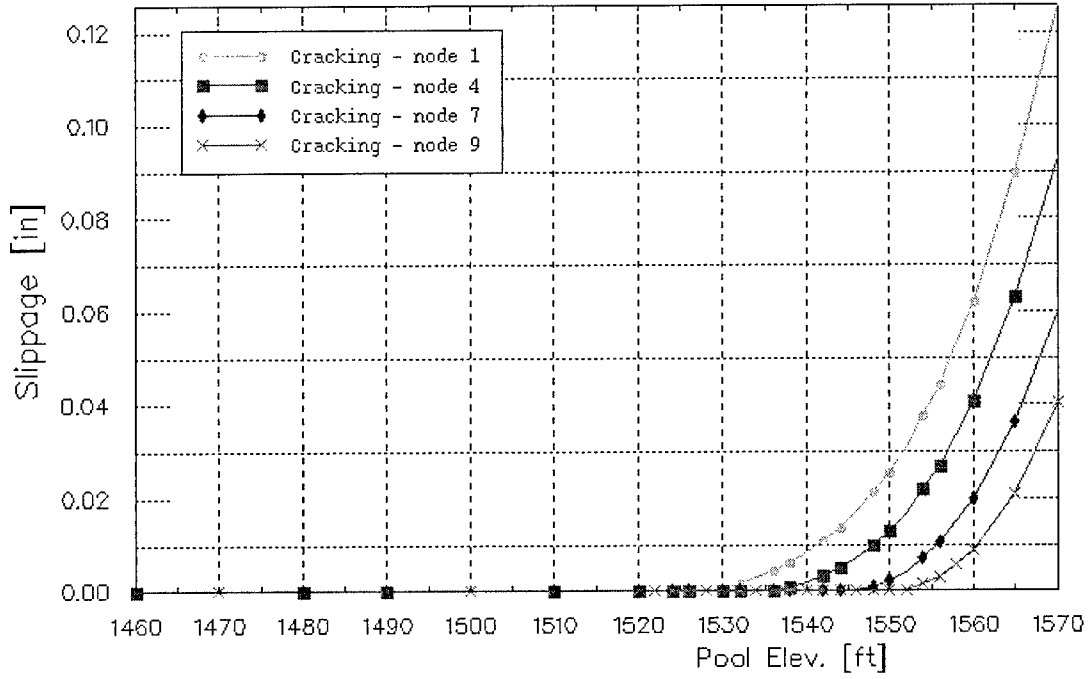


Fig. 4.22. Cracking at the interface around the heel

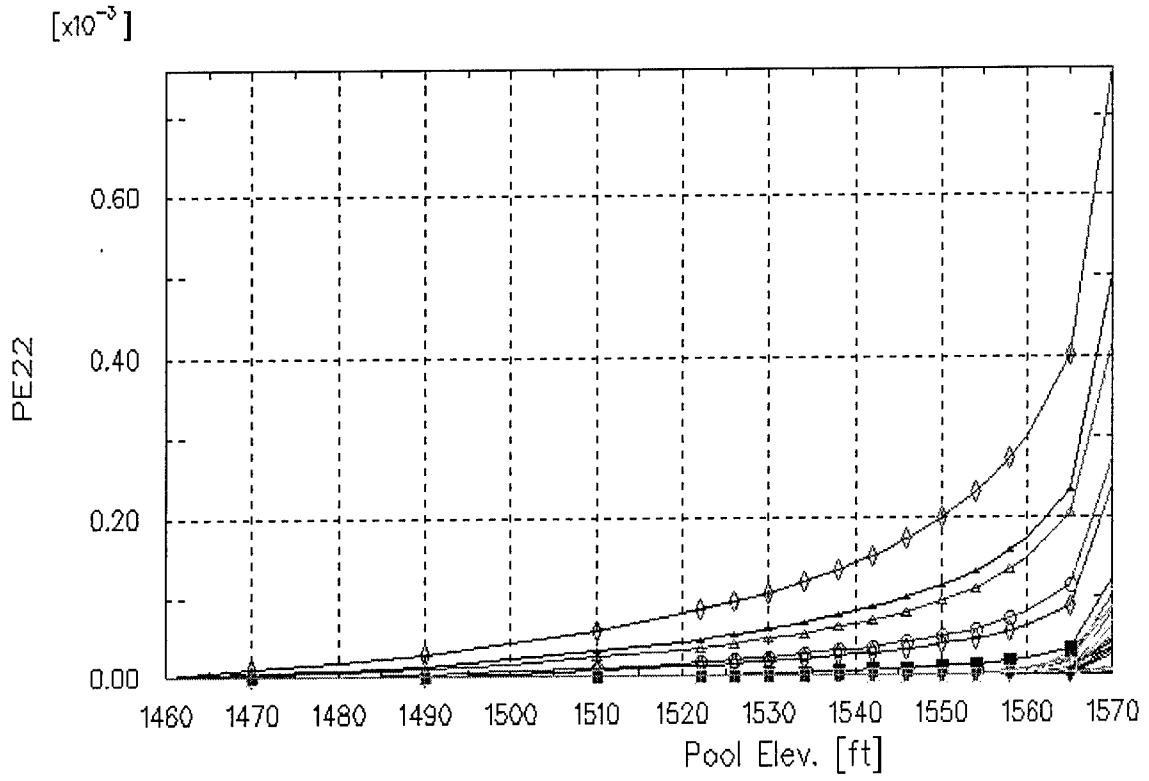


Fig. 4.23. Plastic strain (in vertical direction) in foundation, near the toe of dam

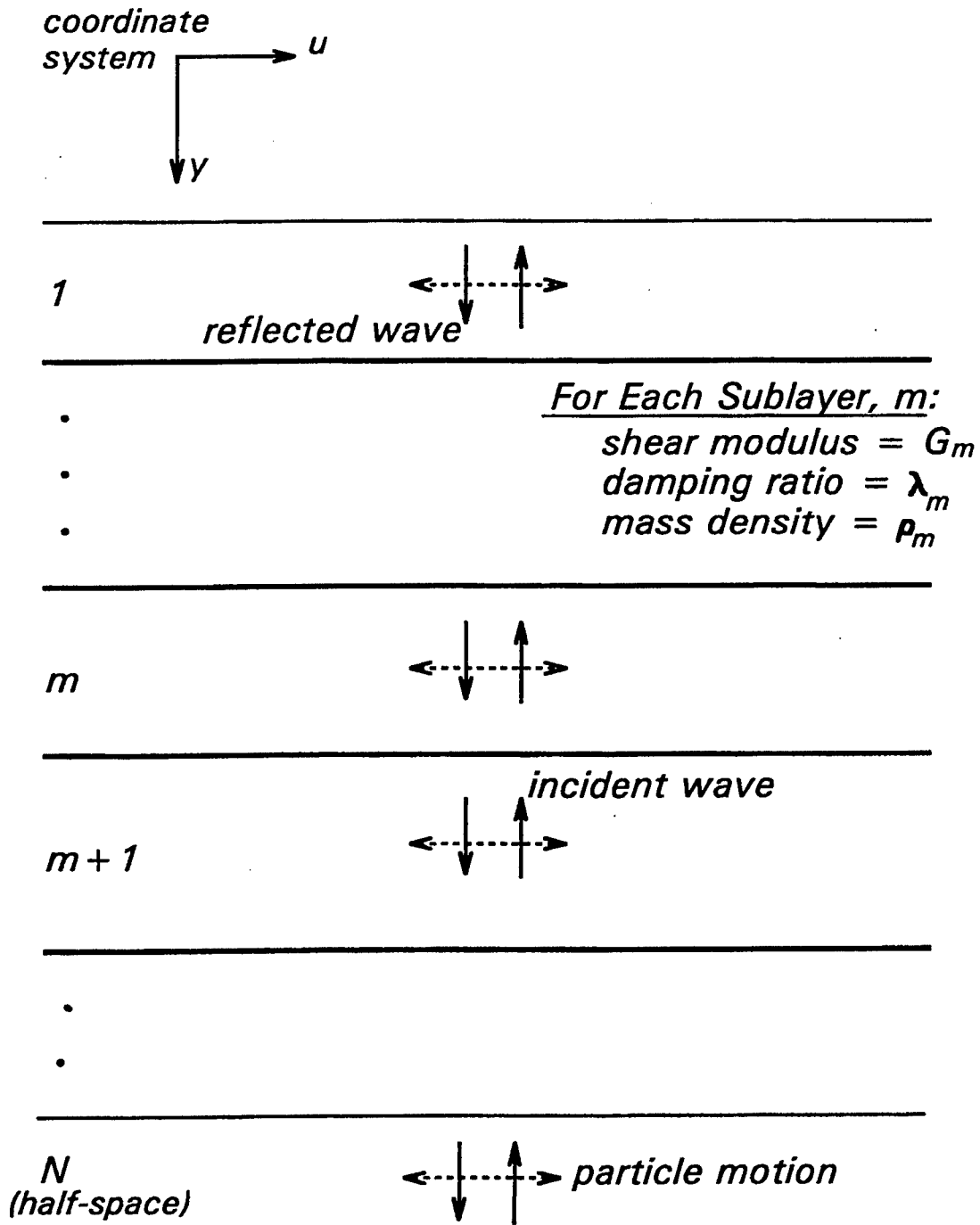


Fig. 4.24. One-dimensional idealization of a horizontally layered soil deposit over a uniform half-space (Idriss and Sun, 1992)

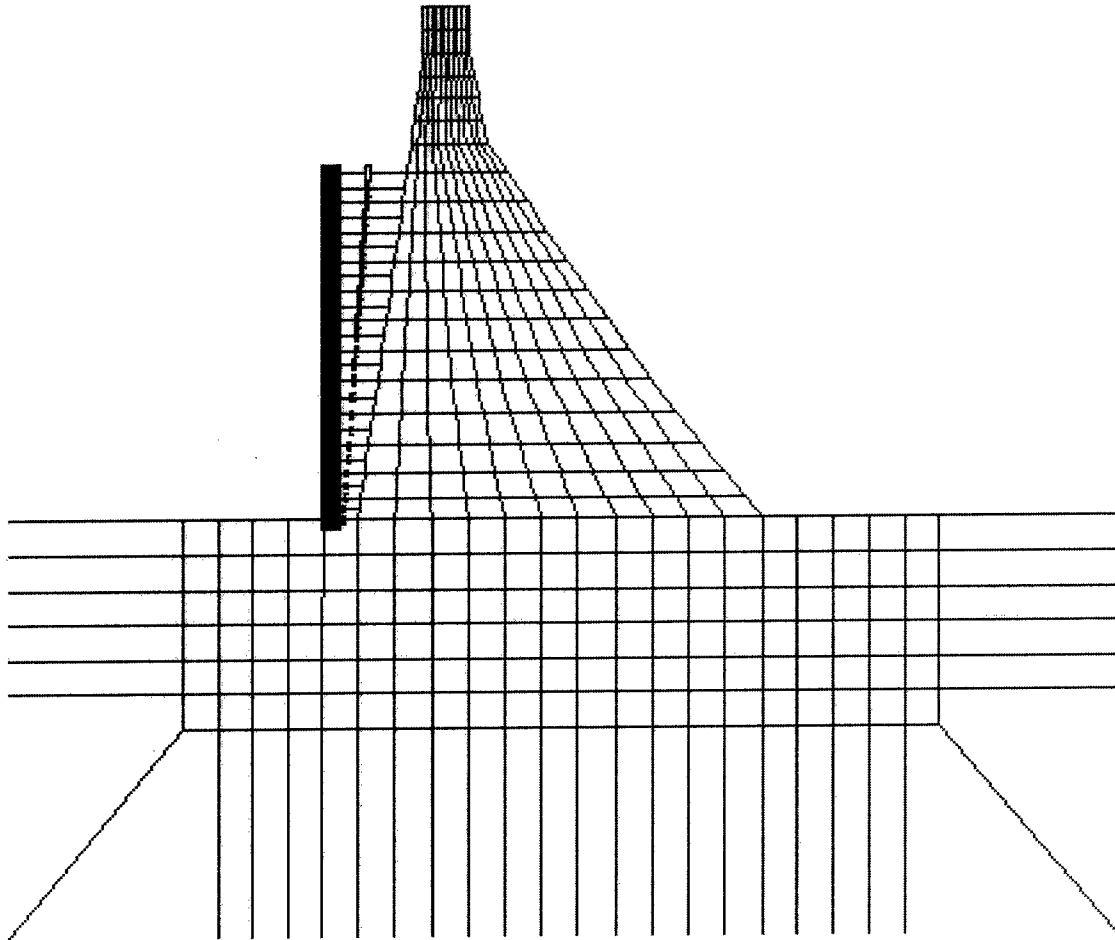


Fig. 4.25. Nonlinear FE model of monolith no. 12 – seismic

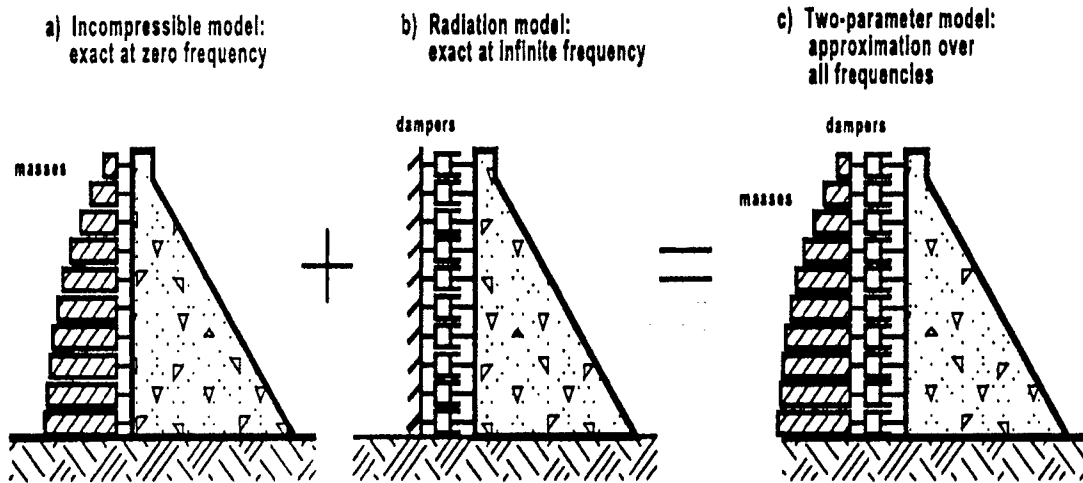


Fig. 4.26. Construction of the two-parameter model (Darbre, 1998)

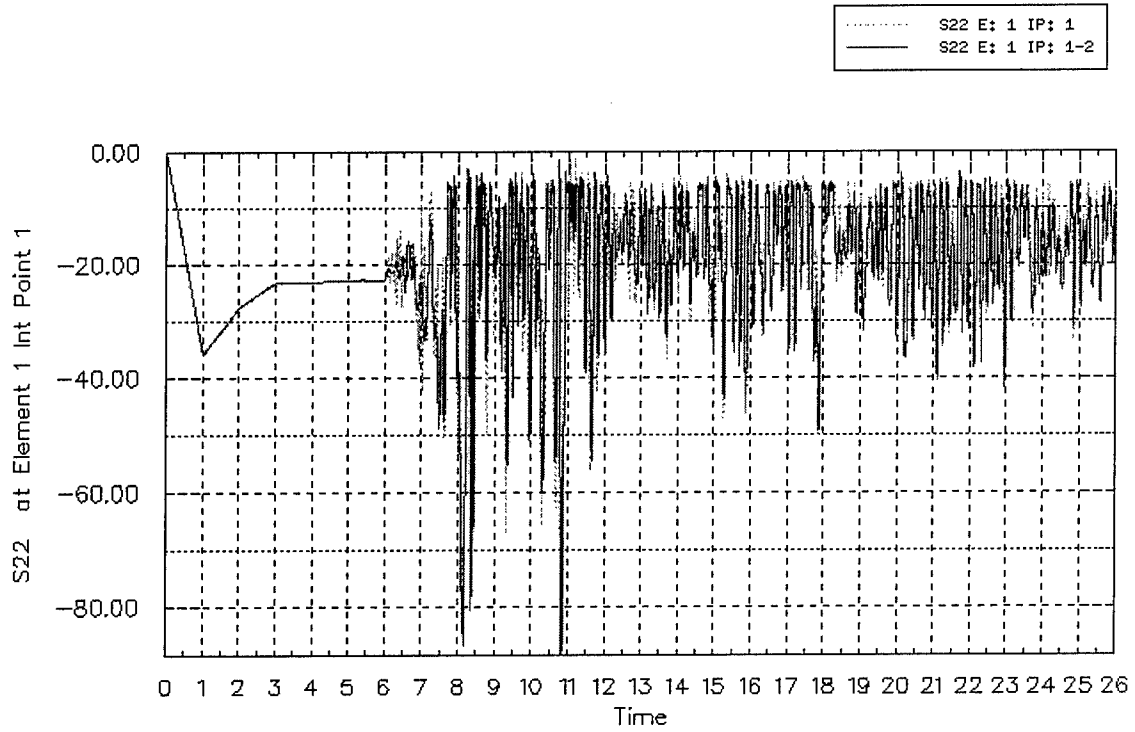
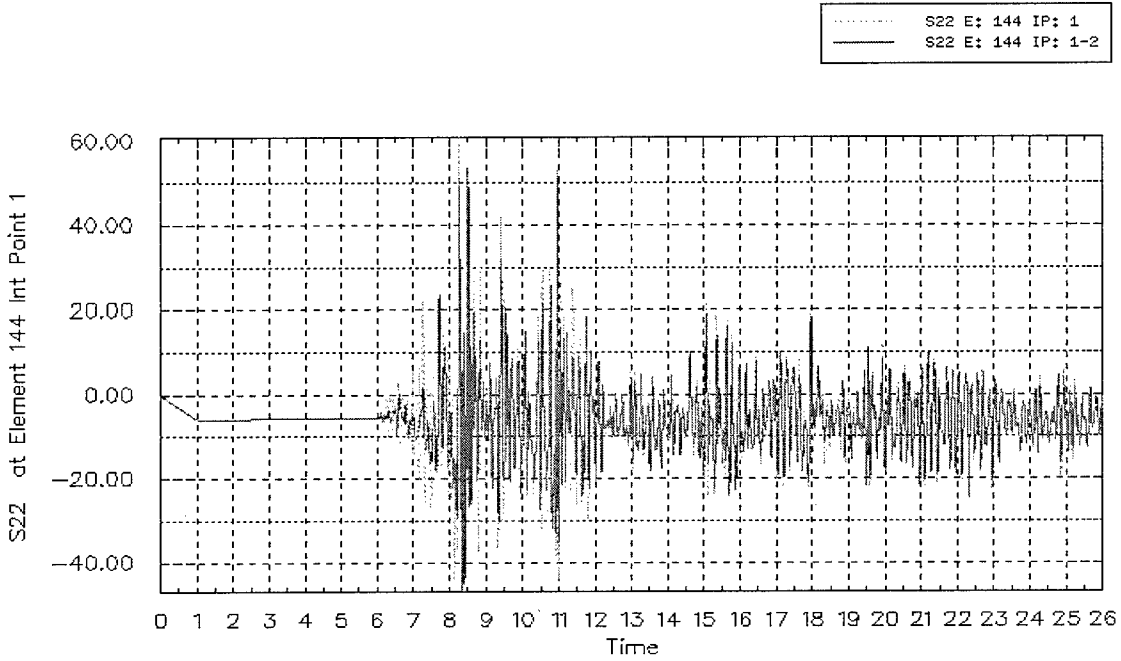
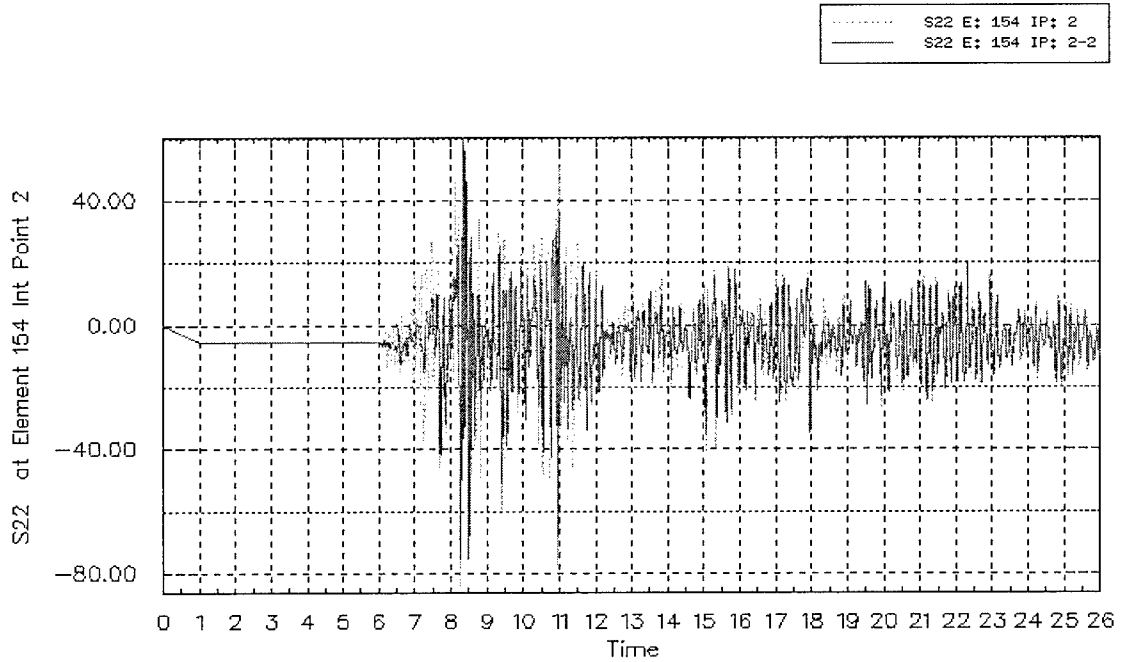


Fig. 4.27. Normal Stress (S22) [ksf] at the heel; El-Centro scaled to $S_a = 0.9g$
(With and without vertical component)



a) Upstream side of the neck



b) Downstream side of the neck

Fig. 4.28. Normal stress [ksf] at neck of dam; El-Centro scaled to $S_a = 0.9g$
 (With and without vertical component)

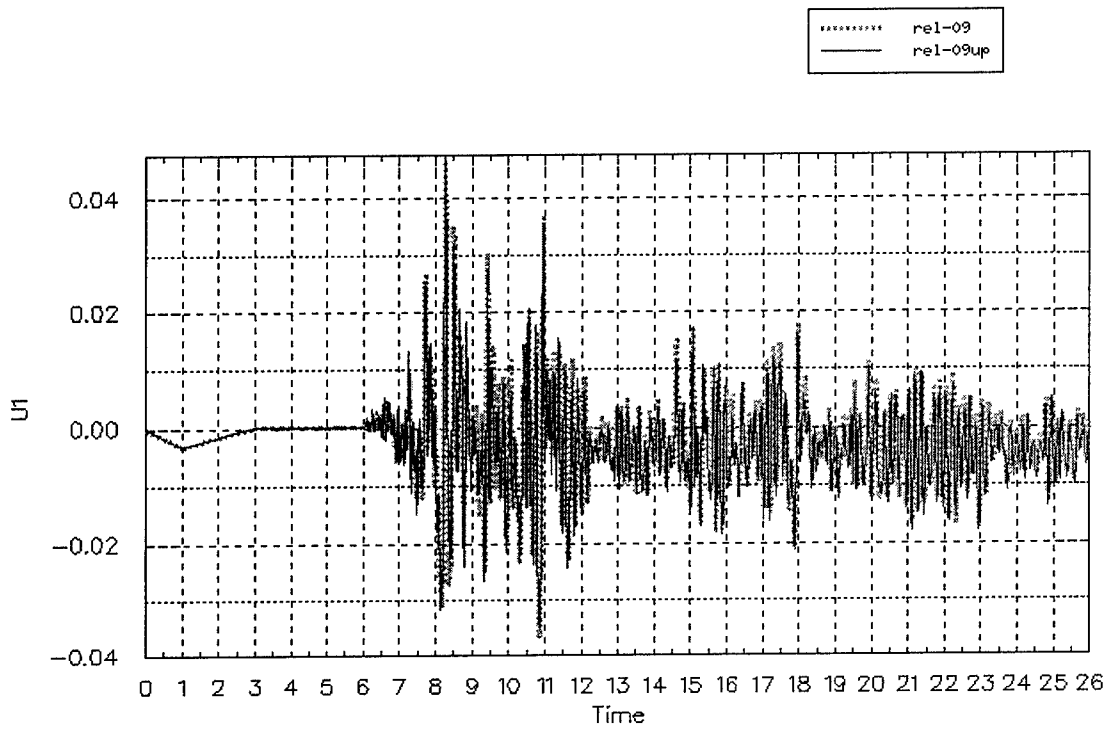


Fig. 4.29. Relative deformation [ft] of top of dam; El-Centro scaled to $S_a = 0.9g$
(With and without vertical component)

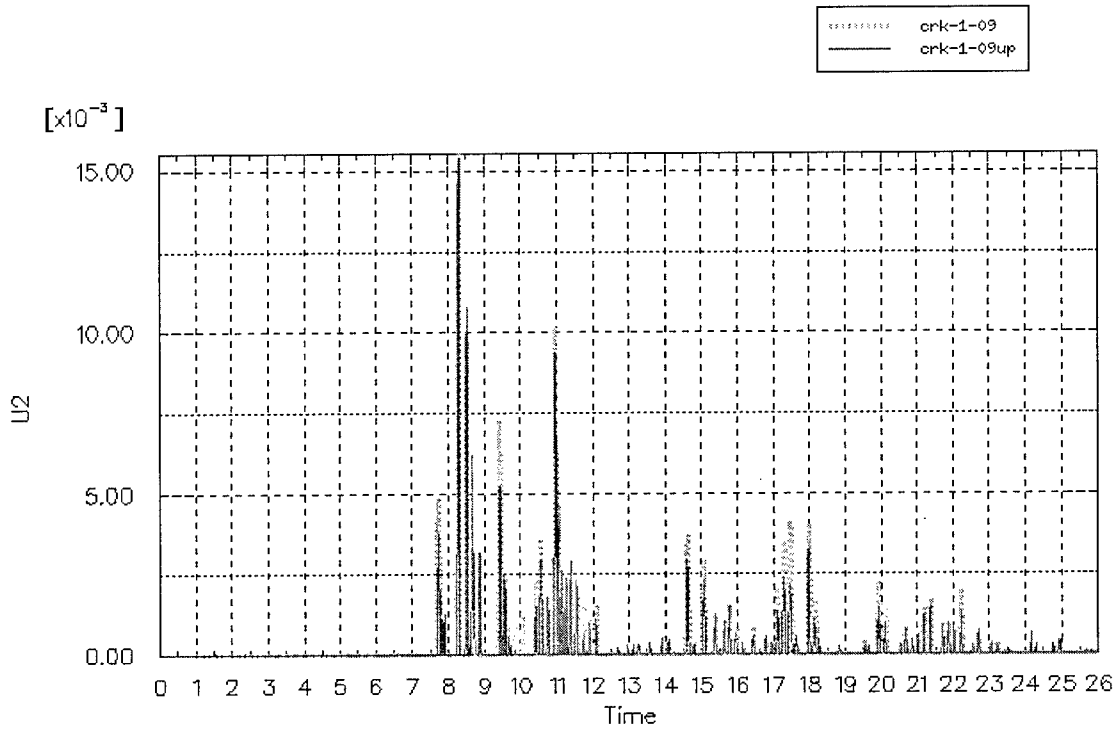


Fig. 4.30. Cracking [ft] at the heel of dam; El-Centro scaled to $S_a = 0.9g$
 (With and without vertical component)

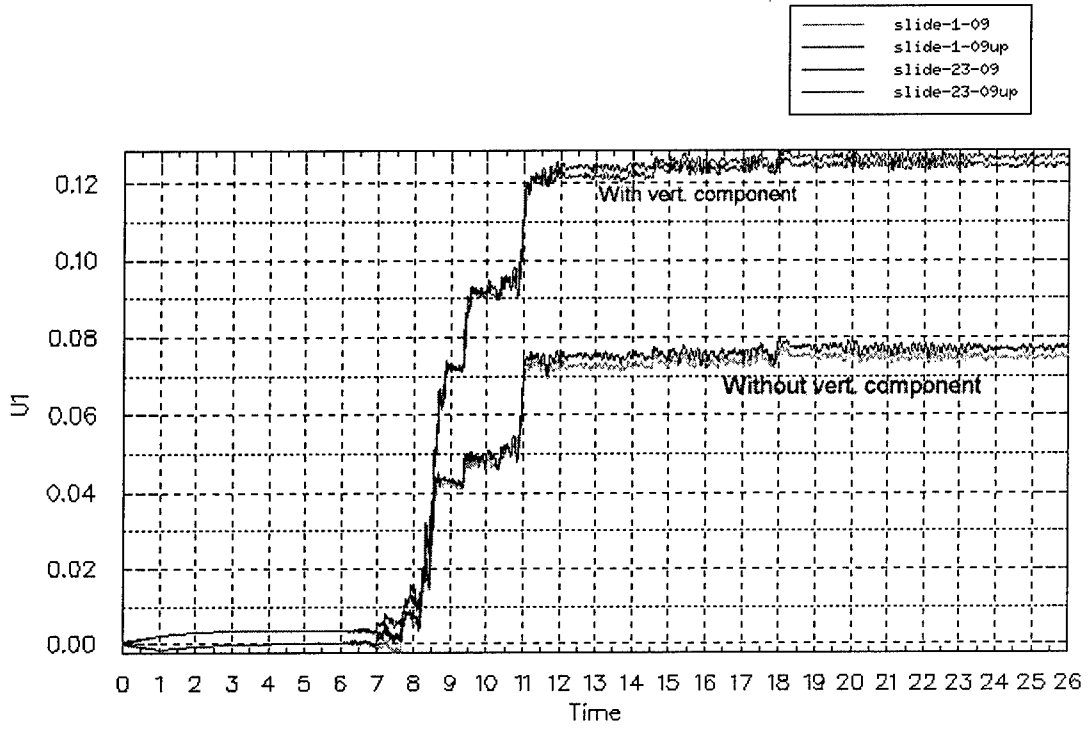
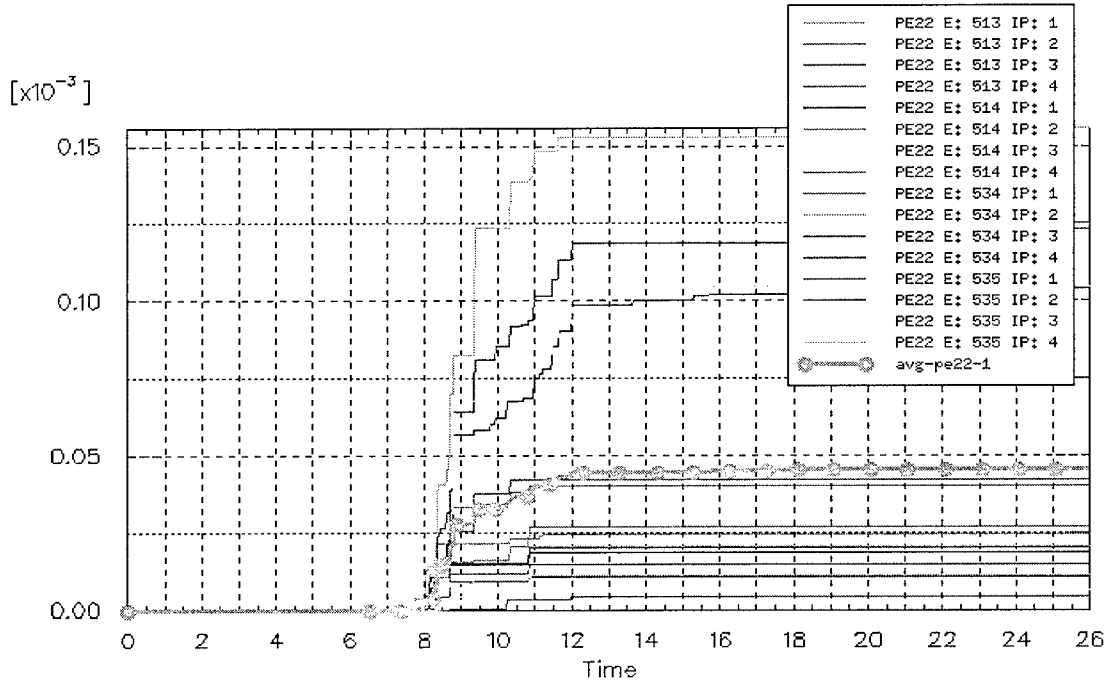
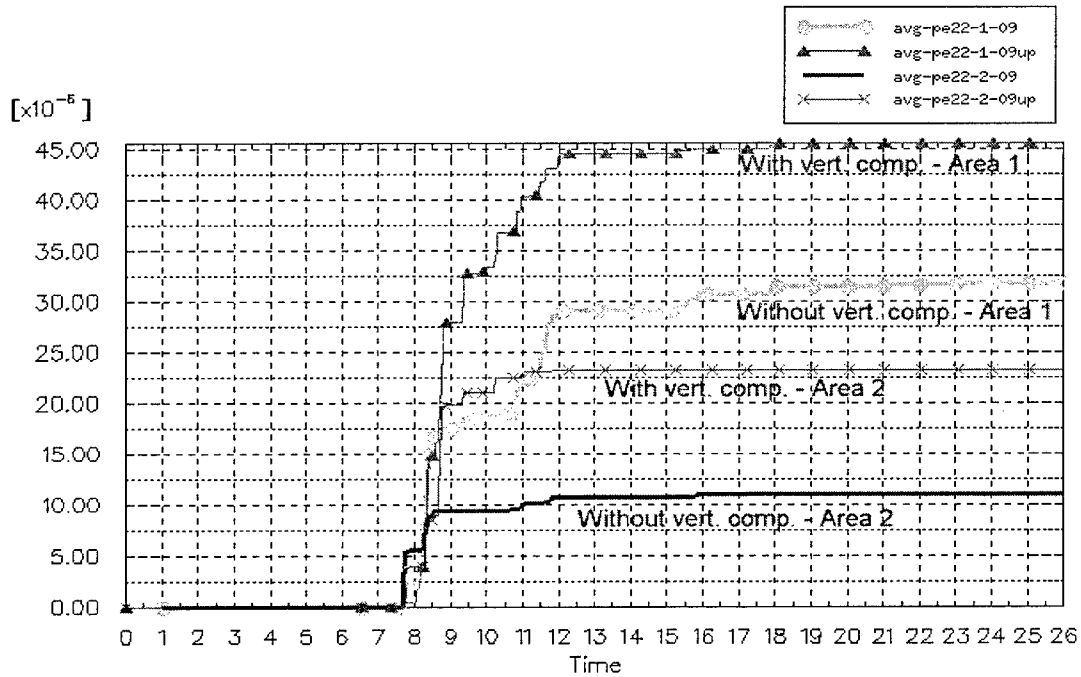


Fig. 4.31. Sliding [ft] at the interface of dam; El-Centro scaled to $S_a = 0.9g$
 (With and without vertical component)



a) Plastic strains at points in foundation (Area 1)



b) Area-averaged plastic strains

Fig. 4.32. Plastic strain in foundation - toe of dam; El-Centro scaled to $S_a = 0.9g$
(With and without vertical component)

Chapter 5

FRAGILITY MODELING

5.1. PROBABILISTIC SAFETY ASSESSMENT

Probabilistic safety assessment (PSA) provides the framework for rational decision-making and management of risk in facilities and/or systems. It can be used to study the viability of a new/ proposed system or the continuing viability of an existing system (Stewart and Melchers, 1997). A system is designed to resist loads and/or demands that are placed on it economically and with an acceptable level of safety. A safety assessment must consider the uncertainties in the demand/ loads and in the resistance of the system, the probabilities of failure to achieve its objectives or to fulfill its requirements, and the consequence(s) of failure. A PSA would enable the Corps of Engineers to devise policies for dam risk mitigation based on likelihood of hazard occurrence, facility safety and performance goals, and project economics, and to explore the expected cost/benefit of designing or retrofitting to achieve different performance levels. Moreover, insights and perspectives are provided on the complexity of dam safety assurance that cannot be obtained through deterministic extreme-event types of analyses alone.

The demands on concrete gravity dams have been presented in Chapter 3.

Similarly, Chapter 4 described the structural behavior of concrete gravity dams subjected to these demands. This chapter is concerned with the assessment of the probabilities of achieving (or failing to achieve) specific performance goals (limit states). The consideration of the consequence(s) of failure involves socioeconomic issues that are beyond the scope of the scope of this study.

In safety or risk assessment of dams, several progressively more severe performance or limit states (*LS*) may be of interest (See Chapter 2). These limit states serve as yardsticks of system performance. Each limit state probability can be expressed as,

$$P [LS] = \sum_y P [LS | Y = y] P [Y = y] \quad (5.1)$$

in which *Y* is a vector of random variables describing the intensity of demand (e.g., reservoir inflow, pool elevation, spectral acceleration of earthquake ground motion, etc.) and other factors, $P[Y = y]$ = hazard, expressed in terms of annual probability, and $P[LS|Y = y]$ = conditional probability of structural failure, given that $Y = y$. This conditional probability of failure is denoted the “fragility”, as described subsequently. Expressing the limit state probability as in Eqn. 5.1 allows the overall risk to be deconstructed into its significant contributors. It is important to note that it is the demand vector that interfaces or couples the hazard and the fragility assessments, which usually are performed independently by different specialists in a system PSA.

Risk assessment, at any level, requires a thorough understanding of how the facility responds as a system to challenges due to operation, the environment, and extreme demands (Whitman, 1984). Detailed understanding of the dam-foundation system and its representation in a logical fashion is required for use in quantitative probabilistic analysis.

An event tree provides a useful graphical tool for visualizing the logic underlying the operation and performance of a complex system. The event tree represents a sequential order in which events occur, each event being described probabilistically. The importance of all components acting in an integrated fashion in a risk assessment is emphasized. Fig. 5.1.a depicts a simple event tree model of a typical concrete gravity dam-reservoir system subjected to hydrologic events. Reading from the left, the performance of the dam-reservoir system, given a specific inflow, q_{in} , depends on the elevation of the gates, whether the sluices are open, the degree to which the penstocks are open, the effectiveness of the drains and ground curtain, tail water elevation, and effective uplift area at the dam-foundation interface. (Climatology and estimation of extreme precipitation and flooding results must precede the determination of q_{in} , as shown in Fig. 5.1.b) With the assignment of probabilities to all outcomes of each node, the probability of any branch in the tree or limit state of interest (which may involve several branches in the tree) can be computed. The part of the event tree involving structural failure of the dam due to hydrologic events and their consequences, as indicated in Fig. 5.1.a, uses the pool elevation as the demand parameter. Analysis of this part of the tree requires that the probability that the dam reaches any one of several limit states (LS) be computed, conditioned on the occurrence of specific values of reservoir pool elevation. In turn, these limit states can be associated with different consequences and maintenance decisions.

The event tree described in Fig. 5.1.a has been presented for illustrative purposes. The probabilities of limit states can be estimated with a much higher accuracy using more detailed descriptions and more rigorous propagation analysis of the uncertainties in the

dam-reservoir system, as will be described in subsequent sections in this chapter, where the focus is on the right hand side of Fig. 5.1.a.

5.2. FRAGILITY MODELING

Fragility analysis is a technique for assessing and displaying, in probabilistic terms, the capability of an engineered system to withstand a specified event (sometimes referred to as a review-level event), often one that is well in excess of the design-basis event. A fragility takes the form of a conditional probability of failure, where the conditioning event is defined by the "control" or "demand" variable indicated on the horizontal axis. The control variable in the fragility must be described in units that are dimensionally consistent with the manner in which hazard is specified. In equation form,

$$\text{Fragility} = P[LS / Y = y, \theta] \quad (5.2)$$

in which $P[LS / Y = y, \theta]$ = conditional probability of limit state (*LS*), given demand y , and θ = vector of fragility parameters. With reference to Eqn 5.1, it can be seen that the fragility is an essential component of a fully coupled risk assessment in which a spectrum of hazards is considered probabilistically.

Fragility analysis of concrete gravity dams is an interdisciplinary endeavor that straddles broad fields of study, including rock mechanics, probability and statistics, earthquake engineering and numerical analysis. The first essential ingredient of a fragility analysis is the identification of all limit states relevant to system performance. These states serve as important performance milestones in the progression of structural response towards failure. They range from the essentially elastic to the nonlinear, inelastic response

states and finally to unstable structural behavior leading to loss of reservoir and downstream consequences. The second essential ingredient is a rational assessment of all sources of uncertainty likely to affect performance. These require a different way of thinking than is typical in customary design, where the emphasis often is on component rather than system behavior and where uncertainties are addressed indirectly with (deterministic) factors of safety or allowable stresses. Finally, computationally efficient tools are required to analyze system response and to compute the required probabilities.

The fragility analysis provides a framework for ensuring that available information on uncertainties is treated consistently. The process leading to the fragility model is transparent and provides an audit trail for decisions regarding safety of a facility. While a PSA is a fully coupled analysis, where both the hazard and the fragility are considered, in fragility assessment, full knowledge of the probabilistic nature of the hazard is not essential as the analysis is effectively uncoupled from the hazard. Once review level hazards are identified, the fragility analysis can give valuable insights into system performance and margins of safety. With proper construction and presentation, a fragility is more readily understood by non-expert personnel involved in the decision-making process. Furthermore, it avoids the interpretation and defense of small probabilities of failure (believed to be on the order of 10^{-4} or less, (National, 1985)) that are derived in a fully coupled PSA. There are limited data to support failure probability estimates of civil structures, and such estimates are highly dependent on the probabilistic models selected. At the current state-of-the-art, fragilities are more robust than limit state probabilities.

The fragility concept has found widespread usage in the nuclear power industry, where it has been used in seismic probabilistic safety and/or margin assessments of

safety-related plant systems (Kennedy and Ravindra, 1984, Ellingwood, 1990, 1994a, 1994b). These fragilities have been determined in a variety of ways: simple heuristics, scaling upward from design calculations, and (rarely) stochastic nonlinear finite element analysis. However, only during the past decade has probabilistic safety assessment begun to emerge as a tool in dam safety decision-making (Bury and Kreuzer, 1985, 1986; Ellingwood, 1995; Hartford and Salmon, 1997).

There are two major natural hazards affecting concrete gravity dams in the United States: extreme hydrologic events and earthquakes. A hydrologic fragility of a concrete gravity dam displays the probability that the dam reaches a limit state (LS) of performance, conditioned on the occurrence of a particular value, y , of some random demand, Y (Eqn. 5.2). The control variable, y , in the hazard must be described in units that are dimensionally consistent with the hazard specified by the hydrologist: reservoir inflow, peak flood elevation at the dam, or other control variable. In a seismic fragility, the demand variable usually is the effective peak ground acceleration or spectral acceleration at the fundamental period of the structure. Thus, the seismic fragility expresses the conditional probability of failure for specific levels of spectral acceleration identified by the facility owner or regulator. An illustration of fragilities for progressively more severe performance/ limit states is presented in Fig. 5.2. In many previous studies, a lognormal (LN) distribution has been postulated for such fragilities (e.g. Kennedy and Ravindra, 1984, Ellingwood, 1990).

All sources of uncertainties believed to affect the performance of the dam should be included in the fragility assessment. Some of these uncertainties are aleatory (inherent) in nature. These inherent uncertainties are not altered in a significant way with increasing sample sizes, though the estimates of the parameters describing the CDF generally stabilize

as sample size increases. In the case of concrete gravity dams, aleatory uncertainties include material properties (concrete, soil and rock), and the natural hazards (precipitation, flood stages and earthquake occurrence and intensity measures).

Other uncertainties are knowledge-based (or epistemic), arising from assumptions made in the analysis of the system and limitations in the supporting databases. In contrast to aleatory uncertainties, these knowledge-based (or epistemic) uncertainties depend on the quality of the analysis and supporting databases and generally can be reduced, at the expense of more comprehensive (and costly) analysis. In the fragility assessment of concrete gravity dams, epistemic uncertainties would include two-dimensional models of dam monoliths used to predict three-dimensional behavior of the dam system, identification of hazard scenarios, and limitations in the data imposed by climatological modeling, short historical records, incomplete foundation/subsurface exploration and other factors.

Frequently, one overall estimate of fragility that reflects both aleatory and epistemic uncertainties in the capacity of the dam/ foundation as a structural system is developed. Such an estimate is provided by the mean fragility, defined to first order as (Ellingwood, 1994a),

$$E [F_R(y)] = \Phi \left[\frac{\ln (y/m_R)}{\beta_C} \right] \quad (5.3)$$

in which $\Phi[]$ = standard normal probability integral, m_R = median capacity (expressed in units that are dimensionally consistent with the demand parameter, y) and β_C , the "combined" uncertainty is,

$$\beta_C = \sqrt{\beta_R^2 + \beta_U^2} \quad (5.4)$$

where: β_R = logarithmic standard deviation describing the epistemic uncertainty, and

β_U = logarithmic standard deviation describing the inherent (aleatory) uncertainty.

In some fragility analyses, it has been customary to determine β_R from supporting databases and to assign β_U based on expert opinion, often expressed by a peer review panel (McCann, et al, 1985). In other cases where data are extremely limited, however, the combined measure, β_C , often is reported directly, with no attempt to distinguish between β_R and β_U . The latter approach is followed herein.

The overall uncertainty in capacity also can be displayed by the family of lognormal CDF's illustrated in Fig. 5.3, defined by parameters (m_R , β_U , β_R). This family can reflect incomplete knowledge regarding the parameters used to estimate the median and the coefficient of variation (or logarithmic standard deviation). Curves 1 through 5, in which the epistemic uncertainties are assumed to affect only the median capacity of the system, are constructed with the median, m_R , fixed with ranges from the 5th to 95th percentile. These curves represent states of perfect knowledge, since the aleatory uncertainties alone are considered. Note that the mean fragility (curve 6, obtained from Eqn 5.3), which includes both the aleatory and epistemic uncertainties, exhibits a larger dispersion than the median fragility (curve 3). It is possible to include different probabilistic models in displays of epistemic uncertainties such the those in Fig. 5.3, but few studies have done so because the level of supporting data required is of higher order.

A clear understanding of the mechanics of dam performance and identification of limit states is required to devise the computational platforms that support the uncertainty analysis and propagation (Ellingwood, 1994a). Furthermore, probabilistic models for the description of the various parameters that play significant roles in the safety assessment are

needed. Construction of fragilities for progressively more severe limit states or performance objectives (as shown in Fig. 5.2) portrays the robustness of dam performance subject to increasing hazard intensity. Policies and priorities for mitigation of such hazards can then be set up accordingly.

5.3. LIMIT STATES

Consistent with the earlier discussion of dam performance (Chapter 2), several limit states were considered in the rigid body, the linear and nonlinear FE analyses. The following limit states (LS) are confined to structural failure modes for Bluestone Dam (Appendix), and are used in both the hydrologic and seismic fragility analyses (cf. Chapter 2):

1. Resultant outside of kern (rigid body analysis) or tension at the heel (FEA),
2. Resultant outside of middle-half of base of dam,
3. Material failure – concrete (at the toe),
4. Material failure – concrete (at the neck of the dam),
5. Material failure – foundation (at the toe),
6. Sliding at the dam-foundation interface,
7. Deflection of the top of dam relative to heel

In current design practice, limit states 1 and 2 are taken as indications of the equilibrium status of the monolith. In the rigid body analysis, limit state 1 is achieved if eccentricity of the resultant vertical force, e , in Eqn. 4.2 is less than $1/3$ of the width of the base, B , or greater than $2/3$ of B , i.e. if the resultant lies outside of the middle third (kern) of the dam. It is usually associated with the onset of tension cracks at the heel of the dam, and

is thus considered analogous to observing tensile stresses at the heel of the dam in the FE analyses. Similarly, in the rigid body analysis, if the resultant force is outside of the middle half, i.e. eccentricity, e , is less than $1/4$ of B or greater than $3/4$ of B , then limit state 2 is achieved. In the linear FE analyses this would be analogous to having $1/6^{\text{th}}$ of the base of the dam in tension. In the nonlinear FE analysis, this limit state is characterized by the formation of a significant crack by tensile forces at the dam-foundation interface, which is assumed to have no cohesion. For the nonlinear FE analyses, fragilities for progressively severe cracking, i.e. crack lengths of 0, 19 and 38 ft, will be presented.

Limit states 3 to 5 are related to material failures. Limit state 3 is achieved if stresses at the toe exceeds the compressive strength of the concrete. For limit state 4 to be realized, the concrete at the neck can fail in tension or in compression. The tensile stresses in the concrete observed around the neck of the dam can be quite significant, as described in Chapter 4. On the other hand, the compressive stresses observed, even for limit state 3, are much lower than the capacity of the concrete. Limit state 5 is achieved in the rigid body analysis if the compressive stresses at the foundation around the toe of the dam are greater than the bearing capacity of the foundation material. In the linear FE analysis, this description is improved by comparing the stresses observed in the foundation around the toe of dam with the Hoek-Brown failure criteria (Hoek and Brown, 1997); the limit state is considered to have occurred if the stress state in a small volume of foundation elements at the toe violates the Hoek-Brown criteria. With the mesh sizes as shown in Fig. 4.2, violation in a three-element volume at the toe was assumed to be local bearing failure. In the nonlinear FE analyses limit state 5 is defined by the relative magnitudes of elastic and plastic strains observed in the elements, which provide a better description of the

nonlinear/post-elastic behavior. From a comparison of the elastic and plastic strains of a series of parametric studies, it was determined that (a) plastic strains of 10^{-4} (i.e. equivalent to the order of magnitude of elastic strains) signify the onset of nonlinear behavior in the foundation around the toe, and (b) the response at the toe of the foundation is dominated by the nonlinear behavior in the foundation if plastic strains exceed 10^{-3} (an order of magnitude higher than the elastic strains). As in the linear FE analysis, the observed plastic strains were averaged over a volume (12x12 ft) around the toe. Thus, in the case of the nonlinear FE analysis, volume-averaged plastic strains of magnitudes 10^{-4} and 10^{-3} will be presented to better capture the progression of the severity of the nonlinear behavior of the foundation.

Limit state 6, sliding failure at the interface between the dam and the foundation, is achieved in both the rigid body and linear FE analyses when the total horizontal force is greater than the resisting frictional force developed at the interface. The magnitude of slippage could not be computed with either model, and thus the limit state only describes whether or not there would be any sliding. In the nonlinear FE model, however, it is possible to compute the amount of sliding observed as the average of the slippage at the nodes around the heel of the dam and the drains. A fragility based on slippage of 0.1 inches (2.54mm) will be presented to compare to results obtained in the rigid body and linear FE analyses. A slippage of 0.5 in may impact the performance of the dam drainage system, decreasing its efficiency. This would increase the uplift pressure at the interface, which in turn would increase the sliding. For limit state 6, a fragility based on slippage of 6.0 in will also be presented. This relatively large magnitude of sliding could cause differential movements between adjacent monoliths in the dam and be a probable cause of eventual

loss of pool control. Finally, limit state 7 is a measure of the horizontal deformation of the top of the dam with respect to the heel. A large deformation in the monolith might impair the internal drainage or function of appurtenant structures. This fragility can not be obtained from the rigid body analysis. As an illustration, fragilities with relative deformations of 0.3 in (7.62mm) and 0.6 in (15.24 mm), or approximately 0.014% and 0.028% of the monolith height, respectively, obtained with FE analyses, will be presented.

All seven limit states described above have been utilized in the hydrologic fragility analysis of the Bluestone dam. In cases when the analysis method is limited and cannot compute the desired response quantities, the limit state is dropped out from comparisons. Limit states 1 to 3 are not used for seismic fragility analysis. The cracking responses (characterized by LS1 and LS2) are not meaningful performance states in seismic analyses. In a seismic excitation, the dam-foundation interface is subjected to intermittent opening and closure, with no residual cracks formed. This opening/ closure is of very small magnitude (as described in chapter 4) and is considered to have little structural significance. Thus, in the seismic fragility analysis, only limit states 4 through 7 have been utilized.

5.4. HYDROLOGIC FRAGILITY

5.4.1. Uncertainty Modeling

In the hydrologic fragility assessment, the performance of the dam-foundation system is characterized by the following random variables: the effectiveness of the drains,

the effectiveness of the grout curtain, the tail water elevation and the effective area of uplift. In addition, the angle of friction and cohesion force of foundation material, the bearing strength of the foundation and compressive strength of concrete are assumed to be random variables. With the exception of concrete compressive strength, which can be modeled by a normal distribution (MacGregor et al, 1983), the necessary statistical data are limited. The uniform distribution is the distribution of "maximum uncertainty" when the random variable is known (from physical considerations) to have a finite lower and upper limit but other information is unavailable. Thus, a uniform distribution was chosen to model the remaining variables, the means of which were defined by the values provided by the US Army Corps of Engineers and are summarized in Table 4.1. The following variables and their assumed ranges are used in both the rigid body and the linear and nonlinear finite element analyses:

Drain effectiveness	= $u(0,1)$
Grout curtain effectiveness	= $u(0,1)$
Tail water elevation	= $u(1360,1400)$ ft
Effective uplift area	= $u(0.33,1.00)$
Angle of friction	= $u(26,34)$ degrees
Cohesion	= $u(3,9)$ ksf
Compressive strength of concrete	= $N(670,770)$ ksf

These values are based on an examination of data summarized for various types of intact rock in sections 1.5 – 1.7 of Afrouz (1992), chapters 4, 5 and 8 of Hoek, Kaiser and Bawden (1997), and chapters 3-6 and 9 of Bienawski (1989). Others (Butler, 1981; Leliavsky, 1958) have asserted that the effective area of uplift is very close to 100%.

For the Hoek-Brown parameters describing the foundation material, mean values of $m_i = 6$ and $GSI = 25$ were chosen from tables provided in Hoek and Brown (1997). The

following parameters used in the FE models were also assumed to have uniform distributions, with the following ranges:

m_i (Hoek-Brown constant)	= $u(4, 8)$
GSI (Geologic Strength Index)	= $u(20, 30)$
Elastic modulus of concrete	= $u(4.52, 5.21)10^6$ psi
Elastic modulus of fdn.	= $u(3.47, 4.43)10^6$ psi
Dilation angle of fdn.	= $u(27, 33)$ degrees

5.4.2. Fragility Analysis

The probability of achieving various limit states for a given pool height is obtained by simulating the performance of many dams (defined by the random variables described above). The computational cost associated with the construction of hydrologic fragilities (compared to seismic fragilities) is relatively low; hence a simple Monte Carlo simulation technique was used. For the rigid body and linear FE analysis, 1000 dams initially were simulated and subjected to increasing pool elevation. The limit states were then identified by post-processing the responses obtained. Comparison of fragilities obtained by simulating only 100 dams showed very good agreement. Consequently, to reduce the computational burden only 100 dams were simulated for the nonlinear FE analyses.

5.4.2.1. Fragilities: Rigid body model

Fragilities obtained from the rigid body model for the limit states identified in the previous section are shown in Fig. 5.4. A lognormal distribution is fitted to fragilities for LS1 and LS2. The fit is very close in both cases. It is observed that fragilities for all but limit states 1 and 2 are zero for the range of pool elevations shown. In addition, the

probability of achieving limit state 1 at pool elevation of 1520 ft, which was the design pool elevation, is small. This result is consistent with the notion that the dam should have a reasonable safety margin against failure at pool elevations at or below that used in the original design. It is also a direct consequence of the fact that the analysis method used for design and safety evaluation is the same, i.e. the rigid body method. But for the revised PMF, the fragilities indicate very high likelihoods of occurrence for LS1 and LS2, i.e. 100% and 43%, respectively. Whether these high probabilities should be of concern depends on the significance one attaches to these simple limits as measures of dam performance.

5.4.2.2. Fragilities: Linear FE model

Fragility curves obtained using the linear FE model are shown in Fig. 5.5. The fragilities for LS1 and LS2 obtained from the rigid body analysis are included for comparison. The fragilities obtained from the linear FE model are sharper than those from the rigid body analyses. There are also considerable differences in the probabilities predicted for higher pool elevations; e.g. at pool elevation of 1556 ft the linear FE model indicates probabilities of 43% and 18% for LS2 and LS5, in contrast to 0% and 18% for the rigid body model. This is because linear FE solutions (for very high loads) often exhibit irregular behavior around points of geometrical discontinuity, leading to relatively high, localized stresses at these points. This behavior is observed particularly around the heel and toe of the dam at pool elevations above 1520 ft. Refinement of the FE mesh does not smooth out these differences.

This irregular behavior is further illustrated in Fig. 5.6, which compares fragilities

for LS1 based on different assumptions, regarding how the limit state is defined, i.e. whether one element exhibiting tensile stress is enough or at least two elements around the heel of the dam must be in tensile stress for LS1 to be achieved. Fig. 5.6 also includes a fragility curve obtained using the modified elastic modulus (according to Hoek and Brown, Eqn. 2.11) for LS1. Likewise, a comparison of fragilities for LS2, including those based on a modified elastic modulus is shown in Fig. 5.7. The fragilities from the rigid body analyses and linear FE analysis (with unmodified elastic modulus) have about the same median values. In contrast, the results obtained using the modified elastic modulus differ significantly in the lower tail of the fragility.

Similar irregular behavior has also been observed for linear FE solutions at the toe of the dam. In this case, the limit state is the local failure of foundation material at the toe, and, as discussed previously, a number of elements defining a finite volume around the toe must achieve that limit state simultaneously for local failure to occur. The resulting fragility curve for LS5 is shown in Fig. 5.5, which gives a probability of failure less than 18% under the revised PMF. Fragilities for the other limit states, except for the relative deformation of 0.3 in, LS7, are zero; the latter, is found to have non-zero probabilities at high pool elevations (Fig. 5.5).

5.4.2.3. Fragilities: Nonlinear FE model

Fragilities obtained from the nonlinear FE analysis are depicted in Figs. 5.8.a and b. For LS3 (not shown) and LS4 (concrete spitting at the neck of dam) the probabilities are zero over the range of pool elevations considered. The other limit states show minimal probabilities for the design pool elevation of 1520 ft. But for higher pool elevations, the

fragilities are substantial. Consistent with the previous results, the fragility for LS1 shows a probability of 100% at pool elevation of 1556 ft. But for LS2 (i.e. crack length of 19 ft) the fragility increases slowly above about 62% at pool elevations greater than 1550 ft. The same phenomenon is also observed for a limit state defined as a crack length of 38 ft, about one-third of the base of the dam.

For LS5, defined as the onset of nonlinear behavior in the foundation around the toe, the (conditional) limit state probability is 13% at the revised PMF (1556 ft), which compares well with the probability of 18% obtained from the linear FE analysis. However, for LS6, defined as the average sliding around the heel and/ or drain holes being greater than 0.1 in (2.54 mm) a probability of 47% is indicated, in contrast to the value zero obtained from both the rigid body and linear FE analyses. More severe definitions of LS5 and LS6, namely, dominant nonlinear behavior in the foundation (LS5) and sliding of 0.5 in (LS6), which are considered detrimental to the structural capacity of the dam-foundation system, result in probabilities of zero at a pool elevation of 1556 ft. Two limit states also are depicted for LS7. The relative deformation of top of dam with respect to heel of 0.3 and 0.6 in show probabilities of 87% and 0%, respectively.

5.4.2.4. Comparison of fragilities

Comparisons of the fragilities obtained from these various analysis methods are illustrated in Figs. 5.9 and Figs. 5.10. The fragilities for LS1 obtained from both the linear and nonlinear FE analyses compare well, while those from the rigid body analysis seem to have underestimated the limit state probabilities (Fig.5.9). In contrast, for LS2 the rigid body and linear FE analyses seem to have underestimated the probabilities compared to

results from the nonlinear FE analysis, for pool elevation up to the revised PMF of 1556 ft. The reverse becomes true, however, for pool elevations greater than 1560 ft. The fragility for a crack length of 38 ft matches the fragility for LS2 from the rigid body analysis closely for pool elevations up to the revised PMF (Fig. 5.9). Comparisons for LS5 and LS7 are illustrated in Fig. 5.10. The fragilities for LS5 obtained from the linear and nonlinear FE analysis show a relatively good correspondence. In contrast, discrepancies for LS7 are large. This is because of the fact that the nonlinear model allows the opening of cracks and thus contributes to the relative deformation. In fact, a plot of fragilities for LS7 and the various crack lengths defined shows that LS7 lies between the fragilities for LS2 and crack length of 38 ft.

Overall, results obtained from the rigid body, linear and nonlinear FE analyses seem to be consistent with each other. The rigid body analysis, though limited in scope, may be a useful tool for preliminary studies and as a benchmark against which subsequent FE models would be compared. The fragilities for the linear FE analysis, however, should be treated cautiously, as they sometimes differ significantly from those predicted by the rigid body and nonlinear FE models. The nonlinear FE model is the most dependable, and though expensive in terms of computational cost and time and effort, it is indispensable for decision-making processes involving considerable risk, capital and labor.

5.5. SEISMIC FRAGILITY

5.5.1. Uncertainty Modeling

The seismic fragility analysis of concrete gravity dams is characterized by many of the same variables used in the hydrologic fragility analysis. Additional variables used in the analysis are the coefficients for Rayleigh damping. A 5% viscous damping ratio was assumed and the Rayleigh coefficients were computed for the 1st and 3rd natural frequencies (see chapter 4), as:

$$C = \alpha M + \beta K \quad (5.5)$$

in which C , M and K are the damping, mass and stiffness matrices and α and β are the Rayleigh coefficients. These coefficients were used as mean values the coefficients with the ranges shown below:

$$\alpha = u(2.04903, 2.50437)$$

$$\beta = u(0.00092115, 0.00112585)$$

The seismic fragility analysis, however, must include the uncertainty that arises from the earthquake ground motion itself. The variability in the seismic ground motion is so large (coefficients of variation of the order of 50% or more) that it may dominate the overall variability in system performance.

Earthquake ground motions are described by various parameters, which include magnitude/ intensity of earthquake, attenuation, local site conditions, frequency content and duration of excitation. Shome and Cornell (1997, 1998) have shown that a suitable ensemble of ground motions for analysis purposes can be created by scaling ground motion

records to the same spectral acceleration at the fundamental frequency of the structure. They concluded that the magnitude/ intensity of ground motion is effectively independent of the nonlinear response of a structure, given that the earthquake records are scaled in this manner. Finally, they demonstrated that spectral acceleration at the fundamental frequency is a good single-parameter measure of the intensity of ground motion. Hence, the spectral acceleration at the fundamental frequency is selected to characterize the ground motion records. Moreover, recent NEHRP recommendations (NEHRP 1998) specify the seismic hazard in terms of spectral acceleration, making this the coupling parameter in both the fragility and the hazard in fully coupled safety assessment, or PSA.

Table 5.1 lists the earthquake records selected to create the ensemble of for the seismic fragility of the Bluestone dam. All occurred between 1940 and 1994 in the US; and have epicentral distances of 8.5 to 47.3 km with magnitudes ranging from 5.6 to 7.5. These records were screened to avoid any apparent “near-source” effects, i.e. records with uncharacteristic pulse-like behavior with large acceleration magnitudes. Fig. 5.11 shows the spectral accelerations of these selected records scaled to 1.0g at the fundamental frequency of Bluestone dam, i.e. 6.11 Hz. Note that all the spectra pass through the “pinch point” at that frequency. The scatter in these response spectra conveys a picture of the aleatory uncertainty in ground motion, conditional on a spectral acceleration of 1.0g.

5.5.2. Fragility Analysis

5.5.2.1. Sampling Procedure

The construction of seismic fragilities a concrete gravity dam is an expensive undertaking. To alleviate the cost of the FE analyses, which is the major component of the effort, efficient sampling plans that minimize sample size and sampling errors and give stable estimates of the desired response statistics are required. Such techniques are available (Rubenstein, 1981). Usually referred to as variance reduction techniques, they include, among others, importance sampling and stratified sampling techniques. One particular technique that has been found to be very useful in reliability problems involving complex systems is denoted Latin Hypercube (LHC) sampling (Imam and Conover, 1980, O'Connor and Ellingwood, 1987). It is a stratified sampling procedure in which the PDF of each input variable, X_i , $i=1, \dots, k$, is divided into N disjoint intervals of equal probability. A value, usually the median of the interval, then is associated with each interval. These values are sampled randomly and without replacement, to form N random samples representing the dam-foundation system. N finite element analyses are performed on these systems, and the response quantities from these analyses are post-processed to extract the required fragilities.

One advantage of the LHC sampling procedure is that it ensures that all portions of the sample space are sampled. It has also been shown (e.g. McKay et al, 1979) to lead to estimators that have very little bias; specifically, the variance in the estimator, which is a measure of sampling error, is less than that in classical Monte Carlo simulation (without variance reduction). Furthermore, the LHC reduces the computational burden considerably

as the number of samples, N , (and thus FE analyses) required for minimal sampling error is quite small.

5.5.2.2. Fragility Analysis

In the construction of the seismic fragility of Bluestone Dam, the spectral acceleration was used as the demand variable (as discussed in previous section). Spectral accelerations of 0.3g, 0.5g, 0.7g, 0.9g, 1.0g and 1.2g were chosen for FE analyses. For each spectral acceleration, twelve FE analyses were carried out, in which the seismic records (in Table 5.1) were scaled accordingly and randomized, and the results were suitably post-processed. Seismic fragilities thus obtained are illustrated in Figs. 5.12 – 5.16. For each performance limit state, two (or more) fragilities are provided to display the structural robustness of the dam-foundation system. The more widely the fragilities are separated, the more robust the dam-foundation system is for that limit state.

The fragility for limit state 4 is shown in Fig. 5.12. The probability of tensile cracking/ splitting of concrete around the neck of the dam (LS4) is about 28% for an earthquake with a spectral acceleration of 1.0g; such an earthquake typically would have a peak ground acceleration of 0.38g - 0.45g (Newmark and Hall, 1982). A fragility showing the occurrence of tensile stresses greater than 350 psi (2.41 MPa), a limit state corresponding to the design strength of the concrete (3000 psi (Appendix)), also is shown; this probability is about two times larger. This analysis shows that in the evaluation of the safety of a structure the median (or mean) estimates of capacity and not the design values should be used. It also shows that designing the dam with a factor of safety equal to 1.3 on splitting strength would reduce the probability of cracking at the neck by a factor of 2. The

fragilities for nonlinear behavior in the foundation (LS5) are depicted in Fig. 5.13. A very low probability is indicated for dominant nonlinear behavior, while a probability of 41% is shown for onset of nonlinearity in the foundation at spectral acceleration of 1.0g. This indicates that the foundation may very well exhibit some nonlinear behavior at this relatively high intensity of excitation, but this behavior will not be dominated by the nonlinear constitutive relationship of the material.

The fragilities for sliding (LS6) at the dam-foundation interface in Fig. 5.14 indicate that probabilities of sliding 0.1 in (2.54 mm) is very high, while the probability of sliding 0.5 in (12.7mm) is about 75%. Some structural damage to the drainage system, particularly at the dam-foundation interface, should be expected from this intensity of seismic excitation. Relatively large sliding (e.g. 6.0 in (152.4 mm)) could cause differential movements between adjacent monoliths in the dam and be a probable cause of eventual loss of pool control. However, Fig. 5.14 shows that the probability of this event is less than 5% for an earthquake with spectral acceleration of 1.0g. The fragilities for the relative deformation of the top of dam with respect to the heel are depicted in Fig. 5.15. A seismic excitation with spectral acceleration of 1.0g would cause relative deformations of 0.3 in (7.6mm) and 0.6 in (15.2 mm) with probabilities of 82% and 16%. These deformations are very small compared to the height of the dam and minimal damage should be expected to appurtenant structures and operation equipment due to these deformations. Moreover, the fact that the overall deformations are on the order of 0.02% of the height of the dam suggests that a rigid body model of the monolith might be an appropriate simplification to the problem, provided that one is not interested in the likelihood of tensile cracking at the neck of the dam.

Fig. 5.16 summarizes how the fragilities for limit states 4 to 7 compare to each other. For the Bluestone dam subjected to an earthquake ground motion with spectral acceleration of 1.0g, probabilities of sliding of 0.5 in or relative deformation of 0.3 in are quite high. Substantial nonlinear responses in the foundation and large magnitudes of sliding (around 6 in) have very low probabilities. However, it could be deduced that some tensile cracking and nonlinear behavior in the foundation are likely to occur (probabilities of 28% and 41%) for such ground motions.

5.6. SENSITIVITY STUDIES

5.6.1. Hydrologic Fragility

A study was undertaken to assess the sensitivity of the hydrologic fragility to the assumptions made regarding the various random variables. This sensitivity is demonstrated by fixing a variable, first at its minimum value and then at its maximum value, and comparing the results obtained at these extremes with the results obtained when it is considered to be a random variable. Variables considered include the effective uplift area, the grout and drain effectiveness, tail water elevation and coefficient of friction.

The analysis was first carried out using the rigid body model of the dam to assess the importance of these variables. Figures 5.17 to 5.21 show the results of the sensitivity analysis obtained from the rigid body model. Variations on the effective uplift area have the greatest influence (Fig. 5.17), while the tail-water elevation has the lowest impact on the fragility curves (Fig. 5.18). The drain and grout curtain efficiencies exhibit comparable impact (Figs. 5.19 and 5.20), though less than that of the effective uplift area.

The effect of perfect correlation in drain and grout curtain effectiveness is also shown in Fig.5.21.

Since the results from the rigid body model had indicated that the effective uplift area had a large impact on the fragility analyses, the effects of this variable were further investigated using the nonlinear FE model. In addition, the effect of the coefficient of friction was investigated. Fig. 5.22 shows the effect of the effective uplift area on fragilities of limit states 1 and 2. These fragilities, obtained by fixing the effective uplift area at 100%, are compared with those obtained in Section 5.4. The effective uplift area has a considerable impact on these fragilities, especially on that for LS2 (cracking of 19 ft), where it has raised the upper portion of the fragility at higher pool elevations. This tendency is consistent with the mechanics of the dam-foundation system, as the uplift force is a destabilizing force acting on the structure. Similarly, Fig. 5.23 illustrates the effects of the effective uplift area for limit states 5 and 6. In these cases also, it exhibits considerable influence on the fragility curves.

The effect of the coefficient of friction on limit states 1 and 2 is presented on Fig. 5.24, in which the fragilities constructed by fixing the coefficient of friction at 0.8816 (friction angle = 41.4°) are compared with those obtained in Section 5.4. The coefficient of friction has minimal impact on the fragilities for LS1 and LS2. In contrast, the coefficient of friction has relatively bigger impact on the limit states 5 and 6, as shown in Fig. 5.25. In this case however, the smaller coefficient of friction reduces the probabilities for limit state 5. This behavior is not unexpected, as loss of frictional resistance causes sliding but does not affect crack propagation at the dam-foundation interface. Sliding at the toe of the dam would also relieve some stresses and thereby reduce the nonlinearity foundation behavior.

5.6.2. Seismic Fragility

An investigation into the sensitivity of the seismic fragility was also carried out. Consistent with the discussion in Sect. 5.6.1, the effective uplift area and the coefficient of friction were considered. Figs. 5.26 and 5.27 show that the seismic fragility is not sensitive to the effective uplift area. The fragility that was constructed by fixing the effective uplift area at 100% is almost identical to that obtained in Section 5.4, in which the variable was assumed to be uniformly distributed between 33% and 100%. This is expected, as the variability in the response of a structure under seismic motion is dominated by the uncertainties in the seismic motion itself, and the rest of the variables do not contribute much. The exception to this is the effect of the coefficient of friction, which is shown in Figs. 5.28 and 5.29. It is shown that fixing the coefficient of friction at 0.88162 (41.4°) has reduced the probabilities for LS4 and LS5, noticeably so for LS5 (onset of nonlinearity). This phenomenon has also been observed in the hydrologic fragilities. As the sliding response is directly dependent on the coefficient of friction, the probabilities should increase, as shown in Fig. 5.29. The coefficient of friction has minimal impact on the fragility for the relative deformation of the dam.

5.7. ADDITIONAL DATA NEEDS

The results of the sensitivity analyses described in the previous section indicate where additional data are required for fragility assessments of concrete gravity dams and

thus where additional investments should be made in supporting research. Moreover, sensitivity analysis suggests those parameters that might simply be assumed to be deterministic. The coefficient of friction between the contact surfaces at the dam-foundation interface was assumed to be the same as that of the foundation. Though the value used for Bluestone dam was considered to be a reasonable value (compared to available literature), more site-specific data is required. This would help to reduce the variance in the estimate of the fragilities.

It is also very important that the effective uplift area be modeled accurately, as it has a significant effect on the hydrologic fragility. It should be noted that the range assumed for the uplift area is quite large. More studies/ experimentation is required to narrow down this range. The effectiveness of the drains and grout curtain is also another area where database improvement is essential.

Table 5.1. List of earthquake ground motion records used in seismic fragility

	Earthquake	Year	Mag.	Epicentral Distance (km)	Component
1	El-centro, CA (Imperial Valley)	1940	6.7	12.9	S00E
2	Olympia, WA (DOT test lab)	1949	6.9	26.2	N04W
3	Kern County, CA (Taft Lincoln)	1952	7.5	44.0	S69E
4	Pugent Sound, WA (U310) (LA Subway Terminal)	1965	6.5	22.5	S58W
5	Parkfield, CA (Parkfield, Cholame 5W)	1966	5.6	35.6	N05W
6	San Fernando, CA (D058) (Hollywood Storage Lot)	1971	6.4	8.5	N90E
7	Anchorage, AKA (Talkeetna)	1975	5.9	47.3	N75E
8	Coalinga, CA (Pleasant Valley)	1983	6.5	10	S45E
9	Elmore Ranch, CA (Imperial Wildlife)	1987	6.2	22.9	N00E
10	Whittier Narrows, CA (Long Beach)	1987	6.1	22	N10E
11	Loma Prieta, CA (Anderson dam)	1989	7.0	26.5	N27W
12	Northridge, CA (Newhall)	1994	6.7	19.1	N90E

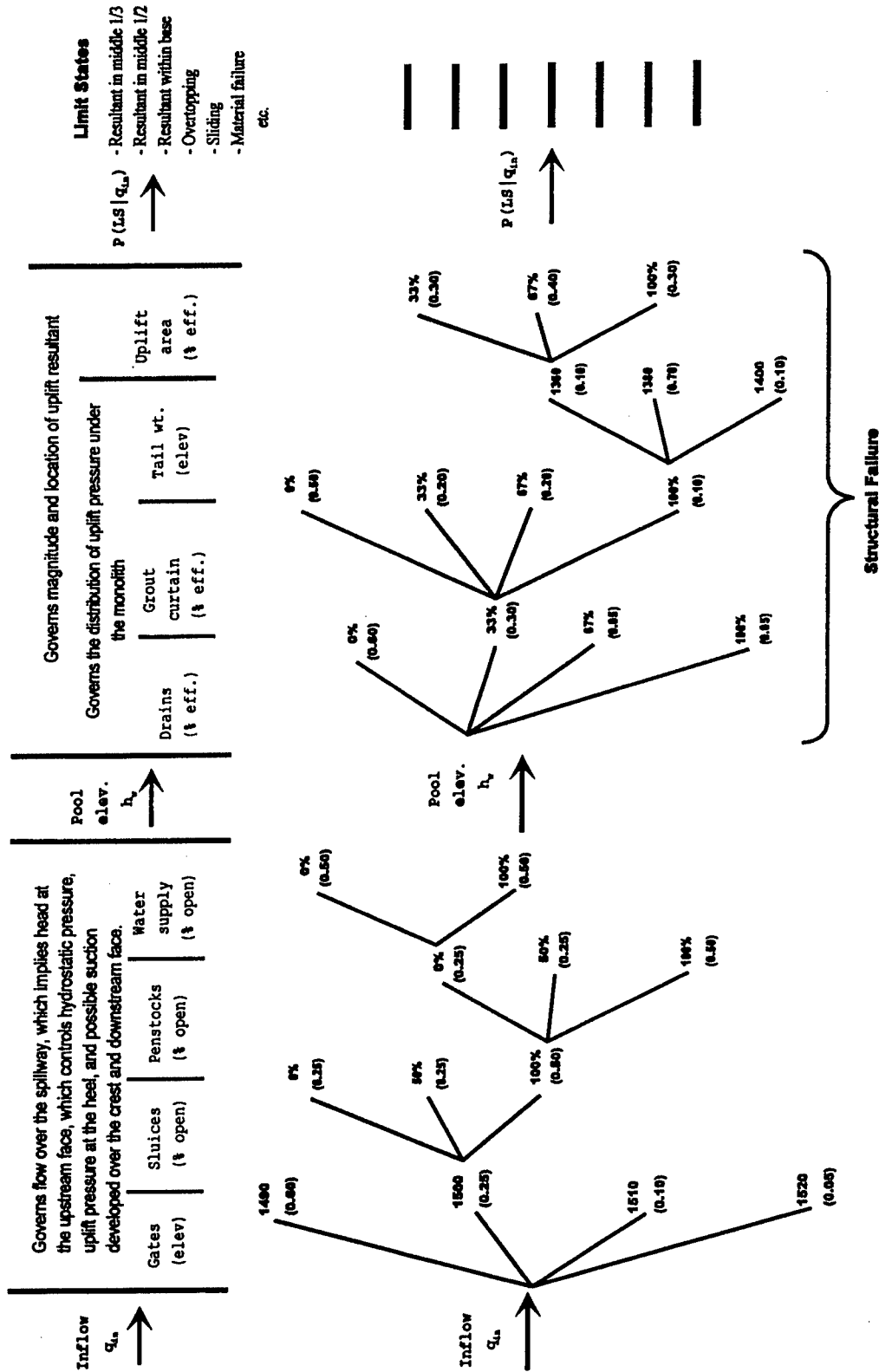


Fig. 5.1.a. Simplified event tree model of a dam-reservoir system

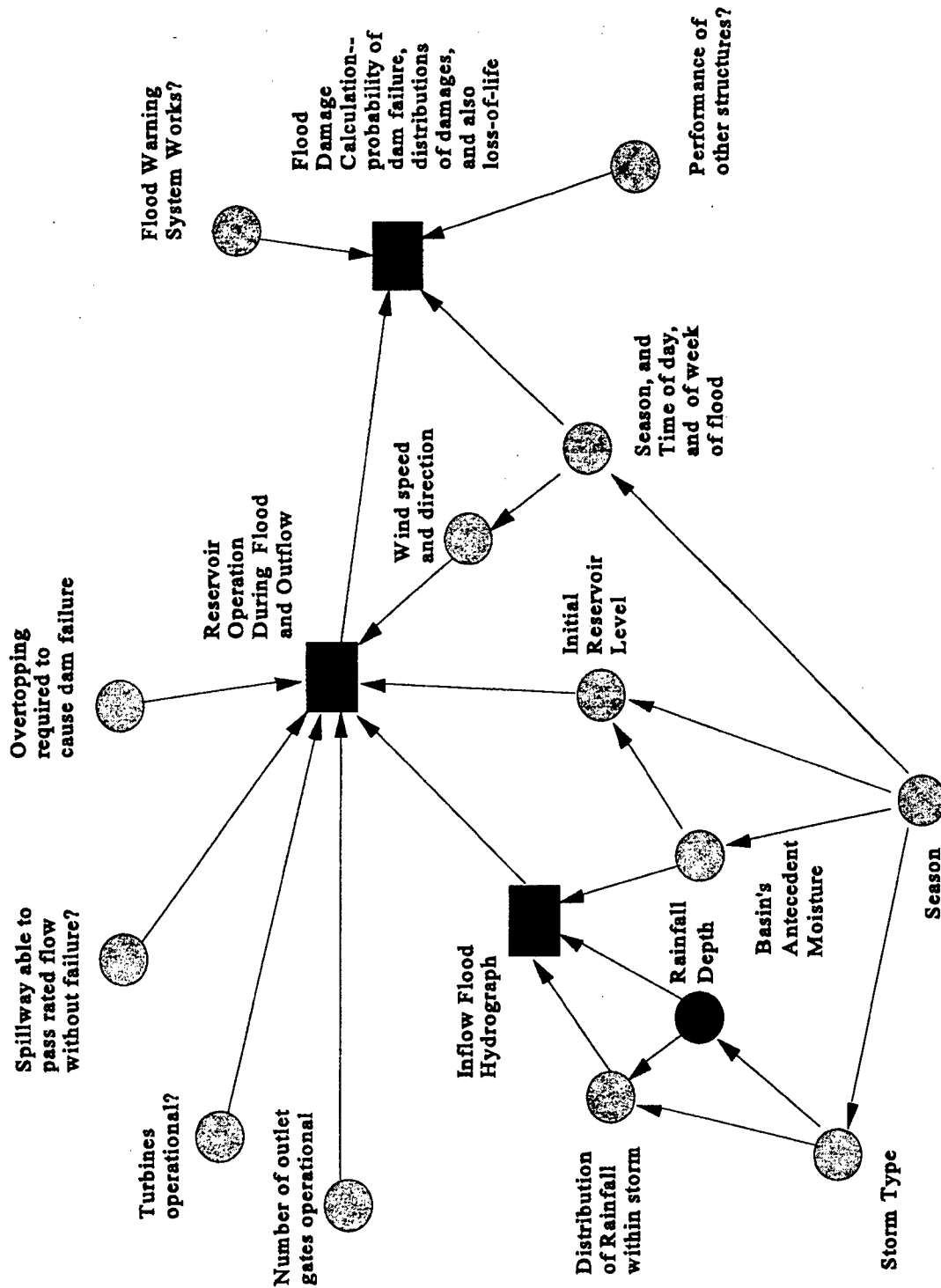


Fig. 5.1.b. Inclusive event tree model of a dam-reservoir system (Stedinger, 1996)

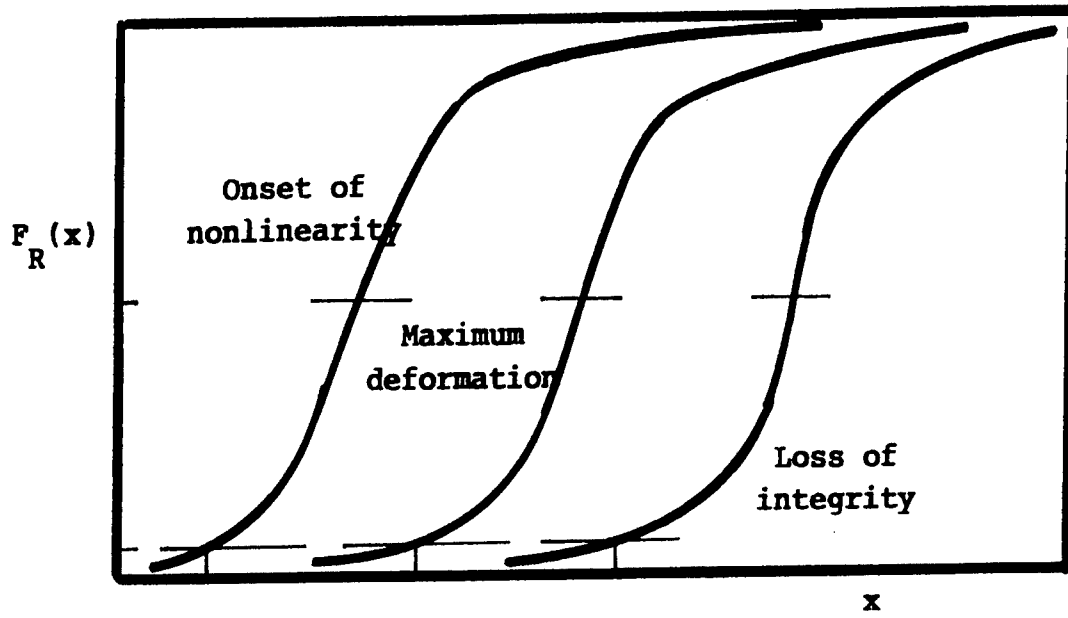


Fig. 5.2. Fragilities for progressively severe limit states

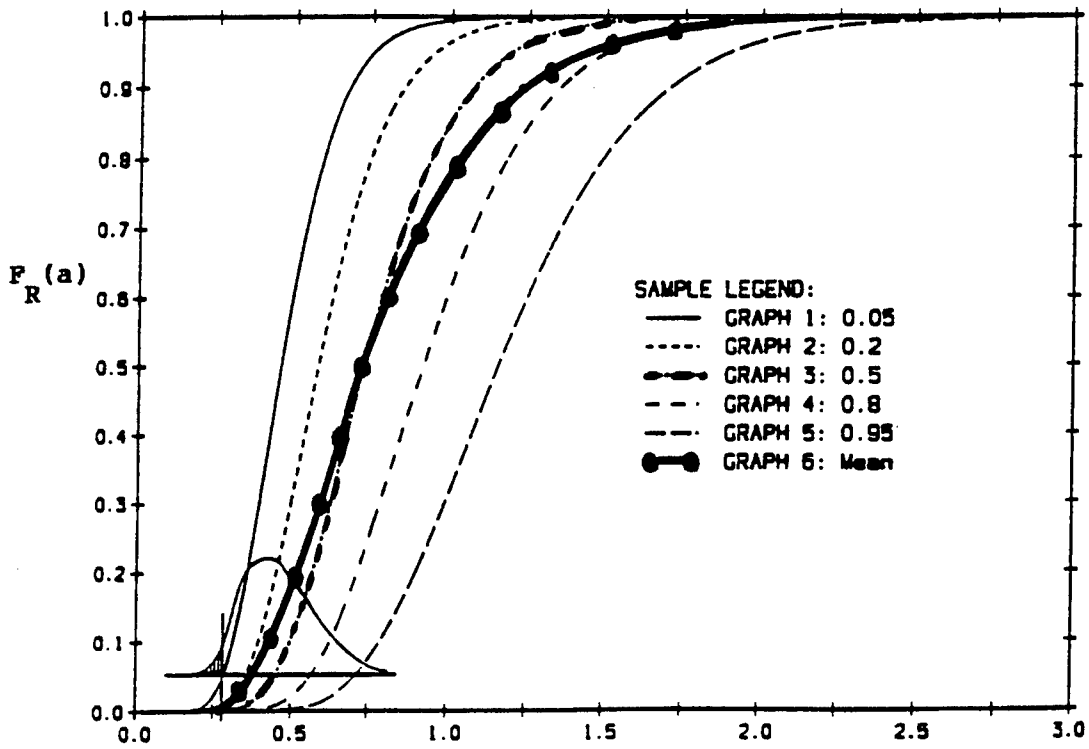


Fig. 5.3. Conceptual illustration of fragility showing both epistemic and aleatory uncertainty

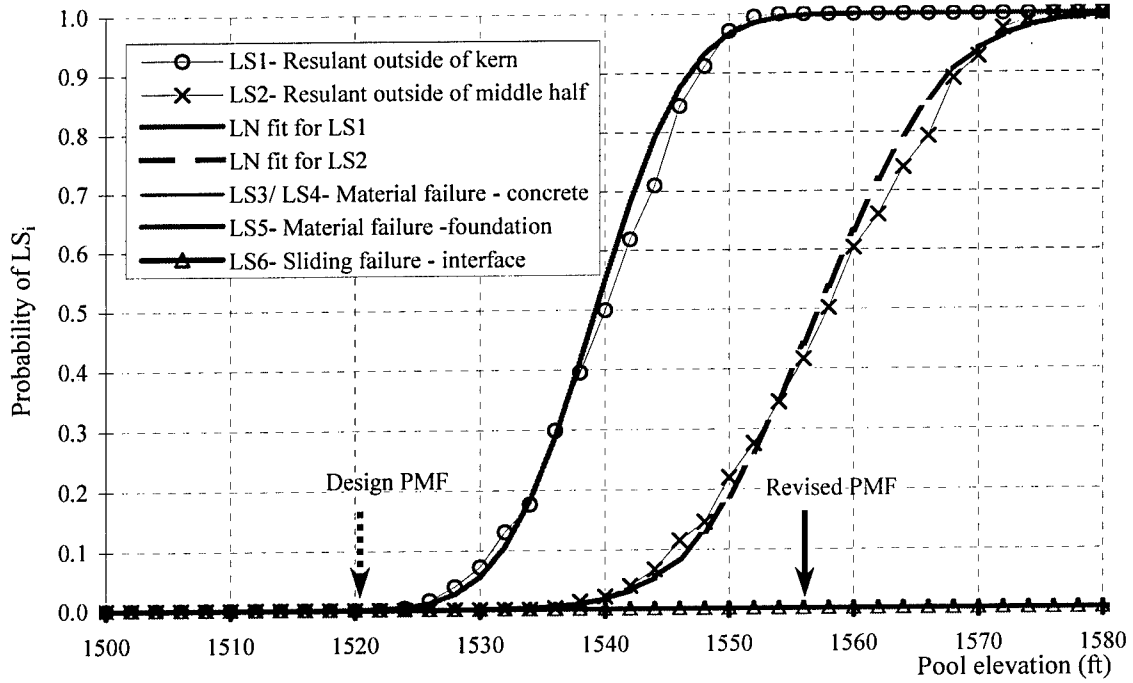


Fig. 5.4. Hydrologic Fragility of Monolith 12 - rigid body analysis

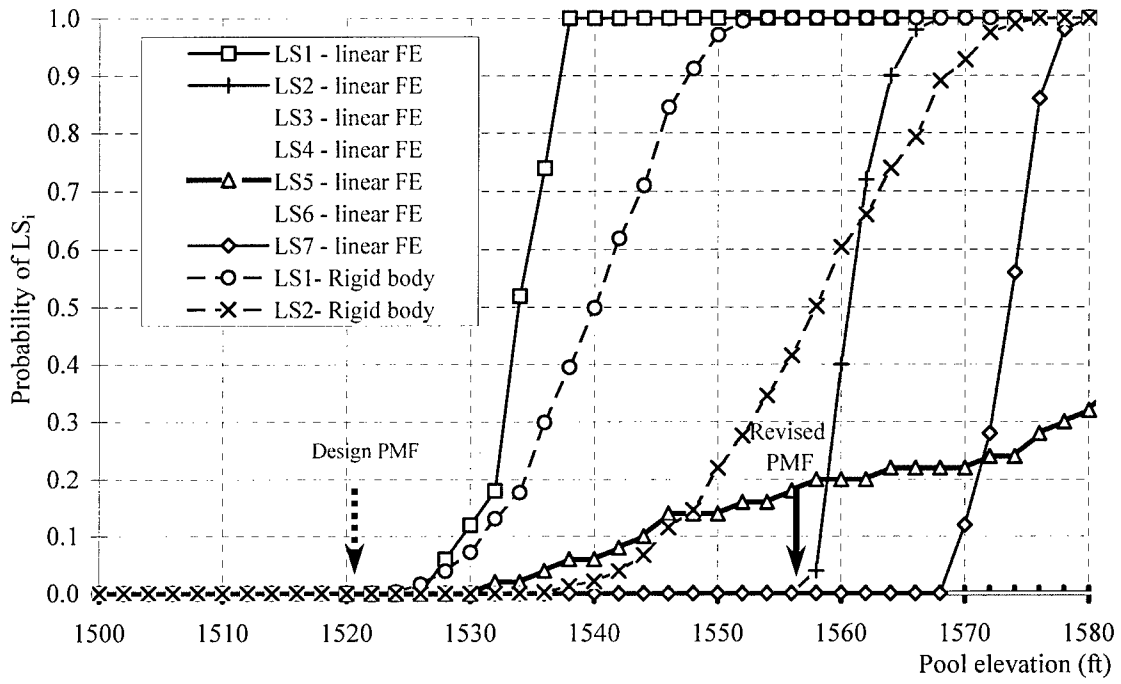


Fig. 5.5. Hydrologic Fragility of Monolith No. 12 - linear FE analysis

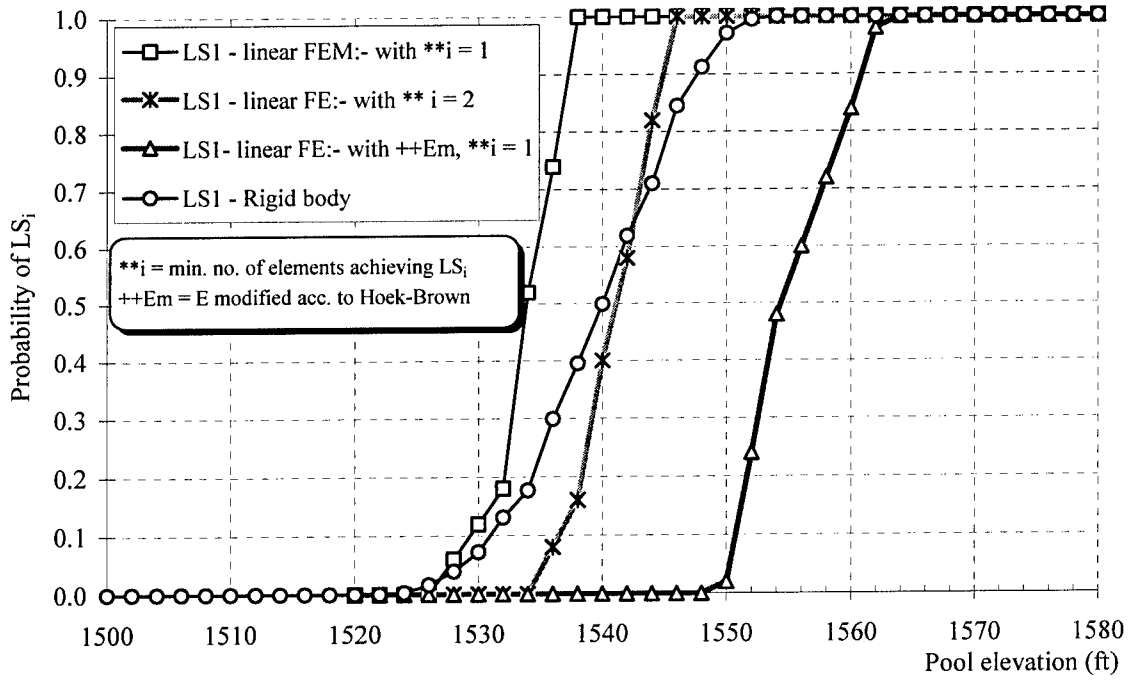


Fig. 5.6. Hydrologic Fragilities for LS1 with different modeling assumptions

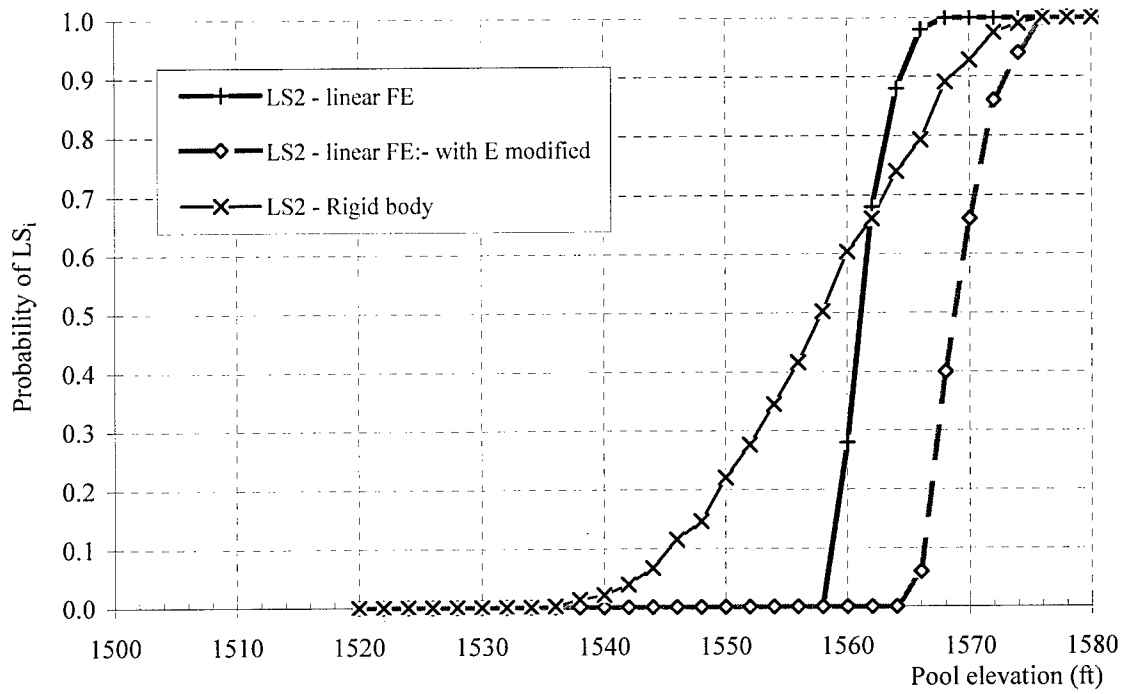
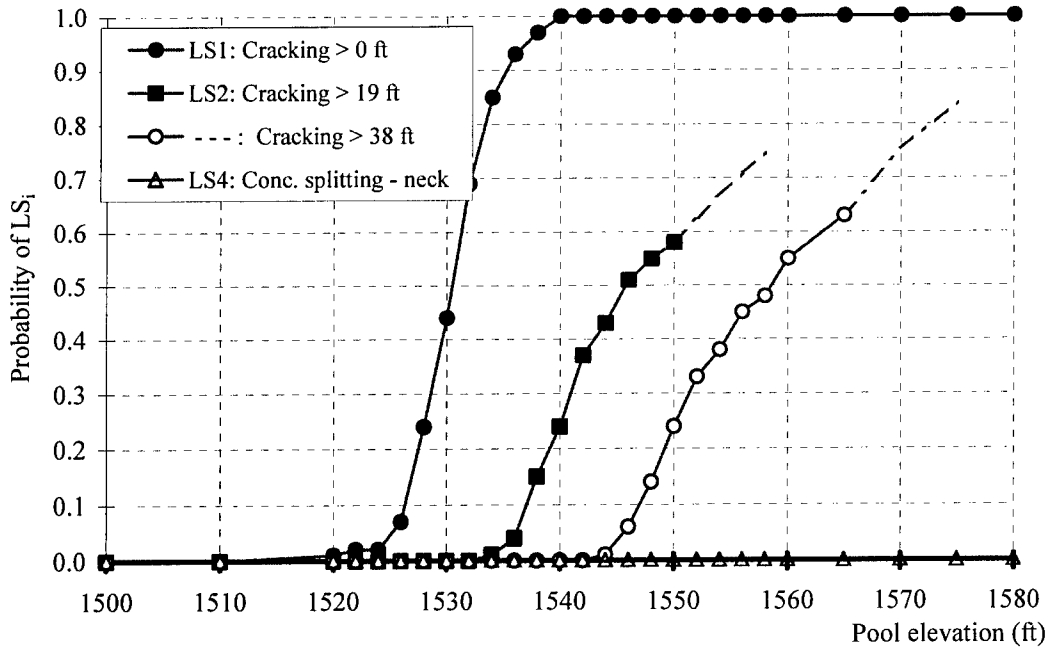
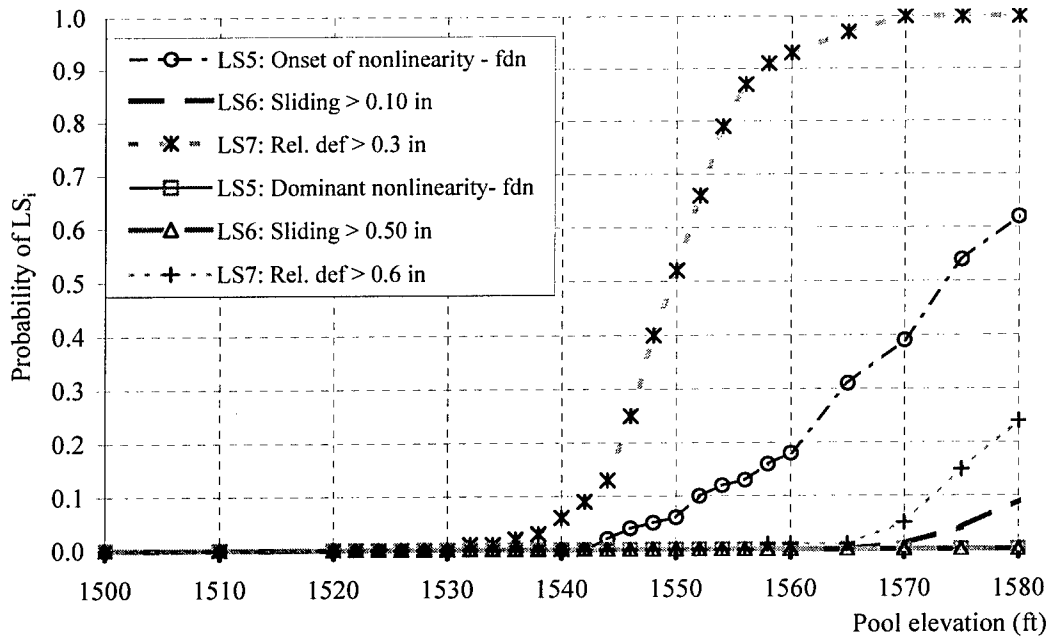


Fig. 5.7. Hydrologic Fragilities for LS2 with modified modulus of elasticity



a) for LS1, LS2, and LS4



b) for LS5, LS6 and LS7

Fig. 5.8. Hydrologic Fragility of Monolith No. 12 - nonlinear FE analysis

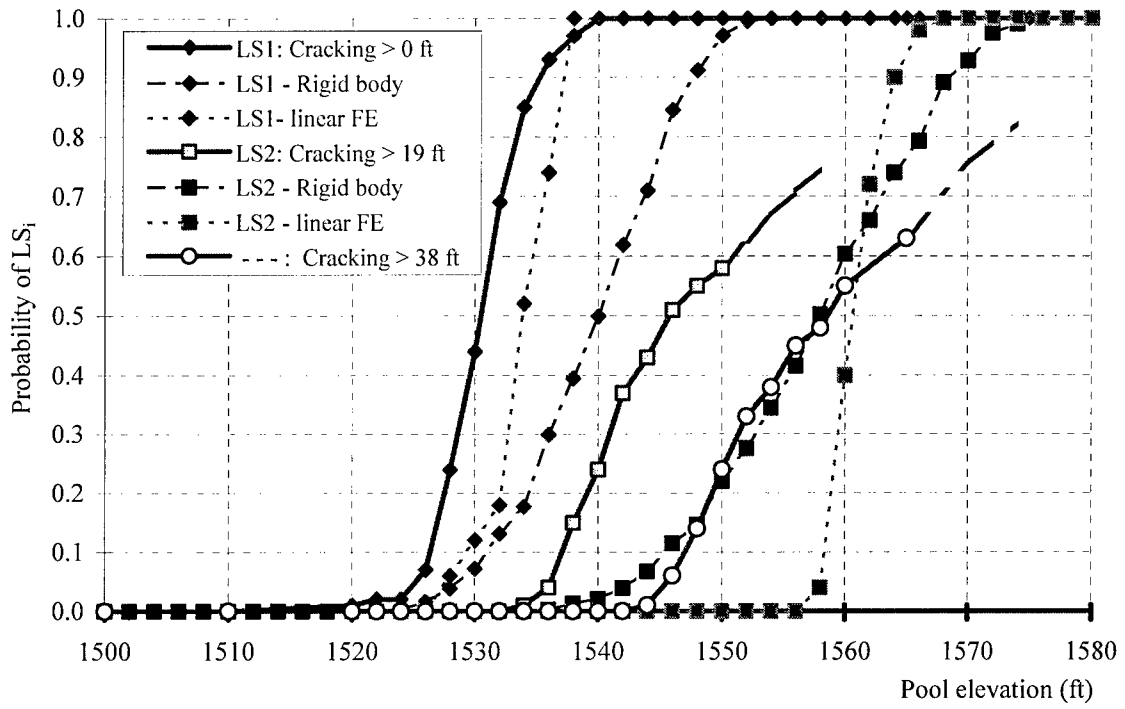


Fig. 5.9. Comparison of Hydrologic Fragilities - LS1 and LS2

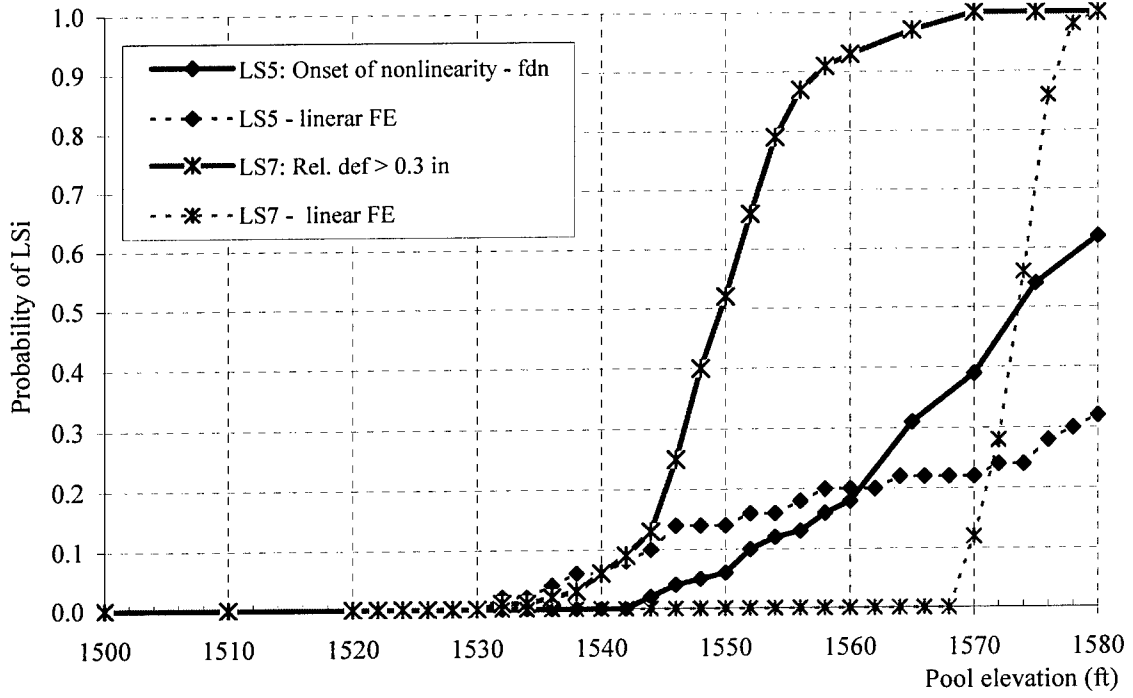


Fig. 5.10. Comparison of Hydrologic Fragilities - LS5 and LS7

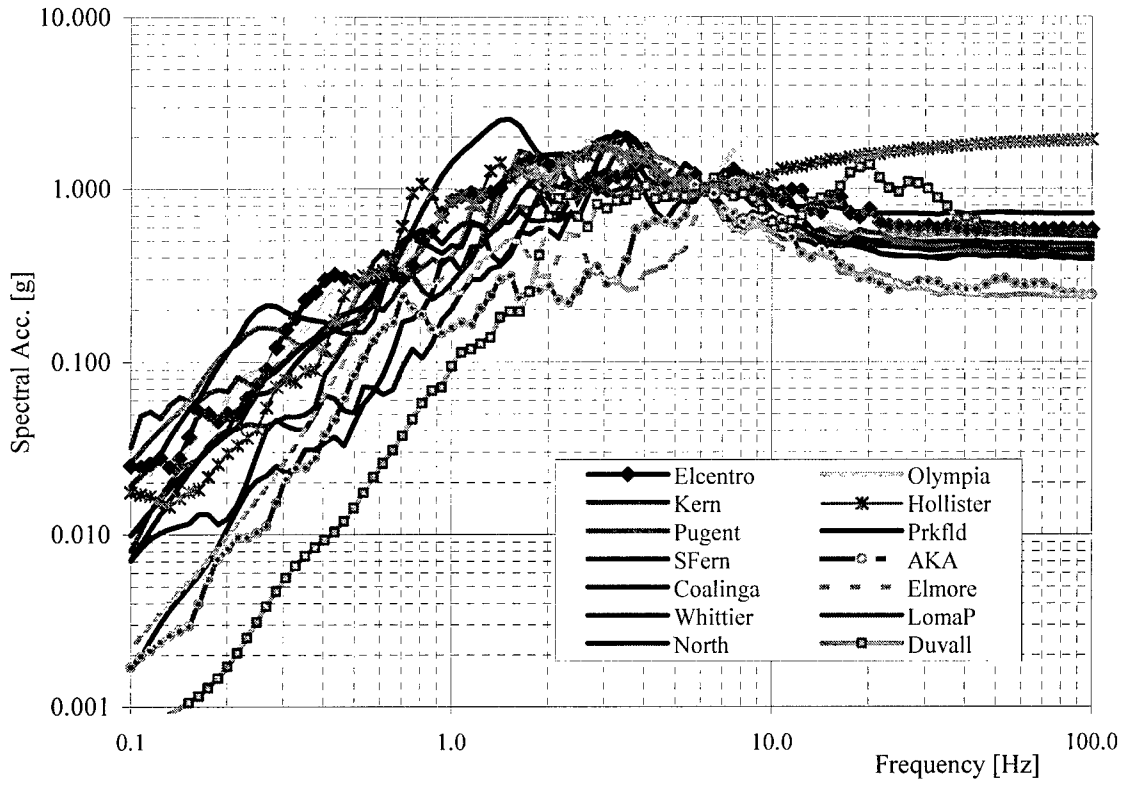


Fig. 5.11. Response spectra of selected earthquake records -
scaled to 1.0g at $w_n = 6.12$ Hz

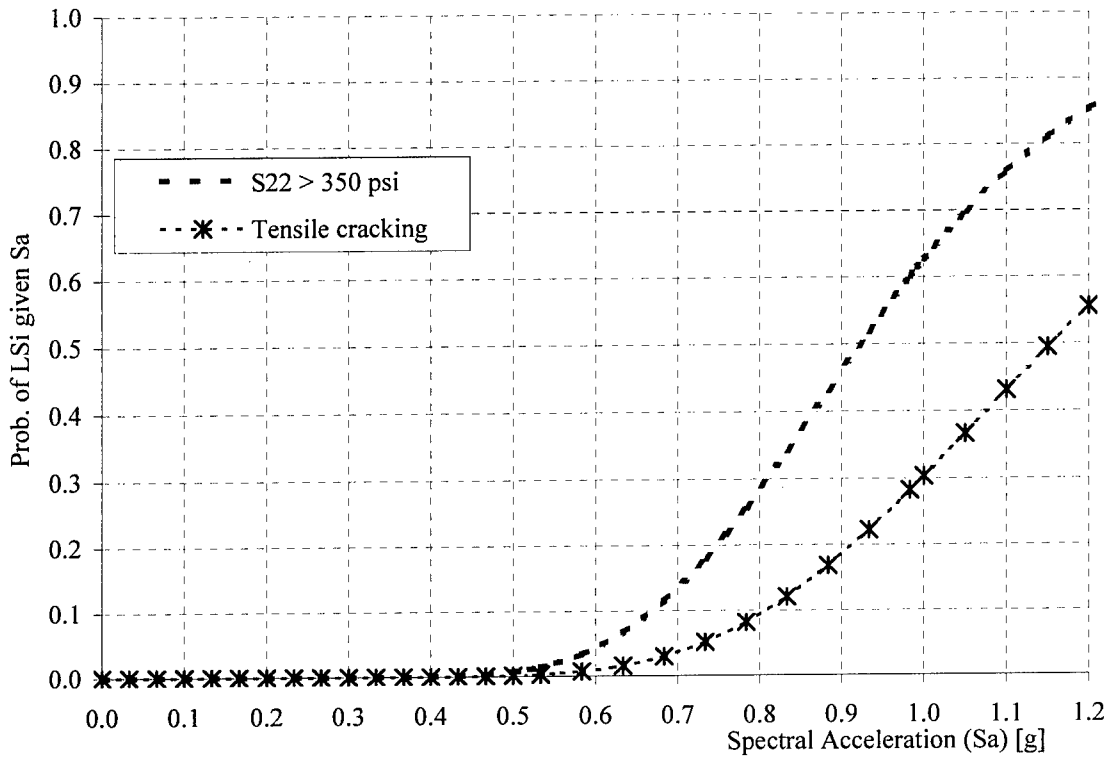


Fig. 5.12. Seismic Fragility of Monolith No. 12

LS4 - Tensile Stress & Cracking

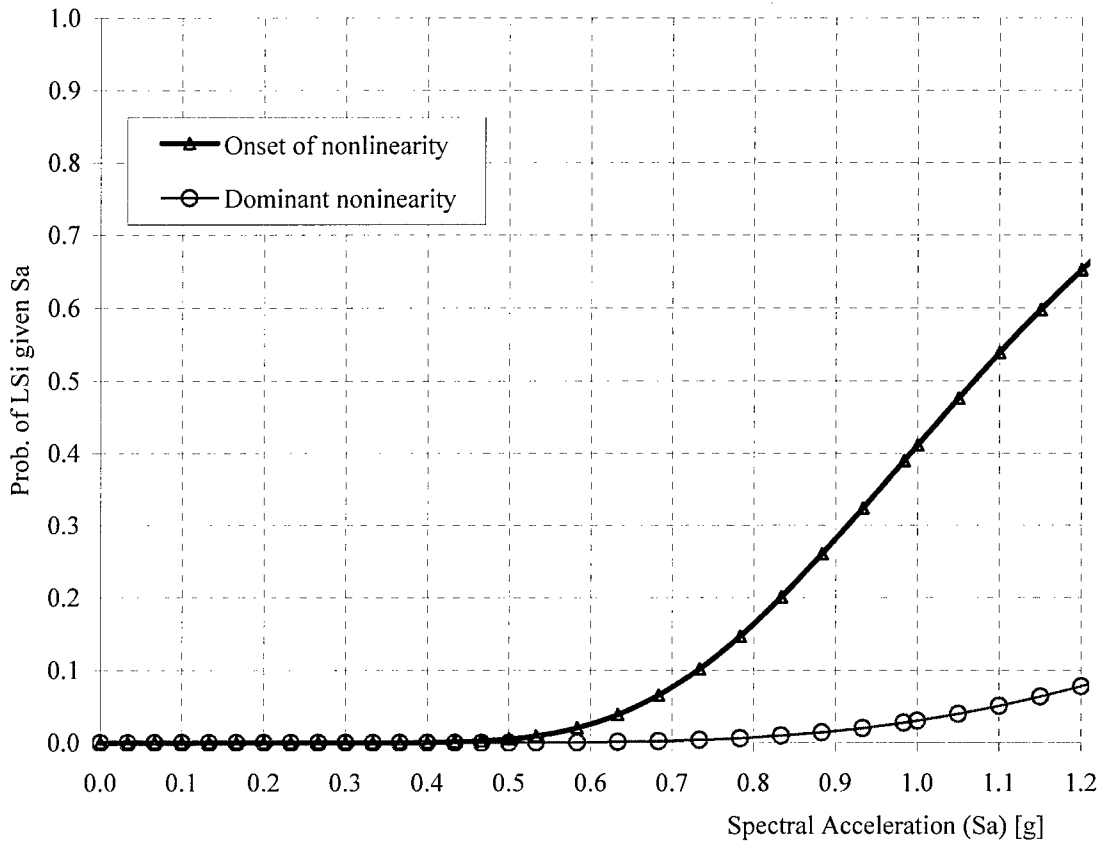


Fig. 5.13. Seismic Fragility of Monolith No. 12
LS5 – Nonlinear behavior in foundation

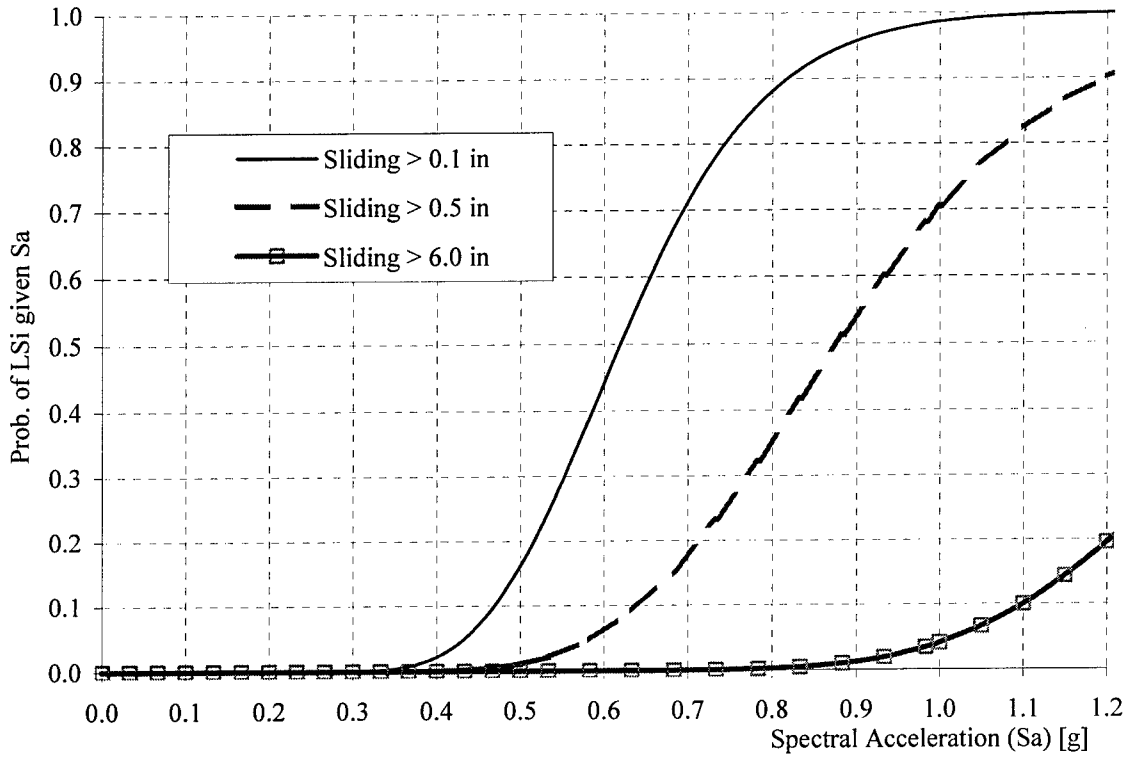


Fig. 5.14. Seismic Fragility of Monolith No. 12
 LS6 – Sliding

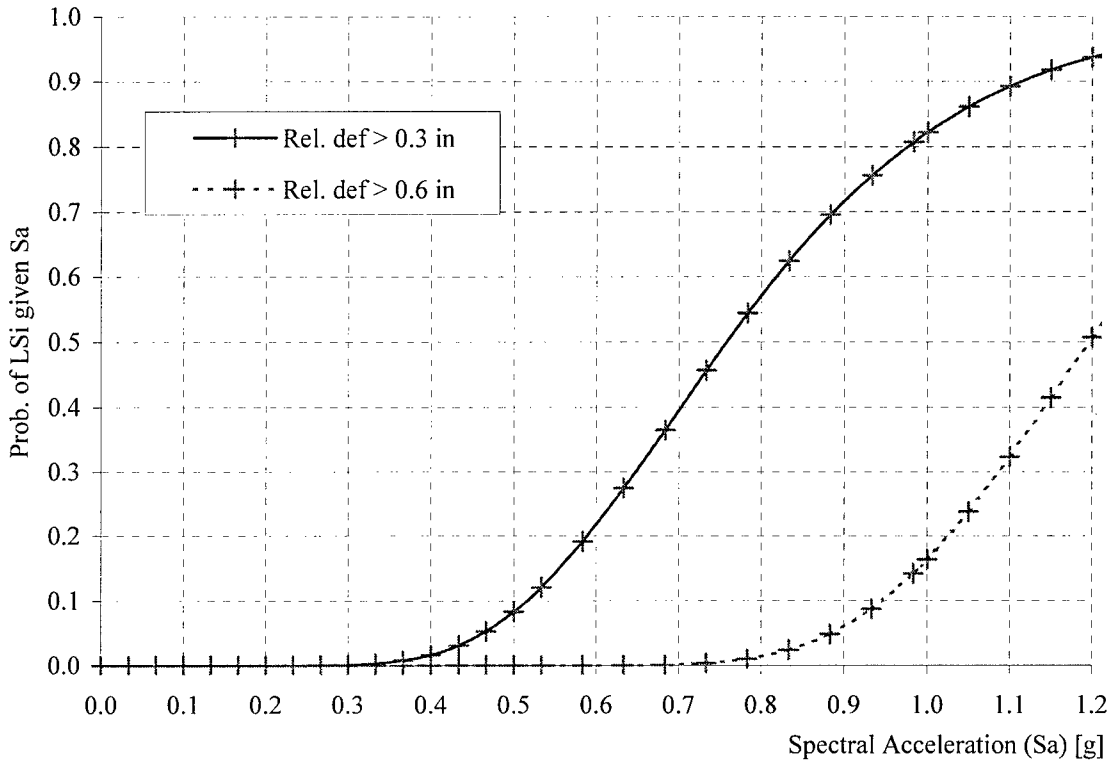


Fig. 5.15. Seismic Fragility of Monolith No. 12
 LS7 - Relative Deformation

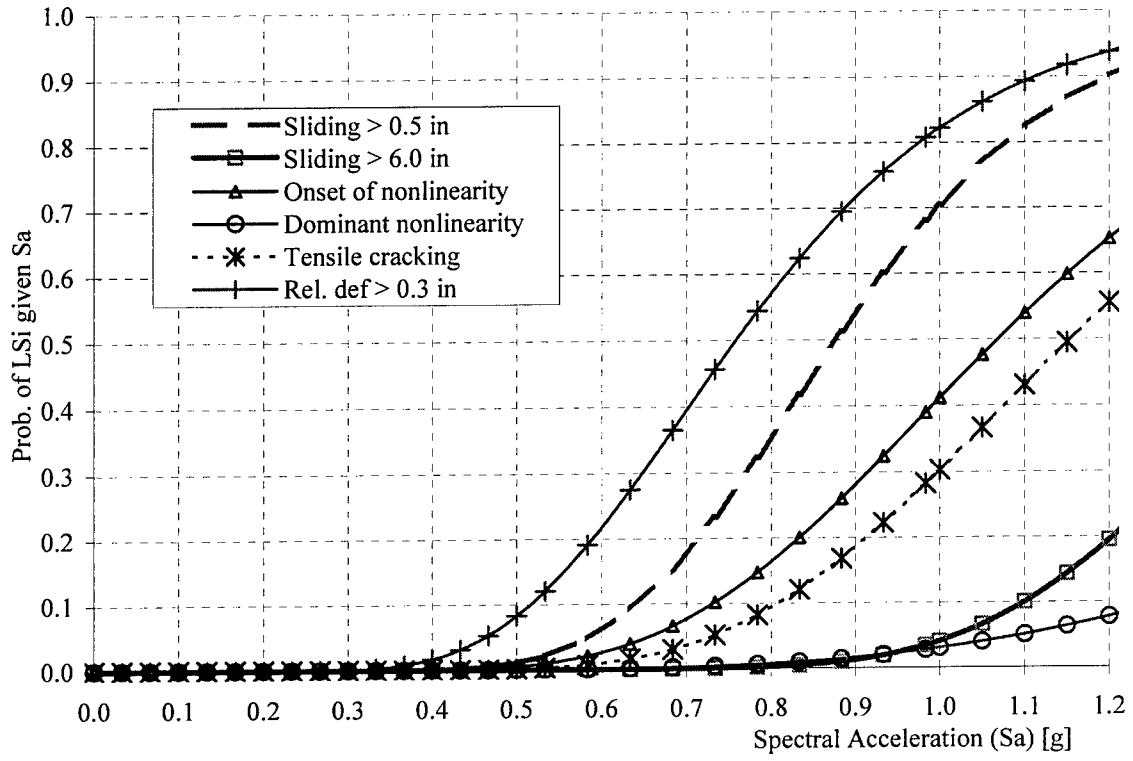


Fig. 5.16. Comparison of Seismic Fragilities

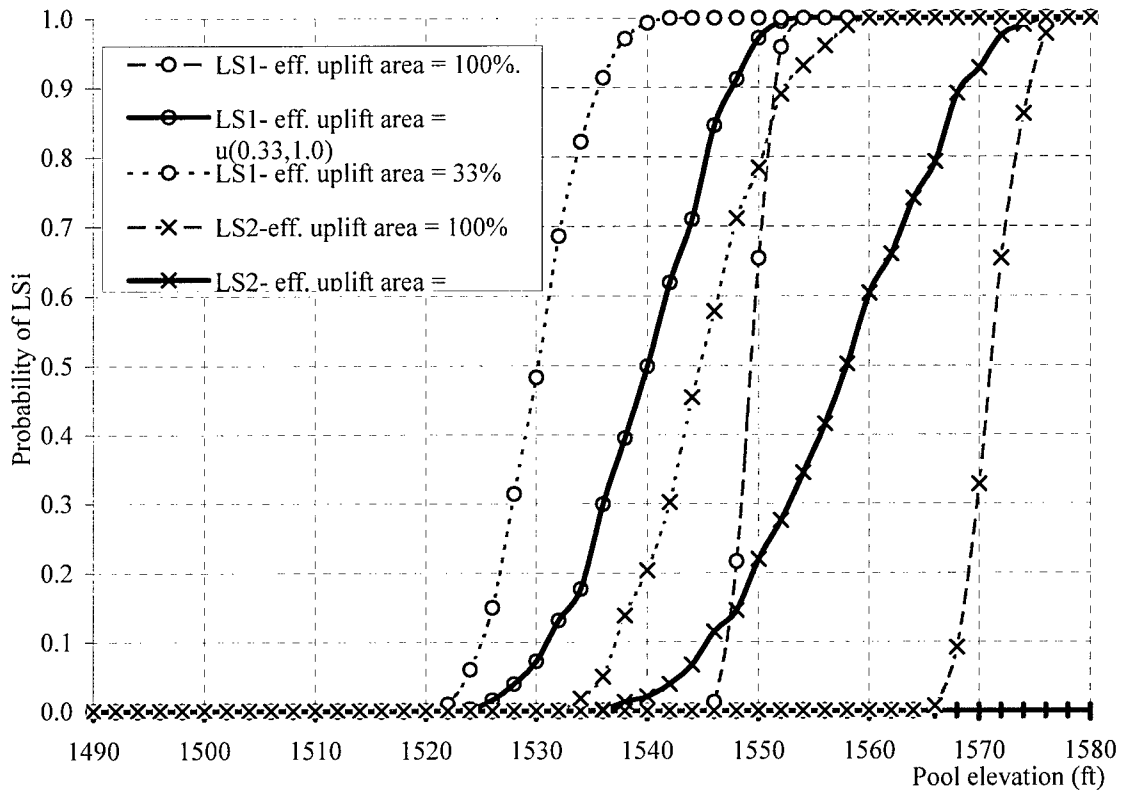


Fig. 5.17. Hydrologic Fragility - Effect of uplift area

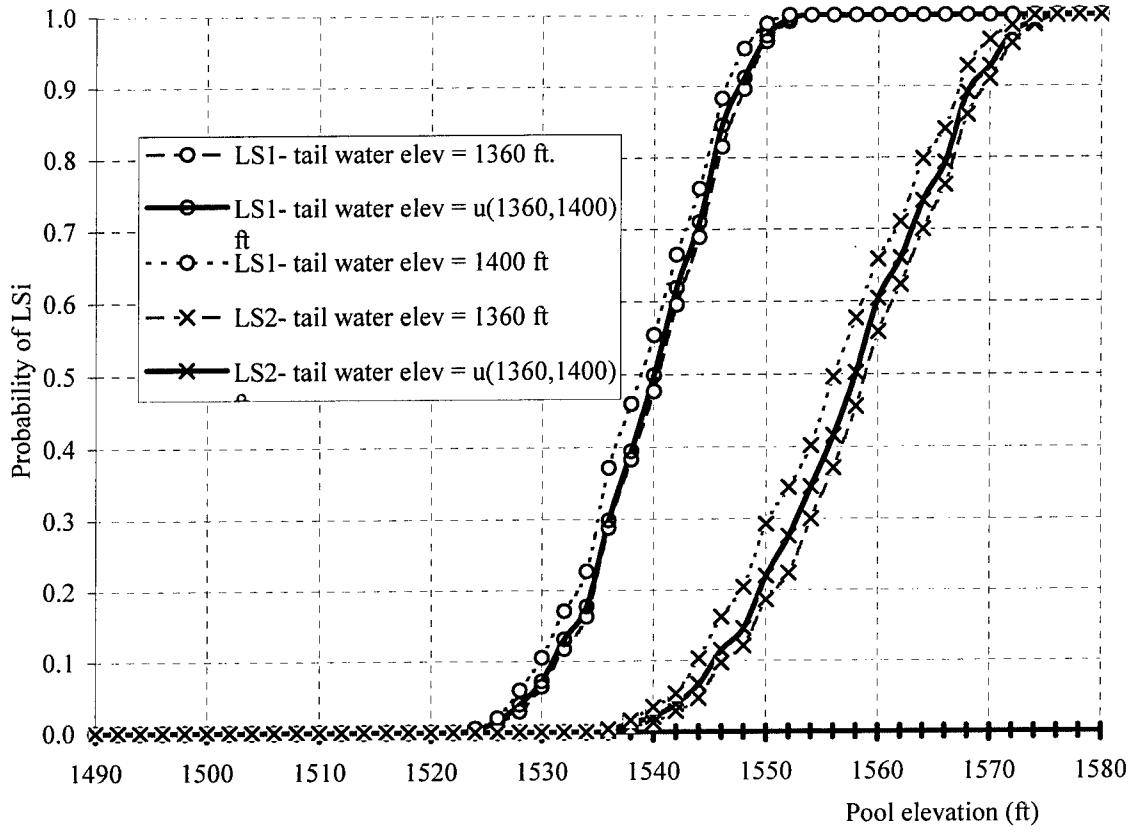


Fig. 5.18. Hydrologic Fragility - Effect of tail water elevation

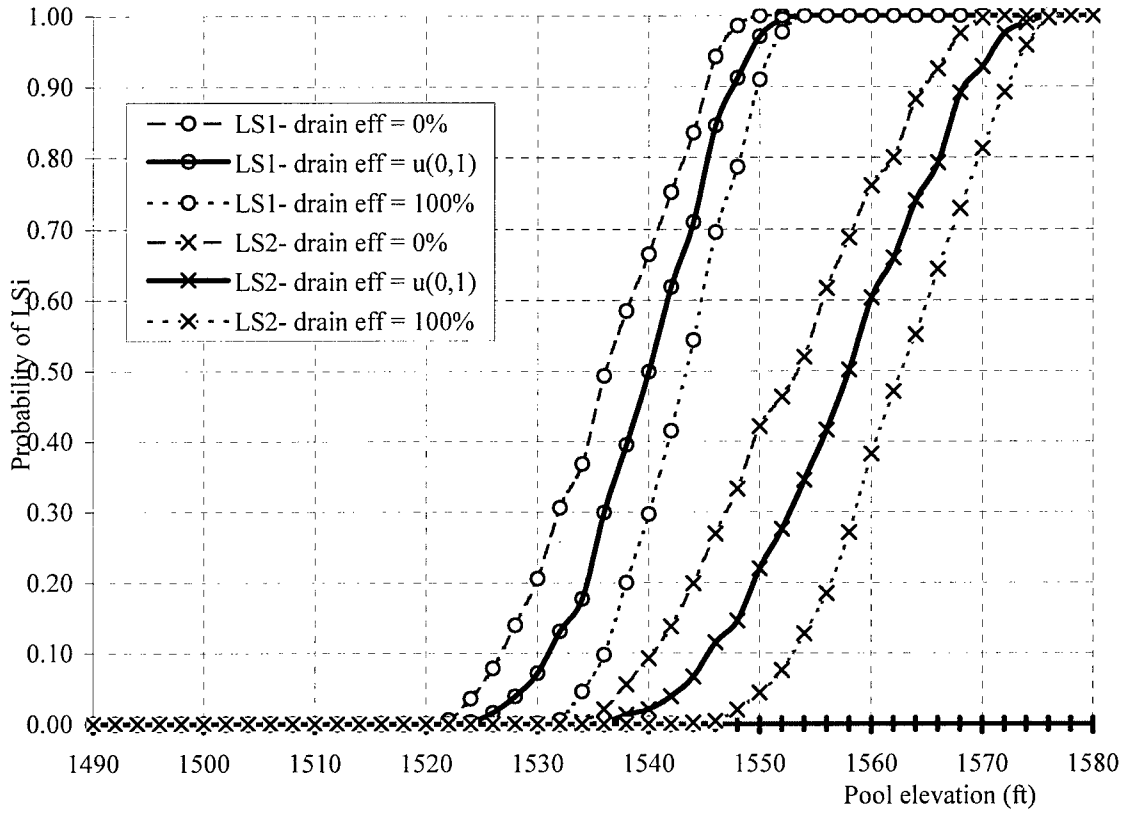


Fig. 5.19. Hydrologic Fragility - Effect of drain efficiency

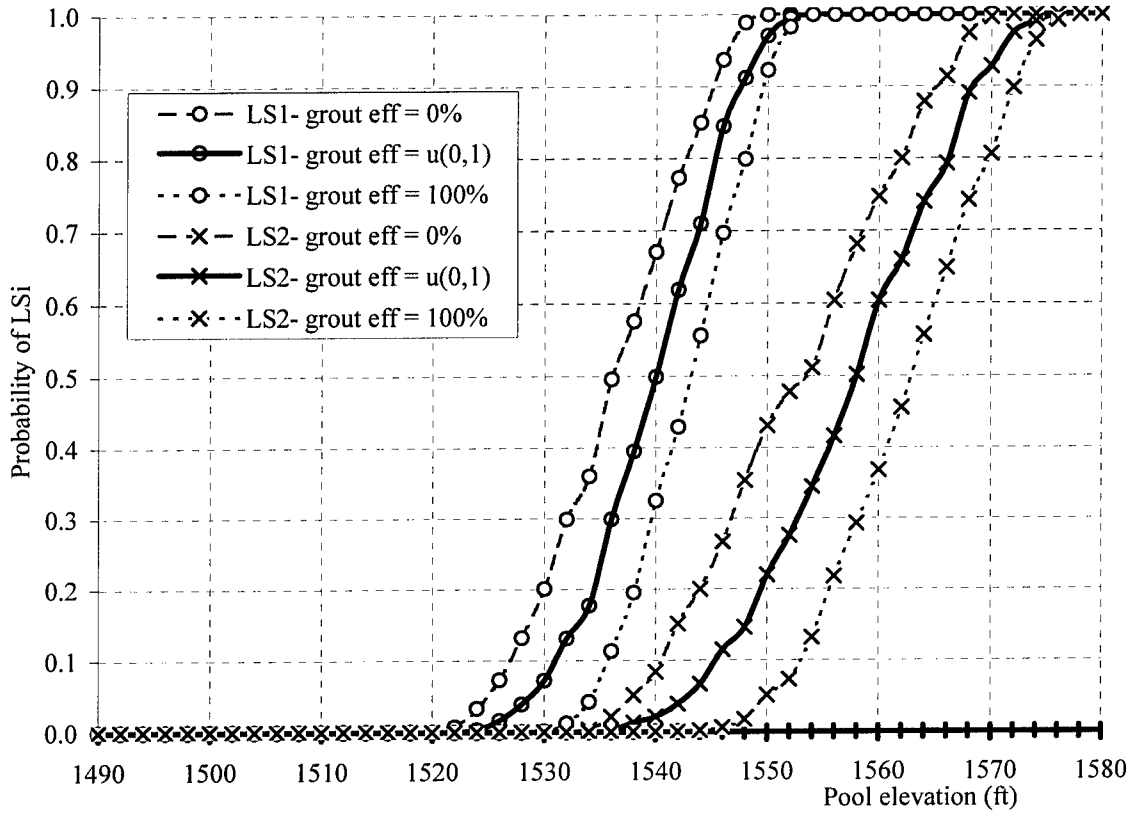


Fig. 5.20. Hydrologic Fragility - Effect of grout efficiency

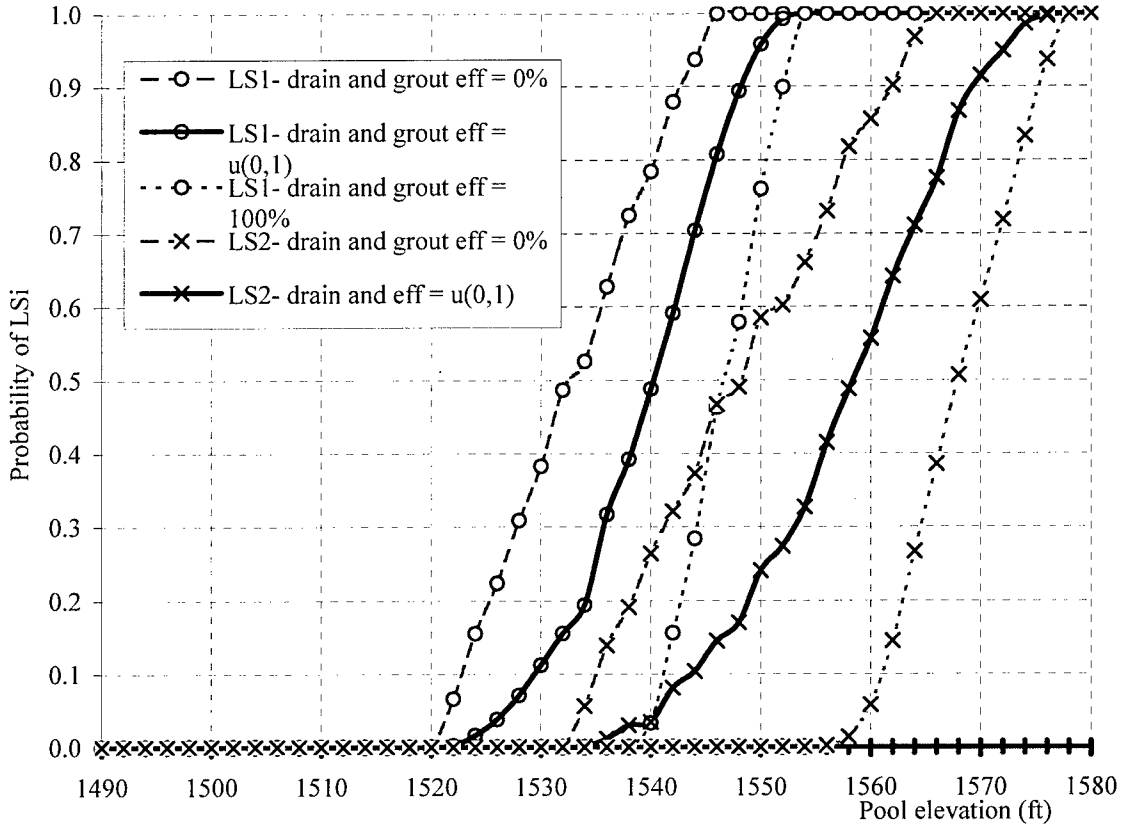


Fig. 5.21. Hydrologic Fragility - Effect of drain and grout efficiencies (perfectly correlated)

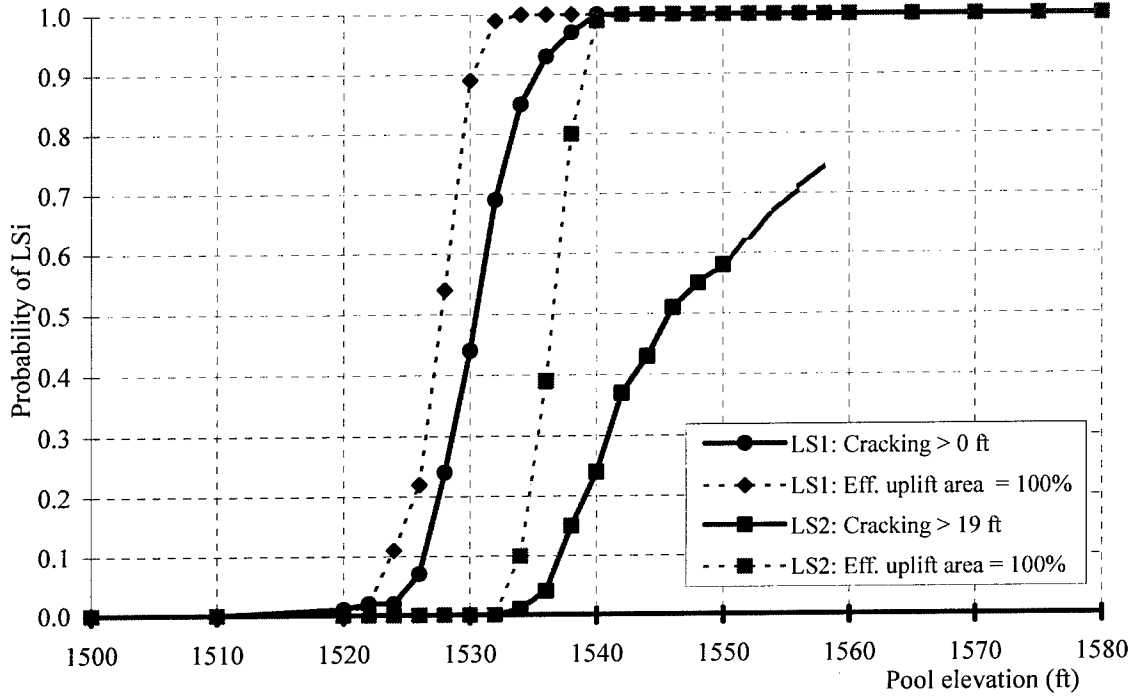


Fig. 5.22. Hydrologic Fragility - effect of effective uplift area; LS1 and LS2

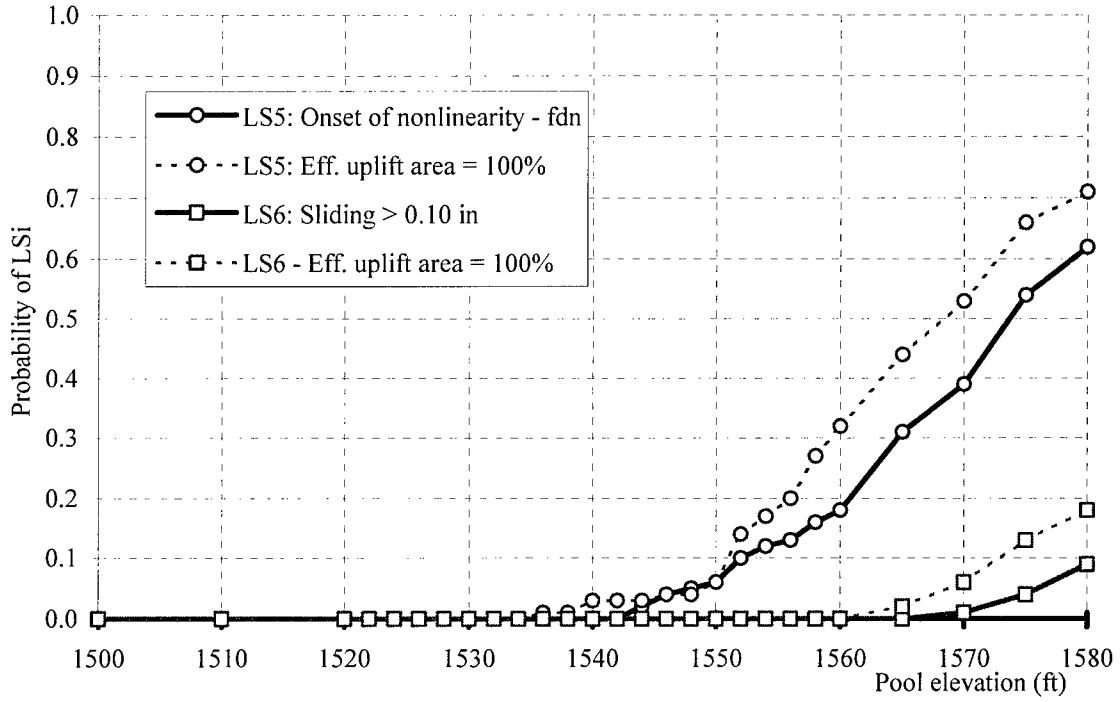


Fig. 5.23. Hydrologic Fragility - effect of effective uplift area; LS5 and LS6

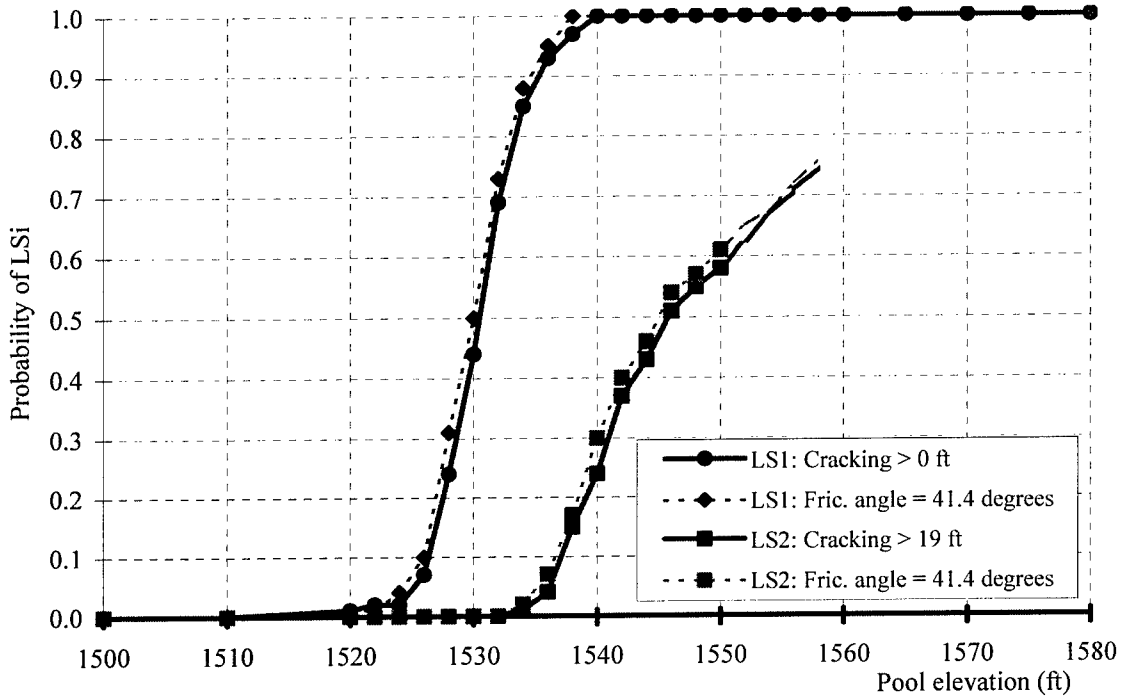


Fig. 5.24. Hydrologic Fragility - effect of coefficient of friction; LS1 and LS2

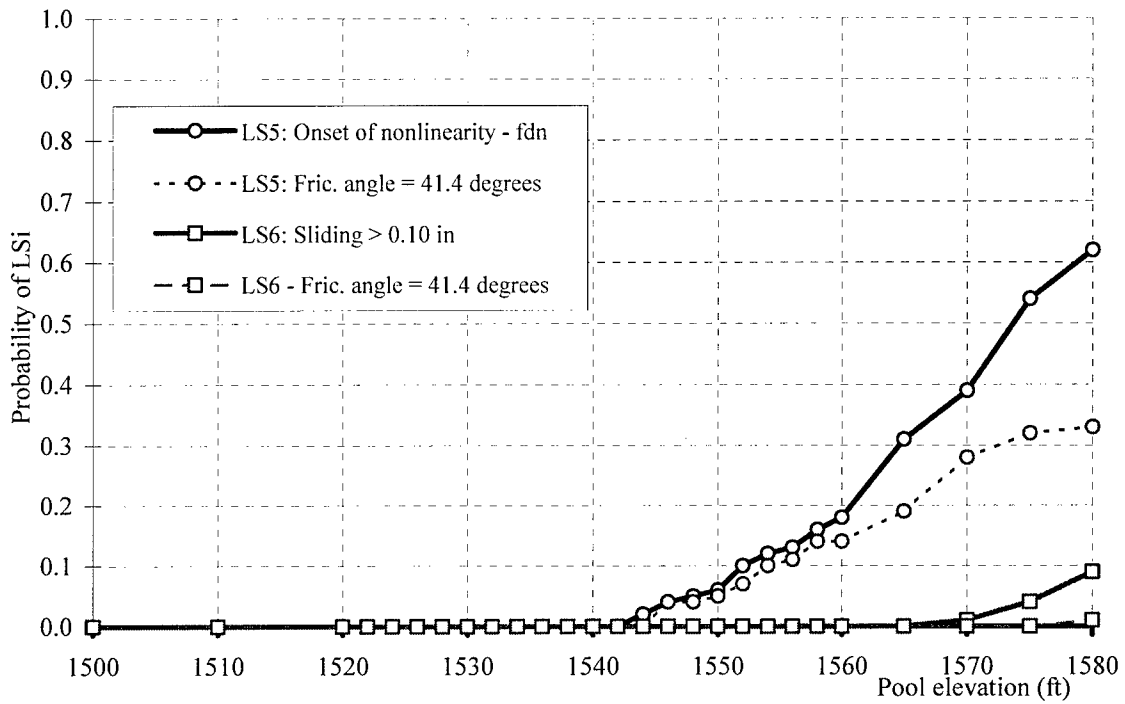


Fig. 5.25. Hydrologic Fragility - effect of coefficient of friction; LS5 and LS6

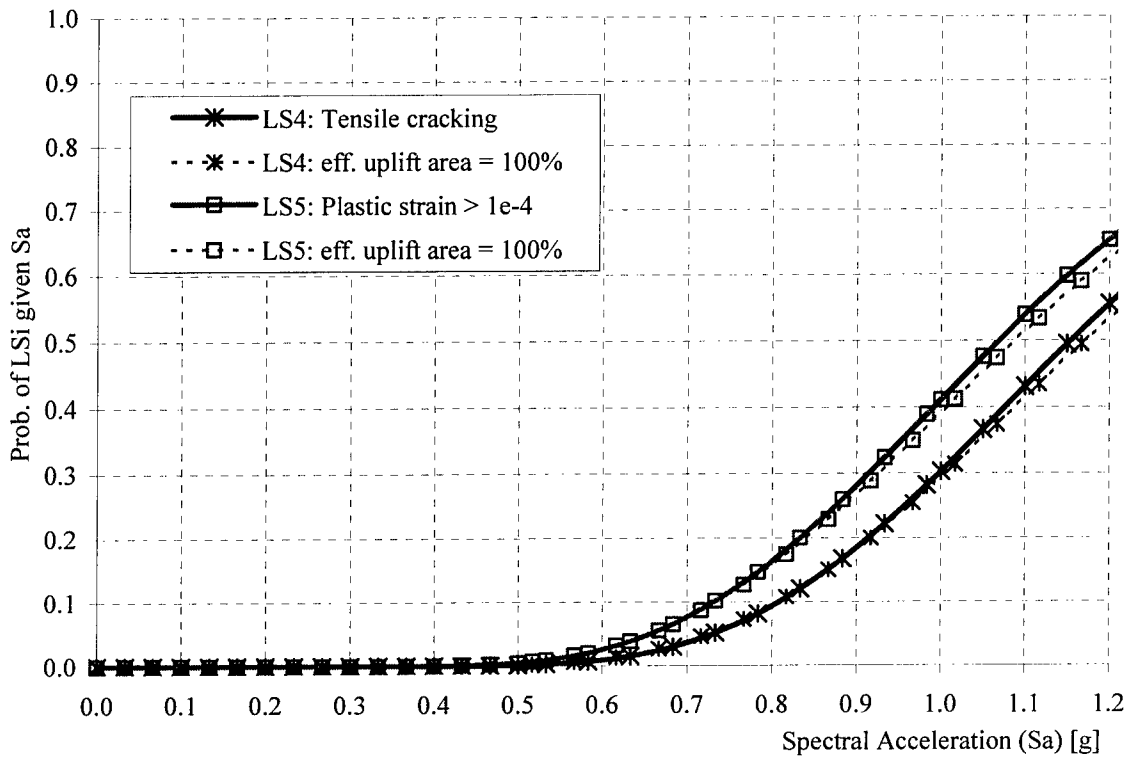


Fig. 5.26. Seismic Fragility - effect of uplift area; LS4 and LS5

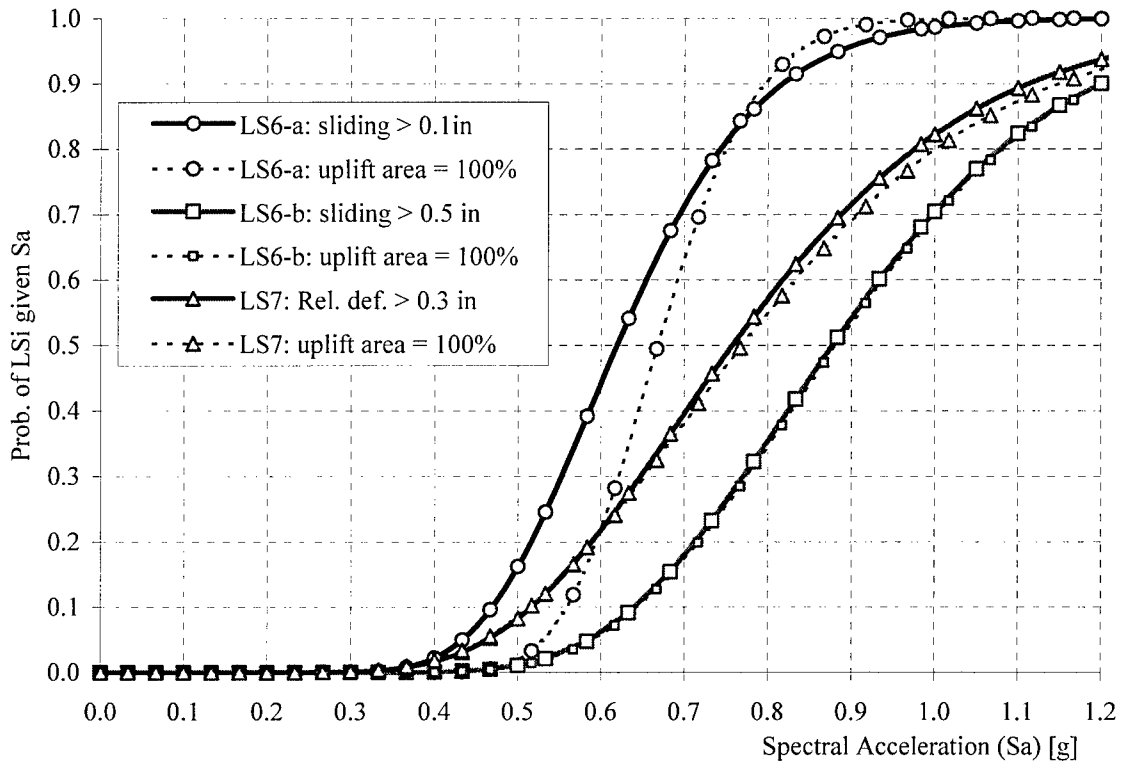


Fig. 5.27. Seismic Fragility - effect of uplift area; LS6 and LS7

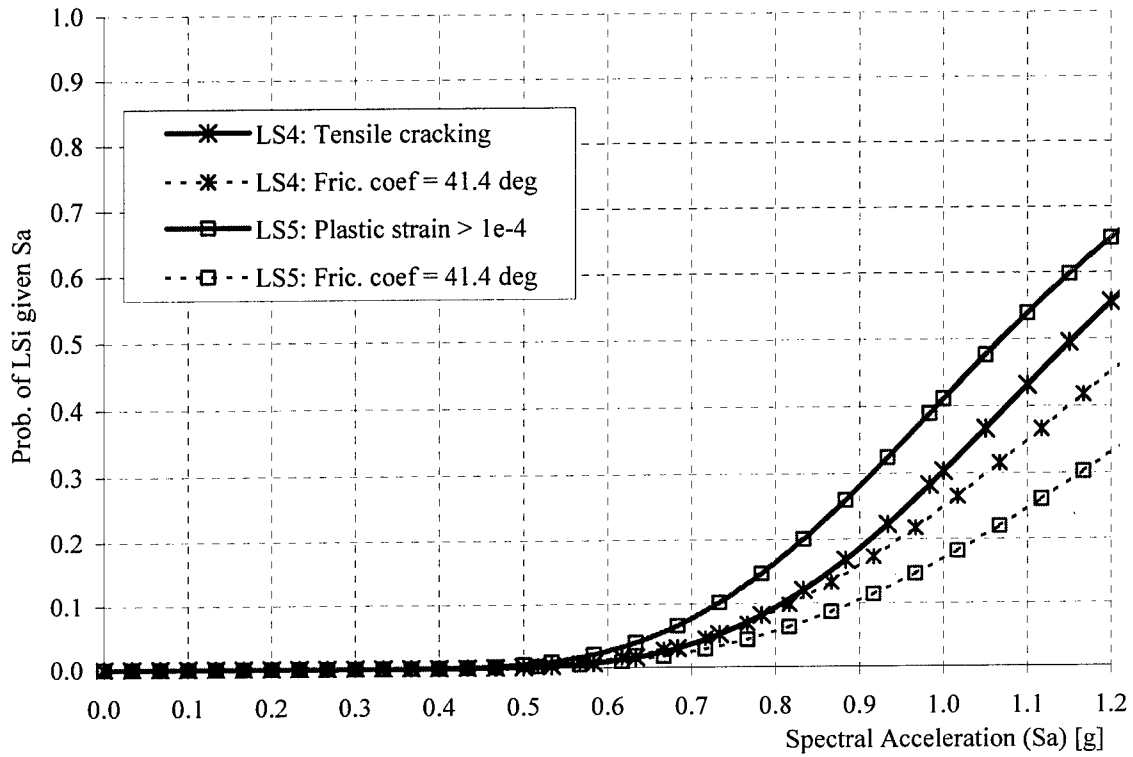


Fig. 5.28. Seismic Fragility - effect of coefficient of friction; LS4 and LS5

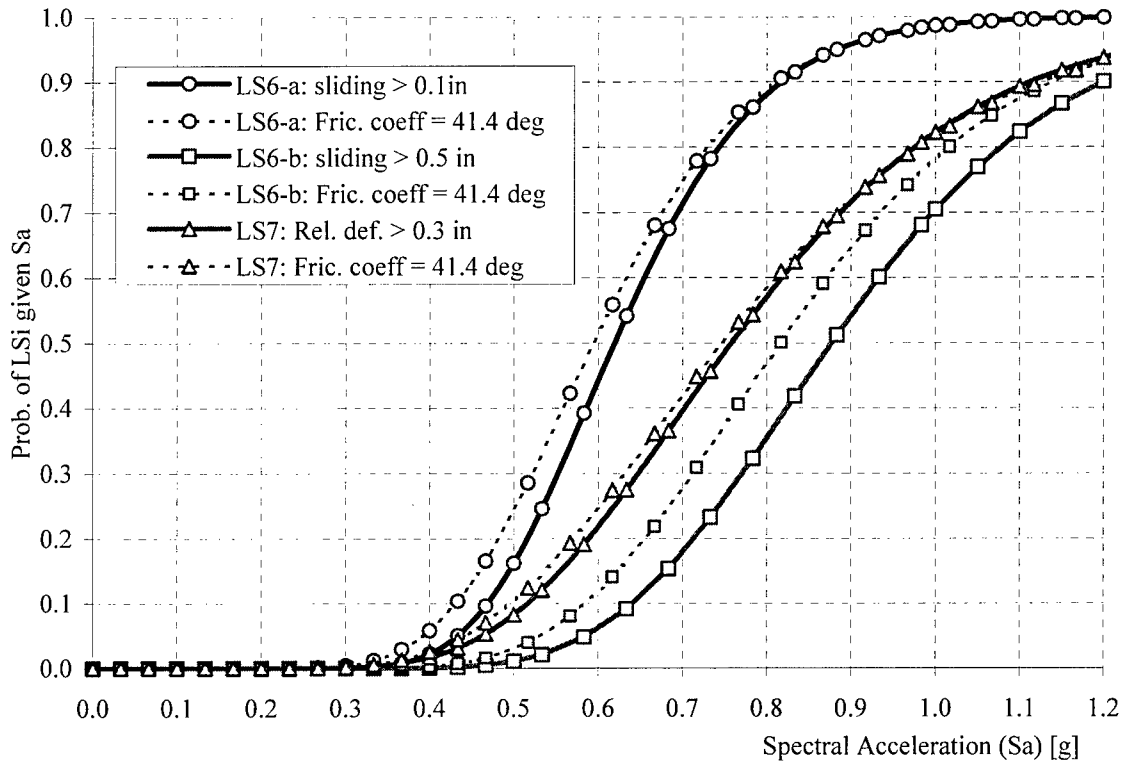


Fig. 5.29. Seismic Fragility - effect of coefficient of friction; LS6 and LS7

Chapter 6

INSIGHTS AND PERSPECTIVES ON RISK

This chapter presents guidelines for the interpretation and implementation of fragilities in the decision-making process. It also illustrates how fragilities are used in a fully coupled PSA to compute the quantitative risk metrics, i.e. limit state probabilities, and to identify ranges of the hazards that are the main contributors to risk. Comparison of these metrics indicates whether the risks due to the competing hazards are balanced. Fragilities and PSA results should be viewed in the context of socially “acceptable risks” in other human endeavors, which are described briefly in this chapter. Approximate procedures of fragility analysis for preliminary risk assessment purposes also are presented.

6.1. INTERPRETATION GUIDELINES

A fragility assessment can be used to identify a level of hazard at or below which there is a high confidence that the dam will survive. It has been common in civil/structural design and safety checking to use a nominal or characteristic strength that has a small probability, typically 5% to 10%, of not being exceeded. Because of the epistemic

uncertainties attendant to the fragility analysis, this 5%-10% exclusion limit is itself a (Bayesian) random variable (described in detail in Section 5.2; see also Fig. 5.3). Selecting a 95% lower confidence interval estimate of such an exclusion limit provides a strength level above which it is "95% likely" that the 5% or 10% exclusion limit falls. Alternatively, one can look at the review level event and assess the safety of the dam-foundation system at that level of the hazard. If the conditional probability (fragility) at the review-level event is greater than the exclusion limit (or, equivalently, if the exclusion limit is below the review-level event), then the structure may be deemed as being deficient and requiring rehabilitation work. Such quantitative measures of performance, when interpreted in a relative sense and in the context of other dam safety analyses, provide perspectives on decisions regarding rehabilitation and retrofit, and can support the development of risk management policies for concrete gravity dams.

Table 6.1 summarizes the results of the hydrologic fragility assessment of the Bluestone Dam, identifying the 5% exclusion limit for the system in its current condition (Table 6.1.a) and the (conditional) limit state probabilities at the revised PMF (Table 6.1.b). The pool elevation at which the LS1 (resultant falling outside of kern for rigid body analysis) is achieved, with a probability of 5%, is 1,528 ft. Interestingly, one obtains about the same result for the onset of cracking at the heel from both linear and nonlinear FE analyses. The pool elevations obtained at the 5% exclusion limit for LS2 are 1,543 ft, 1558 ft, and 1536 ft, for the rigid body, linear and nonlinear FE analyses, respectively. (The reasons for these discrepancies have been discussed in Section 5.4.2). For LS5 and LS6 the pool elevations shown in the last two lines of Table 6.1.a are above the design flood of 1520 ft, confirming that the original design assumptions provided substantial margins of

safety against these particular limit states. A different perspective can be obtained by looking at the probabilities associated with a review level, such as the revised PMF (pool elevation of 1556 ft)(Table 6.1.b). For this pool elevation, there will very likely be cracking at the heel of the dam; the probabilities of crack lengths of 19 ft and 38 ft are as 68% and 45% from the nonlinear FE analyses. The probability for the onset of nonlinear behavior (LS5) at this elevation is 18% or 13%, depending on whether the estimate is obtained from linear or nonlinear FE analysis. However, for LS6 (sliding ≈ 0.1 in), all models predict zero probability, indicating negligible likelihood of overall instability of the monolith in this failure mode.

The results of the seismic fragility assessment of the dam-foundation system are summarized in Table 6.2. At a spectral acceleration of 0.74 g, there is a 5% probability of tensile cracking at the neck of the dam. It is also observed that, with the same probability, the response in the foundation would be dominated by its nonlinear behavior at spectral accelerations of 1.10g. A relatively smaller spectral acceleration, about 0.65g, may cause the onset of nonlinear behavior and sliding of about 0.5 in. Alternatively, choosing a review level event defined by a spectral acceleration of 1.0g (which would be equivalent to an earthquake with a peak ground acceleration in the range 0.38g - 0.45g (Newmark and Hall, 1982), with an estimated return period of 11,000 years at Bluestone Dam (Fig. 3.1)), sliding of 0.10 in is almost certain, while there is a 76% probability of sliding of about 0.5 in. It is possible (with a probability of 28%) that there will be some tensile cracking at the neck of the dam when subjected to this intensity of seismic excitation. A relative deformation of about 0.6 in, has a probability of 16% at excitations with spectral acceleration of 1.0g. It is important to note that the seismic fragility shows a 4% probability of sliding of 6.0 in at a

spectral acceleration of about 1.0g. This merits further consideration in the evaluation of the safety of the dam, as this magnitude of sliding would break the drainage pipes, thereby increasing uplift pressures, cause differential movements between monoliths, and possibly lead to loss of control of pool (See Sect. 5.3).

6.2. FULLY COUPLED RISK ANALYSIS

6.2.1. Basic Concepts

A fully coupled probabilistic safety assessment (PSA) combines the probabilistic/statistical definitions of hazard (demand) and fragility (capacity), and leads to a point or interval estimate of limit state probability, depending on how the epistemic uncertainties are carried through the analysis. The hazard is described by the CCDF of Eqn. 3.1, while the fragility is defined by the CDF of Eqn. 5.2. The limit state probability is defined by Eqn. 5.1, in which the hazard and fragility must have a dimensionally consistent demand variable. This probability can be expressed by the convolution of the hazard (G_Y) and the fragility (F_R) as,

$$P_f = P[LS] = \int_0^{\infty} G_Y(y) \frac{d}{dy} F_R(y) dy \quad (6.1)$$

Because of modeling (epistemic) uncertainties in both hazard and fragility, both G_Y and F_R are random, and the limit state probability, P_f , is a random variable, which can be described by its own distribution. The uncertainties propagated through the analysis of the hazard and fragility (described in Chapters 3 and 5, respectively) give rise to this

distribution, as shown in Fig. 6.1. If G_Y and F_R are the mean hazard and fragility, then the convolution integral in Eqn. 6.1 yields a point estimate of the limit state probability. This point estimate does not necessarily yield the mean of P_f , as the uncertainties are not propagated in the same way. However, this estimate is usually close to the mean of P_f (Ellingwood, 1990; 1994a).

6.2.2. Risk De-aggregation

The conceptual illustration of Eqn. 6.1 in Fig. 6.2 shows that each limit state probability is dominated by hazards within a particular range. This is indicated as the range (y_{min}, y_{max}) of the integrand, which contributes most (say 95%) of the limit state probability. The point, y_m , at which the hazard contribution is greatest, is also indicated. Understanding the behavior of the dam-foundation system to hazards within this particular range is, thus, essential to dam safety/ risk assessment. This range of hazards could also be used to identify review level events for fragility analyses.

If the US Army Corps of Engineers is interested in, say, mitigating the risk of cracking of 38 ft (due to hydrologic hazard) at the Bluestone Dam, then more detailed hydrologic and structural analysis efforts should be focused on events giving rise to pool elevations of 1540 to 1560 ft (see Fig. 6.3). Likewise, the range of interest for LS5, as shown in Fig. 6.4, would be 1530 – 1570 ft. For the seismic risk, spectral accelerations of 0.5g to 0.9g dominate the risk of tensile cracking at the neck of the dam (Fig. 6.5). Similar conclusions could be drawn from Figs. 6.6 – 6.8 for LS5, LS6 and LS7. Corrective or mitigation measures aimed at improving the performance of the dam over these particular

ranges of hazards would push the fragilities towards higher levels of demand, which have smaller probabilities of being exceeded.

This examination/ identification process is referred to as risk de-aggregation in probabilistic risk analysis. Its main objective is to provide insights and perspectives on risk and to focus attention on the range of hazards of interest. This facilitates decisions on allocation of limited resources to mitigate risks posed by taking corrective measures or by changes in policy.

6.2.3. Limit State Probabilities

6.2.3.1. Computation

Using the fragilities obtained in Chapter 5 and the hazards described in Chapter 3, limit state probabilities were computed for Monolith No. 12 of Bluestone Dam. Table 6.3 shows point estimates of such probabilities obtained by convolution of the hydrologic fragilities and hazard. The annual probability of any cracking at the heel (LS1) of the dam is about 2.90×10^{-3} . For cracking lengths of 19 ft and 38 ft at the heel, probabilities of 4.92×10^{-4} and 8.63×10^{-5} were obtained. For LS5 (onset of nonlinearity) a probability of 5.85×10^{-5} was obtained. There is a significant risk of cracking of 38 ft at the heel of the dam, although the dam apparently is reasonably safe from sliding. The probability of observing a relative deformation (LS7) of at least 0.30 in is 3.06×10^{-4} .

Limit state probabilities obtained from convolution of seismic hazard and fragilities are shown in Table 6.4. The annual probability of tensile cracking (LS4) at the neck of the

dam is estimated at 7.69×10^{-5} . A higher probability of 1.72×10^{-4} is observed for sliding of 0.10 in. The smallest probability observed is for dominant nonlinear behavior ($P_f = 3.59 \times 10^{-6}$), followed by sliding of 6.0 in ($P_f = 5.60 \times 10^{-5}$), which are relatively severe performance limit states.

These limit states do not describe structural “failure”, but could be considered as states indicating some degree of structural damage. For purposes of comparison with the “failure” probabilities reported in the literature (discussed briefly in Chapter 2), one can look at the probabilities of the relatively severe limit states, i.e. cracking of 38 ft, dominant non-linearity (LS5), sliding of 6.0 in (LS6), and tensile cracking (LS4). These limit state probabilities, range from 3.59×10^{-6} to 8.63×10^{-5} , and the “failure” probabilities of concrete gravity dams are reported to be about 1.4×10^{-5} (Douglas, 1999). Accordingly, the probability of structural “failure” of the Bluestone Dam appears to be much lower than the values for other dams cited in the literature.

6.2.3.2. Risk Balancing

Limit state probabilities for hydrostatic and seismic events provide a perspective on dam safety and rehabilitation decisions when interpreted in a relative sense. Comparison of the probabilities in Tables 6.3 and 6.4 for hydrologic and seismic events indicates whether the risks due to these two competing hazards are balanced. For example, it is shown that there is some risk (due to seismic hazard) of tensile cracking, sliding of at least 0.5 in, or dominant nonlinear behavior due to seismic hazard, while the hydrologic hazard poses practically no such risk to the facility. It is also noted that there is some probability of

substantial sliding (about 6.0 in) due to seismic hazard, which might cause severe damages leading to failure of the dam-foundation system. Thus, it might be concluded that the facility risk due to seismic hazard is greater than that of hydrologic risk on an annual basis. Considered in this light, costly structural rehabilitation of the dam to reduce hydrologic risk would appear to be a questionable investment. Future rehabilitation efforts or corrective measures for the Bluestone Dam should at least consider the relative values of these risks.

6.3. ACCEPTABLE RISK

Limit state probabilities associated with dams should be evaluated and compared with risks[†] associated with failures of other civil infrastructure facilities (e.g. buildings, bridges) and with other human endeavors. Facility risks should be below a level deemed acceptable to society. Decisions can then be prioritized based on probabilistic safety metrics and on socially “acceptable risk” levels. Though the notion of “acceptable risk” is intrinsic in risk management and policy decision-making, establishing such a criterion is a complex and controversial task.

6.3.1. Decision-Making Agencies

Acceptability of risks is influenced (partly) by the outcomes of formal decision-making processes of agencies concerned with public health and safety issues. The decision-making process is based on risk assessment, cost-benefit analysis, consideration of social,

[†] Many references use "risk" to connote a function of failure probability and consequences of failure, often their product; for purposes of the present discussion, however, they can be used interchangeably.

legal, cultural and political influences and constraints. The decision-making body usually includes risk analysts, engineers, economists, facility managers, policy makers, public interest groups and lawyers. Proper communication of facility risk to non-expert personnel in the decision-making agencies is vital. This undertaking is made difficult by the small probabilities (of failure) involved, usually of the order of 10^{-3} to 10^{-6} , and by limitations in the supporting databases. In addition, the techniques for developing quantitative estimates of risk are complex and involve substantial uncertainties. The variability in the estimated probabilities could be, for example, of the same order of magnitude as the estimate. Nonetheless, it is possible to establish insights on the nature of risk and on strategies for its mitigation (Whitman, 1984; Ellingwood, 1994a).

Differences in attitudes towards formal decision analysis in risk management also influences determination of “acceptable risk”. The degree of public participation in the decision-making process and the level of trust endorsed on the decision-making institutions contribute significantly to these differences. This is illustrated by the widespread acceptance of nuclear power in France (which has traditional respect for technocrats and limited public participation due to the strong central government) and its rejection in the US (whose citizens perhaps have less trust in technology and governments and therefore demand more public participation and control over decisions) (Slovic, 1995; Stewart and Melchers, 1997).

6.3.2. Social Risk Perception

Acceptability of risk is influenced by the perception of the risk by those likely to be exposed to it. This perception varies depending on whether the risk is voluntary or

involuntary, whether the risk is related to a group or an individual, and on perceptions of hazard level and associated severity of consequences. Voluntary risks, such as mountain-climbing, smoking, and sky-diving, are willingly undertaken by an individual having control over his/her actions. Numerous studies over the past 30 years, beginning with Starr's research on the topic (1969), have suggested that risks incurred voluntarily are on the order of 10^{-3} /yr, while those that are involuntary (e.g. building occupancy) are on the order of 10^{-6} /yr. Failure of infrastructure facilities, such as dams, clearly entail involuntary risks.

Risk perception also depends on the number of individuals at risk. When large populations are at risk, as opposed to individuals, social behavior becomes more risk-averse. For example, society will more readily accept 1000 different accidents, each involving one death, than 1000 deaths in a single accident, though the social consequences (in a statistical sense) may be the same. This "risk aversion" tends to lower acceptable levels of risk for risks involving large groups of people.

Levels of acceptable risk are greatly influenced by perceptions of the level of hazard and its consequences. It has been found, for example, that nuclear power plants have one of the highest perceived risks and the lowest expected number of annual fatalities (Slovic et al, 1980), although the actual risks related to nuclear power plants and smoking are reported to be 9×10^{-6} and 4×10^{-3} fatalities/person/year (Stewart and Melchers, 1997). These perceptions are shaped (in part) by psychological aspects, such as the dread (fear) of the catastrophic potential, the "unknown" (unfamiliar) consequences and the high degree of exposure to the hazard.

6.3.3. Acceptable levels of risk

It is natural to compare a facility risk with risks in other human endeavors, obtained from known statistics. The background or "de minimis" individual risk level in the United States (the level where risk tends not to impact public policy) appears to be on the order of 10^{-7} /person/yr (Whipple, 1987; Pate-Cornell, 1994); when the mortality is of the order 10^{-7} or less, action rarely is taken. In contrast, risks with fatality rates greater than 10^{-3} generally are deemed unacceptable. Most engineered infrastructure projects fall in the grey area between 10^{-7} /yr and 10^{-3} /yr. Bridge failure probabilities are on the order of 10^{-4} /yr, dam failure probabilities are on the order of $1/5,000$ (2×10^{-4})/yr (McCann, 1986). Generally, one finds that in this range, the risk is deemed acceptable if the benefits outweigh the risks and government takes specific steps to mitigate the risk through education (health care, vaccinations, etc.) and regulation (speed limits, safety boards, etc).

Typical values of these risks in the United States, usually expressed in mortality rates, are shown in Table 6.5. The overall mortality risk in the United States (uncorrected for exposure) is about 8.6×10^{-3} /yr; of this, heart disease and cancer amount to about 5.7×10^{-3} /yr. Individual risk of death from motor vehicle accidents has stabilized around 2×10^{-4} /yr for many years. One problem with such tabulations is that they often simply divide the number of incidents by the U.S. population. This fails to take into account differences in exposure. For example, if only 20% of the population travels by air in a given year, the fatality/yr would increase by a factor of 5, to 2.2×10^{-5} /yr; even here, some people might only fly once, while others fly weekly. Clearly, the fatality rates for such groups are not the same. Activities that engage the entire population on a more or less equal footing are less prone to such data interpretation problems.

In the evaluation of risk associated with dam failures, F-N diagrams have been used recently (e.g. Whitman, 1984; Hoeg, 1996; Stewart and Melchers, 1997). These diagrams relate the frequency of occurrence to number of fatalities. Fig. 6.9 (adapted from Hoeg, 1996) illustrates a comparison of F-N curves used by different institutions as safety goals. It also presents a proposed F-N curve as a global safety criterion for dams. Another proposal (Lave et al, 1990) is to limit the limit state probability to,

$$P_f = K \frac{10^{-n}}{N^m} \quad (6.2)$$

in which N = number of people at risk, K = social factor based on the nature of the facility, and m, n = constants greater than 1.0; in one study, it was suggested that $m = 1.2$ (Lave et al, 1990). This criterion has "risk aversion" built into it through the factors K and m ; for the B.C. Hydro curve in Fig. 6.9, for example, $m = 1.0$.

The probabilities for the relatively severe limit states computed in Section 6.2.3 were on the order of 10^{-5} . Assuming zero fatality, these probabilities would be located inside the "tolerable" region shown in Fig. 6.9. However, further studies are needed to estimate the "failure" probability and to link this probability to the expected downstream fatalities due to dam "failure". If the results indicate that the "failure" probability is less than 10^{-7} ("de minimis" risk) or if the fatality-probability value plots within the "tolerable" region in Fig. 6.9, then the risk posed by the Bluestone Dam would be deemed "acceptable risk" to the population downstream.

Risk analysis of dams should consider only the incremental increase in risk or damage caused by the presence of the dam. Any damage that otherwise might occur if the dam were not present must be discounted (Bury and Kreuzer, 1986; Lafitte, 1993), i.e.

damage that would occur during floods, if the dam were not in place, need not be ascribed to the dam, but damage that would occur in a so called “sunny day” should be considered. Finally, acceptable risks may be different for existing facilities than for new facilities. With an existing facility, the option of whether or not to build does not exist. Removal of the facility may pose additional risks and cause loss of benefit. Risk of an old facility reaches social equilibrium, with entrenched economic interests and established expectations, whereas a new facility represents the unknown and poses unknown risks.

6.4. SIMPLIFIED RISK ANALYSIS MODELS

The dam fragility analysis described thus far (Chapters 4 and 5) is a complicated and computationally expensive procedure. Procedures that are simple, relatively accurate and computationally cheap are needed. The simplifications could be uncertainty-related or modeling-related, as described below. Such simple risk analysis procedures might be used as a screening tool to determine whether to invest in a more rigorous risk analysis of the dam.

6.4.1. Statistical Simplification

Some studies (e.g. Cornell, 1994; Ellingwood, 1994a; Kennedy, 1997) have suggested that the hazard function (especially seismic hazard) can be approximated, over the range of interest (y_{min} to y_{max} , in Fig. 6.2), by a linear logarithmic function. In equation form,

$$G_Y(y) \approx \left(\frac{y}{u}\right)^{-k} \quad (6.3)$$

Substituting the above and Eqn. 5.3 into Eqn 6.1, and differentiating, one obtains

$$y_m \approx m_R e^{-\beta_C^2 (1+k)} \quad (6.4)$$

$$P_f \approx G_Y(m_R) e^{\frac{(k\beta_C)^2}{2}} \quad (6.5)$$

These approximations enable the limit state probability and the dominant hazard contributors to be estimated without resort to numerical integration. For example, suppose that for a dam fragility $\beta_C = 0.10$ and $k = 5.3$ (Bury and Kreuzer, 1985), one finds that $y_m = 0.94 m_R$ and $P_f = 1.15 G_Y(m_R)$. This indicates that the greatest contribution to the probability comes from hazard levels at about 94% of the median capacity, and the probability (of failure) can be estimated simply by entering the hazard curve at the median dam capacity and multiplying the result by 1.15. Moreover, it can be shown that about 95% of the risk comes from hazard levels between $0.87m_R$ and $1.28m_R$ (cf. Fig. 6.2). This simple analysis emphasizes the importance of being able to estimate the median capacity of the dam and the flood hazard at fractiles close to the median dam capacity.

The above approximation formulae were found to work quite well for the seismic risk of the Bluestone Dam. The approximate values were within 1% of those obtained by numerical integration. However, for the hydrologic risk, the approximations were very inaccurate. The errors in the approximations have been found to be as large as an order-of-magnitude (sometimes even higher). It is thus recommended that numerical integration be carried out for the hydrologic risk, while use of Eqn. 6.5 would suffice for seismic risk.

6.4.2. Structural Simplification

The previous section illustrated the importance of accurate estimation of the median fragility, m_R . It clearly would be advantageous to be able to estimate this fragility by scaling upward appropriately from design conditions. Such a procedure is illustrated conceptually in Fig. 6.10, which shows the increase in deformation and plastic strain beyond the elastic design basis as a function of increasing hazard. Using this approach, the median fragility, m_R , and its variability (or logarithmic standard deviation), V_R , for a given behavior state might be determined by,

$$m_R = m_1 m_2 \dots m_n R_d \quad (6.6)$$

$$V_R = \sqrt{V_1^2 + V_2^2 + \dots + V_n^2} \quad (6.7)$$

in which R_d = design capacity of the dam to withstand the design-basis hazard; factors m_1, \dots, m_n are "median factors of safety" due to design conservatisms, modeling assumptions, and other factors that represent the additional margin of safety beyond the design basis; and V_1, \dots, V_n are coefficients of variation in these individual factors, collectively assumed to be equal to β_C in Eqn 5.4 (the aleatory and epistemic uncertainties in each parameter have been combined). With m_R and V_R determined, the review-level capacity can be determined from the 5-percentile value of the mean fragility:

$$R_k = m_R e^{-1.645 V_R} \quad (6.8)$$

To estimate the median fragility, m_R , a few carefully selected median-centered nonlinear finite element analyses under increasingly severe levels of demand might be used. This was performed for the Bluestone Dam for both the hydrologic and seismic fragilities. For the hydrologic fragilities, the median capacities were estimated from a dam modeled using the median parameters and subjected to increasing levels of pool elevation. Figs. 6.11-12 show the approximate hydrologic fragilities (constructed using $V_R = \beta_C$ obtained from fragilities in Chapter 5). The approximations shown match closely those obtained in Chapter 5. For the seismic case, the simplification required, in addition to a median-centered model, the reduction in the number of earthquake ground motions used. As was suggested by Shome and Cornell (1997, 1998), four ground motion records were used. The approximate fragilities were obtained using LHC sampling procedure (as in Chapter 5). Figs. 6.13-16 show that the approximate seismic fragilities closely match those obtained in Chapter 5, though there is a relatively larger difference for tensile cracking and relative deformation.

This demonstrates that a median-centered fragility analysis yields the median capacity and fragilities based on that estimate could be used at least for preliminary studies to determine whether a more rigorous fragility assessment is necessary. This can be particularly helpful in seismic fragility assessment, which is a computationally expensive endeavor.

Table 6.1. Hydrologic fragilities

a) Behavior at 5-percentile fragility

	Rigid body	Linear FE	Nonlinear FE
LS1 (Cracking-heel > 0 ft)	1528 ft	1528 ft	1525 ft
LS2 (Cracking-heel > 19 ft)	1543 ft	1558 ft	1536 ft
--- (Cracking-heel > 38 ft)	---	---	1545 ft
LS5 (Onset of Nonlinearity- fdn)	> 1580 ft	1537 ft	1548 ft
LS6 (Sliding \approx 0.1 in)	> 1580 ft	> 1580 ft	1576 ft

b) For revised PMF, P [LS | Y = 1556 ft]

	Rigid body	Linear FE	Nonlinear FE
LS1 (Cracking-heel > 0 ft)	100 %	100 %	100 %
LS2 (Cracking-heel > 19 ft)	43 %	0 %	(68) ¹ %
--- (Cracking-heel > 38 ft)	---	---	45 %
LS5 (Onset of Nonlinearity- fdn)	0 %	18 %	13 %
LS6 (Sliding \approx 0.1 in)	0 %	0 %	0 %

¹ Value is taken from extrapolated part of fragility.

Table 6.2. Seismic fragilities

a) Spectral acceleration (S_a) at 5-percentile fragility

		Nonlinear FE
LS4	Tensile cracking	0.74 g
LS5	Onset of Nonlinearity – fdn	0.65 g
	Dominant Nonlinearity - fdn	1.10 g
LS6	Sliding > 0.1 in	0.52 g
	Sliding > 0.5 in	0.63 g
	Sliding > 6.0 in	1.02 g
LS7	Rel. def. > 0.3 in	0.46 g
	Rel. def. > 0.6 in	0.89 g

b) Probabilities at $S_a = 1.0$ g, i.e. $P[\text{LS} | S_a = 1.0 \text{ g}]$

		Nonlinear FE
LS4	Tensile cracking	28%
LS5	Onset of Nonlinearity – fdn	41%
	Dominant Nonlinearity - fdn	3%
LS6	Sliding > 0.1 in	100%
	Sliding > 0.5 in	76%
	Sliding > 6.0 in	4%
LS7	Rel. def. > 0.3 in	82%
	Rel. def. > 0.6 in	16%

Table 6.3. Limit state probabilities (Hydrologic)

Limit State	Probability
LS1: Cracking > 0 ft	2.90×10^{-3}
LS2: Cracking > 19 ft	$4.92 \times 10^{-4\dagger}$
---: Cracking > 38 ft	$8.63 \times 10^{-5\dagger}$
LS5: Onset of nonlinearity	5.85×10^{-5}
LS6: Sliding > 0.10 in	3.62×10^{-7}
LS7: Rel. def. > 0.3 in	3.06×10^{-4}

[†] Extrapolated fragility used in computation of probability

Table 6.4. Limit state probabilities (Seismic)

Limit State		Probability
Tensile stress	S22 > 250 psi	1.64×10^{-4}
	Tensile cracking	$7.69 \times 10^{-5\dagger}$
Nonlinear behavior	Onset of nonlinearity	$9.02 \times 10^{-5\dagger}$
	Dominant nonlinearity	$3.59 \times 10^{-6\dagger}$
Sliding	> 0.1 in	1.72×10^{-4}
	> 0.5 in	1.16×10^{-4}
	> 6.0 in	$5.60 \times 10^{-5\dagger}$
Relative deformation	> 0.3 in	1.49×10^{-4}
	> 0.6 in	$7.22 \times 10^{-5\dagger}$

[†] Extrapolated fragility used in computation of probability

Table 6.5. Annual Individual Fatality Risks (Statistical, 2001)

<u>Source</u>	<u>Fatality/yr</u>
Motor vehicle	1.6×10^{-4}
Air travel	4.0×10^{-6}
Fires	1.4×10^{-5}
Homicide and legal intervention	6.4×10^{-5}
Cancer (all)	2.0×10^{-3}
Cardiovascular disease	3.5×10^{-3}
Natural disasters	7.2×10^{-7}
Flood-related disasters	4.4×10^{-7}

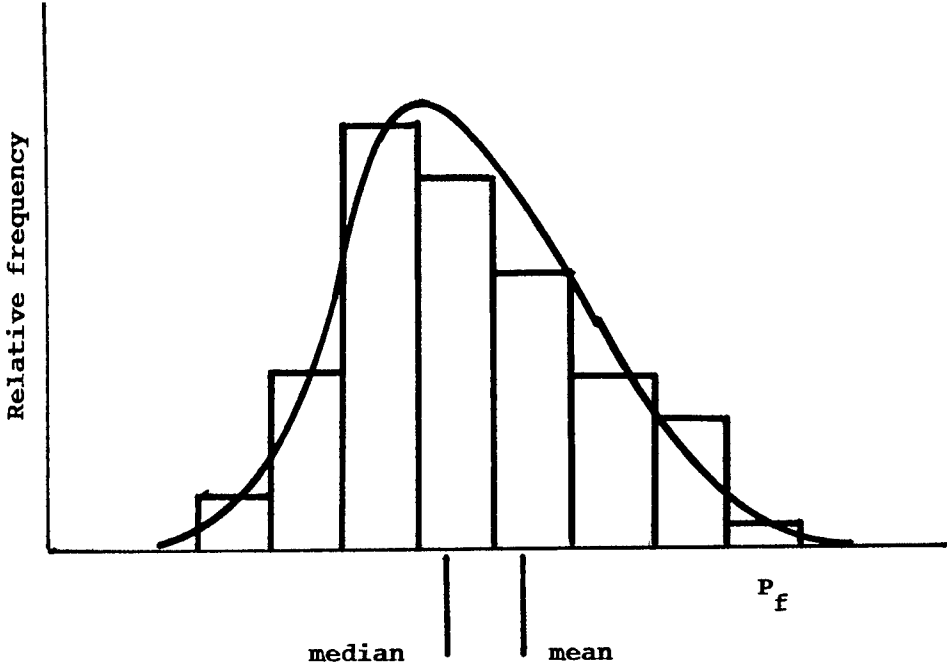


Fig. 6.1. Frequency distribution of estimated limit state probability

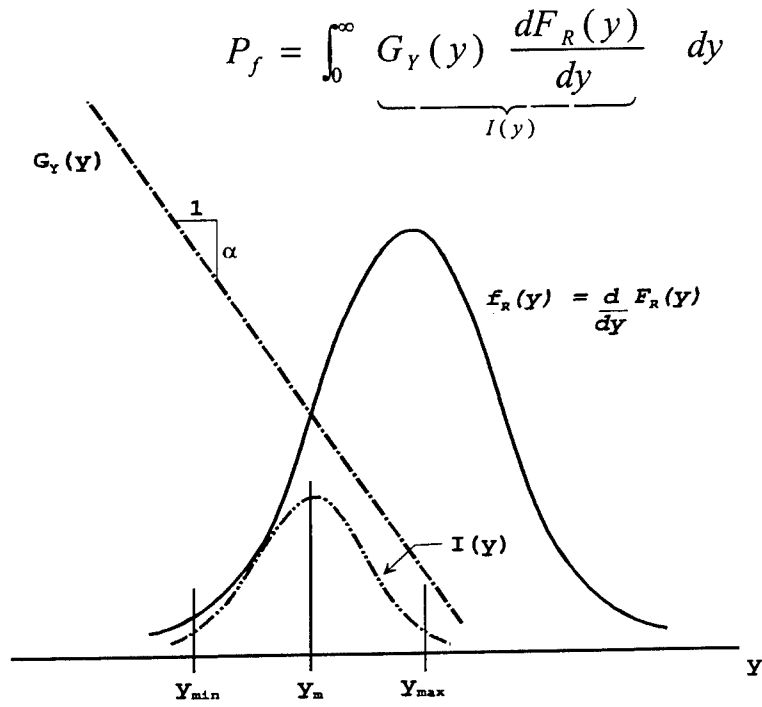


Fig. 6.2. Determination of limit state probability

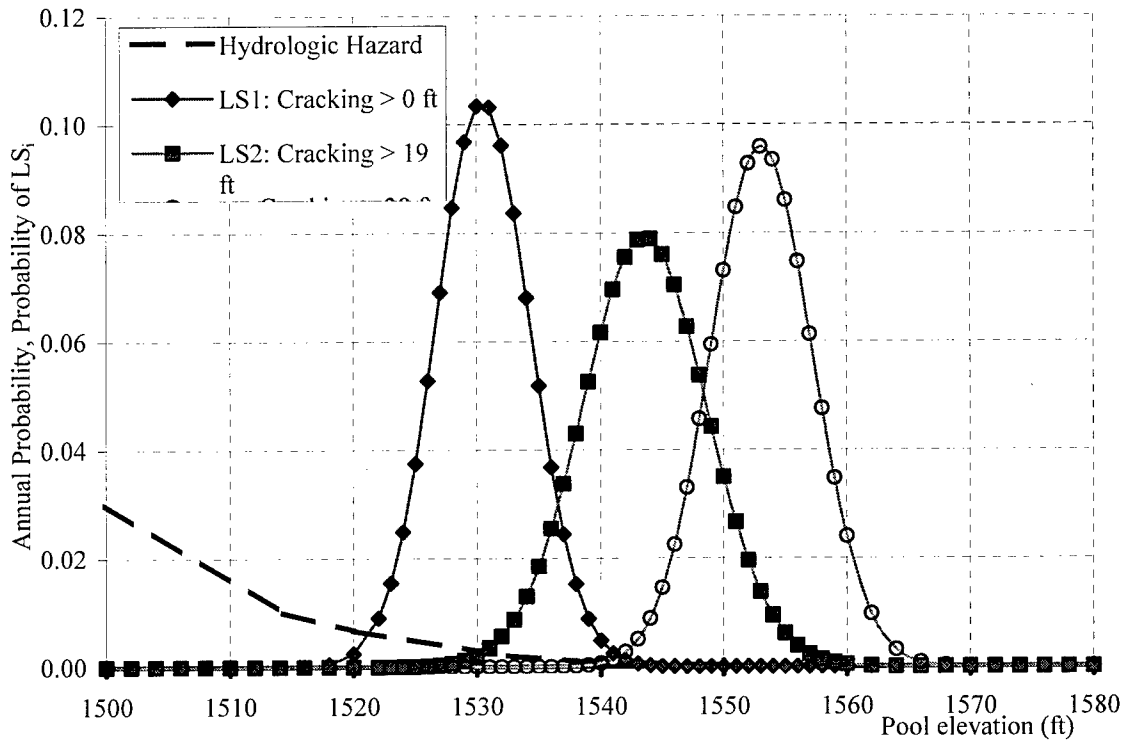


Fig. 6.3. Hydrologic hazard and Limit States for Cracking

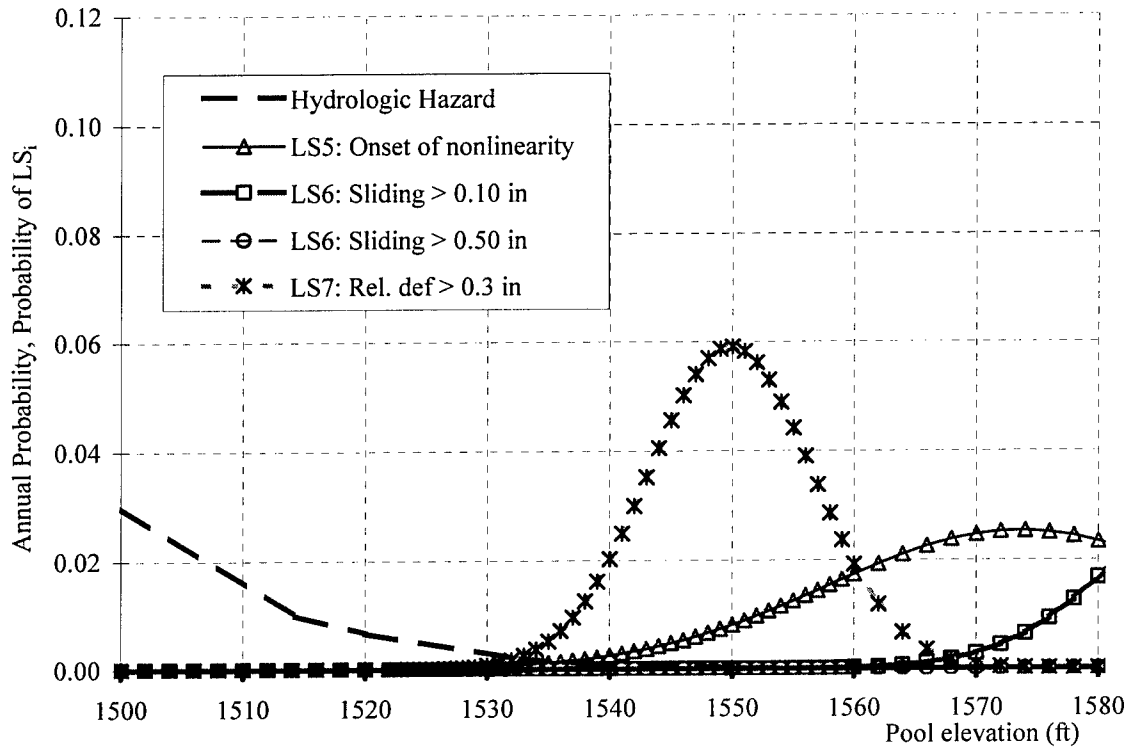


Fig. 6.4. Hydrologic hazard and LS5, LS6 and LS7

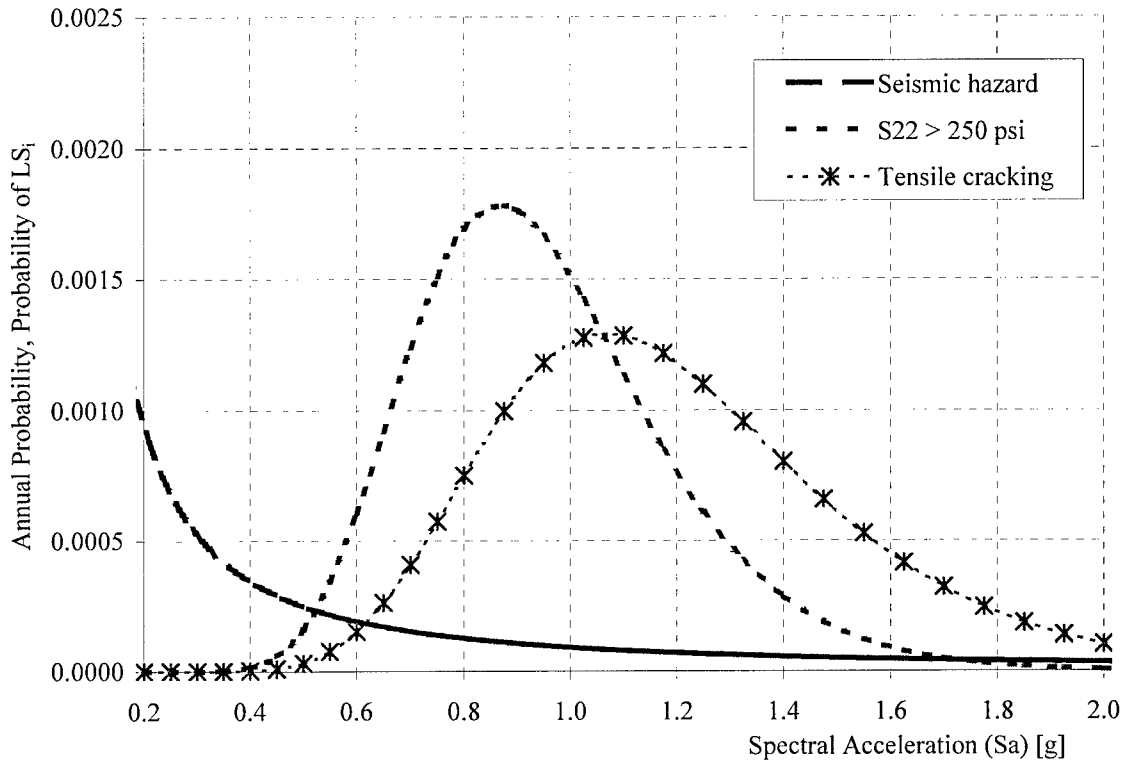


Fig. 6.5. Seismic hazard and LS4 (Tensile Stress & Cracking)

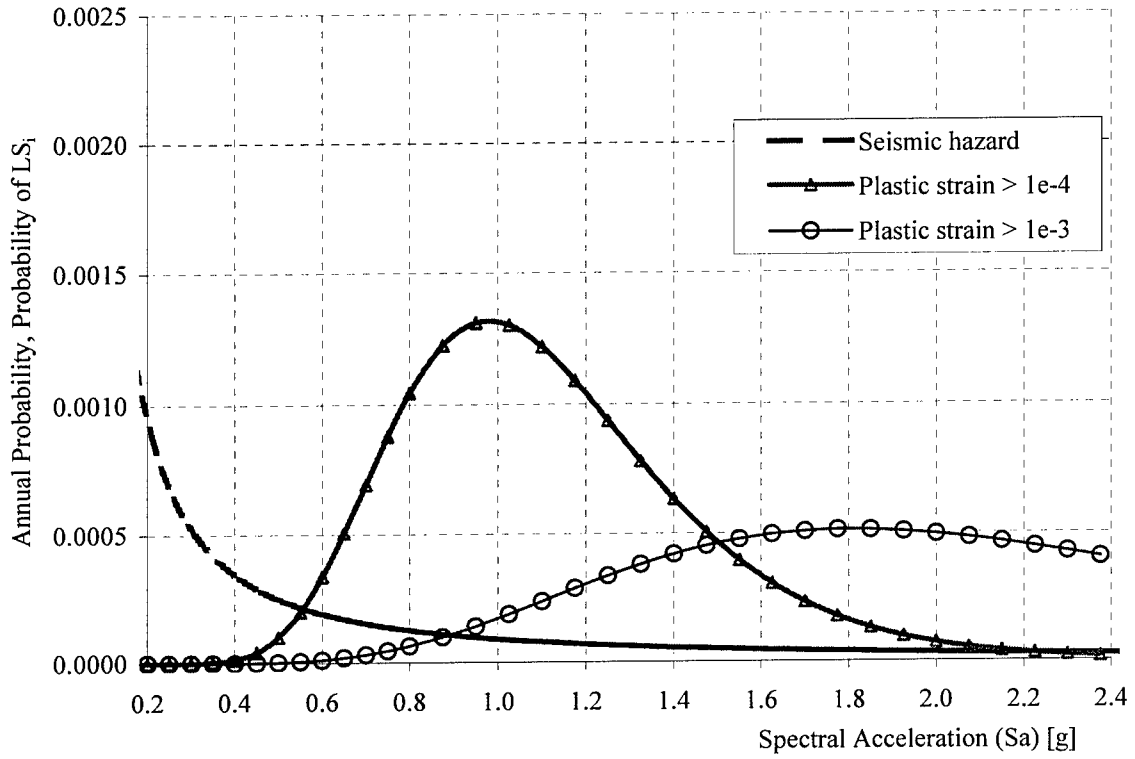


Fig. 6.6. Seismic hazard and LS5 - Plastic Strains

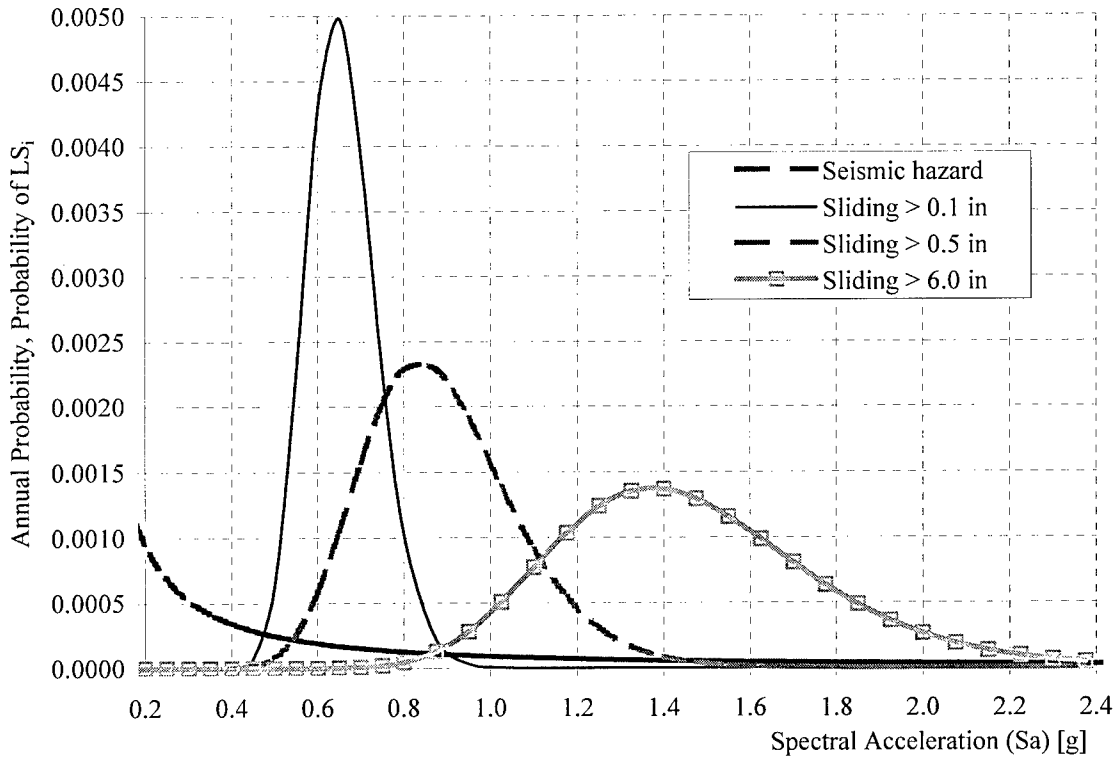


Fig. 6.7. Seismic hazard and LS6 – Sliding

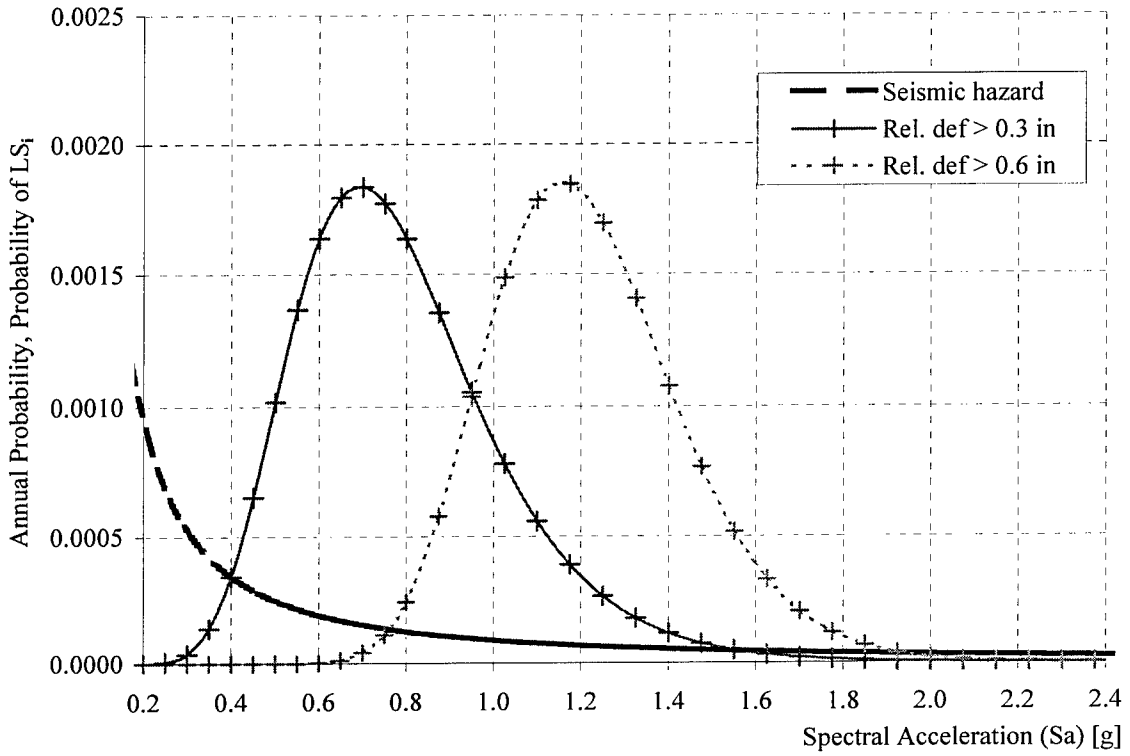


Fig. 6.8. Seismic hazard and LS7 - Relative Deformation

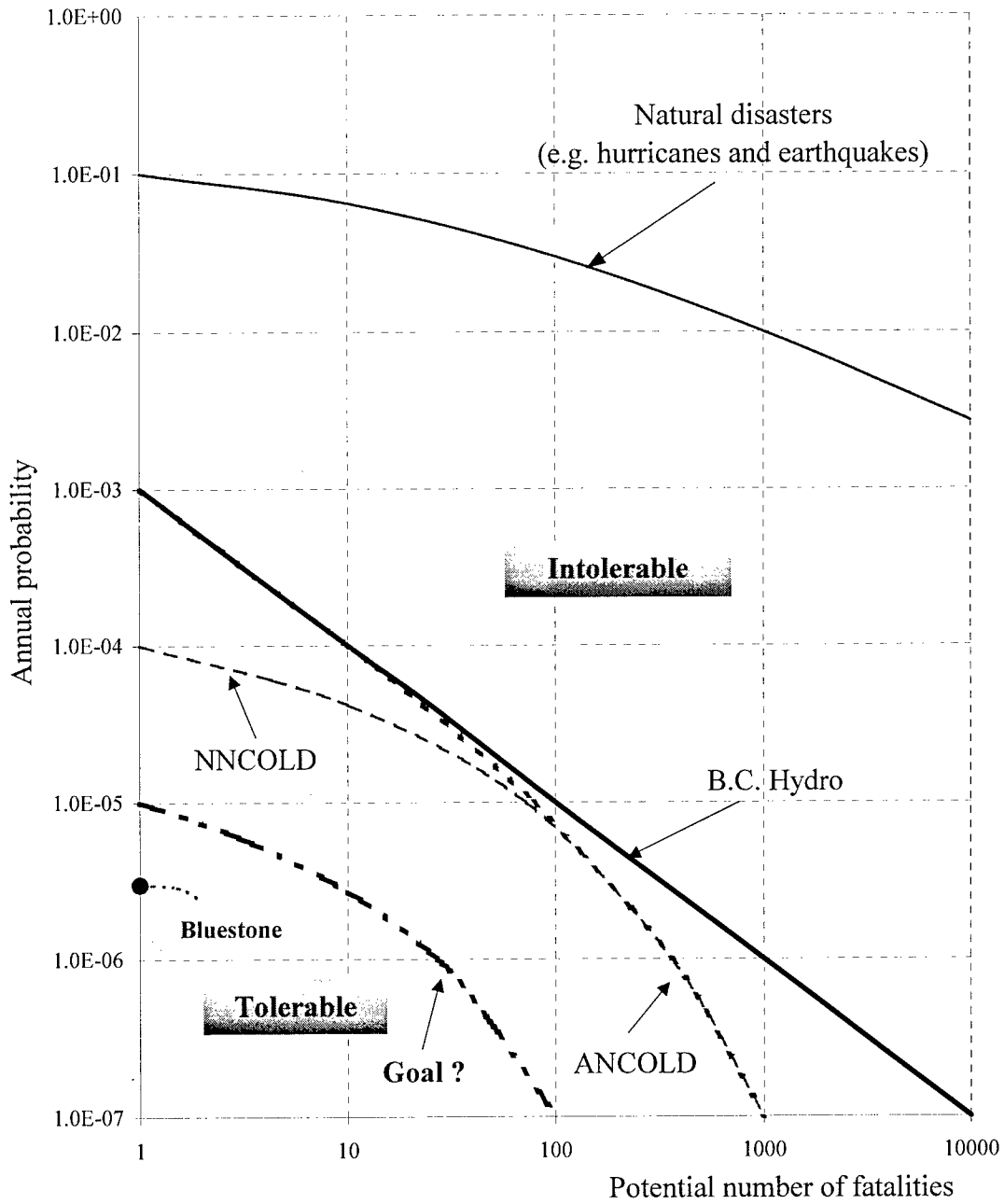


Fig. 6.9. Proposals for F-N curves (adapted from Hoeg, 1996)

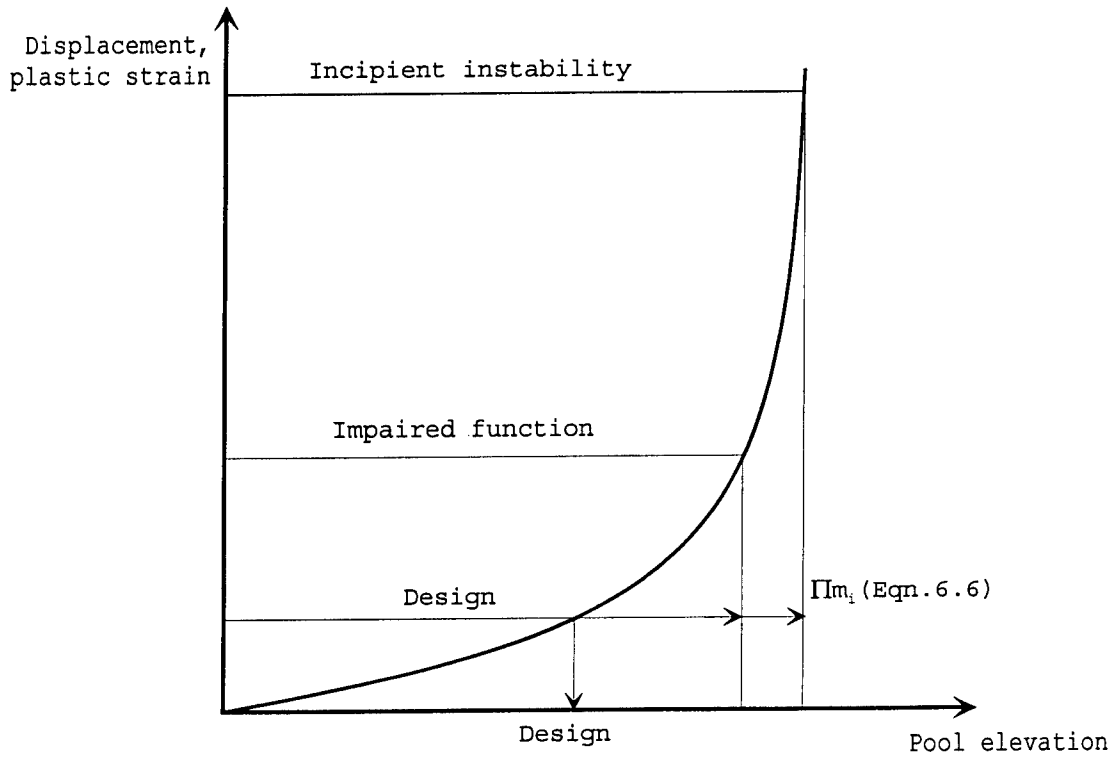


Fig. 6.10. Approximate fragility analysis by scaling upward from design conditions

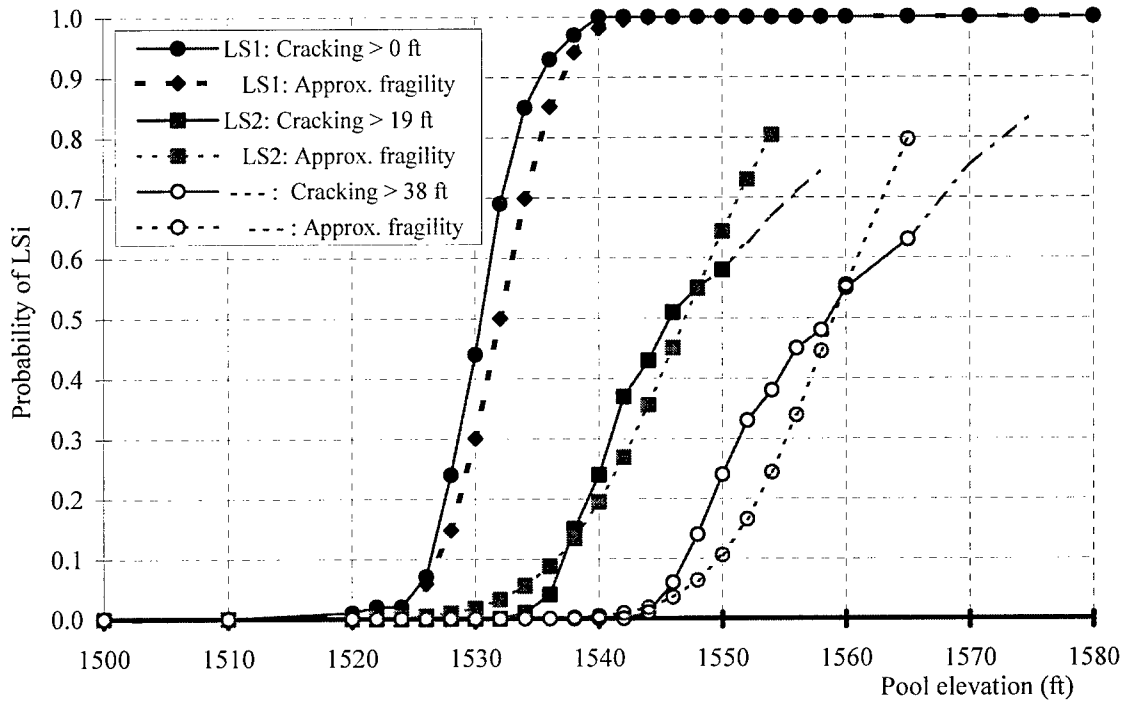


Fig. 6.11. Approximate Hydrologic Fragility for LS1 and LS2

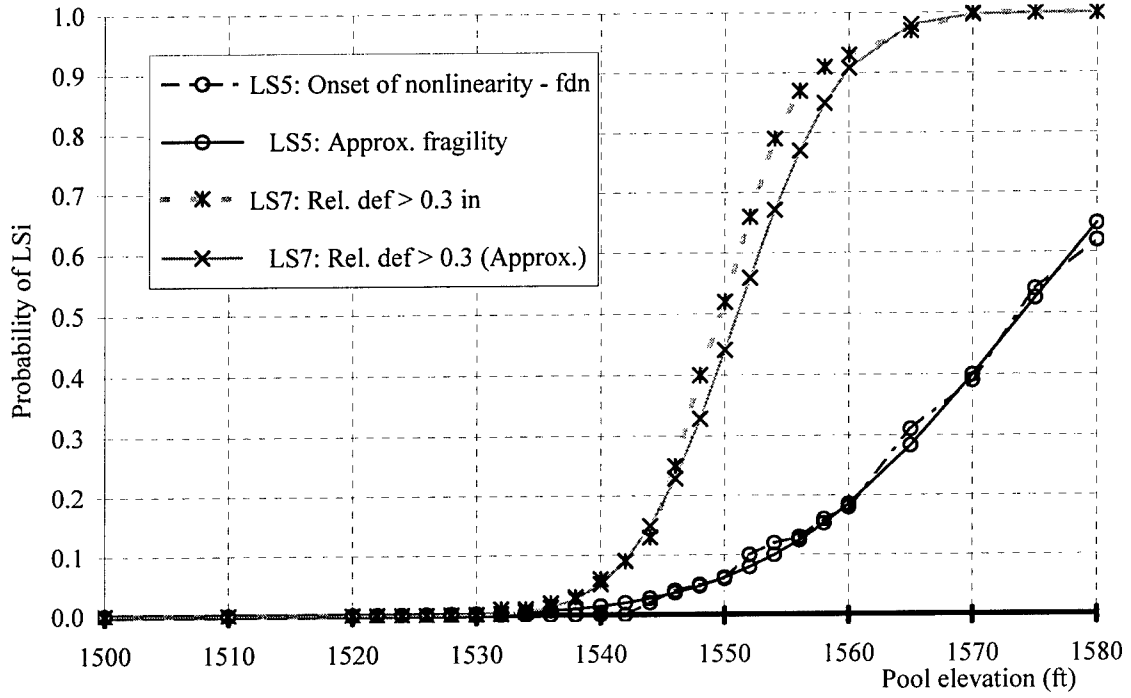


Fig. 6.12. Approximate Hydrologic Fragility for LS5 and LS7

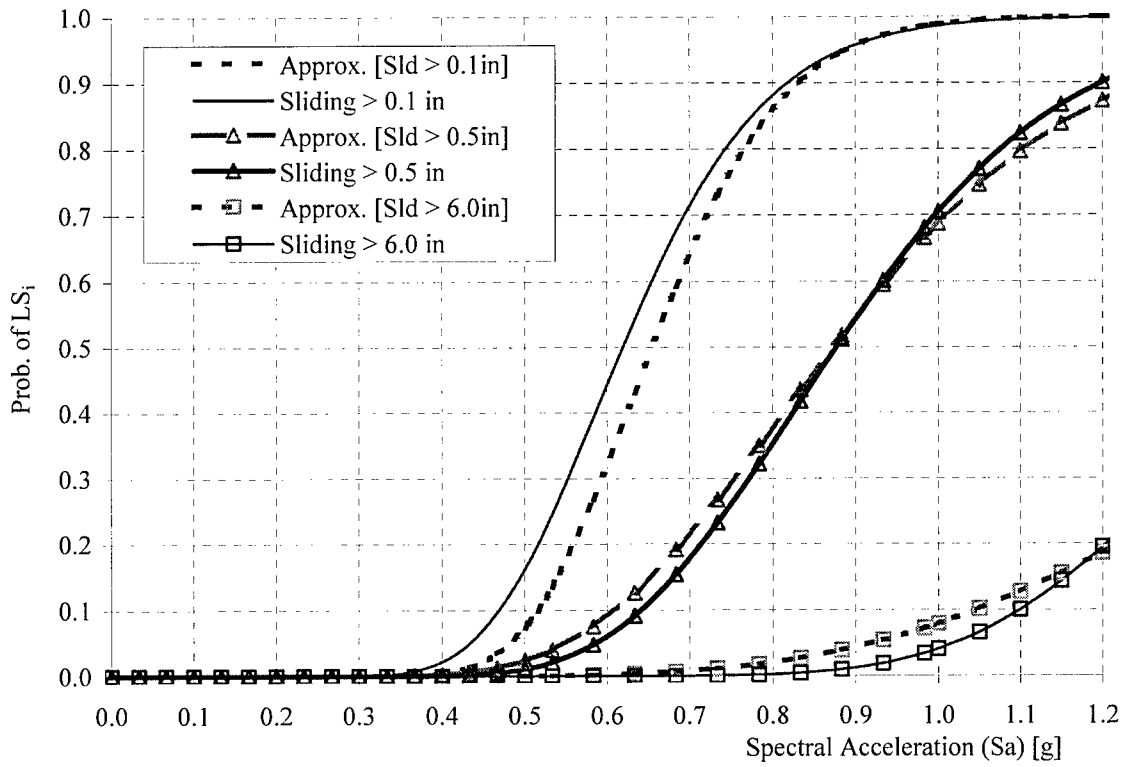


Fig. 6.13. Approximate Seismic Fragilities for LS6 - Sliding

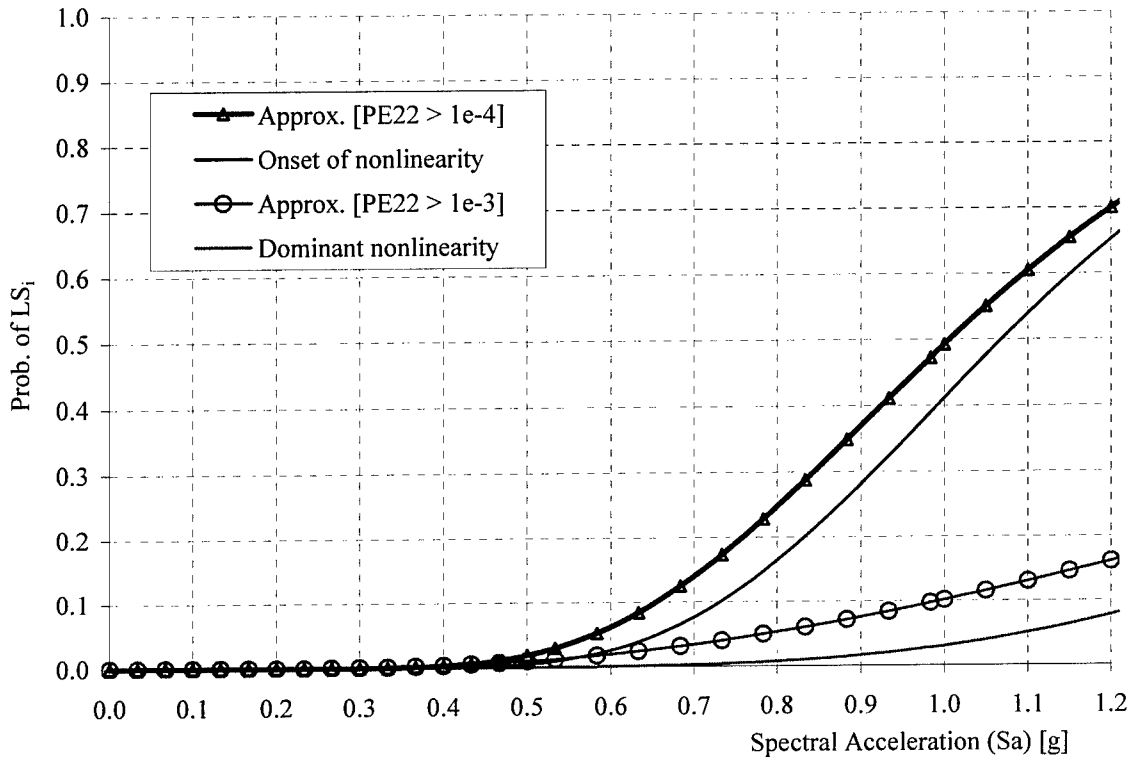


Fig. 6.14. Approximate Seismic Fragilities for LS5 - Plastic Strains

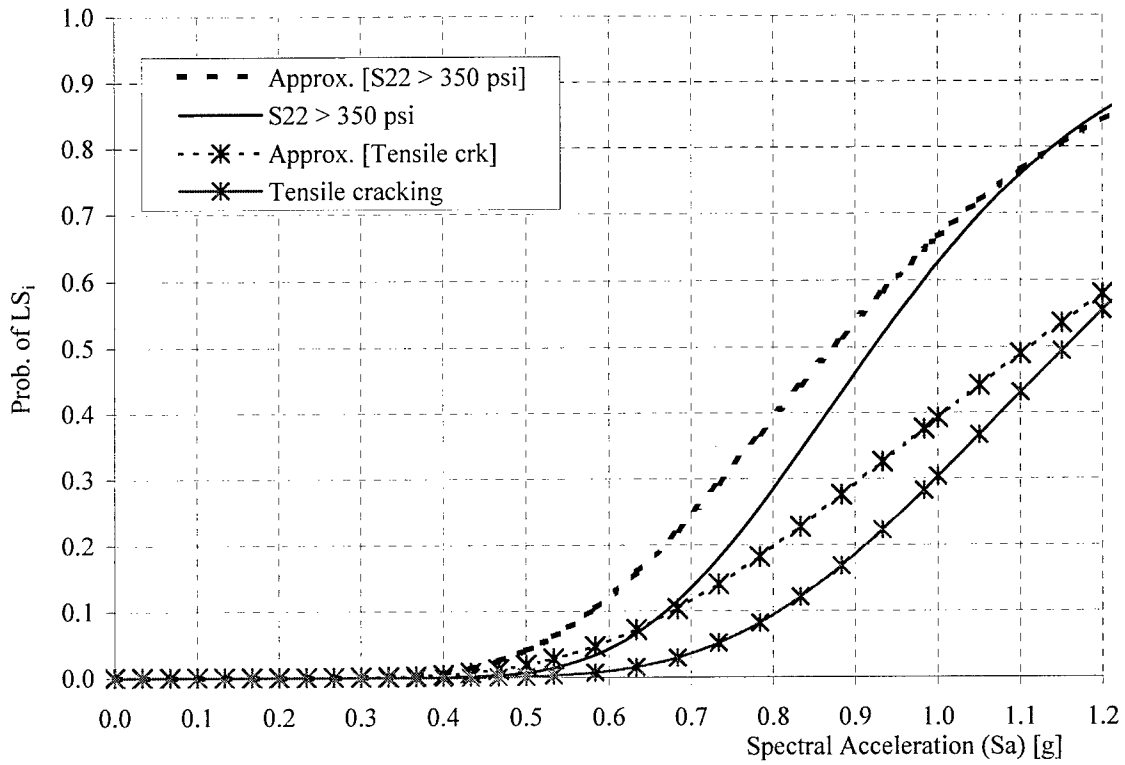


Fig. 6.15. Approximate Seismic Fragilities for LS4 - Tensile Cracking

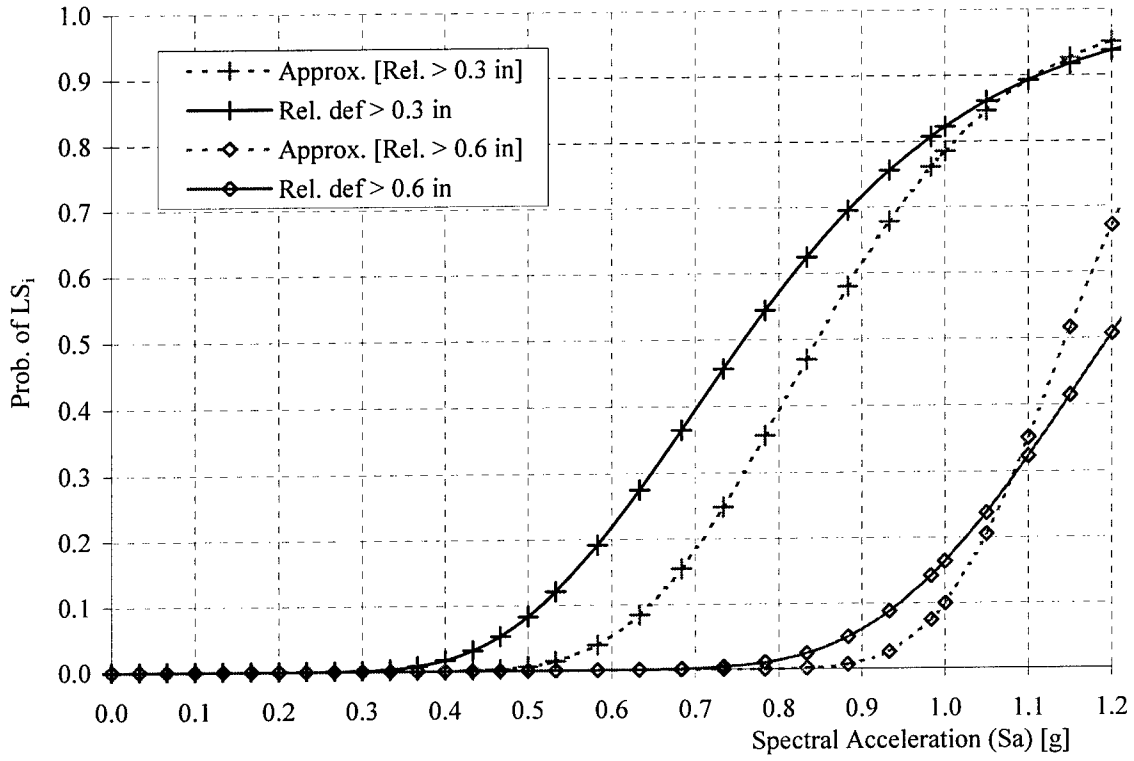


Fig. 6.16. Approximate Seismic Fragilities for LS7 - Relative Deformation

Chapter 7

CONCLUSIONS AND RECOMMENDATIONS

This study has demonstrated the feasibility of performing fragility analysis of concrete gravity dams within the context of a probabilistic safety assessment (PSA). Fragility curves depict concisely the manner in which uncertainties impact the performance of the concrete gravity dam and foundation. It also demonstrated the advantages of using a probabilistic approach vs. a deterministic approach, in which the assessment is based on hypothetical “upper bound” values of hazard. In contrast, the PSA provides a logic structure for the transparent and accountable propagation of uncertainties in the capacity and hazard of the dam. An essentially multi-disciplinary endeavor, the PSA requires a comprehensive understanding of how the facility behaves as a system. The resulting quantitative risk metrics of performance/ safety, when interpreted properly, are indispensable in the decision-making process of risk management agencies. However, the PSA must be easily “readable” by non-technical personnel in these agencies to build confidence and encourage wider use and acceptance.

A major investment in the construction of fragilities is in the development of the structural model that captures the essential features of system behavior. Quantitative risk metrics ultimately are based on these models, and hence, the validation (credibility) and

accuracy of these models is of utmost importance. In this study, models of varying degree of complexity and sophistication were used to construct hydrologic and seismic fragilities for the Bluestone Dam. The pool elevation and spectral acceleration at the fundamental frequency of the dam-foundation system, respectively, were used as demand variables. From a comparison of fragilities obtained from the different models, it was concluded that the rigid body model, though limited in scope, is a useful tool for preliminary studies, while the linear FE model should be treated cautiously, as it might yield misleading results. The nonlinear FE model is the most dependable model and though expensive, it should be employed decision-making processes involving considerable risk, capital and labor. The computational burden of the nonlinear FE models can be reduced by the use of appropriate sampling procedures, and assumptions regarding CDF's of fragilities (confirmed in this study). However, the sophistication of the FE model (or risk analysis) should not exceed the accuracy with which the extreme environmental phenomena can be measured and modeled.

The hydrologic fragilities indicated that the Bluestone Dam is practically safe from sliding for pool elevations of up to 1580 ft, while it is likely that there will be significant cracking at the heel of the dam at the revised PMF of 1556 ft (probability of 45% of observing a crack length of 38ft). The probability for the onset of nonlinear behavior (LS5) at this elevation is about 13% (as obtained from the nonlinear FE model). On the other hand, the seismic fragilities indicated that small sliding (0.10 in) is almost certain, when the dam is subjected to an earthquake with a spectral acceleration of 1.0g (which would be equivalent to an earthquake with a peak ground acceleration of 0.38g - 0.45g (Newmark and Hall, 1982)). However, relatively larger sliding (6.0 in) and dominant nonlinear

behavior in the foundation have low probabilities (4% and 3%, respectively). It is possible (probability of 28%) that there will be some tensile cracking at the neck of the dam at this intensity of seismic excitation.

Sensitivity studies for the hydrologic fragilities indicated that the effective uplift area has considerable influence on the fragilities for all limit states. The coefficient of friction, however, affected only the fragilities for the sliding (LS6) and the nonlinearity in the foundation (LS5). This impact, though, is not as great as that of the uplift area. It was also shown that the drain and grout efficiencies have considerable influence on the hydraulic fragilities. For the seismic fragility, the coefficient of friction was found to have some degree of influence on the fragility for the sliding limit state. Contrary to the observation from the hydrologic case, the effective uplift area had almost no influence on the seismic fragilities.

The fragilities were also coupled with hazard curves (obtained from other sources) to identify the range of hazards that are dominant contributors to each limit state probability ($P[LS]$). The points of greatest hazard contribution to $P[LS]$ were determined, and it was shown that for the relatively severe limit states, the $P[LS]$ is only marginally affected by extremely rare events (e.g. the PMF and MCE). Thus, basing policy solely on the occurrence of such rare events may lead to distortions in identifying the most effective strategies for risk management of the dam. It was also determined that the risks imposed by the two competing hazards (extreme hydrologic events and earthquakes) were not balanced for the Bluestone Dam, with seismic hazard imposing a relatively higher risk.

Levels of socially “acceptable risk” in other endeavors were presented to aid the decision-making process. Limit state probabilities for those that might cause structural

damage (cracking of 38 ft, sliding of 6.0 in, tensile cracking at neck of the dam and dominant nonlinear behavior in the foundation) ranged from 3.59×10^{-6} to 8.63×10^{-5} , which also indicates that “failure” probability is much lower. However, these probabilities are much larger than the “de minimis” risk (10^{-7}) acceptable to society, and further investigation involving benefit-cost analyses to assess the risk posed by the Bluestone Dam appears warranted.

Insights as to whether there is need of more rigorous fragility analysis of the dam can be obtained from approximate, relatively simple procedures and/ or models on safety assessment. The importance of accurate estimates of the fragility (and hazard) at fractiles close to the median capacity of the dam when using such approximate procedures is emphasized. The approximate procedures were found to be very accurate for the seismic fragility and dramatically reduced the computational costs (a reduction to about 25%). These procedures were also effective for the hydrologic fragility. However, it is relatively easier to develop a hydrologic fragility, considering its relatively small computational costs (compared to seismic fragilities).

RECOMMENDATIONS FOR FURTHER RESEARCH

A number of difficulties were encountered in performing the fragility assessments that point out the need for additional research. For one, there is need to tie the qualitative definitions of performance limit states to structural analyses results. For example, the fragilities for the nonlinear behavior of the foundation, differ depending on how big a volume one is looking at, or what values of strains/ stresses are linked to the limit state.

More research is required to determine the strain value to define yielding and how big a volume must yield before the foundation is deemed to be undergoing local yielding or exhibiting nonlinear behavior. Similarly, more research is need to determine what magnitudes of sliding would damage the drains, or render them ineffective, as it has been observed from sensitivity analyses that drain effectiveness has considerable influence on hydrologic fragilities of concrete gravity dams. In addition, the magnitude of relative deformation that would cause damage to appurtenant structures of the dam needs to be ascertained.

There is also need for a more comprehensive database, as the available data was very limited. Efforts should be made to compile data on the effective uplift area, coefficient of friction of the interface, and drain and grout efficiencies. Furthermore, these parameters need to be described by appropriate CDF's.

The present study was restricted to consideration of one monolith, modeled as a 2-D body. The effects of 3-D structural action on fragilities should be investigated, considering the effects of sliding (if any) across construction joints, slip-planes in the foundation or stabilizing influence of adjacent monoliths. Limit state definitions describing these phenomena must be linked to quantitative values obtainable from structural analyses.

Benefit-cost analyses, using the limit state probabilities obtained from the fully coupled risk analyses, should be carried out to identify how the decision-making process is influenced by the PSA, thereby indicating which aspects of the PSA need more attention or improvement. Finally, the potential for using the PSA as basis for standards of design and safety regulation of concrete gravity dams should be investigated.

Appendix - BLUESTONE DAM

The Bluestone Dam is located on the New River near Hinton, West Virginia. It is a concrete gravity dam, designed in the late 1930's as a combined flood control and hydroelectric power facility. Construction of the dam began in 1942. The overall crest length of the dam is 2,062 ft (629 m), consisting of 790 ft (241 m) of spillway, 313 ft (96 m) of intake structure for the power house, and 959 ft (292 m) of non-overflow and assembly bay sections and abutments. The elevation of the base of the dam at the lowest point is 1,360 ft (415 m). The elevation at the top of the non-overflow sections is 1,535 ft (468 m), making the maximum height of the non-overflow section of the dam about 175 ft (53 m). The 790-ft (241-m) spillway section is controlled by 21 gates, each with 30 ft (9 m) clear height. The elevation at the top of the spillway is 1,490 ft (454 m), making the dam height at the spillway approximately 130 ft (40 m). A detailed description of the dam, its design envelope and proposed operation is provided elsewhere (New, 1937).

The foundation material at the site is firm laminated shale and sandstone from 2 to 20 ft (6.1 m) in thickness atop a stratum of fine gray sandstone. Interstratified shale and sandstone are found on the left side of the dam and in both abutments. During the course of construction, a number of foundation problems were encountered, which were addressed mainly through drilling and grouting. There is a grout curtain at the upstream face of the dam, and drilled drain holes extending into the foundation and opening to the inspection

gallery, at floor elevation 1,375 ft (419 m); under normal conditions, these drain by gravity into the tailrace. The combined action of the grout curtain and drains greatly reduces the uplift pressure at the base of the dam, while the grout curtain also seals the seams and crevices in the foundation against leakage from the reservoir. The drainage system has been inspected on a number of occasions during the service life of the dam, and measurements of drain efficiency have been made.

The structural design of the Bluestone Dam conformed to standards that were current in the late 1930's. Consistent with professional practice at the time, the allowable stresses for concrete and foundation materials were estimated very conservatively. More recent (1996) estimates of the actual mechanical properties of the concrete and foundation materials were furnished by the US Army Corps of Engineers. For example, the 28-day compressive strength of concrete was specified at 3,000 psi (21 MPa) in 1937; the allowable stress in compression was 600 psi (4 MPa) (Table II, p.13, of "New," 1937). The actual strength is estimated at 5,000 psi (34 MPa). The impact of such conservatism in design becomes apparent in fragility analysis described in this study.

The power pool elevation for operation of the five hydroelectric turbines is 1,490 ft (454 m). The dam was designed for a maximum flood pool at elevation 1,520 ft (463 m), corresponding to a maximum inflow to the reservoir of 430,000 ft³/s (12,176 m³/s). Recent hydrological studies suggest that this pool level corresponds to approximately a 150-year event. The dam facility is designed to discharge 430,000 ft³/s with all gates and sluices open during a flood at elevation 1,521 ft (464 m). The design considered forces due to dead load [the unit weight of concrete varied from 152-158 lb/ft³ (23.9-24.8 kN/m³)], hydrostatic forces from reservoir and tailwater, ice pressure [20,000 lb/ft (292 kN/m)] at elevation

1,500 ft (457 m)], and silt and saturated earth backfill loads. It also considered earthquake forces, by combining the Westergaard formulae for hydrodynamic interaction forces with assumed inertia forces of the concrete at an acceleration (horizontal and/or vertical) of 0.1g. The critical load combination for design was found to be a pool elevation at 1,520 ft (463 m) and earthquake forces obtained by assuming horizontal and vertical accelerations of 0.1g. Such a design condition would be viewed as unduly conservative, when viewed from the perspective of modern probabilistic event combination analysis, since it is based on the assumptions that the MCE and design flood levels occur concurrently. Other forces, including wave effects, impact from vessels or debris, were not considered.

Estimated hydrologic hazard for Bluestone Dam

Recent hydrologic studies have suggested that the peak flow at PMF is greater than 430,000 ft³/s (12,176 m³/s). With the peak flow at the new PMF, impounding the water behind the dam would require raising the pool upward to 1556 ft (474 m), with tailwater at 1409 ft (429 m). This event is believed to have a return period in excess of 30,000 years. At this level, the current spillway is inadequate to pass the PMF. Preliminary calculations have indicated that the imminent failure flood (IFF) (capacity of current spillway?) elevation is 1,532 ft (467 m), 24 ft (7 m) below the new estimate of the PMF. Several proposals were made for rehabilitating the Bluestone Dam were considered, including raising the crest of the dam and providing an auxiliary spillway. These proposals were not evaluated using modern probabilistic risk analysis concepts.

BIBLIOGRAPHY

"ABAQUS/Standard User's Manual" (2001) Hibbit, Karlsson and Sorensen, Inc., Vol. I-III, Version 6.2 (<http://www.hks.com/>)

Afrouz, A. A. (1992). "Practical handbook of rock mass classification systems and modes of ground failure." CRC Press, Boca Raton, FL.

Algermissen, S.T. et al (1982). "Probabilistic estimates of maximum acceleration and velocity in rock in the contiguous United States." Open File Report 82-1033, US Geological Survey, Denver, CO.

Amadei, B., Illangeasekare, T., and Chinnaaswamy, C. (1991). "Effect of crack uplift on concrete dam stability." Proc. First Conference, Research Needs in Dam Safety, Vol. I, New Delhi, India: I-60 - I-66

Anandarajah, A., Rashidi, H. and Arulanandan, K. (1995) "Elasto-plastic finite element analyses of a soil-structure system under earthquake excitations", Computers and Geotechnics, 17, no. 3: 301-325

Ang, A. H.-S. and Tang, W. (1974). Probability concepts in engineering planning and design, Vol. I. John Wiley and Sons, Inc., New York, NY.

Atkinson, D. and Gobat, J. (last updated in Feb. 2000). <http://felt.sourceforge.net> - URL for an open source finite element analysis, *FELT* (contact: datkinson@clarku.edu or jgobat@sourceforge.net)

Baecher, G., Pate, M.E. and Neufville, R. (1980). "Risk of dam failure in benefit-cost analysis." Water Research 16(3): 449-456.

- Balmer, G. (1952). " A general analytical solution for Mohr's envelope." Proc. Am. Soc. for Testing Materials, vol. 52: 1260-1271
- Barbosa, R. and Ghaboussi, J. (1992). "Discrete finite element method." Engrg. Computations, vol. 9: 253-266.
- Bienawski, Z.T. (1974) "Estimating the strength of rock materials" J. S. Afr. Inst. Min. Metall. 74: 312-320
- Bienawski, Z. T. (1976). "Rock mass classification in rock engineering." In exploration for rock engineering, Proc. of the Symp. (Edited by Bienawski, Z. T.) 1, Balkema, Cape Town: 97-106
- Bienawski, Z.T. (1989). "Engineering rock mass classifications." J. Wiley & Sons, New York, NY.
- Blind, H. (1983) "The safety of dams." International Water Power and Dam Construction, vol. 35: 17-21
- Bolt, B.A. (1993). Earthquakes. W.H. Freeman & Co., New York, NY.
- Bury, K.V. and Kreuzer, H. (1985). "Assessing failure probability of gravity dams." Water Power and Dam Construction, 37(11): 46-50.
- Bury, K.V. and Kreuzer, H. (1986). "The assessment of risk for a gravity dam." Water Power & Dam Construction 38(12): 36-40
- Butler, J. E. (1981). "The influence of pore pressure upon concrete." Magazine of Concrete Research, 33, (114): 3-17
- Casagrande, A. (1961). "First Rankine Lecture: Control of seepage through foundations and abutments of dams." Geotechnique, London, England, II (June): 159-180.
- Casciati, F. and Faravelli, L. (1991). Fragility analysis of complex structural systems. John Wiley & Sons, New York, NY.

Chakrabarti, P and Chopra, A.K. (1973) "Earthquake analysis of gravity dams including hydrodynamic interaction" *International J. Earthquake Engrg. & Str. Dyn*, Vol. 2: 143-160

Chavez, J. and G.L. Fenves (1995). "Earthquake response of concrete gravity dams including base sliding." *J. Struct. Engrg. ASCE* 121(5): 857-864.

Cheng, S.T. (1993) " Statistics of dam failures" *Reliability and Uncertainty Analysis in Hydraulic Design*, (eds. Yen, B.C and Tung, Y-K), Report by the Subcommittee on Uncertainty and Reliability Analysis in Design of Hydraulic Structures of the Technical Committee on Probabilistic Approaches to Hydraulics of the Hydraulics Division of ASCE, New York, NY: 97-105

Choi, S.K. (1992). "Application of the distinct element method for rock mechanics problems." *Engrg. Computations*, vol. 9: 225-233.

Chopra, A.K. (1967) "Hydrodynamic pressures on dams during earthquakes" *J. Engrg. Mechanics Div. ASCE*, vol. 93, no. EM6: 205-223

Chopra, A.K. (1970) "Earthquake response of concrete gravity dams." *J. of Engrg. Mech. Div, ASCE*, Vol. 96, No. EM4: 443-454

Chopra, A.K. and Chakrabarti, P. (1981) "Earthquake analysis of concrete gravity dams including dam-water-foundation rock interaction" *Earthquake Engrg. & Str. Dyn*, Vol. 9: 363-383

Chopra, A.K. and Gupta, S. (1980) "Hydrodynamic and foundation interaction effects in earthquake response of a concrete gravity dam" *J. Str. Div, ASCE*, Vol. 107, No. ST8: 1399-1412

Chopra, A.K. and Zhang, L. (1992) "Earthquake-induced base sliding of concrete gravity dams" *J. Str. Engrg*, Vol. 117, No. 12: 3698-3179

Chow, V.T. (ed.) (1964). *Handbook of Applied Hydrology*. McGraw-Hill, New York, NY.

Cochrane, H.C., Ferrell-Dillard, R. and Baumann, D.D. (1987). "Socioeconomic considerations in dam safety risk analysis." Prepared for U.S. Army Institute for Water

Resources by Planning and Management Consultants, Ltd., IWR Report 87-R-7.

Cornell, C.A. (1968). "Engineering seismic risk analysis." *Bulletin Seismic Soc. Am.* 58(5): 1583-1606.

Cornell, C.A. (1994). "Risk-based structural design." *Proceedings, Symposium on Risk Analysis, Univ. of Michigan, August: 37-48*

Cundall, P.A. (1971) "A computer model for simulating progressive, large-scale movements in block rock systems" *Symp. Intl. Society of Rock Mechanics, Nancy, France: 11-18*

Cundall, P.A. and Strack, O.D.L. (1979) "The distinct element method as a tool for research in granular media." *Report to NSF concerning NSF grant ENG76-20711, Dept. Civ. and Min. Engrg., University of Minnesota.*

"Dam safety assurance program (ER 1110-2-1155)." (1995). *US Army Corps of Engineers, Washington, DC.*

Darbre, G.R. (1996) "Nonlinear dam-reservoir interaction analysis" *11th World Conference on Earthquake Engrg, Acapulco, Mexico: 1055-1062*

Darbre, G.R. (1998) "Phenomenological two-parameter model for dynamic dam-reservoir interaction" *J. of Earthquake Engrg, Vol. 2, No. 4: 513-524*

Darbre, G.R. and Wolf, J.P. (1998) "Criterion of stability and implementation issues of hybrid frequency-time domain procedure for nonlinear dynamic analysis" *Earthquake Engrg & Str. Dyn, Vol. 16, No. 4: 569-581*

Dawdy, D.R. and Lettenmaier, D.P. (1987). "Initiative for risk-based flood design." *J. Hydraulic Engrg. ASCE 113(8): 1041-1051.*

De Boer, R., and Ehlers, W. (1990). "Uplift, friction and capillarity: three fundamental effects for liquid-saturated porous solids." *Int. J. Solids and Struct. 26(1): 43-57.*

- DeSena, M. (1998). "Aging U.S. dams pose serious risk." in U.S. Water News 15(5): May
- Dewey, R., Reich, R.W. and Saouma, V.E. (1994). "Uplift modeling for fracture mechanics analysis of concrete dams." J. Struct. Engrg. ASCE 120(10): 3025-3044.
- Douglas, K, Spannagle, M. and Fell, R (1999) "Analysis of concrete gravity and masonry dam incidents" International J. Hydropower and Dams, no. 6, vol. 6: 108-115
- Duffaut, P. (1986) "Ruptures de barrages et incidents a travers le monde." Travaux, no. 607: 55-57
- "Earthquake engineering for concrete dams: design, performance, and research needs" (1990) Commission on Engineering and Technical Systems, National Research Council, Washington, D.C.
- Ellingwood, B. (1990). "Validation studies of seismic PRAs." Nuc. Engrg. and Des. 123(2): 189-196
- Ellingwood, B., Corotis, R.B., Boland, J. and Jones, N. (1993). "Assessing the cost of dam failure." J. Water Res. Planning and Mgt., ASCE 119(1): 64-82
- Ellingwood, B. (1994a). "Validation of seismic probabilistic risk assessments of nuclear power plants." Report NUREG/GR-0008, U.S. Nuclear Regulatory Commission, Washington, DC.
- Ellingwood, B. (1994b). "Probability-based codified design: past accomplishments and future challenges." Struct. Safety 13(3): 159-176
- Ellingwood, B.R. (1995). "Engineering reliability and risk analysis for water resources investments: role of structural degradation in time-dependent reliability analysis." Report ITL-95-3, U.S. Army Corps of Engineers Waterways Experiment Station, Vicksburg, MS.
- Fenves, G. and Chopra, A.K. (1984a) "Earthquake analysis and response of concrete gravity dams" Report No. UCB/EERC-84/10, Earthquake Engineering Research Center, University of California, Berkeley.

Fenves, G. and Chopra, A.K. (1984b) "Earthquake analysis of concrete gravity dams including reservoir bottom absorption and dam-water-foundation interaction" *Earthquake Engrg. & Str. Dyn.*, Vol. 12: 663-680

Fenves, G. and Chavez, J. (1996) "Evaluation of earthquake induced sliding in gravity dams" *Proceeding of the 11th World Conference on Earthquake Engineering*, Acapulco, Mexico.

Goodman, R.E. and Shi, Gen-hua (1984). "Block theory and its application to rock engineering." Englewood Cliffs, NJ: Prentice-Hall.

Goodman, R.E. (1989). *Introduction to Rock Mechanics* (2nd ed), J. Wiley & Sons, New York.

"Gravity dam design: engineering manual 1110-2-2200." (1958). US Army Corps of Engineers, Washington, DC.

Hartford, D.N.D. and Salmon, G.M. (1997). "Credibility and defensibility of dam safety risk analysis." *Hydropower*, Norway.

Hoeg, K. (1996) "Performance evaluation, safety assessment and risk analysis of dams" *International J. of Hydropower and Dams*, no. 6, vol. 3: 51-58

Hoek, E. and Brown, E.T. (1980) "Underground excavations in rock." *Institution of Min. Metall.*, London

Hoek, E. (1983). "1983 Rankine Lecture: Strength of jointed rock mass." *Geotechnique* 33, No. 3: 187-223

Hoek, E. (1994). "Strength of rock and rock masses." *ISRM New Journal* 2(2): 4-16

Hoek, E. and Brown, E. T. (1997). "Practical estimates of rock mass strength." *Int. J. Rock Mech. Min. Sci.* Vol. 34, No. 8: 1165-1186

Hoek, E., Kaiser, P. K. and Bawden, W. F. (1997). "Support of underground excavations in hard rock." *Balkema*, Rotterdam.

- Hosking, J.R.M, Wallis, J.R, Wood, E.F. (1985) "Estimation of the Generalized Extreme-Value distribution by the method of probability weighted moments" *Technometrics*, 27(3): 251-261
- ICOLD (1971). "Lessons from dam incidents." International Commission on Large Dams, Paris.
- ICOLD (1983). "Lessons from dam incidents." International Commission on Large Dams, Paris.
- ICOLD (1998). "World Register of Dams (Registre Mondial des Barrages)." International Commission on Large Dams, Paris.
- Idriss, I.M. and Sun, J.I. (1992) "SHAKE91: A computer program for conducting equivalent linear seismic response analyses of horizontally layered soil deposits," User's Manual, University of California, Davis, California.
- Imam, R.L. and Conover, W.J. (1980). "Small sample sensitivity analysis techniques for computer models with an application to risk assessment." *Communications in Statistics*, A9(17):1749-1842.
- Jing, L. (1998) "Formulation of discontinuous deformation analysis (DDA) – an implicit discrete element model for block systems" *Engineering geology*, vol. 49: 371-381
- Johnson, F.A. and Illes, P. (1976) "A classification of dam failures." *International Water Power and Dam Construction*, vol. 28, no. 12: 43-45
- Kalustyan, E.S. (1983) "Reliability of rock foundations of concrete dams" *Hydrotechnical Construction*, (Translation from) *Gidrotekhnicheskoe Stroitel'stvo*, no. 6: 7-8
- Karlsson, P.-O. and Haimes, Y.Y. (1989). "Risk assessment of extreme events: application." *J. Water Res. Planning and Mgt.*, ASCE 115(3):299-320
- Kennedy, R.P. and Ravindra, M.K. (1984). "Seismic fragilities for nuclear power plant studies." *Nuc. Engrg. and Des.* 79(1): 47-68.

- Kennedy, R. (1997). "Establishing seismic design criteria to achieve an acceptable seismic margin." Proc. 24th Water Reactor Safety Information Meeting, NUREG/CP-0157, Vol. 1, US Nuclear Regulatory Commission: 221-244.
- Lafitte, L.R. (1993). "Probabilistic risk analysis of large dams: its value and limits." *Water Power & Dam Construction* 45(3):13-16
- Lave, L.B., Resendiz-Carillo, D. and McMichael, F.C. (1990). "Safety goals for high-hazard dams: are dams too safe?" *Water Resources Research* 26(7): 1383-1391.
- Leger, P. and Boughoufalah, M. (1989) "Earthquake input mechanisms for time-domain analysis of dam-foundation systems", *Engineering Structures*, vol. 11, no. 1: 37-46
- Leger, P. and Bhattacharjee, S.S. (1992) "Reduced frequency-independent models for seismic analysis of concrete gravity dams" (Technical note) *Computers and Structures*, Vol. 44, No. 6: 1381-1387
- Leliavsky, S. (1958). "Uplift in Gravity Dams." Constable, London.
- Lemos, J.V. (1999) "Discrete element method of dam foundations" *Distinct Element Modeling in Geomechanics*, eds. Shara, V.M., Saxena, K.R. and Woods, R.D, A.A. Balkema: 89-115
- Lemos, J.V. and Cundall, P.A. (1999) "Earthquake analysis of concrete gravity dams on jointed rock foundations" *Distinct Element Modeling in Geomechanics*, eds. Shara, V.M., Saxena, K.R. and Woods, R.D, A.A. Balkema: 117-143
- Linsley, R.K, Kohler, M.A, Paulhus, J.L.H. (1975). *Hydrology for Engineers*, 3rd ed., McGraw-Hill, New York, NY.
- MacGregor, J. G., Mirza, S. A. and Ellingwood, B. (1983). "Statistical analysis of resistance of reinforced and prestressed concrete members." *ACI Journal* 80(3): 167-176.
- McCann, M., et al, (1985). "Probabilistic safety analysis procedures guide (Vol. 2)." NUREG/CR-2815, U.S. Nuclear Regulatory Commission, Washington, DC.

- McCann, M. W., Jr., editor (1986). "Current developments in dam safety management." Proceedings of a Workshop, Stanford University, Stanford, CA.
- McKay, M.D, Beckman, R.J. and Conover, W.J. (1979) "A comparison of three methods for selecting values of input variables in the analysis of output from a computer code" *Technometrics*, vol. 21, no.2: 239-245
- Mirza, S.A, Hatsinikolas, M. and MacGregor, J. (1979) "Statistical descriptions of strength of concrete", *J. Str. Div., ASCE*, Vol. 105, No. ST6: 1021-1037
- Mustoe, G.W.W, Williams, J.R. and Hocking, G. (1986) "The discrete element method in geotechnical engineering" Barking, Essex, UK: Elsevier Applied Science Publishers
- National Research Council (1985). "Safety of dams: flood and earthquake criteria." (Housner, ed.) Committee on Safety Criteria for Dams, Water Science and Technology Board, National Academy Press, Washington, DC.
- "Natural phenomena hazards design and evaluation criteria for department of energy facilities" DOE STD-1020-94 (1994). U.S. Department of Energy, Washington, DC.
- "NEHRP recommended provisions for the development of seismic regulations for new buildings" (1998) Building Seismic Safety Council, Vols. 1 and 2, prepared for and issued by the Federal Emergency Management Agency, Washington, D.C.
- "New River Bluestone Reservoir Project; Analysis of Dam Design." (1937). US Engineer Office, Huntington, W. VA.
- Newmark, N.M. and Hall, W.J. (1982). *Earthquake Spectra and Design*. Earthquake Engineering Research Institute (EERC), Berkeley, CA.
- Newton, N.W. (1983). "Realistic assessment of maximum flood potentials." *J. Hydr. Engrg. ASCE* 109(6):905-917.
- Novak, P., Moffat, A.I.B, Nalluri, C. and Narayanan, R. (1996). *Hydraulic structures* (2nd ed.). E & F Spon, (Chapman & Hall), London.

O'Connor, J.M. and Ellingwood, B.R. (1987) "Reliability of nonlinear structures with seismic loading" *J. Struct. Engrg., ASCE*, vol. 111, no. 4: 722-739

Ouelette, P., El-Jabi, N. and Rousselle, J. (1985). "Applications of extreme value theory to flood damage." *J. Water Resources Planning and Mgt., ASCE* 111(4): 467-477

Pande, G.N., Beer, G. and Williams, J.R. (1990). "Numerical methods in rock mechanics." John Wiley & Sons, New York, NY.

Paronesso, A. and Wolf, J.P. (1995) "Global lumped-parameter model with physical representation for unbounded medium" *Earthquake Engrg. & Str. Dyn*, Vol. 24: 637-654

Pate-Cornell, E. (1994). "Quantitative safety goals for risk management of industrial facilities." *Struct. Safety* 13(3): 145-157.

Raphael, J.M. (1984) "Tensile strength of concrete" *ACI Journal*, vol. 81, no. 2: 158-165

Reed, D.W. and Field, E.K. (1992) *Reservoir Flood Estimation: Another Look*, IH Report 114, Institute of Hydrology, Wallingford.

Reiter, L. (1990). "Earthquake hazard analysis - issues and insights," Columbia University Press, New York, NY.

Rubenstein, R.Y. (1981). "Simulation and the Monte Carlo method." John Wiley, New York, NY.

Rusch, H. (1969) "Die streuung der eigenschaften von schwerbeton (The variability of the properties of normal concrete)." Preliminary report, Symposium on Structural Safety, International Association for Bridge and Structural Engineering, London, England.

Saouma, V.E. (1995). "Deterministic and reliability based linear nonlinear fracture mechanics based safety analysis of Bluestone dam" Preliminary draft report, Dept. of Civil, Env. and Architectural Engrg, Univ. of Colorado, Boulder, 80309-0428

Schnabel, P.B., Lysmer, J. and Seed, H.B. (1972) "SHAKE: A computer for earthquake response analysis of horizontally layered sites" Report No. EERC 72-12, Earthquake Engineering Research Center, University of California, Berkeley, California.

Serafim, J. L. and Pereira, J. P. (1983). "Consideration of the geomechanical classification of Bienawski" Proc. Int. Symp. on Engineering Geology and Underground Construction, Lisbon 1(II): 33-44

Shalon, R. and Reintz, R.C. (1955) "Interpretation of strengths distribution as a factor in quality control of concrete." Proceedings, Reunion Internationale des Laboratoires d'Essais et de Recherches sur les Materieux et les Constructions, Symposium on the Observation of Structures, vol. 2, Laboratorio Naciano de Engenharia Civil, Lisbon, Portugal: 100-116

Sheorey, P.R, Biswas, A.K. and Choubey, V.D. (1989) "An empirical failure criterion for rocks and jointed rock masses." Eng'g Geol., vol. 26: 141-159

Sheorey, P.R. (1997) Empirical rock failure criteria. A.A. Balkema, Rotterdam.

Shi, G. (1992) "Discontinuous deformation analysis: a new numerical model for the statics and dynamics of deformable block structures" Engineering Computations, vol. 9: 157-168

Shome, N. and Cornell, C.A. (1997) "Probabilistic seismic demand analysis of nonlinear structures" Report No. RMS-35, Reliability of Marine Structures Program, Stanford University, Stanford, CA.

Shome, N. and Cornell, C.A. (1998) " Earthquakes, records and nonlinear responses" Earthquake Spectra, vol. 14, no. 3: 469-500

Slovic, P. (1995) "Perceived risk, trust and democracy" Risk Management Quarterly, US Dept. of Energy, 3(2): 4-13

Slovic, P., Fischhoff, B. and Lichtenstein, S. (1980) "Facts and fears: understanding perceived risk" Societal Risk Assessment: How safe is safe enough?, eds. R.C. Schwing and W.A. Albers, New York, NY: 181-216

Starr, C. (1969). "Social benefit versus technological risk." Science 165: 1232-1238

"Statistical Abstract of the US" (2000??). Department of Commerce

Stedinger, J.R., Heath, D.C. and Thompson, K. (1996). "Risk analysis for dam safety evaluation: hydrologic risk." IWR Report 96-R-13, U.S. Army Corps of Engineers Institute for Water Resources, Alexandria, VA.

Stewart, M.G. and Melchers, R.E. (1997) "Probabilistic risk assessment of engineering systems" Chapman & Hall, London, UK.

Tarbox, G.S, Dreher, K. and Carpenter, L. (1979) "Seismic analysis of concrete dams." Transactions, 13th International Congress on Large Dams, New Delhi, vol. 2: 963-994

Tasuji, M.E, Slate, F.O. and Nilson, A.H. (1978) "Stress-strain response and fracture of concrete in biaxial loading" ACI Journal, vol. 75: 306-312

Tsai, C.S. and Lee, G.C. (1990) "Method for transient analysis of three-dimensional dam reservoir interaction" J. Engrg. Mech., ASCE, vol. 116: 2151-2172

U.S. Water Resources Council (1977). "Guidelines for determining flood flow frequency." Bulletin 17A of the Hydrology Subcommittee, Department of the Interior, Washington, DC.

USCOLD (1976). "Lessons from dam incidents." Prepared by Subcommittee on Dam Incidents and Accidents of the Committee on Dam Safety of the US Committee on Large Dams. Published by ASCE, New York, NY.

USCOLD (1988). "Lessons from dam incidents, USA-II" Prepared by Subcommittee on Dam Incidents and Accidents of the Committee on Dam Safety of US Committee on Large Dams. Published by ASCE, New York, NY.

Wahlstrom, E.E. (1975) "The safety of dams and reservoirs." International Water Power and Dam Construction, vol. 27, no. 4: 142-144

Wei, L. and Hudson, J.A. (1998) "A hybrid discrete-continuum approach to model hydro-mechanical behavior of jointed rocks" Engineering Geology, vol. 49: 317-325

Wepf, D.H, Wolf, J.P and Bachman, H. (1988) "Hydrodynamic-stiffness matrix based on boundary elements for time-domain dam-reservoir-soil analysis" *Earthquake Engrg. & Str. Dyn*, Vol. 16: 417-432

Westergaard, H.M. (1933). "Water pressure on dams during earthquakes." *Transactions, ASCE*, vol. 98: 418-433

Whipple, C. (1987). *De Minimis Risk*. Plenum Press, New York, NY.

Whitman, R.V. (1984). "Evaluating calculated risk in geotechnical engineering." *J. Geotech. Engrg. ASCE*, 110(2): 143-188.

Williams, J.R., Mustoe, G.G.W. and Worgan, K. (1986). " Force transfer and behavior of rubble piles." Iowa: IAHR Ice Symposium, Iowa City.

Wolf, J.P. and Paronesso, A. (1992) "Lumped-parameter model and recursive evaluation of interaction force of semi-infinite uniform fluid channel for time-domain dam-reservoir analysis" *Earthquake Engrg. & Str. Dyn*, Vol. 21: 811-831

Yeh, C.H. and Baier, D.R. (1992). "Pore pressure in finite element analysis of concrete dams." *Proc. 1992 Annual Conference, Assoc. of State Dam Safety Officials*, Lexington, KY, 195-200

REPORT DOCUMENTATION PAGE

Form Approved
OMB No. 0704-0188

Public reporting burden for this collection of information is estimated to average 1 hour per response, including the time for reviewing instructions, searching existing data sources, gathering and maintaining the data needed, and completing and reviewing this collection of information. Send comments regarding this burden estimate or any other aspect of this collection of information, including suggestions for reducing this burden to Department of Defense, Washington Headquarters Services, Directorate for Information Operations and Reports (0704-0188), 1215 Jefferson Davis Highway, Suite 1204, Arlington, VA 22202-4302. Respondents should be aware that notwithstanding any other provision of law, no person shall be subject to any penalty for failing to comply with a collection of information if it does not display a currently valid OMB control number. **PLEASE DO NOT RETURN YOUR FORM TO THE ABOVE ADDRESS.**

1. REPORT DATE (DD-MM-YYYY) September 2002		2. REPORT TYPE Final report		3. DATES COVERED (From - To)	
4. TITLE AND SUBTITLE Fragility Analysis of Concrete Gravity Dams				5a. CONTRACT NUMBER DACW31-99-P-0479	
				5b. GRANT NUMBER	
				5c. PROGRAM ELEMENT NUMBER	
6. AUTHOR(S) Paulos B. Tekie, Bruce R. Ellingwood				5d. PROJECT NUMBER	
				5e. TASK NUMBER	
				5f. WORK UNIT NUMBER	
7. PERFORMING ORGANIZATION NAME(S) AND ADDRESS(ES) Georgia Institute of Technology School of Civil & Environmental Engineering 790 Atlantic Dr. Atlanta, GA 30332				8. PERFORMING ORGANIZATION REPORT NUMBER ERDC/ITL TR-02-6	
9. SPONSORING / MONITORING AGENCY NAME(S) AND ADDRESS(ES) U.S. Army Corps of Engineers Washington, DC 20314-1000				10. SPONSOR/MONITOR'S ACRONYM(S)	
				11. SPONSOR/MONITOR'S REPORT NUMBER(S)	
12. DISTRIBUTION / AVAILABILITY STATEMENT Approved for public release; distribution is unlimited.					
13. SUPPLEMENTARY NOTES					
14. ABSTRACT Concrete gravity dams are an important part of the nation's infrastructure. Many dams have been in service for over 50 years, during which time important advances in the methodologies for evaluation of natural phenomena hazards have caused the design-basis events to be revised upwards, in some cases significantly. Many existing dams fail to meet these revised safety criteria and structural rehabilitation to meet newly revised criteria may be costly and difficult. A probabilistic safety analysis (PSA) provides a rational safety assessment and decision-making tool managing the various sources of uncertainty that may impact dam performance. Fragility analysis, which depicts the uncertainty in the safety margin above specified hazard levels, is a fundamental tool in a PSA. This study presents a methodology for developing fragilities of concrete gravity dams to assess their performance against hydrologic and seismic hazards. Models of varying degree of complexity and sophistication were considered and compared. The methodology is illustrated using the Bluestone Dam on the New River in West Virginia, which was designed in the late 1930's. The hydrologic fragilities showed that the Bluestone Dam is unlikely to become unstable at the revised probable maximum flood (PMF), but it is likely that there will be significant cracking at the heel of the dam. On the other hand, the seismic fragility analysis indicated that sliding is likely, if the dam were to be subjected to a maximum credible earthquake (MCE). Moreover, there will likely be tensile cracking at the neck of the dam at this level of seismic excitation. Probabilities of relatively severe limit states appear to be only marginally affected by extremely rare events (e.g. the PMF and MCE). Moreover, the risks posed by the extreme floods and earthquakes were not balanced for the Bluestone Dam, with seismic hazard posing a relatively higher risk. Limit state probabilities associated with postulated states of structural damage are larger than the "de minimis" risk acceptable to society, and further investigation involving benefit-cost analyses to assess the risk posed by the Bluestone Dam appears warranted.					
15. SUBJECT TERMS Bluestone Dam Gravity dams Structural damage Concrete dams Limit states Reliability Fragility analysis Probabilistic safety analysis Risk					
16. SECURITY CLASSIFICATION OF:			17. LIMITATION OF ABSTRACT	18. NUMBER OF PAGES	19a. NAME OF RESPONSIBLE PERSON
a. REPORT	b. ABSTRACT	c. THIS PAGE			19b. TELEPHONE NUMBER (include area code)
UNCLASSIFIED	UNCLASSIFIED	UNCLASSIFIED		231	